Title
Ionic mechanisms of circadian disruption

Author
Kuljis, Dika Ana

Publication Date
2015

Peer reviewed|Thesis/dissertation

UNIVERSITY OF CALIFORNIA

Los Angeles

Ionic mechanisms of circadian disruption

A dissertation submitted in satisfaction of the requirements for the degree

Doctor of Philosophy in Neurobiology

by

Dika Ana Kuljis

2015

ABSTRACT OF THE DISSERTATION

Ionic mechanisms of circadian disruption

By Dika Ana Kuljis

University of California, Los Angeles, 2015

Professor Christopher S. Colwell, Co-chair

Professor Marie-Francoise Chesselet, Co-chair

The temporal patterning of biological function is regulated by the circadian system on the cellular and systemic levels. In mammals, rhythmic neural output from the suprachiasmatic nucleus (SCN) of the hypothalamus provides the temporal cues needed to sustain synchronous cellular oscillations within tissues throughout the body, and coordinate those rhythms across systems to generate patterns of behavior and physiology essential for health and well-being. Genetic factors that may contribute to the dysfunction of the circadian system include sex, alterations in vasoactive intestinal peptide (VIP) signaling, and the Huntington's disease (HD) causing mutation, all of which are associated with the increased prevalence of behavioral and physiological rhythm disruptions. By examining the SCN for patterns of electrical activity and alteration in the ionic mechanisms that regulate those activities, we determined sex differences in the balance between GABA excitation and inhibition may predispose females to circadian disruption. Secondly, disrupted electrical activity rhythms in animals lacking VIP is associated with deficits in rhythmic behavior/physiology and photic entrainment. Thirdly, reduced A-type/H and enhanced BK potassium currents are associated with the loss of rhythmic SCN electrical activity in the BACHD mouse model of HD.

The dissertation of Dika Ana Kuljis is approved.

Paul E. Micevych

Felix Erich Schweizer

Marie-Francoise Chesselet, Committee Co-chair

Christopher S. Colwell, Committee Co-chair

University of California, Los Angeles

2015

TABLE OF CONTENTS

FIGURES:

SYMBOLS:

Alpha (α)

A-type-K+ current (I_A)

Delta (Δ)

Farad (F)

Hertz (Hz)

Hyperpolarization activated cyclic nucleotide gated current (I_H)

Meter (m)

Micro (μ)

Milli (m)

Molar (M)

Ohm (Ω)

Pico (p)

ACRONYMS:

4’6-diamindino-2-phenylindole, dihydrochloride (**DAPI**)

4-Nitro blue tetrazolium (**NBT**)

5-Bromo-4-chloro-3-indolyl phosphate (**BCIP**)

Action potential (**AP**)

Adenosine triphosphate (**ATP**)

Analysis of variance (**ANOVA**)

Androgen receptor (**AR**)

Arginine vasopressin (**AVP**)

Artificial cerebrospinal fluid (**ACSF**)

Cell-attached recording (**CAR**)

Circadian time (**CT**)

Coefficient of variation (**CV**)

Confidence interval (**CI**)

Constant darkness (**DD**)

Cryptochrome gene (**Cry**)

CRYPTOCHROME protein (**CRY**)

Cyclic-AMP response element binding protein (**CREB**)

Cyclic-AMP responsive element (**CRE**)

Deoxyribonucleic acid (**DNA**)

Diaminobenzidine (**DAB**)

Differential interference contrast (**DIC**)

Dorsal SCN (**dSCN**)

Electron microscopy (**EM**)

Excitatory post-synaptic current (**EPSC**)

Fast delayed rectifier (**FDR**)

Four core genotype mouse model (**FCG**)

Gastrin-releasing peptide (**GRP**)

Gonadectomized (**GDX**)

Gonadotropin releasing hormone (**GnRH**)

Hank’s balanced salt solution (**HBSS**)

Heart rate variability (**HRV**)

Human chorionic gonadotropin (**hCG**)

Huntingtin gene (**Htt**)

HUNTINGTIN protein (**HTT**)

Immunohistochemistry (**IHC**)

In situ hybridization (**ISH**)

Inhibitory post-synaptic current (**IPSC**)

Intrinsically photosensitive retinal ganglion cell (**ipRGC**)

Intraperitoneal (**IP**)

Knock-out (**KO**)

Large-conductance Ca^{2+} activated K^{+} (**BK**)

Luteinizing hormone (**LH**)

Light pulse (**LP**)

Light-dark cycle (**LD**)

Multi-unit activity (**MUA**)

Mutant Huntingtin gene (**mHtt**)

Mutant HUNTINGTIN protein (**mHTT**)

N-methyl-D-aspartate (**NMDA**)

Normal goat serum (**NGS**)

Paraformaldehyde (**PFA**)

Period gene (**Per**)

PERIOD protein (**PER**)

PERIOD2::LUCIFERASE (**P2L**)

PERIOD2::LUCIFERASE (**PER2**::**LUC**)

Phosphate buffer (**PB**)

Phosphate buffered saline (**PBS**)

Pituitary adenylate cyclase-activating peptide (**PACAP**)

Pregnant mare's serum gonadotropin (**PMSG**)

Prokineticin 2 (**PK2**)

RAR-related orphan receptor (**ROR**)

Reactive oxygen species (**ROS**)

Retinohypothalamic tract (**RHT**)

Spontaneous firing rate (**SFR**)

Standard error of mean (**SEM**)

Suprachiasmatic nucleus (**SCN**)

Tetrodotoxin (**TTX**)

Tris-buffered saline (**TBS**)

Ultra-violet (**UV**)

Vasoactive intestinal peptide (**VIP**)

Vasoactive intestinal peptide receptor 2 (**VPACR2**)

Ventral SCN (**vSCN**)

Whole-cell (**WC**)

Wild type (**WT**)

Zeitgeber time (**ZT**)

γ-aminobutyric acid (**GABA**)

GLOSSARY:

Alpha (**α**): activity duration.

Circadian time (**CT**): A standard of time relative to a free-running period.

Free-running period (**tau**): Circadian rhythm period in the absence of environmental zeitgebers.

Zeitgeber time (**ZT**): Time relative to an environmental stimulus that entrains circadian rhythms.

ACKNOWLEDGEMENTS

All chapters of this dissertation represent the collaborative efforts of multiple individuals as directed by PI Christopher S. Colwell. These chapters include materials from manuscripts that have been published, are currently in-press, or are currently in preparation.

Chapter 2 is a version of “Gonadal- and sex-chromosome-dependent sex differences in the circadian system.” by Kuljis, D.A., Loh, D.H., Truong, D., Vosko, A., Ong, M., McClusky, R., Arnold, A.P., Colwell, C.S. (2013) Endocrinology, Apr; 154(4):1501-12. PMID 23439698. Dika Kuljis performed *in vitro* electrophysiology of dorsal and ventral SCN neurons and wrote the manuscript. Dawn Loh and Danny Truong collected and analyzed behavioral rhythms data. Margaret Ong and Andy Vosko performed AR IHC, Rebecca McClusky provided FCG mice and performed GDX surgeries, Arthur Arnold acted as project advisor, and Christopher Colwell acted as project director.

Chapter 3 is a version of “Essential role for VIP in the propagation of photic information within the SCN circuit.” by Vosko, A., van Diepen, H., Kuljis, D.A., Michel, S., Meijer, J., Colwell C.S. (accepted for publication 2015). European Journal of Neuroscience. Andy Vosko performed *ISH* and IHC, Hester van Diepen performed *in vivo* MUA recordings, Dika Kuljis performed *in vitro* whole-cell patch clamp recordings and edited the manuscript, Stephan Michel performed *in vitro* calcium imagining, Johanna Meijer and Christopher Colwell acted as project directors.

Chapter 4 is a version of “Disrupted reproduction, estrous cycle, and circadian rhythms in female mice deficient in vasoactive intestinal peptide.” by Loh, D.H., Kuljis, D.A., Azuma, L., Wu, Y., Truong, D., Wang, H.B., Colwell, C.S. (2014). Journal of Biological Rhythms, Sep; 29(5): 355-69. PMID: 25252712. Dawn Loh wrote the manuscript, collected and analyzed behavioral rhythm data in collaboration with Danny Truong. Dika Kuljis performed *in vitro* whole-cell patch

clamp recordings of dorsal SCN neurons and assisted editing the manuscript. Lauren Azuma performed vaginal cytology, Huei-Bin Wang conducted hormone assays, and Christopher Colwell acted as project director.

Chapter 5 is a version of “Sex differences in BACHD mouse circadian dysfunction.” by Kuljis, D.A., Loh, D.H., Gad, L., MacDowell Kaswan, Z., Ghianni, C., Colwell, C.S. (in preparation, 2015). Dika Kuljis performed electrophysiology experiments and prepared the manuscript. Dawn Loh advised Laura Gad with the collection of behavioral rhythms data, and aided in its analysis. Zoe MacDowell Kaswan performed IHC and stereological analysis. Christina Ghiani directed Dika Kuljis, Mariana Gomez, Crystal Cheung, Jin Yan, Yingfei Wu, Zoë MacDowell Kaswan in brain collection, nissl staining, SCN tracing, and SCN area analysis, to be part the published version of this work, not included in the chapter. Christopher Colwell acted as project director. Additional Colwell Lab colleagues not listed as authors yet provided valuable assistance with motor testing and motor scoring include Huei-Bin Wang and Daniel Whittaker.

Chapter 6 is a version of “Pathophysiological mechanisms of circadian system disruption in the BACHD mouse model of Huntington’s disease.” by Kuljis, D.A., Kudo, T., Colwell, C.S. (in preparation, 2015). Dika Kuljis performed all electrophysiology experiments, Takashi Kudo provided technical advice, and Christopher Colwell acted as project director. Yingfei Wu and Jocelyn Quintanilla assisted with FOS cell counts.

Dika Kuljis drew all diagrams. Richard Baughman assisted with proofreading. Donna Crandall assisted with figure preparation for data figures in chapters 2-6.

PREFACE

The timing of biological function is essential for health and well-being. By coordinating environmental, behavioral, and physiological rhythms, the mammalian circadian system optimizes the function of multiple organ systems throughout the body. When the circadian system dysfunctions, physiological and psychological stress ensues due to sleep disruption, impaired gastrointestinal and immune system function, cardiovascular and metabolic stress, negative-affect, and impaired higher-cognitive function and memory (Wirz-Justice, 2006; McClung, 2007; Cohen et al., 2009; Goel et al., 2009; Mullington et al., 2009; Lange et al., 2010; Besedovsky et al., 2012; Ali et al., 2013). In addition to environmental perturbations that destabilize the circadian system, genetic factors may sensitize or predispose individuals to destabilization. How genetic factors undermine the integrity of biological timing mechanisms is the essential question addressed by this dissertation. By identifying ionic and molecular mechanisms associated with aberrant behavioral and endocrine rhythms, the findings discussed here shed light on the role of sex, vasoactive intestinal peptide (VIP) signaling, and mutant huntingtin protein (mHtt) in the circadian system. This research is driven by the hope that, through the use of genetically modified mice, we will gain important insights into the inner workings of the mammalian circadian system that will aid in the development of medical treatments for dysfunctions of biological timing in humans. Thus, implications and limitations of mouse model findings for the treatment of human disease will be the focus of the ensuing discussion.

VITA: Dika Kuljis

EMAIL: dika.kuljis@gmail.com

EDUCATION

Smith College, Northampton, MA, BA Neuroscience (2003-2007)

RESEARCH

University of California Los Angeles, Los Angeles, CA. Graduate Student Researcher of Christopher S. Colwell PhD: Trained as a whole-cell patch clamp electrophysiologist to answer basic questions about the ionic mechanisms regulating physiological output rhythms from the suprachiasmatic nucleus (SCN) of the hypothalamus. Dissertation research focuses on how factors including sex, the signaling molecule vasoactive intestinal peptide, and the Huntington's disease causing mutation influence rhythmic SCN physiology.

Massachusetts General Hospital Neuroscience Research Department, Harvard Medical School, Charleston, MA (2007-2009). Research Assistant to Florian Eichler, MD: Analyzed hereditary sensory and autonomic neuropathy (HSAN1) mouse model of peripheral neuropathy using EM ultrastructure, and sensory and motor testing. Used dissociated adult dorsal root ganglion cultures to measure neurite outgrowth in response to deoxysphingoid bases, and primary cortical microglial cultures to assess cytokine response to fatty acids of different chain lengths.

Smith College, Northampton, MA (Spring 2007). Undergraduate Research Assistant to Mary Harrington, PhD: Conducted experiments testing hamster and mouse wheel running rhythm responses to IP and subcutaneous treatment of an experimental jet lag drug, and performed statistical analysis of findings.

SELECT PEER REVIEW PUBLICATIONS

Essential role for VIP in the propagation of photic information within the SCN circuit. Vosko, A., van Diepen, H., **Kuljis**, **D.A.**, Michel, S., Meijer, J., Colwell C. (accepted for publication 2015). European Journal of Neuroscience.

Disrupted reproduction, estrous cycle, and circadian rhythms in female mice deficient in vasoactive intestinal peptide. Loh, D.H., **Kuljis, D.A.**, Azuma, L., Wu, Y., Truong, D., Wang, H.B., Colwell, C.S. (2014). Journal of Biological Rhythms, Sep; 29(5): 355-69. PMID: 25252712.

Circadian dysfunction in Huntington's disease. In "Mechanisms of Circadian Systems in Animals and Their Clinical Relevance". **Kuljis, D.**, Schroeder, A.M., Kudo, T., Loh, D.H., Colwell, C.S. (2014) Editor: R Aguilar-Roblero. Springer, NY.

Gonadal- and sex-chromosome-dependent sex differences in the circadian system. **Kuljis, D.A.,** Loh, D.H., Truong, D., Vosko, A., Ong, M., McClusky, R., Arnold, A.P., Colwell, C.S. (2013) Endocrinology, Apr; 154(4):1501-12. PMID 23439698.

Fast delayed rectifier potassium current: critical for input and output of the circadian system. Kudo, T., Loh, D.H., **Kuljis, D.A.**, Constance, C., Colwell, C.S. (2011). Journal of Neuroscience, 31(8):2746-55. PMID: 21414897.

Dysfunctions in circadian behavior and physiology in mouse models of Huntington's disease. Kudo, T., Schroeder, A., Loh, D.H., **Kuljis, D.A.**, Jordan, M.C., Roos, K.P., Colwell, C.S. (2011). Experimental Neurology, 228(1):90-90. PMID: 21184755.

Overexpression of wild-type SPT1 subunit lower desoxysphingolipid levels and rescues the phenotype of HSAN1. Eichler, F.S., Hornemann, T., McCampbell, A., **Kuljis**, **D.A.,** Penno, A., Vardeh, D., Tamrazina, E., Garofalo, K., Lee, H.J., Kini, L., Selig, M., Frosch, M., Gable, K., von Eckardstein, A., Wolf, C.J., Guan, G., Harmon, J.M., Dunn, J.M., Brown Jr., R.H. (2009). Journal of Neuroscience, 29(46):80-90.

Part I. The Circadian System

Chapter 1: Introduction

Time of Life

The Earth's tilted rotation along its orbit around the sun has created daily rhythms of light and ultra-violet (UV) exposure for the Earth's surface for 4.6 billion years. All life forms utilizing land and ocean surfaces responded by developing rhythmic physiology and behavior to best take advantage of predictable daily and seasonal changes to sunlight availability and the resulting environmental conditions. Fossil evidence of Earth's earliest life-forms are called stromatolites, which are cemented sedimentary grains formed by microbial mats, the oldest of these dates to nearly 3.5 billion years ago. Similar life-forms to those that created these most ancient fossils still inhabit the Earth's oceans today and continue to form stromatolites (Schopf et al., 2007). They are called cyanobacteria and are unicellular photosynthetic organisms that move toward ocean surfaces during the day, and to deep dark nutrient-rich waters at night. These behavioral rhythms are coupled to cell cycle rhythms to ensure maximum photosynthesis occurs during the day in the presence of sunlight, while UV-sensitive cell cycle stages occur at night (Mittag and Wagner, 2003). By staggering metabolic function, genomic replication and cell division cycles according to the solar cycle, even the simplest/earliest life forms adaptively aligned their biological rhythms to rhythms in their environment (Wijnen and Young, 2006). From these archaic lifeforms millions of additional species evolved and complex spatial ecologies emerged, as life seeking survival advantage moved to the lands, skies, and waters everywhere from the frigid waters near the poles to the humid jungles of the equator. Endothermic adaptations freed many animal species to occupy greater latitudes, hunt and forage in the cooler hours of the early-morning, evening, and night, and facilitated nocturnality as a mechanism for avoiding diurnal predators. Although the sequence of evolutionary pressures that

led to the development of endothermy in early mammals is debated (Clarke and Pörtner, 2010), it is clear that it expanded the temporal niches available for their occupancy.

Daily variation in physiology and behavior are termed circadian rhythms by biologists because they are biologically generated rhythms and have periods approximately the length of a day (Latin *circa* = about, *dia* = day). The molecular specifics that control circadian rhythms of primitive life-forms such as cyanobacteria vary significantly from those of more complex ones such as humans - as would be expected from billions of years of evolution. More remarkably perhaps is that they *share* many key properties. These properties were first outlined as a set of empirical generalization by Colin Pittendrigh in 1960: they are a biological rhythm whose period is an approximation to the period of the Earth's rotation, they are endogenously generated, self-sustaining, innate, occur at the cellular and whole-organism level, are remarkably precise, are mutable within a range of values that varies by species, show after-effects of their preceding steady-state, nearly temperature independent, light-intensity dependent, are entrained by a restricted class of environmental periodicities, their phase can be shifted by a single perturbation of light and/or temperature, they display transients that precede attainment of a new steady state, and are notably intractable to chemical perturbation (Pittendrigh, 1960). These properties adaptively facilitate the ability of life to predict and respond to daily and seasonal changes in light, temperature, and the availability of other resources, because correctly timing behavior and physiology can be crucial to survival, especially for species that migrate, hibernate or reproduce seasonally.

Molecular clockwork in tissues throughout the body

In mammals, output from the master circadian clock located in the central nervous system regulates physiological rhythms by modifying the phase and amplitude of cellular gene

expression rhythms in tissues throughout the body. These rhythms are genetically regulated by "clock genes" encoding a set of transcription factors whose levels are autoregulated in a negative feedback loop of transcription and translation that cycles with a period close to 24 hours (**Fig. 1.1**). Over the last twenty years, circadian rhythm researchers have identified the mechanism by which this cell-autonomous molecular clockwork generates and regulates rhythms in gene expression in a circadian manner (Dibner et al., 2010; Mohawk and Takahashi, 2011). Briefly, CLOCK and BMAL1 are basic helix-loop-helix PAS-containing transcription factors that heterodimerize and enhance transcription of Period genes (Per1-3) (Albrecht et al., 1997; Shearman et al., 1997; Sun et al., 1997) and Cryptochrome genes (Cry1-2) (van der Horst et al., 1999) through E-box elements (Gekakis et al., 1998; Hogenesch et al., 1998; Takahata et al., 1998). Multiple paralogues of PER and CRY proteins form homo- and heteromeric complexes in the cytoplasm that translocate to the nucleus where they recruit HDAC complex to repress BMAL/CLOCK-mediated transcription (Thresher et al., 1998; van der Horst et al., 1999; Siepka et al., 2007; Duong et al., 2011). This transcriptional inhibition ends when ubiquitination of CRYs targets them for proteosomal degradation, which allows a new cycle to begin (Busino et al., 2007; Siepka et al., 2007; Jagannath et al., 2013). Auxiliary kinase phosphorylation of core clock-protein-complexes advances or delays the rhythm by directing them for degradation or nuclear translocation (Lee et al., 2001; Harms et al., 2004; Gallego and Virshup, 2007; Gavrila et al., 2008), while auxiliary stabilizing transcriptional loops regulate Bmal1 (Preitner et al., 2002; Sato et al., 2004) and other clock genes (Panda et al., 2002; Crumbley et al., 2010) through nuclear receptors from the REV-ERB and ROR families. Working in concert, auxiliary and core circadian molecular networks drive cellular oscillations in gene expression, and function as a highly regulated and resilient timekeeper at the cellular level.

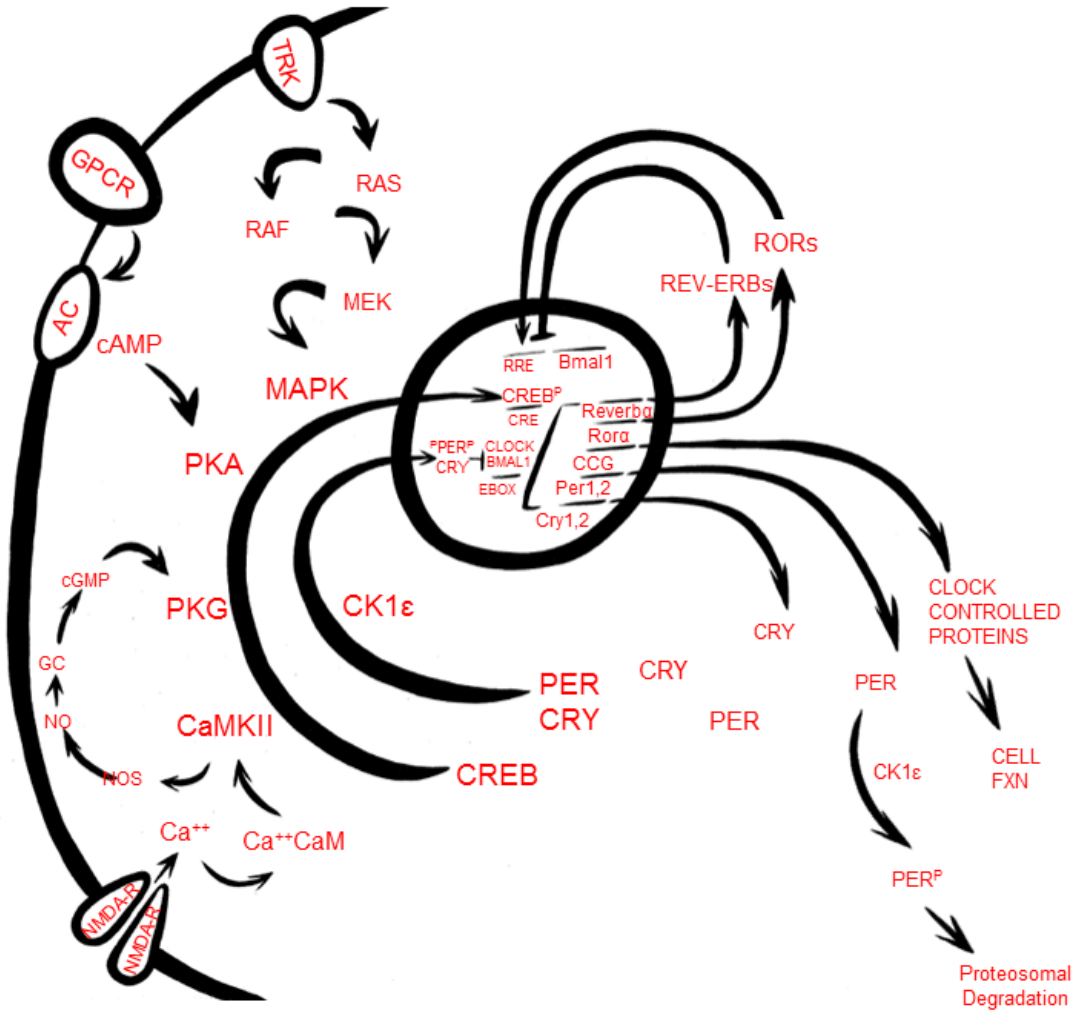

Figure. 1.1: Circadian molecular clockwork. Clock proteins CLOCK and BMAL1 are transcription factors that induce gene expression via EBOX elements, including clock genes Per1 and 2, Cry1 and 2, the auxiliary clock genes Reverbα and Rorα, and other clock controlled genes (CCG) involved in cell-specific function. PER and CRY proteins build-up in the cytoplasm during the day. PER phosphorylation (PER^P) by casein kinase 1 epsilon (CK1ε) targets it for proteosomal degradation, lengthening the time needed for PER and CRY proteins to reach a critical concentration for PER/CRY heterodimerization. CK1ε phosphorylates these dimers targeting them for nuclear translocation where they inhibit BMAL1 and CLOCK transcriptional activity. Auxiliary clock protein REV-ERB inhibits while ROR activates Bmal1 gene transcription via rev response elements (RRE) to affect the timing of the core-clock gene negative feedback loop. In neurons, Per transcription can also be induced when cyclic adenosine monophosphate (cAMP) response-element binding protein (CREB) phosphorylation ($CREB^P$) activates its transcriptional activity via cAMP response element (CRE) which drives expression of downstream genes. CREB phosphorylation is regulated by Ca^{++}/calmodulin (Ca^{++}/CaM)-dependent kinase (CaMKII) via N-methyl-D-aspartate receptor (NMDA-R) activation, cGMP-dependent protein kinase (PKG) activation via nitric oxide synthase (NOS)/ nitric oxide (NO)/ guanylate cyclase (GC)/ cyclic guanosine monophosphate (cGMP) pathway, cAMP-dependent protein kinase (PKA) via G-protein coupled receptor (GPCR) induction of adenylyl cyclase (AC) cAMP production, and the RAS-RAF-MEK-MAPK pathway via Trk receptor activation.

Circadian regulation of gene expression varies with tissue

Each of the major organ systems of the body (i.e. brain, heart, liver, and pancreas) is made up of a network of cellular circadian oscillators with its own clockwork that regulates the transcription of genes important for the specific target organ (Dibner et al., 2010). DNA microarray expression profiling indicates approximately 8 to 12% of genes display circadian oscillations (Panda et al., 2002; Storch et al., 2002; Hogenesch et al., 2003). Many of these rhythmically expressed genes are involved in key rate-limiting steps of biochemical pathways that play critical roles in the rhythmic regulation of cell function (Panda et al., 2002; Baggs and Hogenesch, 2010). For instance in the brain, rhythms in dopamine regulation of motor function are regulated by rhythmic expression of tyrosine hydroxylase, the rate limiting enzyme in the dopamine synthesis pathway, and dopamine receptors at target tissues (Wirz-justice, 1987; Weber et al., 2004). In the hypothalamus rhythmic expression of ion channels regulating action potential dynamics and excitatory and inhibitory drive, generate cell autonomous rhythms in spontaneous electrical activity of neurons (Panda et al., 2002; Wang and Huang, 2004; Choi et al., 2008; Kudo et al., 2011a). In the digestive system, gene expression rhythms regulate glycolysis in the liver (Akhtar et al., 2002), as well as insulin and glucagon secretion from the pancreas, which in combination regulate systemic glucose levels (Vieira et al., 2013). Disrupting the core circadian gene network has dramatic effects on tissue specific gene expression rhythms. For instance, liver-specific overexpression of REV-ERBα results in a 90% reduction of hepatocyte transcriptional rhythms (Kornmann et al., 2007). Loss of BMAL1 results in the loss of leydig cell testosterone production (Alvarez et al., 2008), and the loss of CLOCK results in the blunting of behavioral rhythms related to altered neuronal activity rhythms in the hypothalamus (Kume et al., 1999; Field et al., 2000; Bae et al., 2001; Lee et al., 2001; Preitner et al., 2002; Nakamura et al., 2008b).

SCN circuitry and input

The suprachiasmatic nucleus (SCN) of the hypothalamus contains the “master” oscillatory network necessary for coordinating circadian rhythms in gene expression in tissues throughout the body (Welsh et al., 2010; Mohawk and Takahashi, 2011). This bilaterally paired nucleus is made up of tightly compacted, small-diameter neurons just above the optic chiasm and lateral to the third ventricle (Van den Pol, 1980). Anatomical studies indicate there are at least two distinct subregions of the SCN -- a ventral (core) and dorsal (shell) region (Antle et al., 2009; Golombek and Rosenstein, 2010) (**Fig. 1.2** and **1.3**). Ventral SCN (vSCN) neurons integrate ambient light information from the environment using three major input pathways: the retinohypothalamic tract (RHT), the geniculohypothalamic tract from the intergeniculate leaflet of the thalamus, and the raphe nuclei (Morin and Allen, 2006). Ventral neurons display relatively low amplitude rhythms in clock gene expression and firing rate rhythms (Pauls et al., 2014), but their rhythmic response to photic input acts as a gate for phase altering input (Wang et al., 2008). These neurons express either the neuropeptide vasoactive intestinal peptide (VIP) or gastrin-releasing peptide (GRP), in addition to the neurotransmitter γ-aminobutyric acid (GABA). VIP signaling in particular plays a critical role in SCN circuit function because of its role in gating light-input and synchronizing cellular rhythms. Much effort has been spent in determining how VIP signaling via its receptor VPACR2 works, to synchronize cellular rhythms and powerfully impact the timing of physiological and behavioral rhythms (Cunha-Reis et al., 2004; Aton et al., 2006; Mahoney et al., 2009; Loh et al., 2011; Lucassen et al., 2012).

Light plays the most important role in regulating the timing of biological rhythms. Seasonal changes in the solar day length, or other environmental photic rhythms are communicated to the SCN monosynaptically from intrinsically photosensitive retinal ganglion cells (Hattar et al., 2002; Mure et al., 2007).

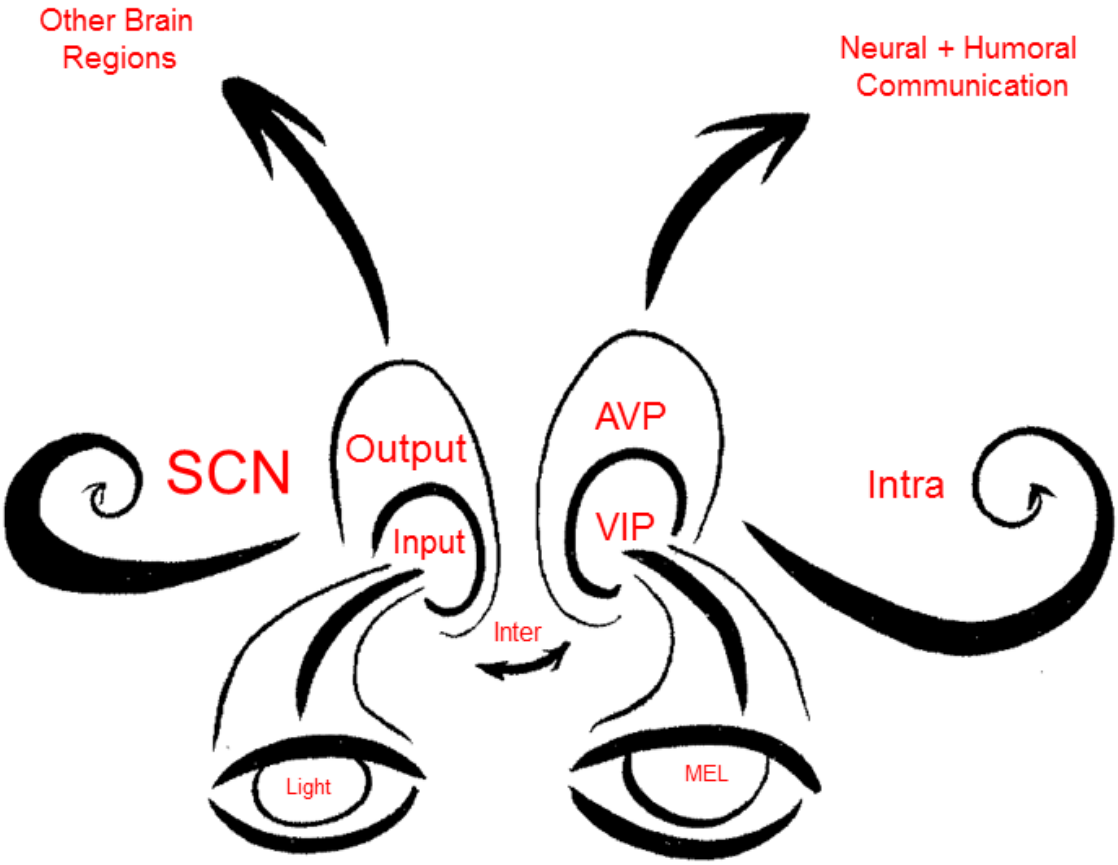

Figure 1.2: Photic regulation of circadian rhythms. Melanopsin (MEL) expressing retinal ganglion cells communicate ambient light information to VIP neurons in the SCN via the retinohypothalamic tract. Intra-SCN VIP signaling is essential for maintaining synchronous neural rhythms that are phase locked to photic environmental rhythms. Rhythmic neural and humoral SCN output temporally regulates the function of extra-SCN brain regions.

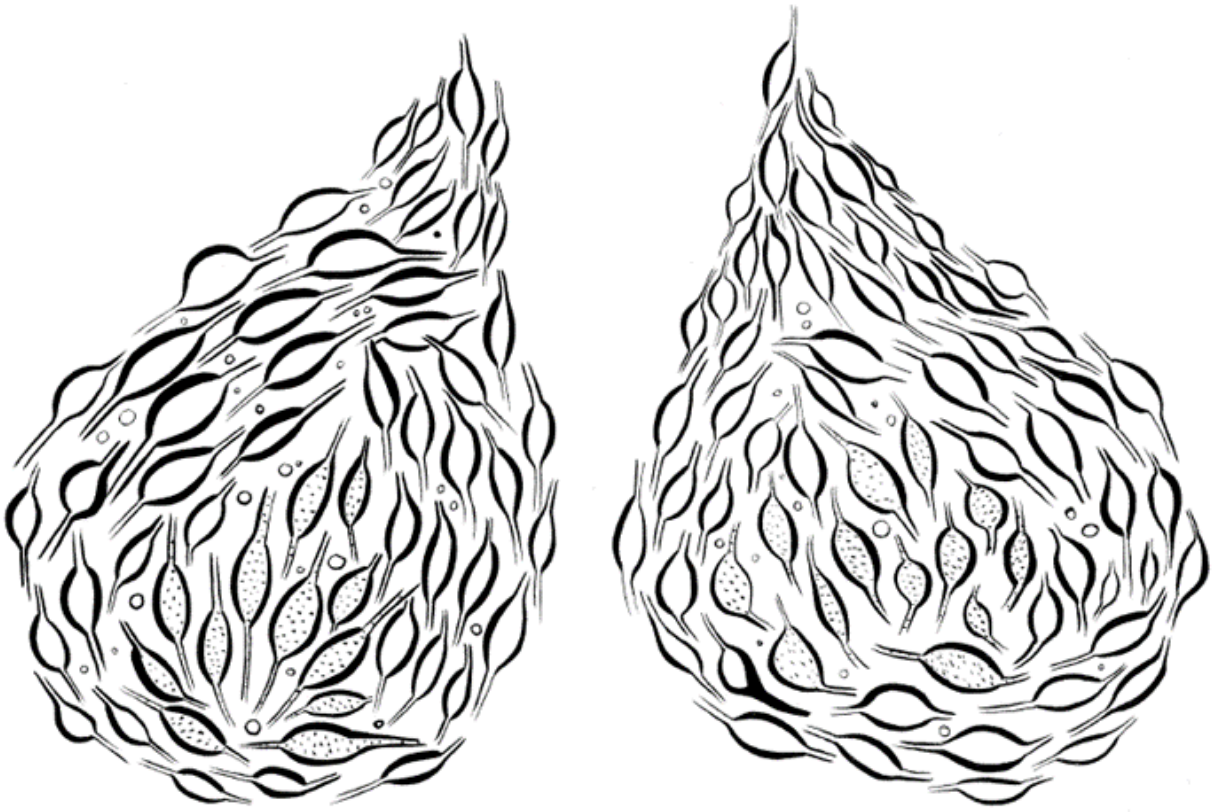

Figure 1.2: Suprachiasmatic nuclei. The suprachiasmatic nucleus (SCN) is a bilateral group of GABAergic multipolar neurons at the base of the third ventricle just above the optic chiasm. Mid-SCN (along rostro-caudal axis), has a tear drop shape in which weakly rhythmic retinorecipient ventral and core neuron (speckled cells) and robustly rhythmic dorsal neurons form anatomically discrete cell populations.

This glutamatergic synaptic connection is responsible for adaptively phase locking internally generated biological rhythms to photic environmental rhythms via a N-methyl-d-aspartate receptor (NMDA-R) dependent mechanism (Colwell et al., 1991; Colwell, 2001; Pennartz et al., 2001; Wang et al., 2008). Night-time NMDA-R activation for retinorecipient SCN neurons selectively induces calcium stimulated intracellular 2nd messenger cascades that activate CREB signaling and change the phase of clock-gene expression rhythms (Moriya et al., 2000; Brown and Piggins, 2007; Wang et al., 2008). Dense projections from retinorecipient ventral neurons to dorsal SCN (dSCN) neurons realign dorsal clock gene and electrical activity rhythms, and thereby adaptively phase biological rhythms regulated by downstream brain regions to environmental rhythms (Antle and Silver, 2005; Gamble et al., 2007; Vosko et al., 2007; An et al., 2011; Hannibal et al., 2011; Loh et al., 2011). Unlike ventral neurons, dSCN neurons generate robust circadian oscillations in gene expression and neural activity that are used as temporal cues for the rest of the brain and body (Yan and Okamura, 2002; Hamada et al., 2004; Nakamura et al., 2005; Webb et al., 2009). Dorsal neurons typically express the neuropeptides arginine vasopressin (AVP) or prokineticin 2 (PK2) in addition to GABA, which are essential for SCN signaling output, especially activity rhythm regulation (Cheng et al., 2002; Li et al., 2009; Maywood et al., 2011). The terms core/shell and ventral/dorsal are standard SCN subnuclear designations, but have nuanced meanings. Core and shell are strictly defined by peptidergic expression, while ventral and dorsal is a spatial anatomical designation only correlated with peptide expression.

SCN outputs coordinate an array of rhythmic tissues

Projections from both the ventral/core and dorsal/shell subpopulations synapse on other medial hypothalamic structures such as the subparaventricular zone surrounding the SCN,

amongst many others (Abrahamson and Moore, 2001; Kriegsfeld et al., 2004; Kalsbeek et al., 2006) (**Fig. 1.4**). Hypothalamic relay nuclei in turn send projections throughout the nervous and endocrine systems, providing multiple pathways by which SCN output conveys environmental time to the rest of the brain and body (Kalsbeek et al., 2006; Dibner et al., 2010). In the absence of environmental light input or other entraining signals, the kinetics of rhythmic clock gene expression drives circadian rhythms of SCN neural output with a period of ~24 hours that synchronize biological rhythms throughout the body and brain. Additionally, circadianly regulated behavioral and physiological outputs, like sleep states and locomotor activity, can "feed-back" to modulate the master clock in the SCN by regulating its neural activity (Meijer et al., 1997; Yamazaki et al., 1998; Schaap and Meijer, 2001; Deboer et al., 2003). These *in vivo* studies highlight the difficulty in disentangling the role of the circadian system on sleep, behavior, and physiology, because altering sleep without impacting the circadian system may not be possible. Nevertheless, *in vivo* and *in vitro* studies focused on identifying the ionic mechanisms that underlie the rhythmic electrical activity of SCN neurons have provided a wealth of information and important insights into the unique circuit properties of the SCN that mediate its ability to generate and sustain rhythmic electrical activity (Bhattacharya et al. 2013a; Wang et al. 2012; Chen & van den Pol 1998; Artinian et al. 2001; Choi et al. 2008; Itri et al. 2010; Gamble et al. 2011; Granados-Fuentes et al. 2012; Cloues & Sather 2003; Lundkvist et al. 2002; Brown & Piggins 2007; O'Neill et al. 2008; Brancaccio et al. 2013; S. An et al. 2011; Itri et al. 2004; Michel et al. 2006; Kononenko et al. 2008; Bhattacharya et al. 2013b; Meijer et al. 1997, amongst others). The subsequent chapters of this dissertation seek to extend this body of research by identifying how genetic factors influence SCN electrical activity.

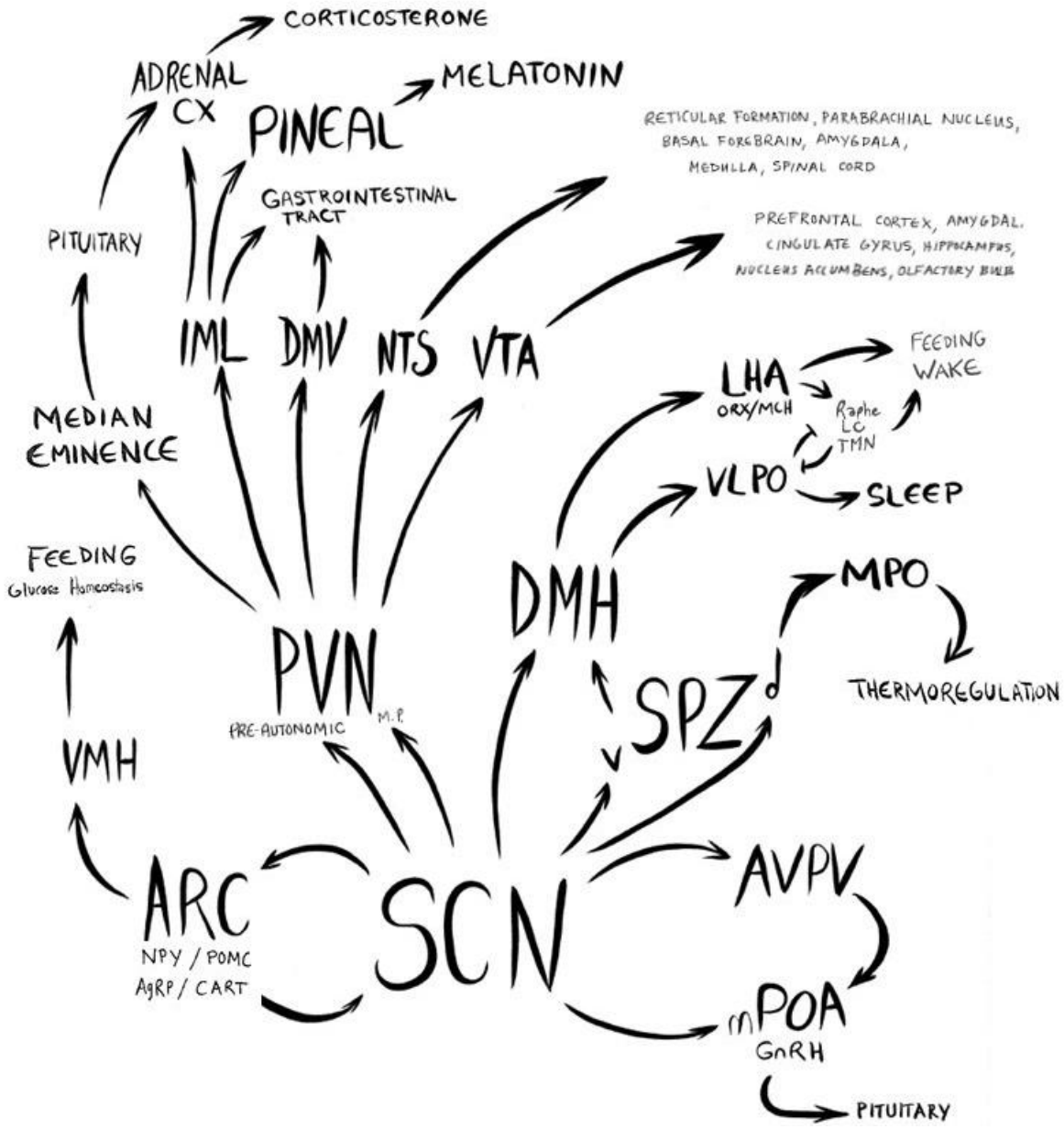

F**igure 1.4:** SCN outputs diagram. Rhythmic SCN output temporally regulates behavioral and physiological rhythms via multisynaptic neural and humoral communication with the following brain regions: arcuate nucleus (ARC); ventromedial hypothalamic nucleus (VMH); anteroventral periventricular nucleus (AVPV); medial preoptic area (mPOA); gonadotropin-releasing hormone neurons (GnRH); dorsal (d) and ventral (v) subparaventricular zone (SPZ); medial preoptic area (MPO); dorsomedial hypothalamic nucleus; lateral hypothalamus (LHA); orexin (ORX); melanin concentrating hormone (MCH); ventrolateral preoptic nucleus (VLPO); locus ceruleus (LC); tuberomammillary nucleus (TMN); paraventricular nucleus (PVN) pre-autonomic and medial posterior (M.P); interomediolateral nucleus (IML); dorsal motor nucleus of vagus nerve (DMV); nucleus tractus solitary (NTS); ventral tegmental area (VTA) (Saper et al., 2005; Dickmeis, 2009; Dibner et al., 2010; Huang et al., 2011; Williams and Kriegsfeld, 2012).

Chapter 2: Sex differences in the circadian system

As far as advancements have come in our knowledge of the mechanisms underlying the molecular machinery mediating circadian rhythms, it could also be said that we only have half the picture considering the majority of circadian rhythms research has focused only on studying male biology. Historically, most neuroscience research has used exclusively male animal models in their experimental designs (Beery, Annaliese and Zucker, 2011), and in the field of circadian rhythms research, this trend was spurred by early observations of estrous cycle-dependent ultradian rhythms in the locomotor activity of female hamsters and rats (Morin et al., 1977; Takahashi and Menaker, 1980; Albers and Elliott, 1981; Wollnik and Turek, 1988). The free running period of female locomotor activity in these rodents changes depending on circulating estrogen levels, causing advanced locomotor activity on the days following highest circulating estrogen levels. Since these early studies, advancements in the understanding and technical manipulability of mouse genetics led to their replacement of earlier mammalian models in most circadian research. Observations of estrous related ultradian rhythms in rats and hamsters still biased many researchers' experimental designs. Female mice have been excluded from many studies due to the belief that needing to control for estrous cycle phase unnecessarily increases experimental complexity and cost.

This bias creates an obvious problem as both male and female circadian rhythms are medically relevant. Furthermore, there is compelling evidence of sex differences in the circadian system. First, behavioral patterning, which is regulated by the circadian system, is different for men and women. Women tend to wake up earlier and have a greater preference for morning activities than men. This difference is likely mediated by gonadal hormones, since starting in puberty, men's sleep times become later than women's, and this sex difference persists until the

end of reproductive years (Roenneberg et al., 2007). Further evidence of gonadal hormone regulation of biological rhythm timing has been shown more directly using rodent models (Malven and Sawyer, 1966; Colvin et al., 1969; Branchey et al., 1971; Itil et al., 1974; Zucker et al., 1980). In humans, in addition to sex differences in the timing of sleep, the dynamics of SCN regulated rhythms in melatonin secretion and core body temperature also differ between the sexes. Women's melatonin secretion rhythms start earlier and have a greater amplitude relative to men's, while men's temperature rhythms have a greater amplitude than women's (Cain et al., 2010). Phase differences in melatonin secretion are likely caused by sex differences in the intrinsic periods of melatonin release as female melatonin rhythm period is typically shorter than 24 hours, and male's are typically longer (Duffy et al., 2011). In experimental settings where subjects are kept in environments without any temporal cues and only their circadian system to drive rhythms in behavior and physiology, a subset of individuals experience spontaneous splitting of their temperature and sleep rhythms. When this occurs, temperature rhythms continue with a similar period for men and women, but sleep rhythm periods, like melatonin rhythms, are shorter for women and longer for men, indicating that circadian regulation of physiological and behavioral rhythms are differentially influenced by sex specific factors (Wever, 1984). Even within the SCN there is evidence of sex differences. During reproductive years males have twice as many VIP expressing SCN neurons (Zhou et al., 1995), and four times the number of androgen receptor (AR) expressing neurons than females (Karatsoreos et al., 2007; Iwahana et al., 2008). AR and VIP are typically expressed on retinorecipient SCN neurons, implicating a sex difference in the mechanism underlying light entrainment and synchronization. Notably, no evidence of sex differences in AVP protein or mRNA expression have been reported, although it is involved in reproduction and reproductive behaviors (Krajnak et al., 1998; Swaab, 2004).

These differences are particularly important for understanding the relationship of sex and sleep disorders. Women are more likely to experience sleep disturbance and daytime fatigue in every geographical region of the U.S. (Grandner et al., 2012). Throughout adulthood, women are more likely to report insomnia symptoms, and by middle age (>45), the ratio of women to men with insomnia increases from 1.4 to 1.7 (Ohayon, 2002). Additionally, there are sex differences in the homoeostatic response to sleep deprivation that are consistent with the notion that women are more vulnerable to its long-term consequences (Koehl et al., 2006; Paul et al., 2006). Considering that much of circadian biological research is conducted with the intention of improving our understanding of the factors that lead to sleep disruption, it is surprising more research is not conducted using female animal models to better reflect the epidemiology of sleep disorders. To re-engage the circadian rhythms research community's interest in the female circadian system, we have reassessed the justification for the sex bias in circadian rhythms research by examining whether ultradian rhythms are present in a commonly used mouse strain. Additionally, with the goal of improving our mechanistic understanding of the circadian system, we sought to determine whether observed sex differences in WT mouse behavior are associated with sex chromosome compliment or circulating gonadal hormones using the four core genotypes (FCG) mouse model.

Materials and Methods

Animals and housing

All experimental protocols used in this study were approved by the UCLA Animal Research Committee. UCLA Division of Laboratory animal recommendations for animal use and welfare, as well as National Institutes of Health guidelines were followed. Experiments for behavior, physiology, and bioluminescence used 2- 3 month-old PER2::LUC knock-in mice on a

C57BL/6J background heretofore referred to as wildtype male and female mice (WT; minimum 12 generations backcrossed (Yoo et al., 2004)). Vaginal smears were conducted to determine estrous cycle phase for those female mice whose tissues were harvested for electrophysiology and bioluminescence. A separate cohort of female mice underwent daily vaginal smears to determine regular cycling.

In order to determine whether gonadal hormones or sex chromosomes underlie sex differences in behavior observed in male and female WT mice, we used the FCG mouse model on a C57BL/6J background for behavioral analysis. FCG testis-determining *Sry* gene is deleted from the Y chromosome (Y^-) and transgenically inserted onto an autosome. When the XY^-*Sry* animal breeds with a WT XX animal they produce the following four core genotypic offspring: XX, XX*Sry*, XY^-, and XY^-*Sry*. Animals carrying the *Sry* transgene develop testis and are referred to as phenotypically male (XX*Sry* and XY^-*Sry),* whereas animals without the *Sry* transgene develop ovaries and are referred to as phenotypically female (XX and XY^-*)*. At 50 days of age, a cohort of 4CG animals were gonadectomized 3 weeks prior to analysis of rhythms in wheel running activity.

Behavioral analysis

Methods used were similar to those described previously (Colwell et al., 2003, 2004). Mice were housed individually and their wheel-running activity recorded as revolutions (rev) per 3 min intervals. Both the running wheels and our data acquisition system were obtained from Mini Mitter Co. (Bend, OR). Animals were exposed to a 12:12 hour light-dark cycle (LD; light intensity 300lux) for two weeks, and then released in 24 hours of constant darkness (DD) to assess their free-running activity pattern for two weeks. The period of this free-running rhythm was used to calculate the duration of one circadian hour (free-running period $\div 24 =$

$circadian\ hour$). FCG mouse circadian time (CT) 16 was determined as four circadian hours after activity onset (or CT12) in DD. A light pulse (LP; white light 100 lux, 10 min) was applied at CT16. Phase shifts in activity rhythm were determined by measuring the phase difference between eye-fitted lines connecting the onset of activity for a period 10 days before and 10 days after the CT16 LP. Phase shift measurements were made by "blind" investigators, without knowledge of subject genotype. Light intensity (lux) was measured with a light meter (BK precision, Yorba Linda, CA), and all handling of mice in DD was carried out with the aid of night vision goggles (FJW Industries, Palantine, IL).

Locomotor activity rhythms were analyzed by periodogram analysis combined with the χ^2 test with $P = 0.05$ significance levels (El Temps, Barcelona, Spain) on the raw data. The periodogram refers to behavioral rhythm amplitude as "power" (%V) or periodicities in the time series for all periods of interest. The power values were normalized to the percentage of variance derived from Qp values of the periodogram (Qpx100/N; N-total number of data points) according to the calculated $P = 0.05$ significance level. Slopes of an eye-fitted line through behavioral onsets were used to confirm period estimates made with the periodogram analysis.

Whole cell patch-clamp electrophysiology

Methods used were similar to those described previously (Itri et al., 2005, 2010; Kudo et al., 2011b). Male and female mice (2-3 months) entrained on a 12:12 LD or DL cycle were anesthetized in an isoflurane chamber at ZT2.5 and ZT12.5 for ZT4-6 (Day) and ZT14-16 (Night) recordings respectively. Anesthetized mice were decapitated, brains extracted, and brains incubated in ice-cold slice solution (chemical composition) for 5 minutes. Coronal slices (300μm) of mid-SCN were collected in slice solution using vibratome, and then incubated for 30 minutes at 32°C followed by 1hr at room temperature in artificial cerebrospinal fluid (ACSF)

while continually being aerated with 95% O_2/5% CO_2. Slices were placed in a recording chamber (PH-1, Warner Instruments, Hamden, CT) attached to the stage of a fixed stage upright DIC microscope (OLYMPUS, Tokyo, Japan), and superfused continuously (2 ml/min) with room temperature ACSF aerated with 95% O_2/5% CO_2.

Whole cell patch clamp SCN recordings were made using electrode micropipettes (3-7MΩ) pulled from glass capillaries (WPI, Sarasota, FL) using a multistage puller (Sutter P-97, Novato, CA). Recording electrodes were filled with standard internal solution (in mM: K-gluconate, 112.5; EGTA, 1; Hepes, 10; MgATP, 5; and $MgCl_2$, 1). Internal solution pH was adjusted to 7.25-7.3 and osmolarity adjusted to 290-300 mOsm. Recordings were obtained with the AXOPATCH 200B amplifier (Molecular Devices, Sunnyvale, CA) and monitored on-line with pCLAMP (Ver 10, Molecular Devices). Each cell was determined to be within vSCN or dSCN by directly visualizing its location with DIC microscopy as being either proximal to the optic chiasm and below the tip of the 3rd ventricle (vSCN), or dorsal to the tip of the 3rd ventricle (dSCN).Cells were approached with slight positive-pressure, maintained until the pipette was lowered to the vicinity of the membrane. By switching to negative-pressure a high-resistance seal (2-10GΩ) was formed, and a second pulse of negative pressure was used to break the membrane. The access resistance of these cells ranged from 15 to 35 MΩ and cell capacitance typically ranged between 6-18pF. A cell's data was not further analyzed if its access resistance values changed significantly (>20%) during the course of the experiment, or if it was not able to decrease firing rate following excitatory treatment. The amplifier voltage-offset was used to cancel the junction potential between the pipette and extracellular solution; however, access resistance compensation was not conducted and therefore we assume error in membrane potential readings. The standard extracellular recording solution was ACSF (chemical composition). Drug treatments were performed by dissolving either gabazine (10μM) or NMDA (25μM; Tocris

Bioscience, Minneapolis, MN) in ACSF and delivered via a rapid gravity feed system into the slice bath during recording.

Spontaneous firing rates (SFR) were recorded with pCLAMP for 1 min. using current-clamp in the whole cell patch configuration. No current was injected during recording. SFR for each cell was determined using the total number of action potentials recorded in the 1 min. time window. SFR for males and females at two time points was determined by averaging data from at least 10 neurons collected from a minimum of 3 animals. Action potential (AP) properties were analyzed using MiniAnalysis (ver 6.0.3, Synaptosoft Inc., Fort Lee, NJ).

Bioluminescence

Methods used for real-time monitoring of bioluminescence of PER2::LUC *ex vivo* tissue explants were similar to those described previously (Loh et al., 2011). Briefly, male and female SCN, pituitary, heart, liver, and adrenal explants were harvested between ZT10 to ZT11 from mice housed in a 12:12 LD cycle. For SCN explants, 300 µm coronal sections were prepared using a vibratome (Dosaka EM, Kyoto, Japan), and the paired mid-SCN (~1mm^2) was then selectively dissected from the rest of coronal slice using 2 cuts from a sterile scalpel. Liver explants (1-2mm^2) were obtained by a single cut from the median lobe using sterile scissors. Halved adrenal explants were obtained by performing a single cut with sterile scalpel. Explants were transferred onto Millicell membranes (0.4um, PICMORG50, Millipore, Bedford, MA) resting on 0.5 mL of recording media that contained freshly added 0.1 mM luciferin (sodium salt monohydrate, Biosynth, Staad, Switzerland). The 35 mm dishes were sealed using autoclaved high-vacuum grease (Dow Corning, Midland, MI). Tissue explants were inserted in the Lumicycle photometer (Actimetrics, Wilmette, IL) no later than ZT12 for bioluminescence monitoring. The explants were monitored at 37°C for 7-10 uninterrupted days. Raw

bioluminescence values were normalized by first subtracting the recorded baseline, then subtracting a running average of 24 hours of this baseline-subtracted bioluminescence, and finally performing a 2-hour smoothing average. Period was calculated from an average of no less than 6 peak-to-peak times. Amplitude was calculated by summing the peak and subsequent trough values. Rate of amplitude damping was calculated from the slope of no less than 6 consecutive amplitudes using the following formula: y = ae^bx, where x indicates the number of days to "damp" for the value of y (amplitude) that is 1/e of the first amplitude, a is the intercept of the exponential regression through amplitude versus time, and b is the x variable coefficient. We report the x value of days to damp as the indicator of damping in our results. Due to using the 24-hour moving average as a normalizing factor, we could not use the first actual recorded peak to determine the phase of the explants, and instead referred to the second recorded peak (or first calculated peak) as the first peak for phase relationships in the results.

AR Immunohistochemistry (IHC)

Brains were collected and processed as described previously. Prior to immunostaining, sections were fixed in 4% paraformaldehyde at room temperature, washed with PBS, and incubated in blocking solution (3% normal goat serum (NGS), 0.1% Triton X-100 in PBS). After blocking, sections were incubated with rabbit polyclonal antibody raised against AR (Santa Cruz Biotechnology, Santa Cruz, CA) diluted to 1:150 in blocking solution at 4°C for 5 days. Sections were then washed and incubated with secondary antibody. Sections were again washed with PBS, cover slipped with Vectashield Mounting Media containing 4'6-Diamindino-2-Phenylindole, Dihydrochloride (DAPI, Vector Laboratories, Burlingame, CA), and stored in the dark at 4°C until imaged. Images from sections were taken to optimize the fluorescence signal to noise in each section.

Statistical analysis

To determine the effects of sex, phenotypic sex, and genotype in behavioral rhythms obtained through wheel running patterning, we applied 2-way ANOVA followed by the Holm-Sidak post hoc test. Paired student *t* tests were used to compare firing rates of SCN neurons under different pharmacological treatments, and unpaired student *t* tests were used to compare firing rates of SCN neurons within sex at the two time points and between sex at the same time point. To determine whether there was a sex difference in response to drug treatment we applied two-way repeated measures ANOVA. Student *t* tests were also used to compare the amplitude (peak to trough ratio) of transcript expression and the parameters of the bioluminescence recordings. All results were reported to be significantly different if $P < 0.05$. All tests were performed using SigmaStat (version 3.5, SYSTAT Software, San Jose, CA). Values are shown as mean ± standard error of the mean (SEM).

Results

Subtle sex difference in diurnal and circadian rhythms of wheel running behavior of WT mice

We compared diurnal and circadian rhythms of wheel-running activity in WT male and female mice (**Fig. 2.1**). Most daily and circadian parameters of behavioral rhythmicity showed no sex differences (**Table 2.1**). Both sexes were behaviorally rhythmic in LD and DD conditions, had similar activity amounts (rev/hr., $P = 0.3$), activity patterning (% activity in light, $P = 0.6$; fragmentation, $P = 0.8$), and period in DD (23.7 ± 0.1 hr., $P = 0.87$). In LD, activity onset was more precise for males (male: 8.3 ± 1.7 min; female: 17.8 ± 3.8 min, $P = 0.006$). In DD, female alpha (or activity duration) was longer (male: 483 ± 32 min; female: 590 ± 34 min). So as not to disturb wheel running behavior, estrous cycle phase was assessed by vaginal smears in a

separate cohort of age-matched females. Most PER2::LUC mice on C57/BL6J background (8/10) had regular 4-day estrous cycle.

No sex differences in diurnal rhythms of WT dSCN and vSCN neuron SFR

SCN controls the timing of rhythms throughout the brain and body via its physiological output, which can be measured by averaging the SFR of individual SCN neurons. WT mouse dSCN SFRs were higher during the mid-morning (ZT4-6) than the early-evening (ZT14-16) in both males ($P = 0.002$) and females ($P = 0.01$); however, males had higher baseline SFRs than females during the daytime (male: 5.7 ± 0.6 Hz; female: 3.4 ± 0.5 Hz; $P = 0.01$). This lower daytime-peak SFR in female dSCN was not due to the effects of circulating gonadal hormones because there was no difference in baseline SFR of female dSCN harvested from animals in proestrus compared to estrus ($n = 5$, $P = 0.4$). This sex difference in daytime SFR was abolished when dSCN neurons were synaptically isolated using the $GABA_A$-R blocker gabazine (**Fig. 2.2**). Under these conditions there was no sex difference in the intrinsic SFRs of male and female mouse dSCN neurons (male: 4.9 ± 0.8 Hz; female: 4.2 ± 0.6 Hz; $P = 0.5$).

Synaptically isolated vSCN neurons were treated with NMDA at ZT4-6 and ZT14-16 to test for photic input pathway gating and sex differences in NMDA responses. Male and female vSCN neurons did not display a significant increase in SFR following NMDA treatment at ZT4-6 (male: $P = 0.06$; female: $P = 0.09$). At ZT14-16, both male and female vSCN neurons did display significant increases in their firing rate following NMDA treatment at ZT14-16 (male: $P = 0.017$; female: $P < 0.001$).

In addition to testing sex differences in SFR, we also looked for diurnal rhythms in AP properties and compared sexes. Male vSCN neurons exhibited synaptically mediated diurnal

rhythms in AP properties. At night, male vSCN APs had a slower rise rate (ZT4-6: 2.76 ± 0.2 ms; ZT14-16: 3.6 ± 0.3 ms) and higher AP threshold relative to baseline (ZT4-6: 6.48 ± 0.7 mV; ZT14-16: 9.89 ± 0.9mV). Both of these differences were abolished in the presence of gabazine, while diurnal rhythms in after-hyperpolarization (AHP) area persisted (ZT4-6: -5253 ± 628 mV·ms; ZT14-16: -8020 ± 1430 mV·ms). Female AP properties did not show diurnal rhythms, yet their vSCN AP AHP areas were larger under all treatment conditions (Female: -4393 ± 630 mV·ms; Male: -2785 ± 270 mV·ms).

Sex differences in PER2 expression in WT periphery

In order to determine whether there are sex differences in the clock-gene transcription/translation feedback loop underlying sex differences in behavior and physiological rhythms, male and female PER2::LUC mouse tissue explants' bioluminescence rhythms were compared (**Fig. 2.3**). In SCN, no sex differences in bioluminescence phase (**Fig. 2.3A**) or amplitude (**Fig. 2.3B**) were detected, but we did observe an increased damping rate for female SCN (female: -0.61 ± 0.05; male: -0.43 ± 0.03; $P = 0.005$) and sex differences in the peak phase and amplitude of some peripheral tissues. Male pituitary and liver bioluminescence peaks were phase advanced compared to female's (**Fig. 2.3A**), while the amplitude of liver and adrenal bioluminescence rhythms was greater in males (**Fig. 2.3C**).

Subtle sex differences in diurnal and circadian wheel running behavioral rhythms of FCG mice

In order to determine whether sex chromosome compliment or gonadal phenotype underlies observed sex differences in wheel running rhythms, we compared the locomoter rhythms of intact (**Fig. 2.4** and **Table 2.2**) and gonadectomized (**Fig. 2.6** and **Table 2.3**) FCG

mice (XX*Sry*, XY$^-$*Sry*, XX, and XY$^-$). Gonadal males and females had similar activity patterning in LD and DD irrespective of XX or XY chromosome compliment (**Table 2.2**). We assessed the expression pattern of AR in SCN, and observed an interaction between gonadal sex and sex chromosome compliment. Gonadal male 4CG mice had greater numbers of AR expressing cells in SCN, and unexpectedly XY- females had greater AR expression than XX females (**Fig. 2.5**). When exposed to CT16 LP, gonadal females displayed greater magnitude phase shifts than gonadal male FCG mice, but we did not detect a sex chromosome dependent difference in gonadal female mice as observed in AR expression. Following GDX, all sex differences in phase shift magnitude were lost (**Fig. 2.7A**), and multiple sex differences in diurnal and circadian wheel running behavior were revealed. Like female WT mice in DD, 4CG mice carrying two X chromosomes (XX and XX*Sry*) had longer alpha (activity duration) than 4CG mice carrying one X and one Y chromosome in DD (XY$^-$and XY$^-$*Sry*; **Fig. 2.7B**). Finally, consistent with previous observations on sex differences in rodent locomotor rhythms we observed that phenotypically male 4CG mice (XX*Sry* and XY$^-$*Sry*) had greater deficits in activity amounts (**Fig. 2.7C**) and rhythm power (**Fig. 2.7D**) than phenotypically female 4CG following GDX.

Discussion

In vivo sex differences in diurnal and circadian rhythms of WT mouse behavior

In LD12:12 conditions, we did not find a sex difference in wheel running activity duration or activity bout numbers. In DD we observed a lengthening of female activity durations. The coupling of two putative oscillators controls activity onsets and offsets (Pittendrigh and Daan, 1976; De La et al., 2000), and since female activity durations are longer than male's in constant conditions, the coupling of these oscillators changes based on photic environment in a sex-

dependent manner. Other studies have observed sex differences in diurnal sleep behavior in the same mouse strain (C57/BL6J) on a LD18:6 photoperiod, when females nap less during their nocturnal active period and spend less time in NREM sleep than male littermates (Paul et al., 2006). Taken together, male activity appears as shorter bouts of high amplitude activity interspersed with naps, with females exhibiting a lower rate of activity over a longer time and fewer active phase naps. Notably, the female WT mouse circadian system drives the same amount of nocturnal activity as in males, but her activity is spread over a longer amount of time. This phenotype may be indicative of a sex difference in the arousal system and/or circadian system output causing a redistribution of behavior *in vivo,* and may indicate that activity amount and bout durations are cooperatively regulated.

In vitro sex differences in SCN and periphery

In vitro there are no sex differences in dSCN firing frequency or AP waveform of synaptically isolated neurons. However, before treatment with the $GABA_A$ blocker gabazine, male dSCN SFR was significantly higher than females. Higher baseline firing rate in males with $GABA_A$-R signaling implicates a synaptically mediated sex difference in physiological output of the SCN neuronal circuit. GABA-excitation is thought to be rare in adulthood, but has been observed in subsets of hypothalamic neurons, including vasopressin expressing magnocellular neurons of the hypothalamus, gonadotropin-releasing hormone neurons, and SCN neurons (Choi et al., 2008; Herbison and Moenter, 2011; Haam et al., 2012). $GABA_A$-R channels are permeable to chloride and depending on the intra- to extra-cellular chloride concentration gradient increases in conductance will hyperpolarize or depolarize membrane potential. Most adult neurons have low intracellular chloride concentrations and inhibitory responses to $GABA_A$-R signaling. However, if they express the sodium potassium chloride co-transporter (NKCC1),

intracellular chloride concentrations are high, and $GABA_A$-R current activation causes membrane depolarization as chloride leaves the cell. Perinatally, gonadally derived androgen provides substrate for neural aromatase-converted estradiol to masculinize brain circuitry via up-regulation of NKCC1 expression to increase the probability of GABA-excitation (Perrot-Sinal et al., 2001; Mccarthy et al., 2002). A similar mechanism may be at play in adult SCN.

No sex differences were observed in the phase or amplitude of the clock gene expression rhythms in SCN, but female SCN had faster damping rates of their bioluminescence rhythms. Thinking of the female SCN as a weaker circuit oscillator with greater risk to circadian system disruptions is consistent with increased prevalence of sleep disruptions reported in women. Weaker oscillators are more easily phase shifted (Abraham et al., 2010), and like her damping WT female SCN counterpart, gonadal female 4CG mice have greater phase shifts in response to LP than gonadal males. Herzog proposes the hypothesis that VIP excitation synchronizes neurons in the SCN, while GABA inhibition desynchronizes them (Freeman and Herzog, n.d.). There is anatomical evidence that some male mammal's SCN have larger VIP cell populations (Zhou et al., 1995), and therefore potentially a greater ability at synchronizing its cellular oscillators through the excitatory effects of VIP signaling. Based on the subtleties of sex differences in GABA signaling in the SCN observed in this work, it may also be that synaptic excitation synchronizes and synaptic inhibition desynchronizes. GABA signaling could function both as a synchronizer and desynchronizer in the SCN circuit based on the sex of the animal, time of day, and age.

Nevertheless, there was no difference in the initial phase or amplitude of the molecular clock indicating there is no sex difference in the timing of entraining output from the SCN. *In vitro* male pituitary and liver were phase advanced suggesting that either there is a sex

difference in the peripheral clockwork of these organs or a sex difference in the mechanism whereby these peripheral tissues respond to entraining output from the SCN.

Light-input pathway

RHT glutamatergic synaptic signaling selectively stimulates increases in neuronal activity, intracellular signaling cascades, and gene transcription that lead to phase shifts of SCN physiological output and circadian control of behavior at night. In LD conditions, male activity onset was more precise, while in DD there was no sex difference. This indicates that the precision of activity onset is uniquely regulated by the light-input pathway in males. Sex differences in vSCN AP waveforms provide clues for membrane currents that may underlie subtle differences in light entrainment. Female vSCN have a larger daytime AHP area than in males. An additional intrinsic current or ionic buffering property that lengthens potassium channel inactivation kinetics in female vSCN neurons may increase AHP area to limit daytime excitability. Male vSCN APs have a higher threshold to initiation relative to baseline inter-spike membrane potential at night that is eliminated by the $GABA_AR$ blocker gabazine. Work in progress will provide important insights on whether intrinsic membrane properties, such as resting membrane potential, are affected by GABA and VIP signaling in male vSCN. Work in other brain regions has shown estrogen can regulate neural excitability and synaptic transmission (Spencer et al., 2008; Kelly and Qiu, 2010).

Beyond the behavioral evidence of sex differences in the light-entrainment pathway, there is also a known anatomical sex difference. Male vSCN expresses four-times the number of AR^+ neurons (Iwahana et al., 2008; Karatsoreos et al., 2011b), and AR signaling has been postulated to play a role in regulating phase shifts in response to light via its activation on mitogen-activated protein kinase (MAPK/ERK) signaling and/or via NMDA-R-mediated

responses to glutamate secreted by retinal afferents (Albers et al., 1981; Schull et al., 1989; Davis et al., 2012; Blattner and Mahoney, 2013). We were unable to detect a sex difference in SFR response to NMDA-R activation in vSCN neurons. In males and females, daytime NMDA treatment produces no net response in average SFR, while nighttime NMDA treatment increases vSCN firing rates to the same degree in both sexes. At night, both male and female vSCN neuronal APs exhibit a faster rise in response to NMDA treatment, indicative of a potentiated NMDA response. Since we were unable to detect sex differences in NMDA response, the role of AR in the light-input pathway is probably downstream to the acute NMDA response of vSCN neurons. Similar to previous studies reporting sex differences in WT AR expression in the SCN (Iwahana et al., 2008), we observed that 4CG gonadal males had about four times the AR expression than XX females. Surprisingly, gonadal female mice with XY^- chromosome compliment have nearly double the amount of AR expression than XX females. XY^- females breed only in early life (Arnold and Chen, 2009), suggesting their fertility and estrous cycling is not on par with their XX littermates, and their circulating ovarian hormones may be reduced. Notably, AR expression does not change depending on estrous cycle phase or following GDX in females (Iwahana et al., 2008), indicating that circulating ovarian hormones do not alter AR expression in the mouse SCN. Therefore even though XY^- females likely have altered ovarian hormone levels, this is likely not affecting AR expression, and our results are consistent with the idea that sex chromosome compliment regulates AR expression in the 4CG mouse SCN.

It has previously been shown that AR expression is associated with the precision of activity onset in WT mice (Karatsoreos et al., 2007). Precise activity onsets indicate the SCN is tightly phase locked to its environmental LD cycle, which may be mediated by stronger coupling and higher amplitude of SCN cellular oscillators. To test this hypothesis, we compared the magnitude of 4CG mouse phase shifts in response to a CT16 light-pulse. Gonadal males were

found to have smaller phase shifts compared to gonadal female 4CG mice. Since a more weakly coupled oscillator is easier to phase shift (Abraham et al., 2010), the greater phase shifts observed in female 4CG mice are consistent with the idea that female SCN oscillators have weaker coupling. This observation is also consistent with the faster damping rate observed in female SCN bioluminescence rhythms. Notably, we were unable to detect differences in phase shift magnitude comparing XY^- and XX female mice, which have different levels of AR expression. This indicates that either increased XY^- female AR expression is insufficient to regulate oscillator coupling as observed in gonadal male 4CG mice who have significantly more AR expression, and/or there is insufficient androgen signaling through ARs in XY^- females to affect SCN coupling.

Sex differences in gonadal hormone regulation of locomotor behavior

Sex differences in phase shift magnitude in 4CG mice are abolished following GDX, providing further evidence that circulating gonadal hormones regulate the light-input pathway. We also observed gonadal hormones in 4CG mice function to converge sex differences in activity duration. Following GDX, XX and XX*Sry* mice display sex-chromosome dependent lengthening of activity duration, and reveal both genes and hormonal environment regulate daily and circadian phenotype. In the 4CG mouse model bout length is regulated by sex chromosome compliment rather than circulating hormones. Coupling strength between putative morning and evening oscillators controls activity duration (Pittendrigh and Daan, 1976), and weaker coupling in XY animals may shorten alpha, while stronger coupling in XX animals might lengthen alpha. The prevalence of sleep disorders increases following menopause, and based on our present results, female genetics may be regulating increased activity durations and delayed sleep onsets.

Sex differences in the role of gonadal hormones on daily and circadian activity levels have previously been shown. Following GDX, there is a dramatic reorganization and drop in male mouse activity, but there is only a mild effect on female locomotor rhythms (Iwahana et al., 2008). Using the 4CG mouse model, we were able to show that sex chromosome compliment does not contribute to this gonadal sex difference.

Conclusion

Major circadian parameters in wheel running rhythms like period and activity amount are similar in males and females. Neural activity within the SCN is thought to directly reflect the daily and circadian patterning of wheel-running activity and we found that firing rates showed no sex difference in synaptically isolated SCN neurons. The phase and amplitude of the underlying molecular clockwork as assessed by PER2 expression in the SCN are also similar. Subtle sexually divergent behavioral patterning phenotypes such as more precise male activity onset and longer female alpha may therefore reflect divergent neural circuit properties of the SCN. An important question to consider is whether these differences justify the exclusion of females from experimental designs in the future. Over the past 5 years, circadian research using mouse models has predominantly been conducted using only males (60%), and female mice were reportedly included in less than 20% of primary research articles. Due to the subtle nature of the sex differences we observed in young adult mouse behavioral rhythms, we conclude female mice are well suited for inclusion in biological rhythms research, and considering the increased prevalence of sleep disturbance in women, believe there is a strong practical argument for the increased utilization of female mice in translational circadian and sleep studies.

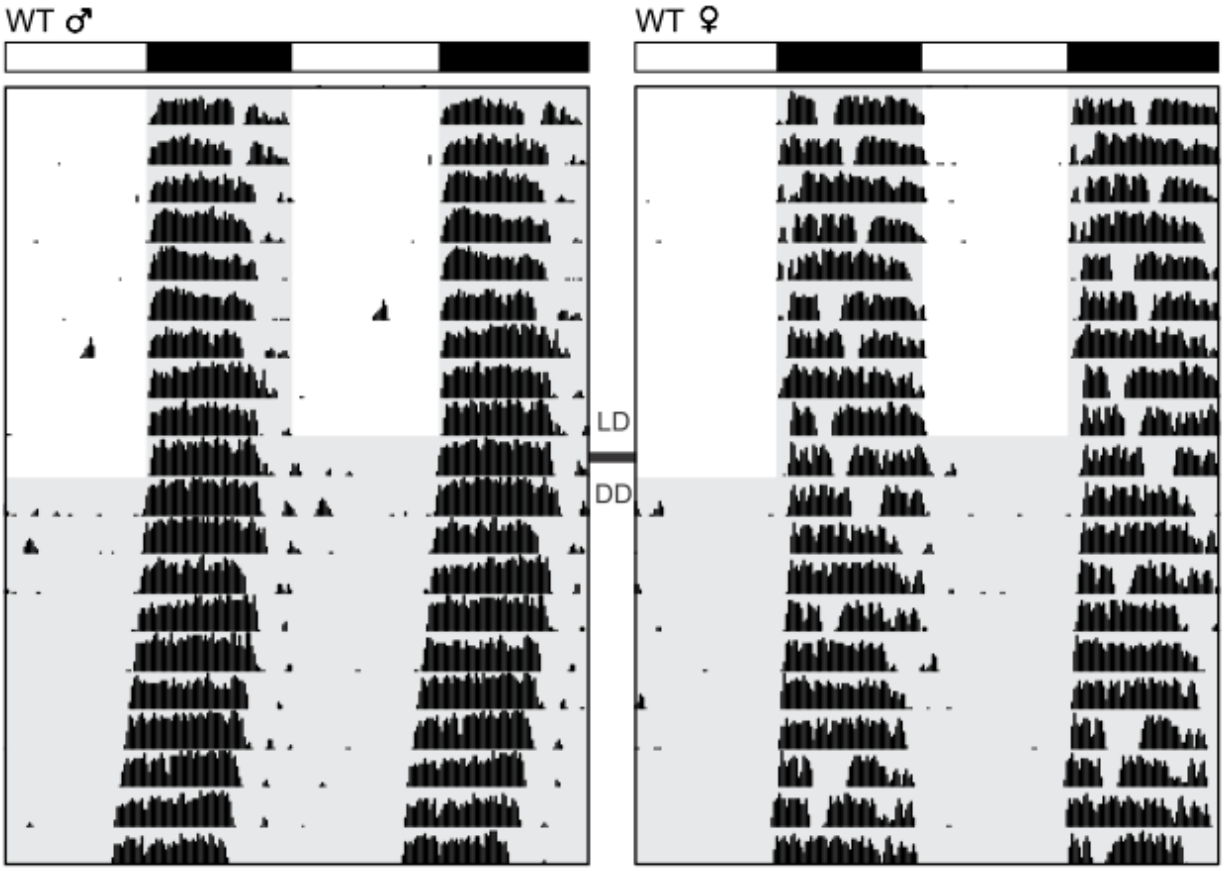

Figure. 2.1: Sex differences in WT mouse wheel running activity rhythms. Representative example of a male (left) and female (right) actogram in 12:12 LD cycle (day 1-10) and constant darkness (day 11-20). Male mice have more precise activity onset in LD than females. Female mice have longer activity duration in DD than males.

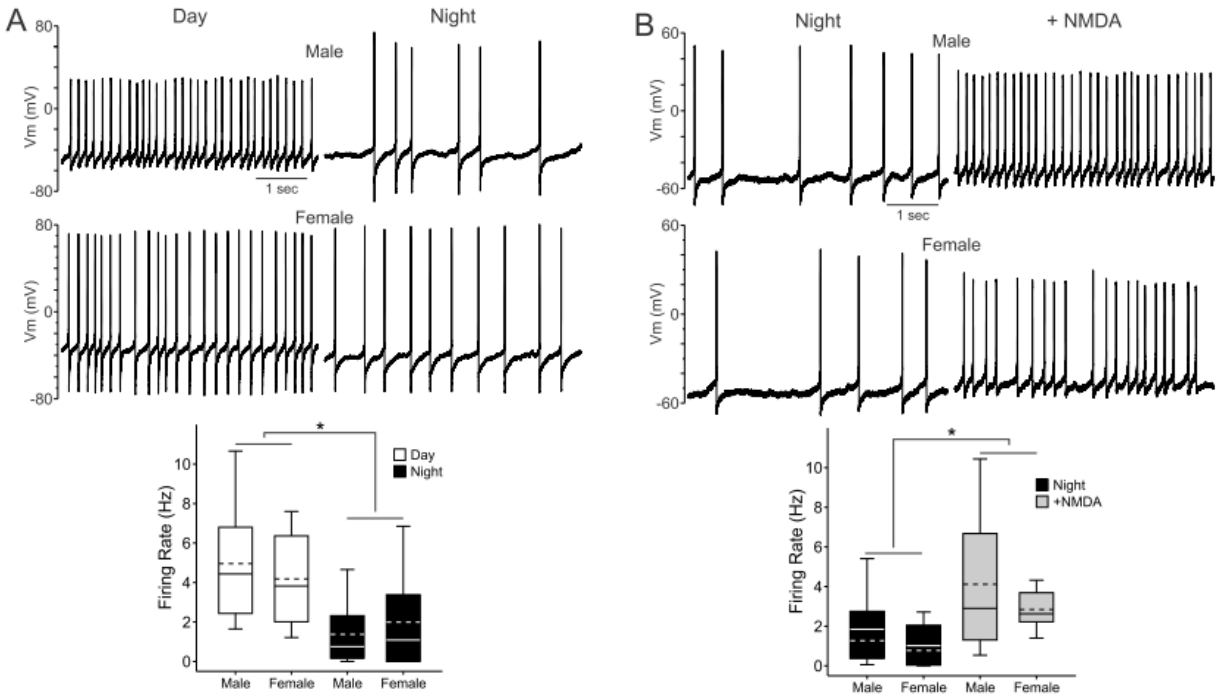

Figure 2.2: No sex differences in SCN firing rate. **(A)** Top, example traces. Bottom, box plots of firing rates. Daytime (ZT4-6) firing rates are higher than nighttime (ZT14-16) firing rates in males ($P < 0.003$) and females ($P < 0.05$). There is no significant difference between male and female firing rates in the presence of gabazine at either time point ($P = 0.9$). **(B)** No sex difference in early evening NMDA response in vSCN. Male and female vSCN neurons show a significant increase in firing rate following NMDA treatment at ZT14-16 (Male, $P = 0.02$; Female, $P < 0.001$). The range of firing rates following NMDA treatment is greater in male SCN neurons, however there is no statistically significant interaction between sex and NMDA response ($P = 0.6$). Dashed lines indicate mean.

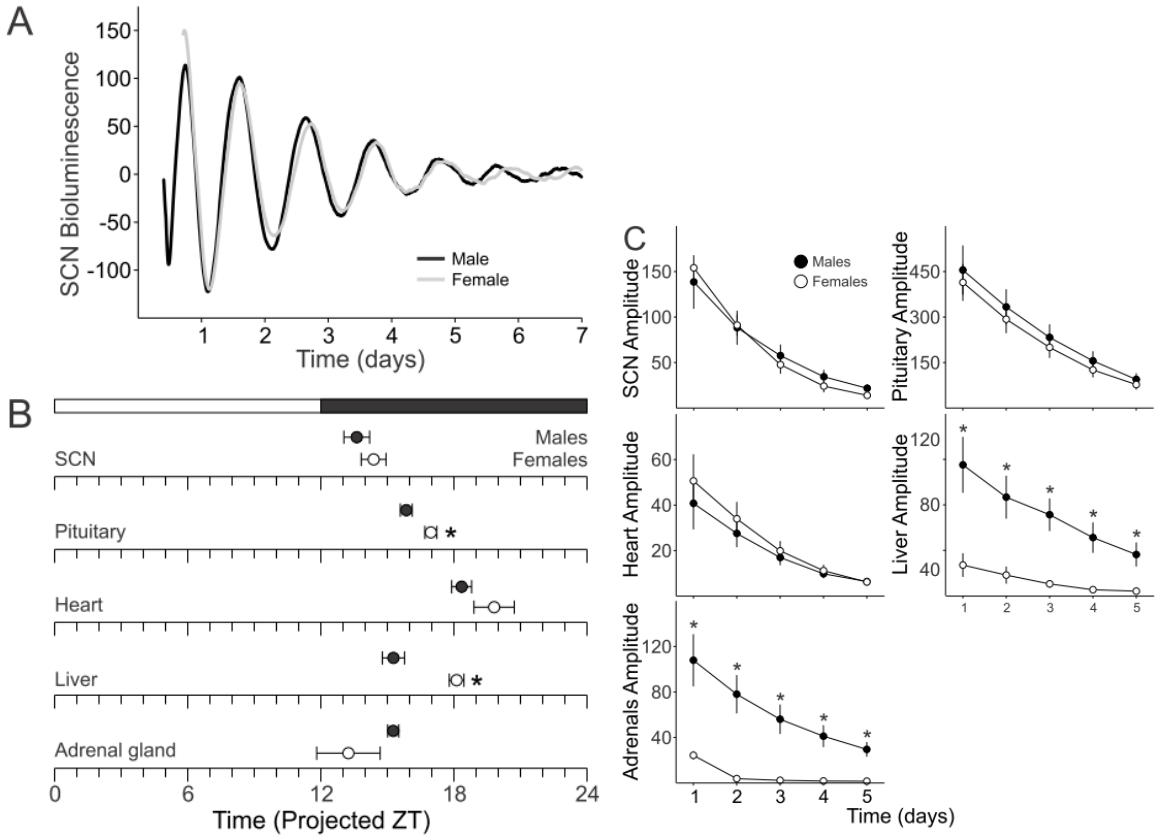

Figure 2.3: Sex differences in bioluminescence rhythms of central and peripheral oscillators. No sex difference in bioluminescence phase or amplitude in SCN **(A** and **B)**. Peak phase of pituitary and liver rhythms are phase delayed in females relative to males **(B)**. Amplitude of liver and adrenal bioluminescence rhythms is higher in males than females **(C)**.

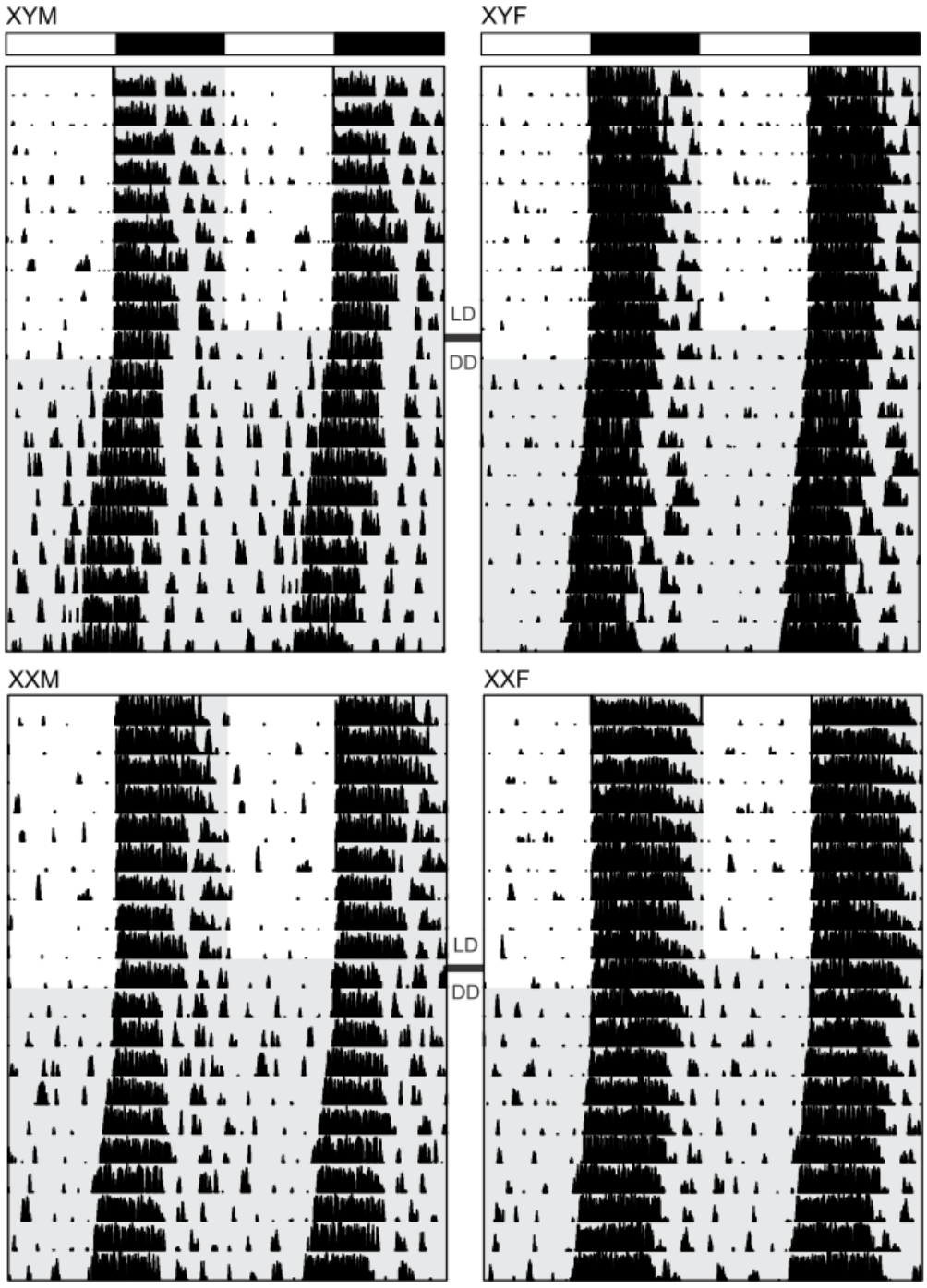

Figure 2.4: FCG wheel running activity rhythms. Left column: XY^{-}*Sry* (M; top) and XX*Sry* (M; bottom). Right column: XY^{-} (F; top) and XX (F; bottom). Gonadal males (left column) and females (right column) have similar activity patterning irrespective of XX or XY chromosome compliment.

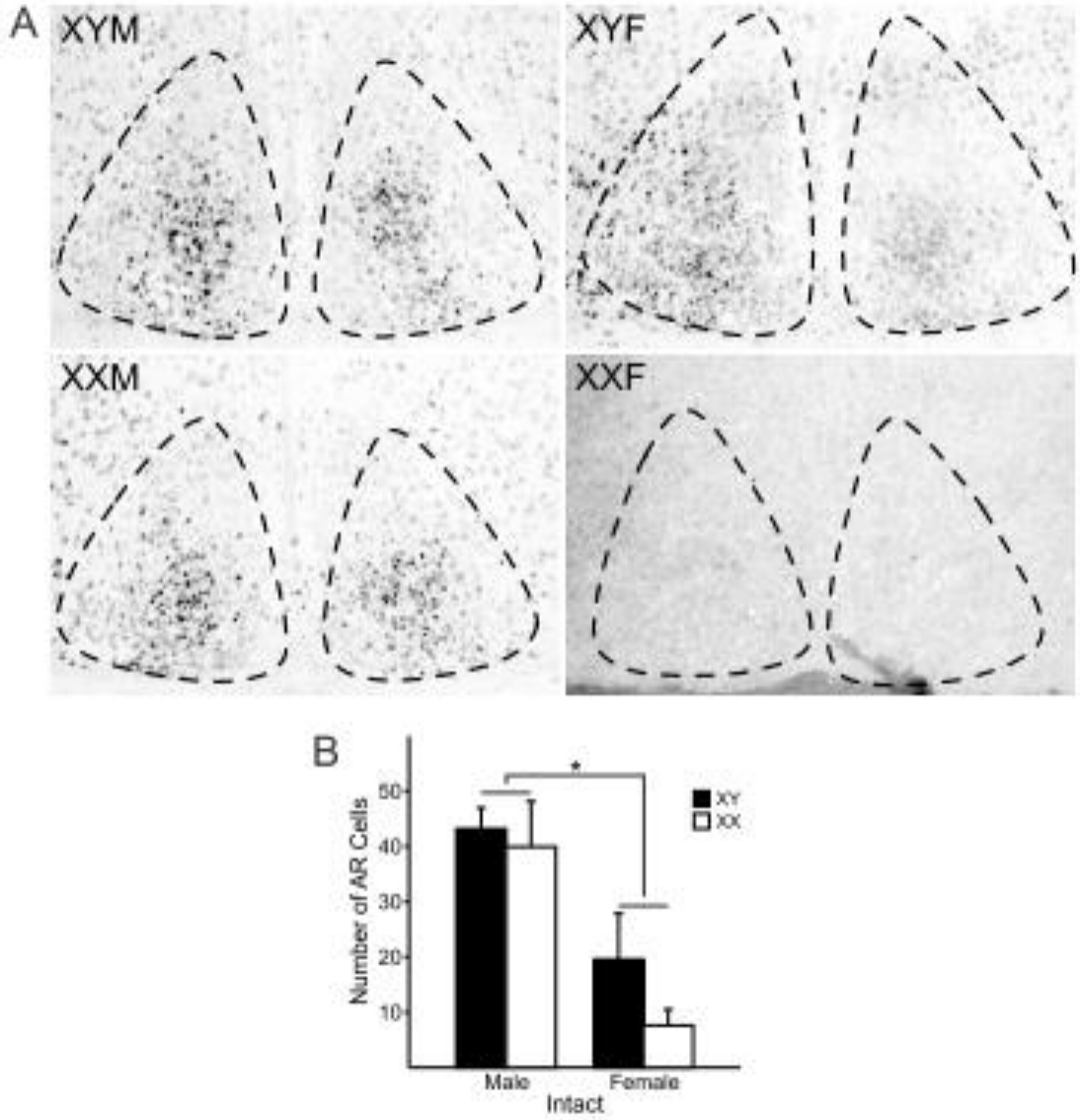

Figure 2.5: AR expression in 4CG mice. **(A)** XX*Sry*, **(B)** XY^{-}*Sry*, **(C)** XX, **(D)** XY^{-}. Gonadal male 4CG mouse SCN (top row) expresses more AR^{+} cells than SCN from gonadal female 4CG mice (bottom row). Gonadal female 4CG mice with XY chromosome compliment have more AR+ cells than gonadally female mice with XX chromosome compliment.

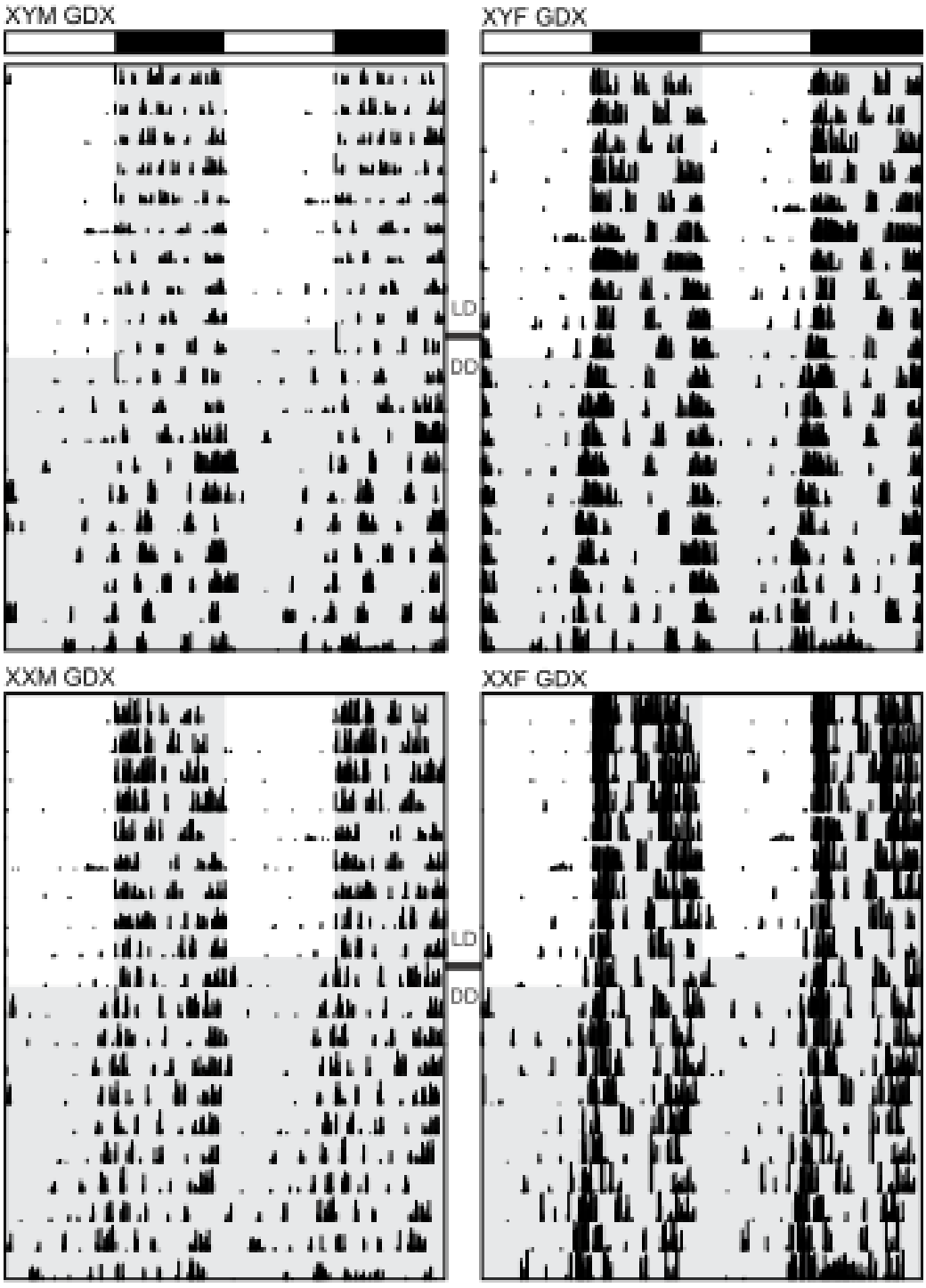

Figure 2.6: GDX FCG wheel running activity rhythms. Left column: XY$^-$Sry (M; top) and XXSry (M; bottom). Right column: XY$^-$ (F; top) and XX (F; bottom). Following GDX, gonadal male 4CG mice (left column) have a greater decrease in activity levels than gonadal female 4CG mice (right column). In DD, 4CG mice with XX chromosome compliment have longer activity duration than those with XY chromosome compliment.

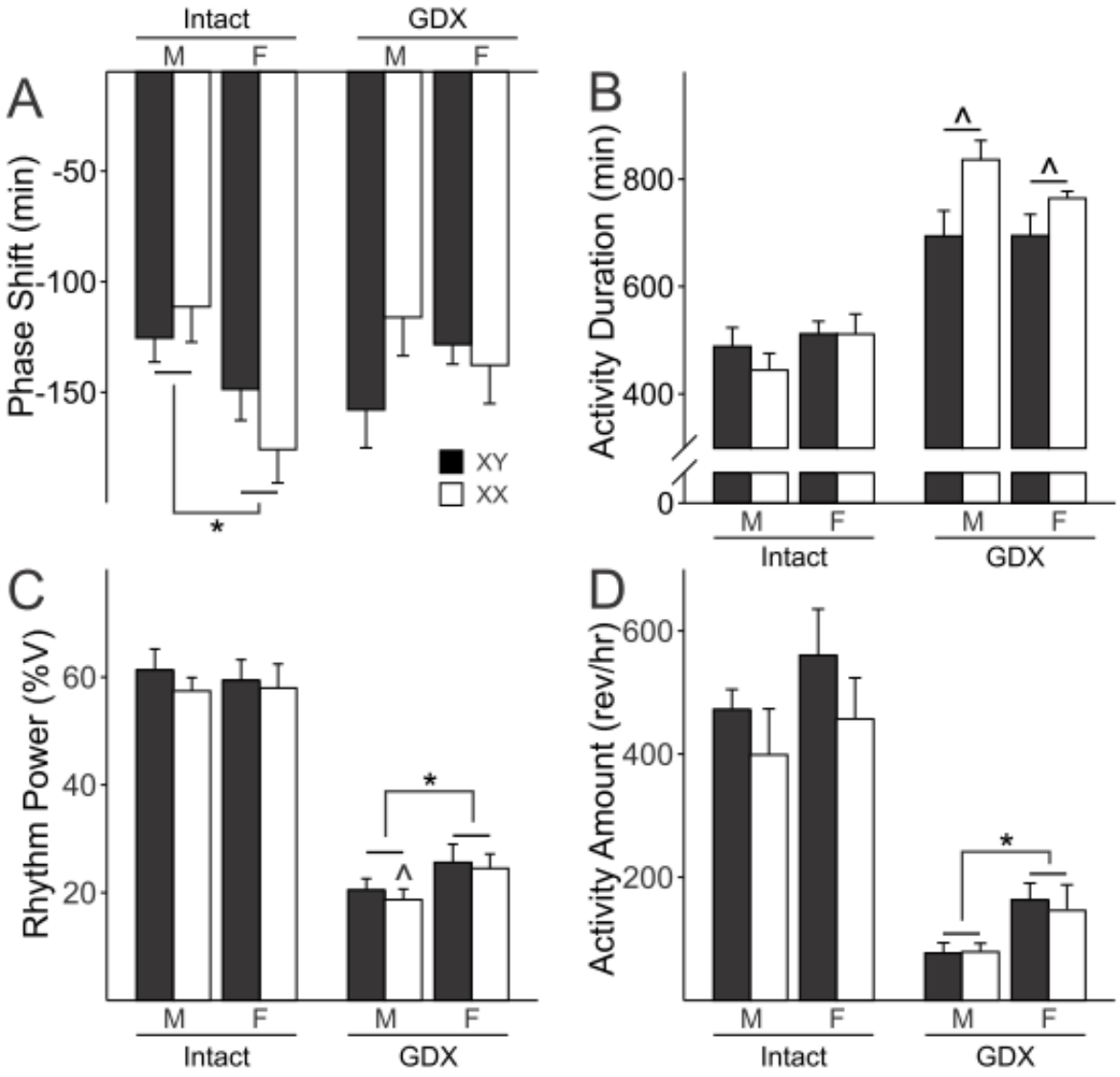

Figure 2.7: Genetic and hormonal influence on wheel running activity rhythms of 4CG mice. Before GDX, phenotypic female mice respond to CT16 LP with greater phase shifts than male mice. Following GDX there is no difference in phase shift **(A)**. XX chromosome compliment confers longer activity duration than XY chromosome compliment **(B)**. Phenotypic male mice have lower total activity than phenotypic female mice **(C)**. Phenotypic male 4CG mice have greater deficits in wheel running rhythm power than phenotypic female 4CG mice. Power of wheel running activity rhythms has a greater decrease in XX phenotypic male mice than XY phenotypic male mice **(D)**.

		Males	Females
LD	% V	60.2 ± 3.4	54.4 ± 4.3
	rev/hr	383.4 ± 33.3	331 ± 25.2
	% Activity in Light	4.2 ± 0.8	4.0 ± 0.8
	Alpha (min)	560 ± 37.6	648 ± 37.3
	Precision (min)	8.3 ± 1.7	17.8 ± 3.8**
	Fragmentation (bouts/day)	4.6 ± 0.5	5.1 ± 0.3
	Phase Angle (min)	-6.5 ± 2.4	-8.8 ± 3.7
DD	Period (hr)	23.7 ± 0.1	23.7 ± 0.1
	% V	49.5 ± 4.9	44.9 ± 4.2
	Activity rev/hr	335 ± 37.1	321 ± 32.1
	Alpha (min)	483 ± 32	590 ± 33.8*
	Precision (min)	17.3 ± 3.7	37 ± 11.1
	Fragmentation (bouts/day)	6.5 ± 0.7	6.3 ± 0.5
	LD-DD Phase Angle (min)	-29.5 ± 5.0	-21.7 ± 5.8

* gonadal sex $p < 0.05$
** gonadal sex $p < 0.01$

Table 2.1: Sex differences in wheel running activity rhythms of WT mice. Most circadian parameters are not sexually dimorphic. Male mice have more precise activity onset in LD ($P < 0.05$). Female mice have longer alpha in DD ($P < 0.05$).

		Gonads Intact			
		XYM	XXM	XYF	XXF
LD	% V	55.1 ± 6.5	60 ± 2.7	54.6 ± 6.6	46.8 ± 6.2
	rev/hr	352.5 ± 55.5	437.3 ± 48.2	525.1 ± 86.2	412.4 ± 93.8
	% Activity in Light	10.3 ± 4.2	4.8 ± 0.4	6.9 ± 1.8	13.9 ± 6.3
	Alpha (min)	428.8 ± 25.6	512 ± 42.3	503.5 ± 24.9	544.7 ± 34.9
	Precision (min)	13.4 ± 1.2	9.6 ± 1.2	12 ± 1.9	12.6 ± 1.3
	Fragmentation (bouts/day)	5.1 ± 0.5	5 ± 0.6	6 ± 0.6	19.6 ± 3.3
	Phase Angle (min)	2.1 ± 2.4	4.4 ± 2.4	6.3 ± 1.8	6.3 ± 1.9
DD	Period (hr)	23.6 ± 0.04	23.8 ± 0.04	23.67 ± 0.08	23.6 ± 0.04
	% V	61.4 ± 3.9	57.5 ± 2.5	59.5 ± 3.8	58.1 ± 4.5
	Activity rev/hr	474 ± 32.3	400 ± 74.7	561 ± 74.9	458 ± 66.9
	Alpha (min)	490 ± 34.8	446 ± 31.1	513 ± 23.2	513 ± 37.2
	Precision (min)	14.8 ± 1.9	11.2 ± 1.5	13.1 ± 3.4	14.9 ± 1.8
	Fragmentation (bouts/day)	6.4 ± 0.4	6.4 ± 0.5	5.8 ± 0.5	5.9 ± 0.4
	LD-DD Phase Angle (min)	-22.9 ± 2.1	-16.6 ± 5.8	-30.4 ± 11.5	-13.6 ± 12.3
	Phase Shift (min)	-126 ± 10.9	-112 ± 16	-149 ± 14.1**	-176 ± 15.1**

* gonadal sex $p < 0.05$

** gonadal sex $p < 0.01$

Table 2.2: No sex differences in 4CG running wheel activity rhythms.

		GDX			
		XYM	XXM	XYF	XXF
LD	% V	24.8 ± 2.5	29.5 ± 3.1	36.6 ± 6.3*	34.5 ± 4.1*
	rev/hr	84.3 ± 12.7	117.4 ± 24.7	166.9 ± 34.5*	174.3 ± 47.7*
	% Activity in Light	7.7 ± 0.8	8.0 ± 2.4	6.8 ± 3.8	5.6 ± 1.8
	Alpha (min)	711.5 ± 8.3	638 ± 39.5	639.5 ± 54.1	727.2 ± 28.8
	Precision (min)	25.3 ± 5.8	29.4 ± 14.5	17.1 ± 5.7	86.4 ± 77.7
	Fragmentation (bouts/day)	6.6 ± 0.4	15.1 ± 9.6	4.8 ± 0.8	20.4 ± 1.4
	Phase Angle (min)	2.1 ± 5.1	1.5 ± 2.0	2.6 ± 3.6	23.1 ± 21.9
DD	Period (hr)	23.9 ± 0.06	24.1 ± 0.1	23.9 ± 0.06	23.9 ± 0.1
	% V	20.6 ± 2.1	18.8 ± 1.9	25.7 ± 3.4*	24.6 ± 2.6*
	Activity rev/hr	77.8 ± 16.7	79.7 ± 14.0	164.0 ± 27.3	147.0 ± 41.7
	Alpha (min)	695.2 ± 47.1	837 ± 35.8^^	696.3 ± 39.2	766 ± 13.0^^
	Precision (min)	80.5 ± 23.9	52.8 ± 13.9	27.6 ± 4.2**	25.3 ± 4.0**
	Fragmentation (bouts/day)	6.9 ± 0.8	8.2 ± 0.6	7.3 ± 0.5	7.6 ± 0.3
	LD-DD Phase Angle (min)	16.2 ± 20.2	67.3 ± 61.0	73.6 ± 61.9	55.3 ± 62.0
	Phase Shift (min)	-158 ± 17.2	-117 ± 17.4	-129 ± 8.9	-135 ± 17.4

^^ chromosome $p < 0.01$ * gonadal sex $p < 0.05$

** gonadal sex $p < 0.01$

Table 2.3: Chromosomal and gonadal sex differences revealed in 4CG running wheel activity rhythms following GDX.

Part II. The role of VIP in rhythmic physiology

Chapter 3: VIP and SCN physiology

Light is the most powerful environmental cue to which circadian rhythms synchronize (Czeisler et al., 1981; Khalsa et al., 2003). Photic cues are detected by specialized intrinsically photosensitive retinal ganglion cells (ipRGCs) containing the photopigment melanopsin (Lucas et al., 2012). The axons of ipRGCs form the RHT which terminates on the ventral aspect of the SCN (Morin and Allen, 2006). RHT terminals release glutamate, and under certain conditions, the neuropeptide PACAP (Hannibal et al., 2008) with the result of photic stimulation being the increase in firing rate of SCN neurons (Shibata et al., 1984; Meijer et al., 1998). For SCN neurons, NMDA receptor activation and resulting increases in intracellular calcium (Ca^{2+}) (Colwell, 2001; Irwin and Allen, 2007) play a special role in mediating the effects of RHT activity. The influx of Ca^{2+} in retinally-innervated SCN neurons triggers a number of signal transduction pathways that promote the transcription of a set of genes through cyclic AMP-responsive element (CRE)-binding protein (CREB) phosphorylation, which include the clock gene *Per1* (Travnickova-Bendova et al., 2002; Yan and Silver, 2004) and the immediate early gene cFOS (Kornhauser et al., 1996). These molecular light-evoked changes in gene expression are thought to be necessary to cause light-induced phase shifts in physiology and behavior (Albrecht, 2012).

Although the detailed mechanism by which the SCN circuit operates remains unknown, a major role for VIP in photic resetting is indicated by multiple experimental observations. Behaviorally, VIP-deficient mice show clear deficits in their circadian light response (Colwell et al., 2003) and our hypothesis was that the light-evoked changes in SCN physiology would also be compromised. In the present study, we first examined the SCN response to light *in vivo* using MUA recordings of freely-moving VIP KO mice and littermate wild-type (WT) controls. We then measured NMDA-evoked responses in ventral SCN neurons of both genotypes using a brain slice preparation. Next, Fura2 calcium imaging techniques were used to measure the

calcium transients evoked by electrical stimulation of the RHT *in vitro*. Finally, digoxigenin *in situ* hybridization (ISH) was used to follow the light-induction of *Per1* message over time and within sub-regions in the SCN for both genotypes. Light induction of cFOS in the SCN was also examined with immunohistochemical (IHC) techniques.

Materials and Methods

Animals and Housing

Experimental protocols used in this study were approved by the University of California, Los Angeles or Leiden University Animal Research Committee. Recommendations for animal use and welfare, as dictated by the UCLA Division of Laboratory Animals and guidelines from the National Institutes of Health were followed. Adult male (1.5 to 5 months of age) WT C57Bl/6 mice and mice lacking the gene encoding for the neuropeptide VIP (VIP KO) (Colwell et al., 2003) were obtained from a breeding facility at the University of California, Los Angeles or from the breeding facility at Leiden University. Mice were group housed until they were used for experiments. A total of 102 C57Bl/6 mice were used with half being VIP KOs.

In vivo SCN recordings

Mice were implanted with a tripolar stainless steel micro electrode (Plastics One, Roanoke, VA USA) using a stereotaxic instrument (Stoelting, Wood Dale, IL, USA) as previously described (Lucassen et al., 2012; Van Diepen et al., 2013). Two polyimide-insulated and twisted electrodes were aimed at the SCN and a third uncoated electrode was placed in the cortex as a reference. Mice were anaesthetized using a mix of ketamine (100mg/kg), xylaxine (20mg/kg) and atropine (1mg/kg). The electrodes were implanted under a 5˚ angle at the same rostrocaudal level as bregma 0.61 mm lateral to midline and 5.38 mm ventral to the dura mater.

The electrode was fixed to the skull using three screws and dental cement. After a week of recovery animals were placed in a custom designed recording chamber to measure SCN electrical activity and behavioral activity simultaneously using passive infrared sensors. Animals were connected to the recording system using a counterbalanced swivel system in which they were able to freely move. The electrical signal was amplified and bandwidth filtered (0.5-5kHz). Window discriminators were used to convert action potentials into digital pulses that were counted in two second epochs. Physiological responses were used to confirm electrode placement within the light-responsive part of the SCN.

Animals were recorded over at least two days in continuous darkness. After those two days the animals were exposed to 5 minutes of light (fluorescent light source; 150 µW/cm2) at CT 14-16 (2-7 pulses). The animals received multiple 5-minute pulses within the same day at this phase. The circadian time of the light response was calculated per day on the basis of the onset of behavioral activity recorded by a passive infrared sensor in the recording chamber. For quantification of the response, the increases in SCN electrical activity were compared to baseline levels. Baseline levels were defined as 50 seconds before lights on, and the level of sustained light-induced increase was defined as the average firing rate during lights on (>5 seconds after light onset). At the end of each recording, animals were sacrificed and brain tissue was collected for histological verification of the electrode location. After brain fixation in a 4% paraformaldehyde solution containing ferrocyanide, brains were sectioned coronally and stained with cresyl violet. The position of the electrode was determined by microscopic inspection. Electrodes outside the SCN were excluded from analysis.

Whole cell patch clamp electrophysiology

Mid-SCN coronal slices were collected with a vibratome in slice solution (in mM: 26 $NaHCO_3$, 1.25 NaH_2PO_4, 10 glucose, 125 NaCl, 3 KCl, 5 $MgCl_2$, 1 $CaCl_2$) at ZT 11.5 from

PER2::Luciferase (P2L) mice and VIP KO x P2L littermates between one-and-a-half and three months of age housed in reverse LD 12:12. Slices were attached to the stage of a fixed-stage upright DIC microscope (Olympus, Tokyo, Japan), and superfused continuously with aerated (95% O_2/5%CO_2) artificial cerebrospinal fluid (ACSF in mM: $NaHCO_3$, 26; NaH_2PO_4, 1.25; glucose, 10; NaCl, 125; KCl, 3; $MgCl_2$, 2; $CaCl_2$, 2). Recording electrodes (4-8MΩ) were pulled from glass capillaries (WPI, Sarasota, FL) on a multistage puller (Sutter P97, Novato, CA, USA) and filled with standard internal solution (in mM: K-gluconate, 112.5; EGTA, 1; Hepes, 10; MgATP, 5; GTP, 1; leupeptin, 0.1; phosphocreatine, 10; NaCl, 4; KCl, 17.5; $CaCl_2$, 0.5; and $MgCl_2$, 1). Recordings were obtained using the AXOPATCH 200B amplifier (Molecular Devices, Sunnyvale, CA, USA) and monitored on-line with pCLAMP (Ver. 10, Molecular Devices). Each cell was visualized to be within the SCN by means of DIC microscopy. Ventral cells were identified as being adjacent to or in close proximity with the optic chiasm. Dorsal cells were identified as being dorsal to the tip of the third ventricle within the mid-SCN slice. After forming a high resistance seal (>1 GΩ) in voltage clamp configuration, a second pulse of negative pressure was used to break the membrane. Most cells had a capacitance between 6 and 15pF, and cells with access resistance higher than 60 MΩ or holding currents larger than -30 pA (at V_{Hold}= -70 mV) were excluded from additional analysis. Junction potential between the pipette and extracellular solution was cancelled by voltage offset of the amplifier before establishing a seal. All solutions' pH was adjusted to 7.25-7.3 and osmolarity adjusted to 290-310 mOsm.

Spontaneous firing rates (SFR) were recorded between ZT4-6 for daytime recording and ZT14-17 for nighttime recordings using current-clamp mode in whole cell patch clamp configuration. After entering whole cell mode in voltage clamp and switching to current clamp mode, neuronal firing was allowed 3-5 minutes to stabilize. Baseline SFR was then calculated using the number of action potentials detected over the subsequent 60 sec. Gabazine (10 μM) was then applied for 3-4 minutes, followed by NMDA (25μM) for 2-3 minutes, and SFR was

calculated using the number of action potentials detected during the subsequent minute of gabazine and/or NMDA treatment. Following NMDA treatment, ACSF was used to wash slices and determine whether cells were able to re-hyperpolarize following pharmacological excitation to insure only healthy cells were included in analysis. All baseline vSCN neuron recordings were made in presence of the $GABA_A$ receptor blocker gabazine to isolate NMDA responses (10μM; Tocris, Minneapolis, MN, USA). Chemicals were purchased from Sigma-Aldrich (St. Louis, MO, USA) unless otherwise noted.

Resting Membrane Properties

Previous studies have shown that Per1::GFP SCN neurons show daily rhythms in multiple resting membrane properties (Kuhlman and McMahon, 2004). A similar protocol was used to examine the intrinsic excitability of SCN neurons in this study, but without the use of a fluorescent marker of gene expression to guide neuron selection. Resting membrane properties of dSCN neurons were examined during the daytime and nighttime in slices treated for at least two minutes with TTX (1 μM; Tocris Bioscience, Minneapolis, MN) and gabazine (10 μM; Tocris Bioscience) to block action potential and GABAergic synaptic potentials. Multiple neuronal recordings were attempted per slice, so between recordings, drugs were washed off for 2-5 minutes, or long enough to partially unblock voltage gated sodium and GABA channels. The partial restoration of action potentials allowed discrimination between neurons, or electrically active cells, and glia, non-electrically active cells, both of which are found in the SCN. After forming a high resistance seal, going whole-cell, and obtaining membrane parameters for the selected neuron, the amplifier was switched from voltage-clamp to current-clamp mode. Cells typically reached a stable membrane potential within the first 10 seconds of the switch. Resting membrane potential was then recorded over the subsequent one to three minute period and

calculated as the average membrane potential during that time. Neurons were then treated with increasingly hyperpolarizing current steps (500 msec, -5 to -25 pA in 5 pA steps). Each neuron was treated three times. Membrane voltage response traces were filtered for electrical interference before analysis (harmonics 1:1, 119 cycles to average, auto-reference frequency). For each replication, peak hyperpolarization (using 5 smoothing points) was examined for each current injection step, then averaged. For all other parameters, the average trace of the three replications was used to identify hyperpolarization peak time, area, and slope of the response between 10 and 90% of its value. Cells which weren't able to maintain steady membrane potential between current injection treatments were excluded from analysis. Two-Way ANOVA was used to identify effects of time and genotype on resting membrane potential and input resistance ($P < 0.05$). Three-Way ANOVA was used to identify effects of time, genotype, and magnitude of negative current injection on neuronal voltage responses ($P < 0.05$). When significant effects were detected, post-hoc multiple pairwise comparisons using the Holm-Sidak method were used to identify statistically significant group differences ($P < 0.05$).

In vitro Ca^{2+} imaging

Brain slices containing the SCN were collected as described above from animals 6-10 weeks of age and loaded with the ratiometric Ca^{2+} indicator dye fura-2-acetoxymethyl ester (Fura-2-AM, Teflabs, Austin, TX, USA) as previously described (Michel et al., 2013). The slices were prepared at ZT 11 and the recordings made between ZT 15 - 17. A monochromator (Polychrome V, TILL Photonics, Gräfeling, Germany) was used to deliver paired 50 ms light pulses of two excitation wavelengths (340 and 380 nM). Emitted light (505 nM) was detected by a cooled CCD camera (Sensicam, TILL Photonics), and images were acquired at two second intervals (0.5 Hz). Single-wavelength images were background subtracted, and ratio images (340/380) generated. Cells were defined as ventral or dorsal based on proximity to the optic chiasm or third ventricle

respectively, and the mean ratio values for these region-of-interest-defined cells were used to calculate intracellular Ca^{2+} concentration. Experiments were conducted using imaging software TILLvisION (TILL Photonics).

For electrical stimulation of the RHT, a concentric bipolar electrode (125 µm/Rnd/ 25 µm Pt-Ir, purchased from FHC, Bowdoin, ME, USA) connected to a Grass S88 Stimulator (Warwick, RI, USA) was placed in the center of the optic chiasm of a coronal hypothalamic slice . The stimulation strength was adjusted to elicit clear Ca^{2+} transient with a fast recovery to baseline levels. The cells were stimulated at 10 Hz for one second with pulse duration of 200 µs. This train of stimuli was repeated three times with a 60 second pause between stimulations.

Data were collected and analyzed using Tillvision, Igor Pro (Wavemetrics, Portland, OR), Excel (Microsoft, Redmond, WA), and SPSS 20 (IBM, Armonk, NY). First, baseline Ca^{2+} concentration were examined using mean and SD of signal 14 seconds before each peak in every cell. Cells with a baseline intracellular Ca^{2+} concentration $[Ca^{2+}]_i$ larger than 600 nM were excluded from the data set. Values that were greater than two SDs from the mean were identified as outliers by the SPSS software and excluded from the analysis.

Digoxigenin ISH

A plasmid (pCRII; Invitrogen, Carlsbad, CA, USA) containing the cDNA for Per1 (340–761 nucleotides, accession number AF022992) was generously provided by Dr. D. Weaver (University of Massachusetts), and insert identity was confirmed by sequencing using the M13R primer. To generate antisense and sense templates for hybridization, plasmids were linearized overnight, phenol-chloroform extracted, ethanol precipitated and re-suspended in diethyl pyrocarbonate (DEPC)-treated water.

Digoxigenin-labeled riboprobes were generated from 1µg of template cDNA in a reaction mixture containing 2µl of 10X concentrated digoxigenin (DIG) RNA Labeling Mix (Roche Applied Science Indianapolis, IN, USA), 2µl of 10X concentrated Transcription Buffer (Roche Applied Science, Indianapolis, IN, USA), 40U Rnase Block (Stratagene, La Jolla, CA, USA), and 2µl of the appropriate RNA transcriptase (SP6, or T7; Roche Applied Science, Indianapolis, IN, USA) for two hours at 37°C. The *in vitro* transcription reaction was terminated by the addition of 2µl of 0.2 M EDTA and precipitated with 2.5µl of 4 M LiCl and 100% ethanol overnight at -20°C. The precipitate was extracted with 70% ethanol and reconstituted in 100µl of sterile water. Probe yield estimates were determined by comparison to known concentrations of untranscribed linearized plasmid in gel electrophoresis and also from serial dilutions of cross-linked riboprobe spotted to nitrocellulose membranes, bound to alkaline phosphatase-conjugated anti-DIG antibody (Roche Applied Science, Indianapolis, IN, USA), and visualized with 4-Nitro blue tetrazolium (NBT) and 5-Bromo-4-chloro-3-indolyl phosphate (BCIP) (Roche Applied Science, Indianapolis, IN, USA).

Prior to brain collection, wheel running activity was measured as described previously (Loh et al., 2013). Male VIP-deficient mice were housed in cages containing running wheels (Mini Mitter Co., Bend, OR) from 6-7 weeks of age and their wheel-running activity recorded as revolutions (rev) per three minute intervals. Animals were exposed to a 12:12hr light-dark cycle (LD; light intensity 350 lux) for 10 days, and then released to 24hrs of constant darkness (DD) to assess their free-running activity pattern for 7-10 days. Animals were exposed to light (10 min, light intensity ≈ 50 lux) at circadian time (CT) 16 based on wheel running activity records (CT 12 was defined as activity onset) and sacrificed after either 30, 60, 90, or 120 minutes under anesthesia (n = 3 to 5 in each condition). Control animals were culled at the same time without a light pulse. Brains were removed, flash-frozen, sectioned at 20µm and slide mounted, then stored at -80°C until used for ISH or immunofluorescence.

On the first day of hybridization, slides were warmed to room temperature and fixed in 4% paraformaldehyde. Following brief washes in PBS, slides were placed in prehybridization buffer (50% formamide, 5X SSC, 1% SDS, 0.2% Tween-20, 0.1% heparin, and 50 ng/mL Torula RNA) at 60°C for one to two hours. Sections were then hybridized overnight at 60°C in hybridization buffer (50% formamide, 5X SSC, 1% SDS, 0.2% Tween-20, 0.1% heparin, and 50 ng/mL Torula RNA), and ≈ 50-100 pg/μL of riboprobe) in sealed slide mailers. Following hybridization, slides were washed briefly in 5X SSC, and then for one hour in 0.2X SSC at 60°C to remove unbound probe. Slides were then briefly washed with maleic acid buffer (0.1M maleic acid, 0.15M NaCl) and blocked in 20% heat-treated sheep serum in maleic acid buffer. After blocking, slides were incubated with 1:500 anti-DIG antibody conjugated to alkaline phosphatase (Roche Applied Science, Indianapolis, IN, USA) in a humid chamber at 4°C overnight. After antibody incubation, slides were washed in maleic acid buffer and then in Tris buffer (0.1 M Tris (pH 9.5), 0.1 M NaCl, and 5 mM MgCl2). For revelation, slides were incubated in a color reaction solution (Tris buffer, 0.3375% NBT, 0.35% BCIP, 1mM levimasole) at room temperature overnight in a humid chamber. After revelation, slides were washed with PBS and color was preserved via a final incubation in 4% paraformaldehyde containing EDTA. Slides were then cover-slipped and imaged on a Zeiss microscope using Axiovision software (Carl Zeiss Inc., Thornwood, NY). Sense probe hybridization showed no positive staining.

For quantification, SCN sections were imaged and SCN borders were determined by 4',6- Diamidino-2-Phenylindole, Dihydrochloride (DAPI) and arginine vasopressin (AVP) distribution dorsal to the optic chiasm in the anterior hypothalamus. For each SCN, a template was created to define core and shell subregions delineated by AVP expression. This delineation was confirmed by additional double immunostaining against AR to confirm that a lack of AVP signal coincided with the SCN core. Templates from adjacent sections were superimposed onto

both Per1+ and c-FOS+ sections and the resulting mid-SCN image (unilateral) for each animal was counted by an experimenter blind to condition.

Immunohistochemistry

Brains were processed as described above, and alternate sections were used to delineate SCN subregions chemo-architecturally. Sections were fixed in 4% paraformaldehyde at room temperature, washed with PBS, and incubated in blocking solution (3% normal goat serum (NGS), 0.1% Triton X-100 in PBS). After blocking, sections were incubated with a guinea pig polyclonal antibody raised against arginine-vasopressin (AVP, 1:000; Bachem, Torrance, CA), a rabbit polyclonal antibody raised against cFOS (1:30,000; Merck Millipore, Darmstadt, Germany), or a rabbit polyclonal antibody raised against androgen receptor (AR; 1:150; Santa Cruz Biotechnology, Santa Cruz, CA) in blocking solution at 4ºC for 4 days. Sections were then washed and incubated with Alexa Fluor® 568-conjugated goat anti-guinea pig IgG antisera (Molecular Probes, Eugene, OR), diluted to 1:300 with blocking solution at room temperature. If tissue was processed for double immunostaining, primary antibody incubation was carried out with both the primary AVP antibody and a rabbit polyclonal antibody raised against androgen receptor (Santa Cruz Biotechnology, Santa Cruz, CA) diluted at 1:150. Also, during the secondary antibody incubation, Alexo Fluor® 488-conjugated secondary antisera (Molecular Probes, Eugene, OR), diluted at 1:200, was additionally used. After incubation with secondary antibody, sections were again washed with PBS, cover slipped with Vectashield Mounting Media containing DAPI (Vector Laboratories, Burlingame, CA), and stored in the dark at 4ºC until imaged.

Statistical measurements

The data sets were analyzed for equal variance and normal distribution to help select the appropriate statistical test. Significance for electrophysiological recordings and Ca^{2+} imaging was assessed using Two-Way Analysis of Variance (ANOVA), with genotype and light or NMDA exposure as factors. Post-Hoc Paired Student's *t*-tests were used to detect significant changes due to pharmacological treatment and Unpaired Student's *t*-tests were used to assess differences in spontaneous electrical activity due to genotype. Effects were reported to be significant if $P < 0.05$. For ISH, the data sets were analyzed by Two-Way ANOVA, with genotype and light exposure as factors. If significant group differences were detected ($P < 0.05$) by ANOVA, then the Holm–Sidak method for pair-wise multiple comparisons was used. For all tests, values were considered significantly different if $P < 0.05$. All tests were performed using SigmaStat software (version 3.5, Systat Software, San Jose, CA, USA). Values are shown as mean ± SEM.

Results

In vivo electrophysiology finds no deficits in light evoked responses in SCN of VIP mutants

Using *in vivo* extracellular recording techniques, SCN electrical activity was measured in both VIP KO (n=7) and WT controls (n=5). Physiological responses were used to confirm that the electrode was placed in a light-response region of the SCN and histological analysis confirmed that each of these recordings was made in the SCN. Successful recordings showed high SCN electrical activity during the day and low electrical activity during the night. Light exposure induced an increase in the SCN electrical discharge pattern with a transient overshoot at lights on and a sustained elevation in SCN electrical activity throughout light exposure (**Fig. 3.1A**). No differences in light response characteristics were detected between VIP KO and WT

mice (KO: 12 ± 2 % change; WT: 16 ± 6 %; *t*-test: $P > 0.05$; **Fig. 3.1B**). Both genotypes showed a significant increase in SCN electrical activity upon light exposure during the night (CT 14-16) (**Fig. 3.1C**). As analyzed by two-way ANOVA, there was not a significant difference between genotypes in baseline (P = 0.5) or in the light-response (P = 0.7). These results demonstrate that photic information is reaching the retinorecipient cells in the SCN in the VIP KO mice.

In vitro electrophysiology demonstrates reduced activity and robust NMDA-evoked changes in vSCN neurons

A variety of evidence suggests that the effects of light on the mammalian circadian system are mediated by glutamatergic mechanisms and that the NMDA receptor plays an important role in this regulation. Using the whole cell patch-clamp recording technique in current clamp mode, we measured the SFR responses of vSCN neurons in a brain slice preparation to bath application of NMDA (25μM, 3min). Each of these cells was determined to be within the vSCN by directly visualizing the location of the cell as being immediately adjacent to or in close proximity with the optic chiasm using infrared DIC video microscopy. Two-way ANOVA identified main effects of NMDA treatment ($P = 0.006$) and genotype ($P = 0.003$), but no interaction effect of genotype and treatment ($P = 0.3$). WT mouse vSCN neurons responded to bath application of NMDA with an increase in SFR (**Fig. 3.2,** $P < 0.001$). The VIP KO also showed a significant response to NMDA treatment ($P = 0.02$), but there were differences between the genotypes. First, the absolute SFR was reduced in mutant SCN compared to WT in both baseline (WT: 1.76 ± 0.4 Hz vs. VIP KO: 0.48 ± 0.2 Hz, $P = 0.03$) and NMDA treatment conditions (WT: 4.11 ± 1.0 Hz vs. VIP KO: 1.44 ± 0.4 Hz, $P = 0.04$). Consistently, inter-spike membrane potential was hyperpolarized in VIP KO neurons (-5.4 ± 1.6 mV, $P = 0.025$). Second, whereas all WT neurons (16/16) responded to NMDA treatment with increased firing rates, only

9 out of 13 mutant neurons did (Fisher's Exact Test, $P < 0.001$). In all but one of the VIP KO neurons that responded to NMDA treatment with no change or decreased firing rate, membrane potential did however depolarize. Thus, in the vSCN region, while the absolute levels of neural activity were reduced in VIP deficient mice, NMDA still evoked a significant change in firing of these neurons although the excitatory effects were less uniform than in WT.

RHT-stimulation-induced Ca^{2+} transients are normal in vSCN but deficient in dSCN in VIP KO mice

Release of glutamate from RHT terminals in the SCN after electrical stimulation will lead to an increase in $[Ca^{2+}]_i$ (Irwin and Allen, 2007) and ultimately, phase shifts of the circadian system. Optical imaging techniques and the fura2-AM indicator dye were used to measure RHT-stimulated Ca^{2+} transients in SCN cells in the night. RHT stimulation produced a reliable increase in $[Ca^{2+}]_i$ in a subset of SCN neurons of ventral (WT: 40%; KO: 38%) and dorsal (WT: 20%; KO: 19%) SCN cell populations. In vSCN, the magnitude of the RHT-evoked Ca^{2+} transient was enhanced in the VIP-deficient mice (**Fig. 3.3A**). In the dSCN, there was a 30% reduction in the amplitude of RHT-evoked Ca^{2+} increases (**Fig. 3.3B**). The baseline in Ca^{2+} levels measured during the night were low and did not vary between the genotypes (**Fig. 3.3C**). Two-way ANOVA revealed effects of genotype ($P = 0.02$), RHT-stimulation ($P = 0.001$), and an interaction of genotype x RHT stimulation ($P = 0.01$) on the Ca^{2+} transients. Thus, as measured by Ca^{2+} transients, the vSCN cell population appears to be receiving the signal from the RHT, but in the absence of VIP, dSCN cells exhibit a weakened response.

The loss of VIP alters the temporal and spatial distribution of light-evoked increases in Period1 expression in the SCN.

To establish how light-induced *Per1* expression varies between the genotypes, *in situ* hybridization using digoxigenin probe for *Per1* was performed on SCN tissue at 30, 60, 120 min after light exposure at CT 16 (50 lux, 10 min). SCN photomicrographs illustrate that WT and VIP deficient mice differ in their spatio-temporal expression profiles of *Per1* (**Fig. 3.4, 3.5**). As previously reported (Yan and Silver, 2004), WT SCN *Per1* is photically induced in two separate waves -- one in the core followed by one in the shell. The majority of immediate light-induced *Per1* expression occurs during the first wave in the SCN core. This is followed by a second wave in the shell, which is characterized by a steady increase of *Per1* from 30 to 90 min. In VIP KO mice, the two waves of *Per1* induction follow a different pattern. Although a sizable induction of *Per1* is seen 30 min. after initial light exposure in the SCN core, this first wave of *Per1* induction dissipated at least one hour earlier in the VIP KO. Additionally, the second wave of *Per1* induction in the SCN shell was markedly attenuated in VIP KO mice. In fact, shell *Per1* levels were similar to untreated mutant controls, although more animal to animal variation was observed than in WT controls. Two-way ANOVA revealed effects of genotype ($P = 0.01$), light treatment ($P = 0.001$) and interaction of genotype x light treatment ($P = 0.01$) on light-induced *Per1* expression levels in the mouse SCN.

We also examined the light induction of cFOS in the core and shell SCN (**Fig. 3.6**). Compared to untreated controls, WT SCN exhibited significant cFOS induction when measured 60 and 120 min. after light exposure (50 lux, 10 min.) in both the core and shell regions. In contrast, the VIP KO mice only exhibited a significant cFOS induction when measured 60 min after light exposure in the core SCN. At 120 min., the cFOS counts were back to baseline levels in the core, and never increased in the shell region. Two-way ANOVA revealed effects of

genotype (P = 0.001), light treatment (P = 0.001) and interaction of genotype x light treatment (P = 0.001) on light-induced cFOS expression levels in the mouse SCN. Thus in the VIP KO mice, the light-induction of cFOS and *Per1* are attenuated in duration and most significantly impacted in the shell region of the SCN.

The loss of VIP alters spontaneous firing rate rhythms of dorsal SCN neurons in vitro

Considering the deficits observed in RHT-induced calcium transients and gene induction for the dorsal region of VIP KO mouse SCN, we also examined these neurons for changes in rhythmic electrical output. First, spontaneous firing rates (SFR) and inter-spike membrane potentials (ISMP) were examined under baseline conditions and following synaptic isolation using the $GABA_A$-R blocker gabazine. Three-Way ANOVA was used to test for effects of genotype, time, and gabazine treatment on SFR and ISMP, and when significant effects were detected, post-hoc Holm-Sidak pairwise multiple comparison procedure was used to identify significant genotypic and time-related group differences, and Paired TTESTs were used to identify significant effects of gabazine treatment. A significant interaction between genotype and time was found for SFR (P < 0.001) and ISMP (P = 0.02). Under baseline conditions (**Fig. 3.7**), WT SFR was significantly higher during the daytime than at night (Day, 5.15 ± 0.42 Hz.; Night, 1.70 ± 0.47 Hz., P < 0.001), but VIP KO SFR did not vary between the day and night (Day, 2.82 ± 0.41 Hz.; Night, 3.37 ± 0.41 Hz.; P = 0.34). Gabazine treatment (**Fig. 3.8**) significantly reduced SFR of WT neurons during the day (-0.69 ± 0.28 Hz; Paired TTEST, P = 0.027), but not at night (-1.01 ± 0.67 Hz.; Paired TTEST, P = 0.17), and WT SFR was still significantly higher during the daytime than at night in the absence of synaptic signaling (Day 4.96 ± 0.67 Hz., Night 1.37 ± 0.83 Hz.; P < 0.001). For VIP KO dSCN neurons, gabazine did not have a significant effect on SFR during the daytime (-0.33 ± 0.58 Hz, Paired TTEST, P = 0.96),

but at night it had an excitatory effect (+0.85 ± 0.37 Hz; Paired TTEST, *P* = 0.04), so that VIP KO SFR was significantly lower during the day than at night (Day 2.16 ± 0.75 Hz., Night 4.55 ± 0.72 Hz.; *P* = 0.007). Additionally, VIP KO SFR was significantly lower than WT during the daytime (-3.16 ± 0.5 Hz.; *P* < 0.001) and significantly higher than WT at night (+2.28 ± 0.5 Hz.; *P* = 0.004).

No effect of time of genotype was found for ISMP under baseline conditions (WT: Day -44.3 ± 1.77 mV, Night -45.7 ± 2.1 mV; VIP KO: Day -48.8 ± 2.0 mV, Night -45.3 ± 1.4 mV; Genotype, *P* = 0.28; Time, *P* = 0.59; Interaction, *P* = 0.22), but in gabazine VIP KO neuron ISMP was significantly lower during the daytime than at night (Day, -48.4 ± 2.1 mV; Night -41.3 ± 2.0 mV; *P* = 0.01), and during the daytime it was significantly hyperpolarized compared to WT neuron ISMP (-4.37 ± 1.0 mV, *P* = 0.03), while WT ISMP was not rhythmic (Day -44.1 ± 1.8 mV, Night -47.2 ± 2.1 mV; P = 0.27).

We also examined resting membrane properties to determine whether the antiphase rhythms in dSCN SFR and ISMP we detected in the presence of gabazine were regulated by alterations in the intrinsic excitability of VIP KO neurons (**Fig. 3.9**). Two-Way ANOVA was used to detect effects of genotype and time on resting membrane potential (**Fig. 3.9C**), and post-hoc multiple pairwise comparison testing using the Holm-Sidak method was used to identify significant group difference. WT neurons show depolarizing resting membrane potentials during the daytime and hyperpolarized potentials at night (Day: -47.2 ± 3.4 mV, Night: -55.2 ± 4.2 mV, T = 2.6, *P* = 0.01), but this rhythm was lost in VIP KO neurons (Day: -51.6 ± 5.5 mV, Night: -50.0 ± 5.3 mV, T = 0.5, *P* = 0.6). Three-Way ANOVA was used to detect effects of genotype, time, and magnitude of negative current injection on peak membrane potential responses, and although there was a trend toward larger deflections during the day (+4.7 ± 5.0 mV, $F_{1,366}$ = 3.4, *P* = 0.07), significant day/night differences in voltage responses were not detected for either WT

or VIP KO neurons (**Fig. 3.9A** and **3.9B**). The lack of a rhythmic voltage response to negative current injection is inconsistent with a previous report (Kuhlman and McMahon, 2004), and raises the possibility voltage responses are too variable across SCN neurons to detect rhythms without GFP fluorescent markers of clock gene expression to guide neuron selection as were previously used.

Discussion

VIP is an important component of the mechanism by which the circadian system entrains to photic environmental rhythms. Experimental manipulations of VIP have similar effects to light on behavior and physiology. When VIP alone (Piggins et al., 1995) or in combination with other peptides (Albers et al., 1991) is microinjected into hamster SCN, it causes a similar phase shift in behavioral rhythms as would light. Additionally, application of VIP onto brain slices containing the SCN, causes the induction of clock gene expression (Nielsen et al., 2002) and phase shifts circadian vasopressin release and neural activity rhythms (Watanabe et al., 2000; Reed et al., 2001). Behaviorally, the loss of VIP signaling alters the synchronization of the circadian system with environmental rhythms. A normally entrained animal will start its activity from a phase predicted from the prior LD cycle. For a WT mouse this is typically 30 minutes before the time of lights-off in the prior LD cycle, but for VIP and VIPR2 KO mice it is 8 to 10 hours before (Harmar et al., 2002; Colwell et al., 2003; Aton et al., 2005; Brown and Piggins, 2007; Hughes and Piggins, 2008; Ciarleglio et al., 2009). Also, VIP KO mice are unable to entrain to a skeleton photoperiod (one or two light exposures per 24 hour cycle), do not respond to short light exposures with phase shifts of their locomotor activity rhythm (Colwell et al., 2003), and do not show behavioral and physiological adaptations to short or long photoperiods (Lucassen et al., 2012). These data indicate VIP is required for normal light-induced synchronization of the circadian system.

To determine where in the SCN circuit VIP acts to mediate photic phase shifts, we first tested whether loss of VIP impaired retinorecipient neurons' responses to light-input. Previous studies have shown that light-responsive SCN neurons recorded *in vivo* from WT mice increase their electrical impulse frequency following retinal illumination (Meijer et al., 1998; Nakamura et al., 2004; Drouyer et al., 2007; Brown et al., 2011; Van Diepen et al., 2013), and here we found VIP KO mice light-responsive SCN neurons exhibit robust light-responses indistinguishable from those of WT mice (**Fig. 3.1**). Prior work has established the RHT mostly innervates neurons in the vSCN (Ibata et al., 1989; Morin and Allen, 2006; Kiss et al., 2008), and we assume that the greatest percentage of the light-responsive units we recorded *in vivo* were also located in the vSCN where VIP is expressed. Given the severe behavioral deficits in the photic responsivity of VIP KO mouse behavior (Colwell et al., 2003), these results were unexpected, as they indicate retinal illumination is reaching the SCN of the mutant mice and is able to excite neurons there without difficulty.

NMDA receptors play a critical role in transducing glutamatergic excitation from the RHT into an photic phase resetting electrical response within the SCN (Colwell et al., 1990; Ding et al., 1997; Colwell, 2001; Pennartz et al., 2001; Wang et al., 2008). Therefore, we next directly measured NMDA-evoked changes in vSCN firing rate at the single-cell level using a brain slice preparation. One caveat here is that in order to isolate the NMDA responses, we blocked GABA mediated synaptic transmission which could influence the findings. Focusing on neurons in the retino-recipient vSCN, we found that VIP KO and WT mice exhibited clear NMDA-evoked changes in firing rate (**Fig. 3.2**). This observation fits with the extracellular recording described above. Additionally, the single cell resolution of the whole cell patch clamp recordings offers a more nuanced view of the impact of the loss of VIP on neural excitability. The absolute level of SCN activity and inter-spike membrane potential was significantly reduced in the absence of VIP and a smaller percentage of neurons exhibited NMDA-evoked increases in firing rate --

genotypic changes that would be very difficult to detect using the extracellular recording technique described above. Even though there were some genotypic differences, VIP KO mice still exhibit a clear NMDA response.

After NMDA receptor activation, the next step in the signaling cascade mediating photic phase shifts of SCN neurons is an increase in intracellular Ca^{2+} mediated both by glutamate receptor activation and depolarization driven activation of voltage sensitive Ca^{2+} channels (Kim et al., 2005; Irwin and Allen, 2007; Colwell, 2011). Using optical imaging techniques and the fura2-AM indicator dye we found that RHT-stimulated Ca^{2+} transients of SCN cells at night, we found that the percentage of cells responding to RHT stimulation did not vary between the genotypes, but the magnitude of responses in ventral and dorsal cell populations varied significantly. In vSCN, the RHT-stimulation-evoked Ca^{2+} transients were actually enhanced in the VIP-deficient mice compared to WT (**Fig. 3A**), while in the dSCN, there was a 30% reduction in the amplitude of RHT-stimulation-evoked Ca^{2+} transients (**Fig. 3B**). VIP KO vSCN neurons were less active than WT neurons, which may underlie their enhanced responsiveness to RHT-stimulation, while in the dSCN neurons were more active than WT neurons, which may underlie their reduced responsiveness to additional excitation induced by RHT-stimulation. After blocking GABA signaling, VIP KO dSCN rhythms are antiphase, and specifically at night they are firing faster and their inter-spike membrane potentials are depolarized compared to WT neurons (**Fig. 3.8**). Altered VIP KO dSCN rhythm phasing to photic environmental rhythms likely accounts for the 8 to 10 hour difference in activity onsets VIP KO animals exhibit relative to WT mice when released from LD into DD. Taken together, these findings raise the possibility that loss of VIP alters the phase of rhythmic SCN properties, which may in and of itself effect the spread of photic information from the ventral to the dorsal regions within the SCN circuit, and fits with recent observations suggesting VIP and its receptor (VIPR2) are necessary for circuit-level integration within the SCN (Pauls et al., 2014).

To further test this model we used anatomical techniques to track time-dependent spread of photic input information within the SCN. Increased intracellular Ca^{2+} activates a number of signaling pathways that converge to alter transcriptional and/or translational regulators. One such action of Ca^{2+} is the phosphorylation of CREB. Phosphorylated CREB translocates into the nucleus where it can bind to CREs in the promoter regions of *c-Fos* and Period1 (*Per1*) to drive their transcription over the course of hours (Kornhauser et al., 1996; Shearman et al., 1997; Shigeyoshi et al., 1997; Gau et al., 2002; Travnickova-Bendova et al., 2002). We previously found that the photic induction of *Per1* in the SCN was reduced in VIP KO mice 60 minutes after light exposure (Dragich et al., 2010). In our final set of experiments, we examined light-evoked changes in *Per1* and cFOS in the SCN of the VIP KO mice with greater spatial and temporal resolution. For each SCN, a template was created to define core and shell regions, as delineated by the expression of AVP (shell) and androgen receptor (core). As previously reported (Hamada et al., 2004; Yan and Silver, 2004; Koch et al., 2009), we found photic induction of WT SCN *Per1* transcription occurs in two separate waves: a large first wave in the core, followed by a second smaller wave in the shell during which *Per1* steadily increases from 30 to 90 min (**Fig. 3.4, 3.5**). Light-induced *Per1* expression in VIP KO SCN showed a strikingly different pattern. Consistent with the acute physiological responses, light exposure induced a sizeable first wave of *Per1* expression in the core SCN of VIP KO mice; however, the first wave of *Per1* induction dissipated faster in VIP KO mice and the second wave of *Per1* induction in the SCN shell was markedly attenuated. As far as we know, this pattern of gene expression has only been reported once before, in mice heterozygous for a mutation in the NaV1.1 channel (*Scn1a* $^{+/-}$) that show normal light induction of *c-Fos* and *Per1* mRNA in vSCN, and impaired induction in dSCN (Han et al., 2012). Antiphase SFR rhythms in VIP KO dSCN may contribute to the rapid dissipation of *Per1* signal in SCN, if enhanced GABA release from fast firing dSCN neurons (**Fig. 3.7** and **3.8**) were inhibiting vSCN neurons via their reciprocal

connections. However, we detected reduced vSCN neural activity even in the absence of GABA signaling. Notably, neural excitability is reduced in both *Scn1a* $^{+/-}$ and the vSCN of VIP KO mice, indicating that even if it is possible to acutely excite vSCN neurons, absolute levels of neural activity are likely important in the regulating photic responsivity of SCN neurons.

Our findings indicate SCN neurons are responsive to photic information from the retina in the absence of VIP signaling, but raise additional questions about the mechanisms underlying impaired photic entrainment of VIP KO mice. Ventral/core cells receive most of the retinal input in the SCN (Ibata et al., 1989; Morin and Allen, 2006; Kiss et al., 2008), respond most robustly to light-induced changes in electrical activity and gene expression (Shibata et al., 1984; Meijer et al., 1998; Antle et al., 2009), in addition to expressing VIP, gastrin-releasing peptide, and the neurotransmitter GABA. Dorsal shell neurons receive dense innervation from ventral cells (Yan et al., 2007), generate more robust circadian oscillations in gene expression (Yan and Okamura, 2002; Hamada et al., 2004; Nakamura et al., 2005; Pauls et al., 2014), and express AVP, prokineticin 2, and GABA. Therefore VIP is well positioned to mediate core to shell communication. VIP receptors (VIPR2) are expressed throughout the SCN, but their expression is more abundant in the dorsal region (An et al., 2012), especially in the mid-SCN where our physiological recordings were performed.

Light exposure or treatment with gastrin-releasing peptide and/or VIP can cause persistent increases in neural activity within the SCN at night (Kuhlman et al., 2003; Gamble et al., 2007, 2011; Lesauter et al., 2011; Kudo et al., 2013). Considering the long-lasting changes in excitability peptide transmitters affect within the SCN network, we speculate VIP and gastrin-releasing peptide regulate the excitability of the neurons within the SCN circuit. VIP is expressed by a subset of GABAergic interneurons found throughout the central nervous system, and has been shown to alter the excitability of several neural populations (Jeftinija et al., 1982;

Pawelzik et al., 1992; Lee and Cox, 2006; Hermes et al., 2009). There is also evidence that SCN neurons from VIPR2$^{-/-}$ mice may be chronically hyperpolarized (Pakhotin et al., 2006), which is consistent with the findings in the present study for vSCN neurons and dSCN neurons during the daytime, but not for dSCN neurons at night which actually showed depolarized ISMPs (**Fig. 3.9**). Our findings also suggest that VIP-induced changes in electrical activity may be critical for inducing light-evoked changes in gene expression, especially in the dorsal SCN. During the night, SCN neurons are normally silent and respond to photic stimulation transduced by ipRGCs to generate action potentials up to 20 Hz. (Meijer et al., 1998; Berson et al., 2002; Warren et al., 2003; Tu et al., 2005; Irwin and Allen, 2007). This RHT-stimulated neural activity drives synaptic communication with the rest of the cells in the SCN circuit. At night SCN neurons are typically silent and therefore most responsive to excitatory input, but VIP KO dSCN neuron action potential rates were already high at night, and their failure to respond to additional excitation may be related to their already excited state. Our findings indicate that in the absence of VIP, retinorecipient neurons are still responsive to photic stimulation, but their ability to communicate photic information to the rest of the SCN is impaired, possibly due to altered phasing of excitability rhythms within dSCN (**Fig. 3.8**). This may explain why the loss of VIP or its receptor, causes dramatic photic entrainment impairments, including the inability of the SCN to encode seasonal information.

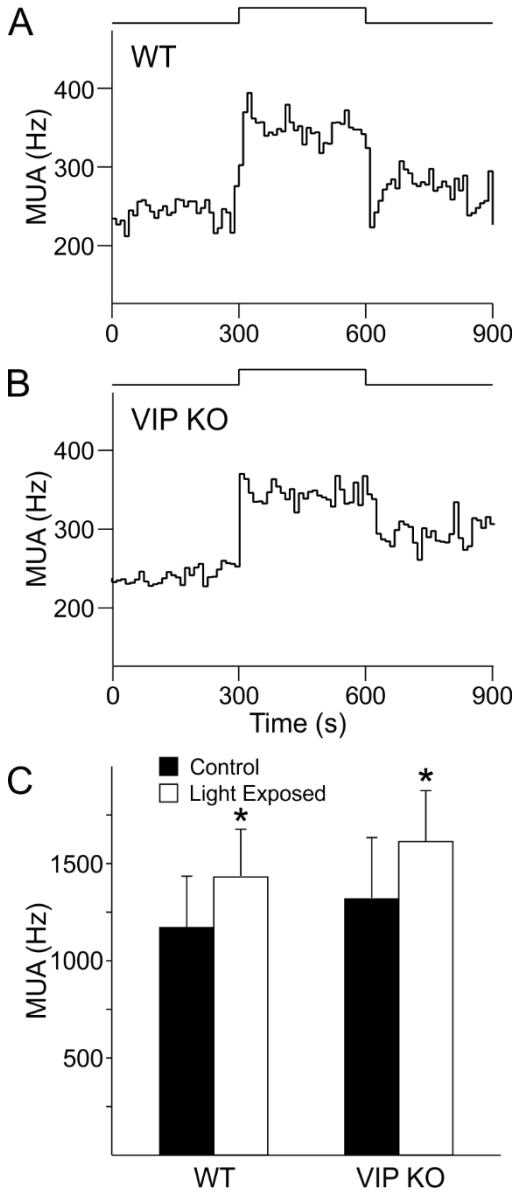

Figure 3.1: Light-evoked changes in multiunit activity (MUA) recorded from the SCN of freely moving mice. **(A, B)** Representative examples of MUA rhythms recorded from the SCN of a WT and VIP KO mouse during the night. Light pulses are indicated above the graphs. SCN firing rate is increased in both VIP KO and WT mice, with a response latency of 0.04 sec. Bin size is 0.01 sec. **(C)** Bar graphs show mean and SEM of the MUA before and during light exposure. Significant effects of light and genotype were tested with Two-Way ANOVA followed by the Holm-Sidak method for multiple comparisons (Light, $*P < 0.05$, Genotype, NS).

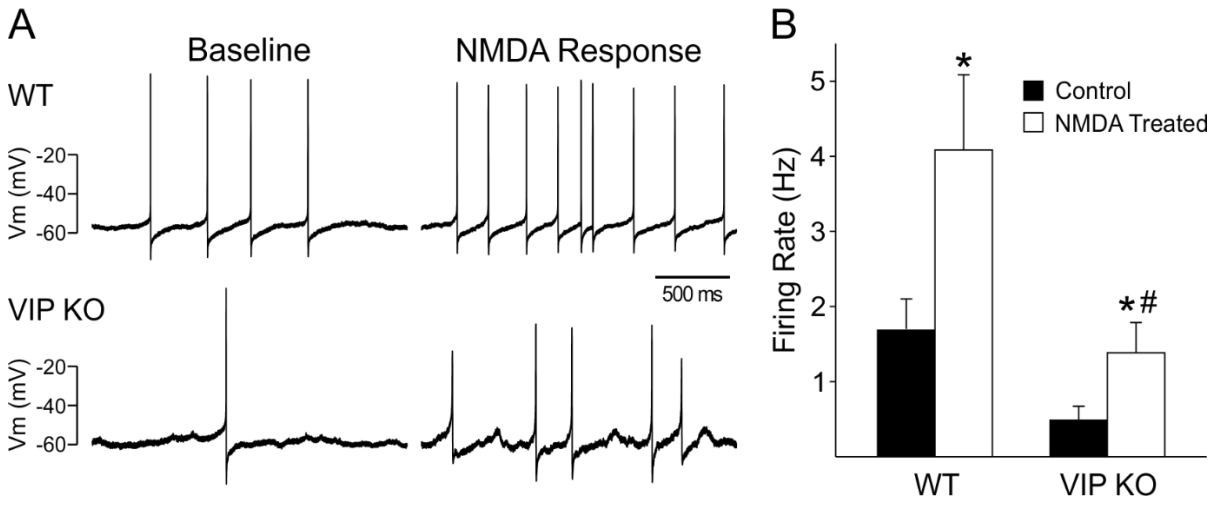

Figure 3.2: Application of NMDA increased the firing rate of ventral SCN neurons during the night *in vitro*. **(A)** Representative examples illustrating the NMDA-induced increase in firing rate in a vSCN neuron from the VIP KO and WT control mice. **(B)** Bar graphs depict average firing rates for each group (+SEM). Genotype and NMDA treatment effects on firing rate was assessed with Two-Way ANOVA followed by the Holm-Sidak method for multiple comparisons (Genotype, $^{\#}P < 0.05$; Treatment, $^{*}P < 0.05$).

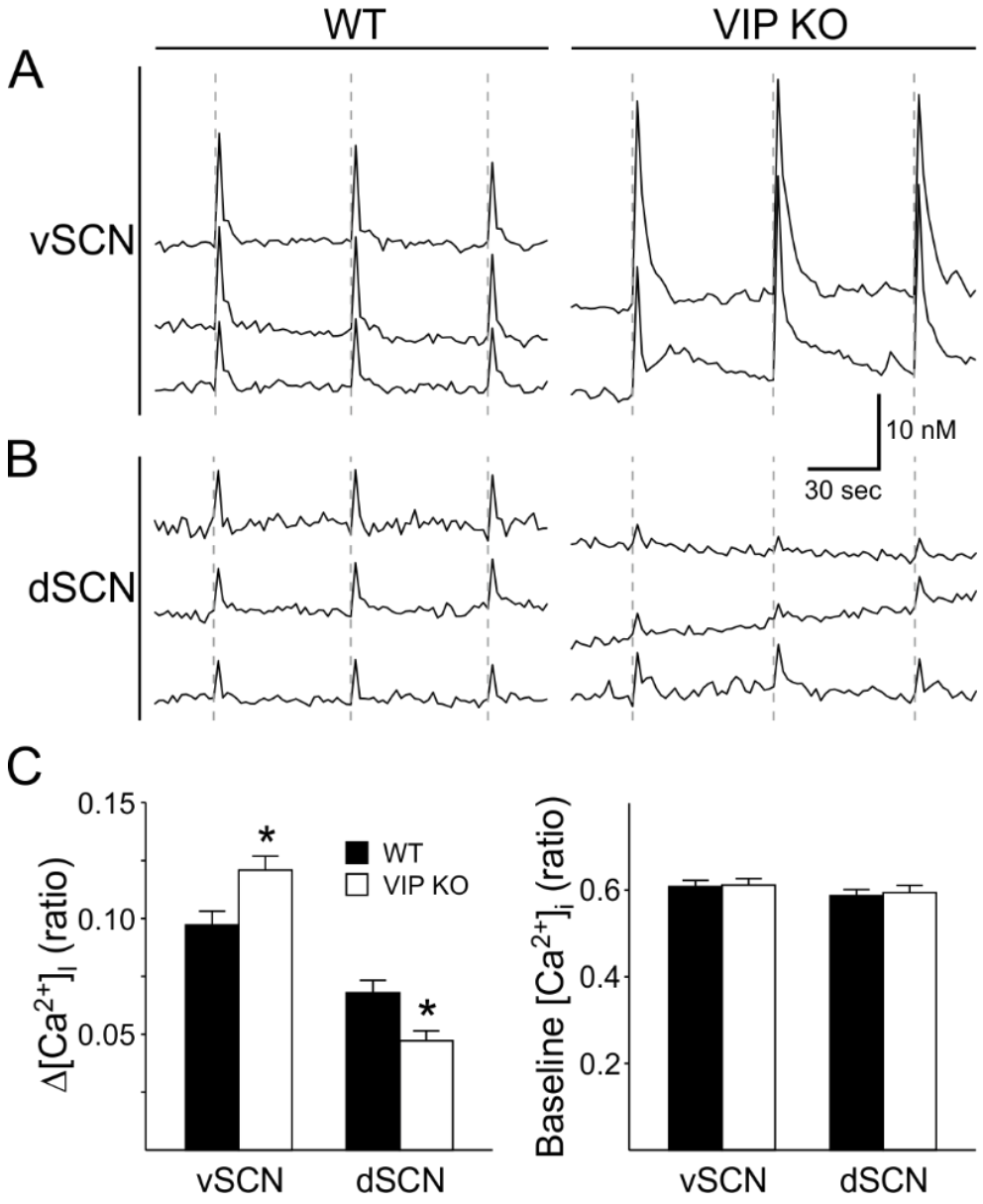

Figure 3.3: Evoked Ca^{2+} transients in the SCN of VIP KO and WT controls in response to RHT stimulation in a brain slice. **(A)** Examples of increases in $[Ca^{2+}]_i$ after electrical stimulation of the RHT (dotted line; 10Hz for 1 sec) in the ventral and dorsal region of the SCN for both WT and VIP KO mice. Each line represents the response of one cell to three repeated stimuli. **(B)** Average change in $[Ca^{2+}]_i$ expressed in ratio (340 nm/380 nm) after RHT stimulation. Compared to WT controls, the VIP KO mice show higher responses in the ventral SCN ($P = 0.005$), but lower responses in the dorsal SCN ($P = 0.003$) after RHT stimulation. Error bars represent SEM. Effects of genotype and RHT stimulation on $[Ca^{2+}]_i$ were tested using Two-Way ANOVA followed by the Holm-Sidak method for multiple comparisons (Genotype, $^*P < 0.05$; Stimulation, $P < 0.05$). **(C)** Average baseline $[Ca^{2+}]_i$ does not differ between the genotypes, nor between ventral and dorsal SCN.

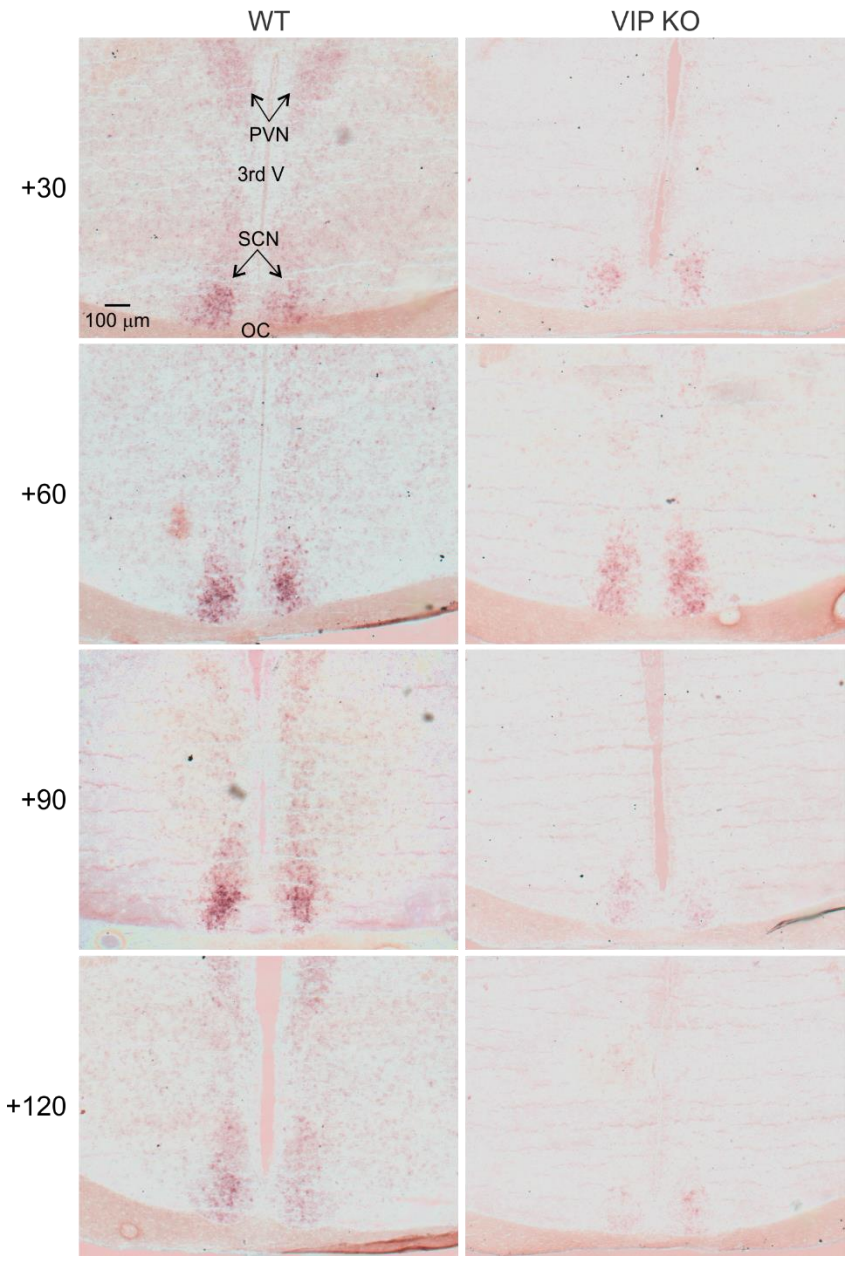

Figure 3.4: Examples of the temporal pattern of light-evoked changes in *Per1* mRNA. SCN photomicrographs following digoxigenin ISH for *Per1,* reveal a time course of *Per1* induction in WT mice following a CT16 light-pulse. Message begins to appear around 30 minutes after the beginning of the light pulse, well-defined expression in a subpopulation of cells in the ventro-middle region of the nucleus occurs 45 to 60 minutes after the initial pulse. Message expression spreads across the nucleus and disappears by 4 hours after the initial pulse. This pattern is disrupted in the VIP KO mice in which the initial induction of the *Per1* in response to light is strong but the signal is not sustained ventro-middle SCN nor communicated to the shell SCN region. Upper left panel is labeled with PVN (paraventricular nucleus), SCN (suprachiasmatic nucleus), OC (optic chiasm), and 3rd V (3rd ventricle) as an aid for the reader.

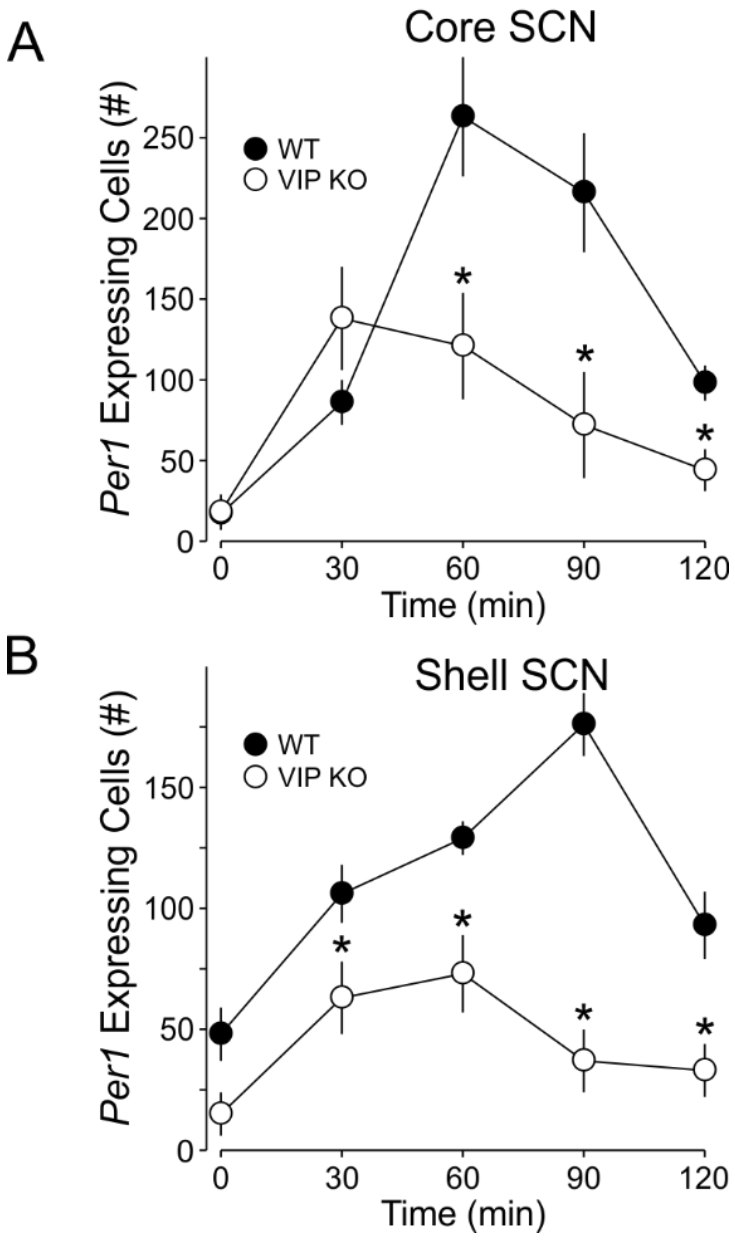

Figure 3.5: Quantification of the temporal patterns of light-evoked *Per1* expression in the core **(A)** and shell SCN **(B)**. Cell counting of *Per1*+ cells following ISH reveals that *Per1* is significantly induced by a CT 16 light pulse at all-time points measured in WT mice, but only at 30 and 60 min post pulse in VIP KO mice. Post hoc analyses reveal significantly reduced *Per1*+ cell counts in the VIP KO compared with controls at 30, 60, and 90 min time points in the core SCN (denoted by *). In the shell, all *Per1*+ cell counts were significantly reduced. Significant difference (*P<0.05) compared to controls analyzed by Two-Way ANOVA followed by Holm-Sidak method for multiple comparisons.

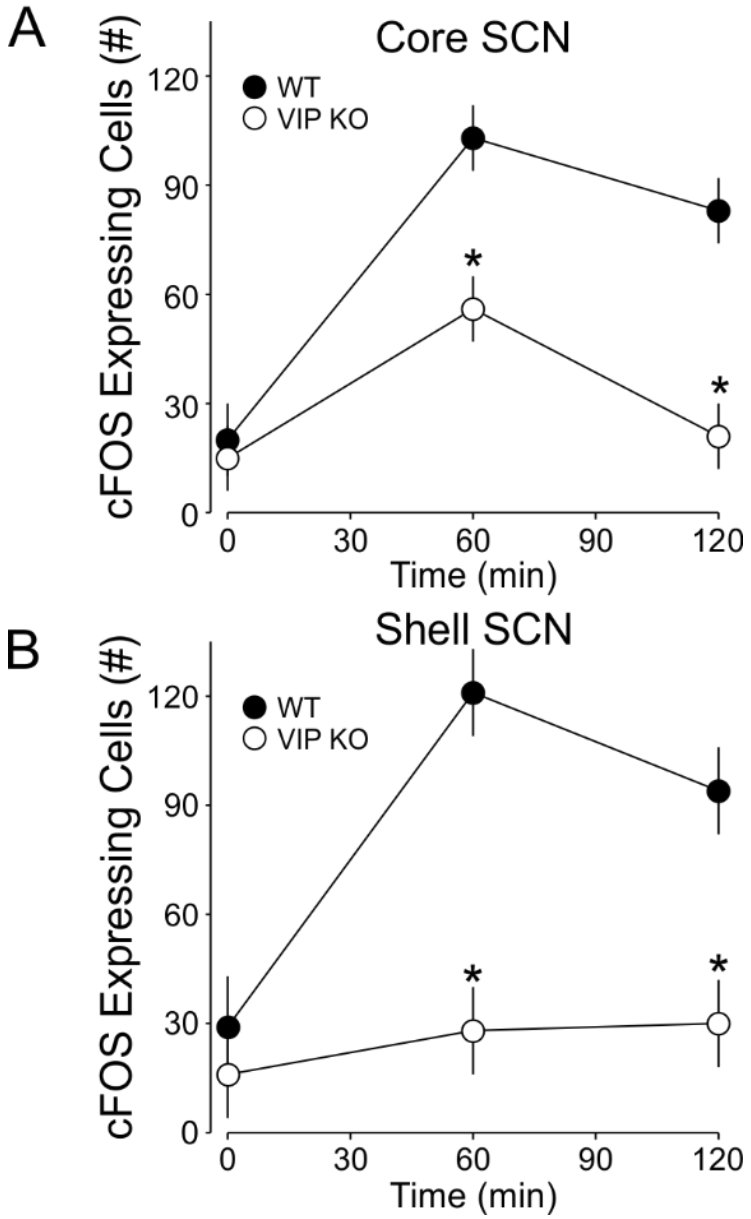

Figure 3.6: Quantification of the temporal patterns of light-evoked c-FOS expression. In core **(A)** and shell SCN **(B)**. Cell counting of c-FOS+ cells in the SCN core following immunofluorescence reveals that c-FOS is significantly induced by a CT16 light pulse at both 60 and 120 min following light exposure in WT mice, but only at 60 min post pulse in VIP KO mice. In the SCN shell, c-FOS is significantly induced at both 60 and 120 min following light exposure in WT mice. There was no significant c-FOS induction in the SCN shell of the mutant mice. *Post hoc* analyses reveal significantly reduced c-FOS+ cell counts in VIP KO mice compared with controls at both the 60 and 120 min time points. * indicates significant difference ($P<0.01$) compared to controls analyzed by Two-Way ANOVA followed by Holm-Sidak method for multiple comparisons.

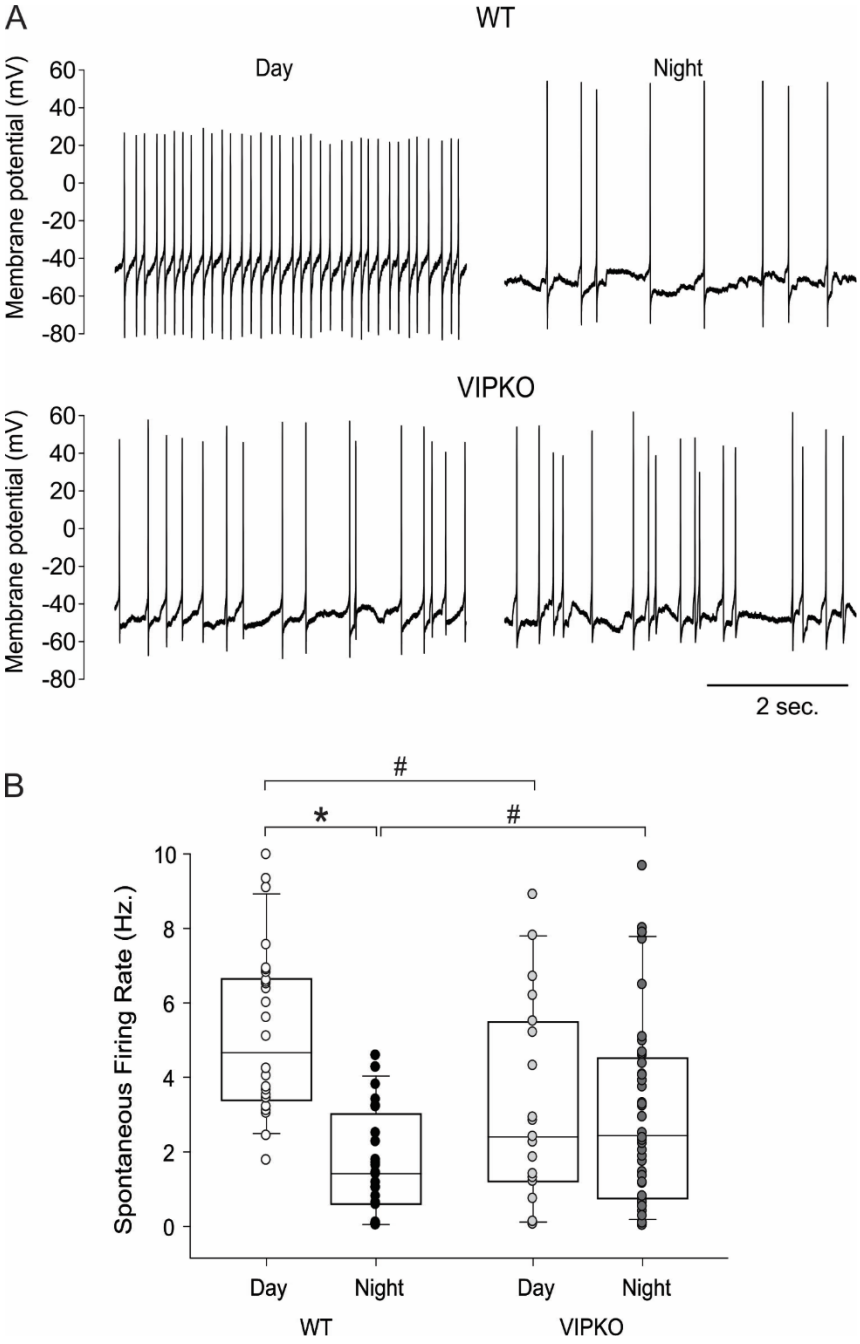

Figure 3.7: Loss of spontaneous firing rhythms in VIP KO dorsal SCN. **(A)** Trace examples of a WT (top) and VIP KO (bottom) dSCN neuron's SFR. **(B)** Box plots representing first and third quartile (box), medians (middle line), and data range (whiskers) with individual WT day (white dots), WT night (black dots), VIP KO day (light gray dots), VIP KO night (dark gray dots) data points superimposed. Two-Way ANOVA was used to test for effects of genotype and time on SFR, followed by Holm-Sidak method for multiple comparisons (*Day/night, $P < 0.05$; $^{\#}$Genotype within time, $P < 0.05$).

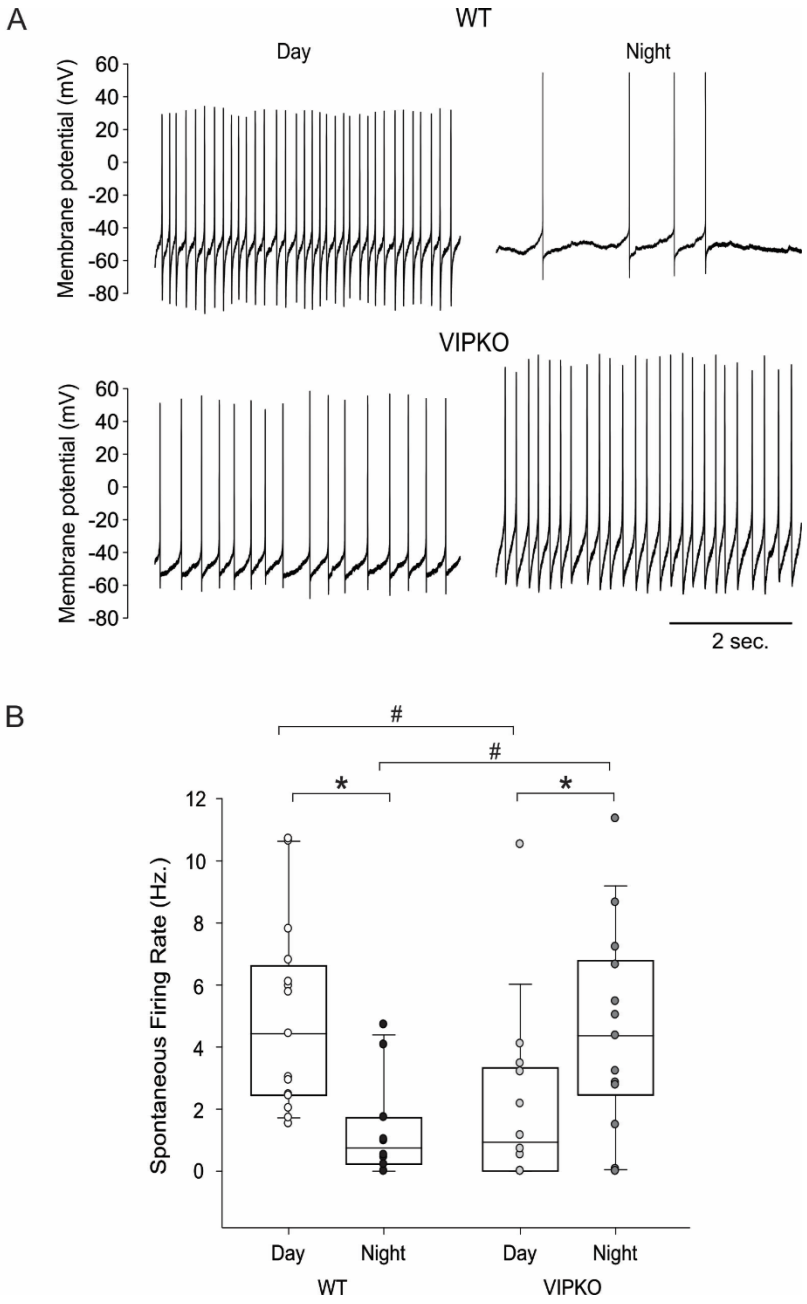

Figure 3.8: Antiphase SFR rhythms of synaptically isolated VIP KO dSCN neurons. **(A)** Trace examples of a WT (top) and VIP KO (bottom) dSCN neuron's SFR. **(B)** Box plots representing first and third quartile (box), medians (middle line), and data ranges (whiskers) with individual WT day (white dots), WT night (black dots), VIP KO day (light gray dots), VIP KO night (dark gray dots) data points superimposed. Three-Way ANOVA was used to test for effects of genotype, time, and gabazine treatment on SFR, by Holm-Sidak method for multiple comparisons (*Day/night, $P < 0.05$, $^{\#}$Genotype within time, $P < 0.05$).

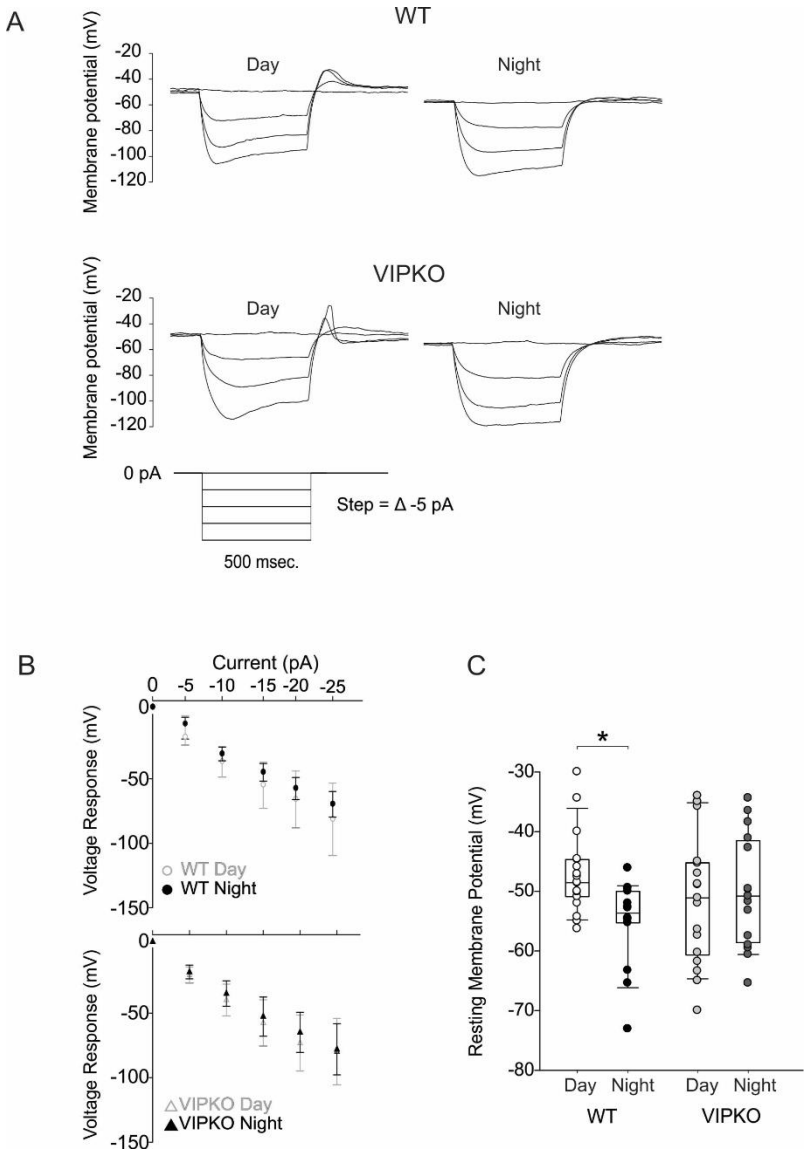

Figure 3.9: Loss of resting membrane potential rhythms in VIP KO dSCN neurons. **(A)** Representative traces of WT and VIP KO membrane potential responses to negative current step injection. **(B)** Peak voltage response group means (± 95% CI) plotted as a function of current. Three-Way ANOVA was used to test for significant effects of genotype, time, and current step magnitude on peak voltage response (Current, $P < 0.05$). Both (B) and (C) examined the same number of neurons. **(C)** Box plots representing first and third quartile (box), medians (middle line), and data range (whiskers) of resting membrane potentials with individual WT day (white dots, n = 18), WT night (black dots, n = 14), VIP KO day (light gray dots, n = 17), VIP KO night (dark gray dots, n = 15) data points superimposed. Two-Way ANOVA was used to detect effects of genotype and time on resting membrane potential, followed by Holm-Sidak method for multiple comparisons (*Day/night, $P < 0.05$).

Chapter 4: VIP's role in the circadian regulation of female fertility

Many people in our society experience chronic disruptions of their sleep/wake cycle. While not explicitly tested, there is every reason to suspect that disrupted sleep also disrupts and/or misaligns the circadian system through increased sleep-phase light-exposure and locomotion. There are a number of lines of evidence that link circadian disruption and declining reproductive success. For example, several studies have demonstrated reduced fecundity in mice with mutations in their core clock genes (Kennaway et al., 2004; Miller et al., 2004; Dolatshad et al., 2006; Alvarez et al., 2008; Ratajczak et al., 2009). Likewise, in *Drosophila*, clock mutants show reduced reproductive fitness (Beaver et al., 2002). Environmental disruptions of circadian timing also reduce reproductive success (Endo and Watanabe, 1989; Summa et al., 2012), although this phenomenon is understudied. Finally, epidemiological studies have linked shift work to decreases in human reproductive success (Mahoney, 2010; Mong et al., 2011).

The female reproductive cycle is controlled by a finely-tuned multi-organ feedback loop, involving hypothalamic control of pituitary hormone secretion and corresponding steroid release from the ovaries. In female rodents, ovulation occurs spontaneously in regular 4 to 5 day cycles, and is gated by the circadian system (Everett and Sawyer, 1950; Turek et al., 1984; Barbacka-Surowiak et al., 2003). With the isolation or ablation of the master pacemaker of the circadian timing system, the suprachiasmatic nuclei (SCN), pre-ovulatory hormone surges are lost in female rats (Nunez and Stephan, 1977; Gray et al., 1978; Mosko and RY, 1979; Wiegand et al., 1980). Along with ablation studies in rodents, the observed deficits in clock mutants, deliberate circadian disruption models, and human epidemiological studies, many lines of evidence demonstrate circadian disruption is negatively correlated with fertility and inspires further examination of links between female circadian and reproductive cycles.

Previous anatomical studies have established that the connectivity from the SCN to gonadotropin-releasing hormone (GnRH) neurons in the medial preoptic area consists of both a direct connection with neurons expressing vasoactive intestinal peptide (VIP) (Van Der Beek et al., 1997; Kriegsfeld et al., 2002; Ward et al., 2009) and an indirect connection with kisspeptin- and arginine vasopressin (AVP)-positive neurons via the periventricular nucleus (de la Iglesia and Schwartz, 2006; Robertson et al., 2009; Vida et al., 2010; Williams et al., 2011). Physiologically, exogenous VIP increases the electrical activity of GnRH neurons during the surge (Christian et al., 2005; Christian and Moenter, 2008), suggesting that VIP provides an excitatory signal from the circadian clock that helps time the GnRH surge. Additionally, transient reduction of VIP by infusion of anti-sense *Vip* mRNA or antibodies against VIP leads to a dampening of the magnitude of the LH surge in female rats (Harney et al., 1996; Van Der Beek et al., 1997; Gerhold et al., 2005), but the impact of the loss of VIP on the female circadian and reproductive cycles has not been explored.

We postulate that VIP-deficiency may be particularly detrimental to the SCN-GnRH circuit and affect downstream measures of reproductive function in female mice, including fertility, regularity of the estrous cycle, and LH-induced ovulation. Additionally, the loss of VIP ($VIP^{-/-}$) in *male* mice results in severe disruption in behavioural rhythms (Colwell et al., 2003), which stems from loss of neuronal synchrony (Aton et al., 2005; Ciarleglio et al., 2009) that results in altered phasing of peripheral oscillators (Loh et al., 2011). The impact of VIP-deficiency on female rhythms has been understudied, and we suggest that while female VIP KO mice exhibit circadian disruption, there may be ameliorating sex differences that should be acknowledged.

Materials and Methods

Animals and housing

The experimental protocols used in this study were approved by the UCLA Animal Research Committee, and all recommendations for animal use and welfare were followed, as dictated by the UCLA Division of Laboratory Animal Medicine and the guidelines from the National Institutes of Health. *VIP*$^{-/-}$ mutants (VIP KO; also deficient in histidine isoleucine [PHI] encoded by the same locus) backcrossed to the C57BL/6 strain (Colwell et al., 2003) were crossed to PERIOD2::LUCIFERASE (PER2::LUC, *Per2*^{Luc}) mice also on a C57BL/6 background (Yoo et al., 2004) as previously described (Loh et al., 2011). All wild-type (WT) and VIP KO mice described in this study were maintained as homozygotes for the PER2::LUC knocked-in fusion gene. All mice were housed under 12:12 light-dark (LD) conditions for a minimum of 2 weeks prior to any experimentation.

Measurement of fertility

Female WT (*n* = 8) and VIP KO (*n* = 8) littermates at 2 months of age (mo) were paired with male WT mice (2 mo) to determine fecundity in terms of number of litters, number of pups born, and number of pups weaned. Breeders were checked daily for pregnancy and births, and dams were left undisturbed to avoid maternal stress leading to litter loss. As such, the number of pups born could only be accurately determined from P7.

Determination of estrous cycles by vaginal lavage

WT (*n* = 24) and VIP KO (*n* = 24) female mice (2 mo) housed under a 12:12 LD cycle were monitored using vaginal lavage at zeitgeber time (ZT) 0-1 (within 1 hr of lights on). Care

was taken to avoid insertion of the lavage pipet, and the lavage samples were spotted in small (~100 µl) drops onto glass microscope slides. Cell types contained within each vaginal smear were determined using light microscopy (10X power) and scored for estrous state (Caligioni, 2009), where proestrus is indicated by the predominance of nucleated epithelial cells, estrus is denoted by the absence of nucleated cells and the presence of cornified squamous epithelial cells, while lavages from mice in metestrus and diestrus contained leukocytes. Mice were scored as having regular estrous cycles if they exhibited 4-5 day cycles throughout the monitoring period (14-21 days). Conversely, if mice exhibited more than 3 days in metestrus or diestrus, more than 2 days in proestrus, more than 1 day in estrus, or did not follow the order of progression of estrus states, they were scored as having irregular estrous cycles. The percentage of proestrus or estrus states was determined over the number of days sampled, and the percentage of proestrus smears followed by estrus were determined by visually scoring the number of proestrus smears that were immediately followed by an estrus-positive smear and dividing that by the total number of proestrus smears within each mouse.

Measurement of serum hormones

Serum was collected from 3 month old WT (*n* = 10) and VIP KO (*n* = 10) female mice at ZT6 (mid-day) on the day of a proestrus smear using methods previously described (Loh et al., 2008). Serum was assayed for estradiol using radioimmunoassay by the National Peptide and Hormone Program laboratory at Harbour-UCLA (Torrance, CA). For measurement of luteinizing hormone (LH) concentrations, serum was collected from a separate cohort of age-matched WT (*n* = 4) and VIP KO (*n* = 4) females at hourly intervals between ZT7 (7 h after lights on) and ZT15 (3h after lights off) housed under a 12:12 LD cycle on the day of a proestrus smear. The serum samples were assayed for LH using the Milliplex MAP mouse pituitary magnetic bead

assay (MPTMAG-49K, EMD Millipore, Billerica, MA). Assay sensitivity was reported as 1.7 pg/ml, with intra- and inter- assay %CVs reported as < 15 and < 20 respectively for LH. No other analytes were run in this panel, thus ruling out cross-reactivity with other antibodies. Pituitary standard samples run in this assay contained LH ranging from 4.9 pg/mL to 20 ng/ml.

Determination of spontaneous oocyte release during estrus

Vaginal smears were monitored for 2 estrous cycles for WT (*n* = 12) females or at least 7 days until a proestrus smear for VIP KO (*n* = 12) females. During the estrous stage, mice were sacrificed at ZT0-1, and the ovaries with oviducts attached were removed by cutting the ovary fat pad and the uterus. The ovary and oviduct were further dissected in Hank's Balanced Salt Solution (HBSS; Gibco, Invitrogen, Carlsbad, CA) to remove the fat and uterus, and transferred to fresh solution in an indented microscopic slide for analysis under a dissecting microscope. Each oviduct was carefully examined for released oocytes by making a small incision in the oviduct and teasing out the contents along its entirety. The cumulus mass was dissociated by treatment in HBSS containing 300 µg/ml hyaluronidase (Sigma-Aldrich, St Louis, MO) and the oocytes were distinguished from other detritus by their spherical nature. Sampling at earlier time points (ZT 12 - 23 on the day of a pro-estrus smear) revealed an absence of oocytes in both WT (*n* = 5) and VIP KO (*n* = 3) oviducts.

Oocyte release in response to ovarian stimulation

In a separate cohort, ovulation was induced using a combination of pregnant mare serum gonadotropin (PMSG) and human chorionic gonadotropin (hCG). Female WT (*n*=6) and VIP KO (*n*=6) mice (2 mo) were hormone primed with an intraperitoneal (*ip*) injection of 5 IU of

PMSG (G4877, Sigma-Aldrich) applied at ZT11 on the day of metestrus, and ovulation was induced 48 hr later by *IP* injection of 5 IU of hCG (Novarel, Ferring Pharmaceuticals, Parsippany, NJ). On the morning following the hCG injection, mice were sacrificed between ZT0 and 1, and the number of oocytes released into the oviducts were counted.

Wheel running activity

Adult female mice (2-4 mo; WT n = 10, VIP KO n = 10) were singly housed in cages containing wheels, and wheel running activity was recorded as previously described (Colwell et al., 2003). Mice were entrained to a 12:12hr LD cycle for a minimum of 2 weeks prior to collection of 10-14 days of data under LD conditions, followed by 10-14 days in constant darkness (DD) to obtain free-running activity. Data was recorded using Mini Mitter (Bend, OR) data loggers in 3 min bins, and 10 days of data under each condition were averaged for analysis. Free-running period (tau) was determined using the χ^2 periodogram and the power of the rhythm was calculated by multiplying the Q_p by 100/n, where n = number of data points examined using the El Temps program (Barcelona, Spain). Activity duration (alpha) was determined by the duration of activity over the threshold of the mean using an average waveform of 10 days of activity. The phase of activity onset was also defined as the time at which activity crossed the threshold of the mean of total activity. To calculate the phase angle of entrainment revealed by release into DD, the difference on the day of lighting change was determined between best-fit regression lines drawn through activity onset prior to and after release into DD. Precision was determined by calculating the daily variation in onset from best-fit regression lines drawn through 10 days of activity in both LD and DD conditions using the Clocklab (Actimetrics, Wilmette, IL). Fragmentation was defined as bouts/day with a maxgap of 21 min.

Measurement of spontaneous firing rate in SCN

Whole cell patch-clamp electrophysiology methods similar to those described previously were used (Kudo et al., 2013). Young female mice (2-3 mo) were anaesthetised in an isoflurane chamber in the day (ZT 2.5) or in the night (ZT 12.5). 300 µm coronal sections were prepared and superfused continuously with room temperature artificial cerebral spinal fluid (ACSF) aerated with 95% O_2/ 5% CO_2 in a recording chamber (PH-1, Warner Instruments, Hamden, CT) attached to the stage of a fixed stage upright DIC microscope (OLYMPUS, Tokyo, Japan). Whole cell patch clamp SCN recordings were made using electrode micropipettes (3-7MΩ) and filled with standard internal solution (in mM: K-gluconate, 112.5; EGTA, 1; Hepes, 10; MgATP, 5; and MgCl2, 1). Internal solution pH was adjusted to 7.25-7.3 and osmolarity adjusted to 290-300mOsm. Recordings were obtained with the AXOPATCH 200B amplifier (Molecular Devices, Sunnyvale, CA) and monitored on-line with pCLAMP (Ver 10, Molecular Devices).

For these experiments, recordings were made from cells located in the dorsal SCN (dSCN) as defined by being dorsal to the tip of the 3rd ventricle. The access resistance of these cells ranged from 15 to 35 MΩ and cell capacitance typically ranged between 6-18pF. Data were not collected if access resistance values changed significantly (>20%) during the course of the experiment and/or if a neuron was not able to decrease firing rate following excitatory treatment with NMDA (25µM). Drug treatments were performed by dissolving gabazine (10µM) in ACSF and delivered via rapid gravity feed system into the slice bath during recording. Spontaneous firing rates (SFR) were recorded with pCLAMP for 1 min using current-clamp mode in whole cell patch configuration. No current was injected during recording. SFR for each cell was determined using the total number of action potentials recorded in a one minute time window. SFR for WT and VIP KO females at both time points was determined by averaging data from at least 10 neurons collected from a minimum of 3 animals.

Monitoring of PER2::LUC bioluminescence

Female WT (*n* = 7) and VIP KO (*n* = 10) mice (2-3 mo) were housed under a 12:12 LD cycle for at least 2 weeks prior to sampling. Vaginal smears were performed during the second week to determine estrous state, and mice in proestrus (nucleated cells) were sampled at ZT 10-11. SCN explants were dissected from 300 µm coronal sections, dissected ovaries were further halved, and 1-2 mm^3 explants were dissected from the pituitary and mid-point of the uterus. PER2::LUC bioluminescence recordings using a Lumicycle photometer (Actimetrics, Wilmette, IL) were conducted and analysed as previously described (Loh et al., 2011; Kuljis et al., 2013). Briefly, bioluminescence readings were taken every 10 min, and for analysis, were baseline-subtracted, de-trended (24 hr window) and smoothed (2 hr window). Due to this process, we do not report the first recorded peak but instead the first calculated peak for phase of PER2::LUC expression. Amplitude of each cycle was determined by the sum of the peak and subsequent trough values, and period was determined from a minimum of 4 consecutive cycles.

Statistical Analysis

For comparison of female WT and VIP KO measures, that passed normality and equal variance tests, we applied Student's t-tests and deemed differences as significant if $P < 0.05$. For parameters that failed either normality or equal variance tests, rank sum *t*-tests were applied. Two-factor repeated measures analysis of variance (ANOVA) was applied to examine the relative contributions of genotype and time of day of pro-estrus serum LH concentration. *Post hoc* Bonferroni comparisons were performed to compare the effect of genotype at each sampling time. Values are reported as mean ± standard error mean (SEM).

Results

Female reproduction is greatly reduced in the VIP-deficient mice.

To determine if VIP is critical for reproduction, we paired naïve WT and VIP KO female littermates with WT males. VIP KO females produced dramatically fewer pups (10.6 ± 1.5) than their sisters (21.5 ± 3.0, $P < 0.01$) over 6 months of breeding, demonstrating reduced fecundity. The mean number of pups per litter was not significantly different between the genotypes (WT 4.8 ± 1.7, VIP KO 4.0 ± 1.6 pups/litter; $P = 0.32$), but fewer litters were born to VIP KO dams (2.9 ± 0.3) compared to WT females (4.5 ± 0.3, $P < 0.01$). Furthermore, VIP KO females spent a smaller percentage of time either pregnant or nursing (46.8 ± 3.1 %) versus WT females (76.9 ± 5.2 %, $P < 0.001$). We can conclude from these findings that although VIP KO females are capable of reproduction, they are sub-fertile, spending less time pregnant or nursing, and producing half the number of offspring compared to their sisters held under the same conditions.

The regularity of the estrous cycle is greatly reduced in the VIP-deficient mice.

To determine if the basic reproductive biology underlying ovulation is affected by VIP-deficiency, we examined the estrous cycle by daily vaginal lavage in WT and VIP KO female littermates (representative examples shown in **Fig. 4.1A**). We found irregular estrous cycles in the majority of VIP KO females (20/24), while the majority of the WT females exhibited regular cycling through proestrus, estrus, metestrus and diestrus (19/24). Cycle duration, as determined by the time between estrus phases, was found to be longer in VIP KO females (8.18 ± 1.05 days) compared to typical WT cycles (4.64 ± 0.17 days; $P < 0.001$; **Fig. 4.1B**). A common finding in VIP KO females was that not every proestrus smear was followed by an estrus smear (51.6 ± 6.5 %; **Fig. 4.1A,C**), whereas almost every proestrus smear in WT females was

immediately followed by an estrus smear (84.4 ± 5.5 %, $P < 0.001$; typical example depicted in **Fig. 4.1A**, top). Additionally, VIP KO females exhibited elongated duration in diestrus/metestrus, as indicated by the presence of leukocytic cells (57.69 ± 3.88 %), compared to WT females (44.68 ± 2.06 %, $P = 0.008$**; Fig. 4.1D**). Over the entire period in which estrous cycles were assessed, VIP KO females had significantly fewer percentages of days in proestrus (15.9 ± 1.8 %) compared to WT females (20.7 ± 1.2 %, $P < 0.01$), and had fewer days in estrus (14.7 ± 2.6 % vs. WT 20.5 ± 1.6 %, $P < 0.05$). Our data indicates that VIP is essential for regular estrous cycles, and VIP-deficiency results in long spells in the diestrus and metestrus states. Furthermore, estrus is not guaranteed after proestrus, which further adds to the longer duration between estrous states in mutant females.

Serum estradiol levels were not altered by the loss of VIP.

To determine if the steroidal signals that define the ovulatory process are affected by the VIP mutation, we measured serum concentrations of estradiol during proestrus. The rise in circulating estradiol during the day of proestrus precedes the activation of GnRH neurons, which initiates the LH surge and in turn stimulates ovulation (Legan et al., 1975). The mid-day (ZT 6) serum concentration of estradiol was no different in VIP KO females (52.9 ± 4.2 pg/µl) from WT females (54.4 ± 3.8 pg/µl, $P = 0.77$; **Fig. 4.2A**). We also performed hourly measurements of LH from ZT7 to ZT15 to determine if surge time and/or concentration were altered in VIP KO females. The maximum LH measured in VIP KO females (0.2 ± 0.04 pg/ml) was not significantly different from WT females (1.1 ± 0.8 ng/ml; rank sum test, $P = 0.11$). The maximum LH concentration in WT females was found to be lower than surge-like concentrations of LH (>5 ng/ml), despite hourly sampling on the day of proestrus. Coupled with the high variability in LH concentrations within WT females, we are unable to draw conclusions about genotypic

differences in LH surge concentration. We ascertained that the temporal window of peak LH concentration within animals was not significantly altered by the loss of VIP (WT ZT 11.3 ± 1.4, VIP KO ZT 11.4 ± 1.3; Rank Sum Test, $P = 0.73$). Our findings indicate that mid-day rise in estradiol concentration during proestrus is not altered in the VIP KO mice, which do not exhibit any measurable changes in LH concentration or peak timing.

Spontaneous ovulation is dependent on VIP

Mice ovulate spontaneously following estrus, and we examined the number of oocytes released in both WT and VIP KO mice on the day following a proestrus smear. We found that 6 out of 12 VIP KO females did not release any oocytes after a proestrus smear compared to 2 out of 12 WT females. Of the mice that released oocytes, significantly fewer oocytes were found in VIP KO oviducts (5.3 ± 0.7 vs. WT 10.7 ± 0.7 oocytes/pair of oviducts, $P < 0.001$; **Fig. 4.2B**). To determine if the reduced number of oocytes released by VIP KO females during ovulation is due to an inability of the ovaries to release the oocytes, we hormone-primed female mice using the PMSG-hCG ovarian stimulation technique commonly used to increase fertility in the production of transgenic mice. Following ovarian stimulation, we found that VIP KO mice release 26.7 ± 1.7 oocytes, which is not significantly different from the 24.7 ± 2.8 oocytes released by WT females ($P = 0.51$; **Fig. 4.2C**). In contrast to our finding, 50% of VIP KO females do not spontaneously ovulate on the day after proestrus, yet the entire cohort of hormone primed VIP KO females released oocytes, demonstrating that the VIP KO ovaries are able to respond to gonadotropin stimulation.

Circadian behaviour is disrupted in female VIP-deficient mice.

Several studies have characterized the circadian phenotype in male VIP-deficient mice (Colwell et al., 2003; Aton et al., 2005; Ciarleglio et al., 2009), while surprisingly neglecting to describe the behaviour of female mutants. We used wheel-running activity to determine the impact of the loss of VIP on diurnal and circadian rhythms of behaviour in female mice **(Fig. 4.3).** In LD conditions, the diurnal rhythms are largely similar between the genotypes with the only significant change seen in the extent of fragmentation of the nocturnal activity bout (**Table 4.1**). It is in DD that the full extent of the circadian phenotype in these mutant animals emerge. We observed significant decreases in the power and precision of the wheel running activity. Additionally, there is a significant decrease in the free-running period and a dramatic decrease in the magnitude of light-induced phase shifts to light exposure at CT16 (**Table 4.1**). Overall activity levels are not altered, highlighting the general conclusion that the loss of VIP does not produce a gross motor phenotype. A characteristic feature of the behaviour of VIP KO mice is the vastly advanced angle of entrainment to the LD cycle, as revealed when the mice are placed in DD. Like males, VIP KO females are abnormally entrained to the LD cycle, but their advanced angle of entrainment has a significantly smaller magnitude than VIP KO males, suggesting a sex-dependent effect of the mutation (**Table 4.2**). It is worth noting that there was no problem measuring key circadian parameters in WT female mice despite their likely estrous cycling. Overall, the female VIP-deficient mice showed clear and dramatic disruption of their circadian rhythms in wheel running activity.

SCN neural activity is compromised in female VIP-deficient mice.

SCN neurons are spontaneously electrically active cells that generate rhythms in action potential frequency with peak activity during the day (Colwell, 2011). We examined day-time

(ZT4-6) and night-time (ZT14-16) neural activity of dSCN neurons from WT and VIP KO mice using whole cell patch clamp electrophysiology. As expected, female WT mice exhibit a day-night difference in SFR, with higher frequency of firing during the day (3.57 ± 0.56 Hz) than during the night (1.25 ± 0.44, *P* = 0.011; **Fig. 4.4A**). In comparison, female VIP KO dSCN neurons exhibited lower firing rates during the day (-1.89 ± 0.33 Hz, vs WT, *P* = 0.019), a trend toward higher firing rates during the night (+4.9 ± 0.7 Hz, vs WT, *P* = 0.064), but no significant day-night difference in SFR (*P* = 0.30; **Fig. 4.4B**). When the cells were synaptically isolated using a GABA-blocker (gabazine), VIP KO dSCN neurons were again found to have lost the day-night differences in SFR (day 2.61 ± 0.56 Hz vs. night 3.29 ± 1.10 Hz, *P* = 0.54; **Fig. 4.4C**). Responsiveness of neurons to excitation was tested using NMDA, and were found to increase firing rates for both WT and VIP KO neurons (**Fig. 4.4C**). The reduced daytime SFR in the dSCN at a time when it should be at its peak in female VIP -/- mice, demonstrates that the mutants exhibit a weakened output or altered output phasing from the SCN circuit *in vitro* and suggests that the rest of the circadian system is getting a low amplitude signals from the SCN *in vivo*, or the phase of the signal is altered.

PER2 rhythms in the SCN, pituitary and reproductive organs are differentially affected in female VIP-deficient mice.

The circadian timing system consists of a central clock located in the SCN and peripheral clocks found throughout the body (Albrecht, 2012; Mohawk et al., 2012). To determine the impact of the loss of VIP on the molecular clockwork, we measured the phase of the expression of a critical circadian gene, *Period2*, using the PER2::LUC reporter which drives expression of luciferase fused to the PERIOD2 protein in double transgenics for the VIP mutation and the reporter (Loh et al., 2011). To control for the effects of estrous cycle-driven

hormones, we only used proestrus female mice. While the period and phase of peak PER2::LUC bioluminescence in the SCN was not affected by loss of VIP (**Fig. 4.5A; Table 4.3**), the phasing of the pituitary and uterus were advanced in VIP KO PER2::LUC explants (**Fig. 4.5B**). Conversely, the amplitude of the oscillations in the peripheral explants is unaffected by loss of VIP (**Fig. 4.5D**), whereas the amplitude of PER2::LUC bioluminescence in the SCN and pituitary are blunted in the mutant mice (**Fig. 4.5A, D**). The loss of VIP did not affect the period of PER2::LUC rhythms in any of the explants (**Fig. 4.5C**). We can thus conclude that VIP is not needed for intrinsic rhythmicity of peripheral oscillators in the ovary or uterus, since the period and amplitude of these rhythms are not different from WT controls. In contrast, VIP is important for the amplitude of PER2::LUC bioluminescence in the SCN and the pituitary and is also critical for the normal phasing of the pituitary and uterus.

Discussion

We wished to the address the impact of VIP-deficiency on the reproductive success of female mice, due to the importance of both VIP and the circadian timing system on reproduction. Anecdotal evidence from our colony indicated difficulty maintaining the homozygote VIP-deficient line. Careful measurements over 6 months confirmed that the VIP KO females are sub-fertile, spending less time pregnant or nursing, and producing half the number of offspring compared to their sisters held under the same conditions. Low fecundity has also been reported in VIPR2 knock-out mice (Dolatshad et al., 2006). These studies indicate that the loss of VIP signalling can result in the decline of reproduction and raise questions about the underlying mechanisms.

Previous studies have established that VIP expressing neurons provide one of the connections between the SCN and GnRH neurons in the medial preoptic area (Van Der Beek et

al., 1997; Horvath et al., 1998; Kriegsfeld et al., 2002; Ward et al., 2009; Vida et al., 2010). One of the receptors for VIP (VIPR2) is expressed on GnRH neurons (Smith et al., 2000), and physiologically, the exogenous treatment of VIP increases the electrical activity of GnRH neurons, while blocking the receptor decreases firing (Christian and Moenter, 2008). Therefore, we examined the impact of the loss of VIP on the estrous cycle. We found that VIP-deficient female mice have irregular and lengthened estrous cycles, due to a failure to progress from proestrus to estrus (**Fig. 4.1**). The VIPR2 KO mice show a disrupted estrous cycle, yet also spent more time in estrus (Dolatshad et al., 2006). We cannot explain the differences between the mutant lines but point out that VIPR2 also binds PACAP. Both lines of mutants are able to reproduce and the AVP and kisspeptin pathway most likely allows for continued, albeit lower fertility. Current thinking places greater importance on the indirect multi-synaptic connection between the SCN and GnRH neurons via AVP and kisspeptin (Robertson et al., 2009), which may be timed or gated by the direct VIPergic connection (Williams and Kriegsfeld, 2012). In rats, a sophisticated model of internal desynchrony within the SCN provides evidence that the AVP and VIP expressing subdivisions need to have coupled cross-talk to achieve maximal GnRH-dependent LH surge activity (Smarr et al., 2012). Ovulation involves the coincidence between high estrogen levels sensitizing the gonadotrophs with a gating signal from the SCN controlling time of ovulation (Legan et al., 1975; Christian and Moenter, 2010). We predicted a blunted LH surge in the mutant females, as has been seen in rats treated with anti-sense against *Vip* (Harney et al., 1996; Gerhold et al., 2005), but were unable to successfully measure the surge with hourly sampling. We were however able to determine that the necessary rise in serum estradiol is not impacted by the loss of VIP (**Fig. 4.2**). The end measure of the estrous cycle in females is ultimately ovulation, which we found to be deficient in the VIP KO female, in which oocytes were released less frequently and in fewer numbers than in WT controls. VIP has been shown to mediate the development and survival of female rat ovarian follicles (Flaws et al.,

1995; Cecconi et al., 2004; Chen et al., 2012), as well as a steroidogenic role in ovaries (Ahmed et al., 1986; Kowalewski et al., 2010). In our study, ovarian stimulation in response to exogenous treatment with gonadotropins did not vary between the genotypes (**Fig. 4.2**), demonstrating that the deficit in the mutants is not in the oocyte content of the ovaries but rather in the luteinizing signal. Additionally, the comparable proestrus concentration of serum estradiol in VIP-competent and VIP KO females suggests that VIP is not critical for ovarian steroidogenesis. Prior studies examining the effect of VIP on ovarian development, survival and steroidogenesis used in vitro manipulations supplementing cultures with exogenous VIP. In contrast, our VIP KO model's development may have occurred through redundant pathways, e.g. PACAP (Cecconi et al., 2004), allowing for reproduction to continue, albeit at sub-optimal levels. The disruption in the estrous cycle provides a proximate explanation for the observed decline in reproductive success and is likely a common consequence of circadian disruption.

The circadian timing system of female VIP-deficient mice is compromised at several levels. Behaviorally, the female mutant mice have severe deficits in circadian rhythms of locomotor activity, characterized by a shortened free-running period, lowered rhythm power, and poor precision of cycle-to-cycle activity onset (**Fig. 4.3; Table 4.1**). A further characteristic observed in both male and female VIP KO mice is the abnormally advanced angle of entrainment revealed when mice are released from LD to free-running DD conditions. This suggests the mice are abnormally entrained to the prior LD cycle, and we and others have reported phase-advanced physiology and behavior in VIP KO and VIPR2-/- males under an LD cycle (Colwell et al., 2003; Aton et al., 2005; Ciarleglio et al., 2009). Although the VIP KO female mice also exhibit an advanced phase angle of entrainment, its magnitude is half that of their male counterparts (**Table 4.2**), suggesting there is a sex-dependent effect of the mutation. Additional sex-dependent effects include the reduced amount of activity specific to the VIP KO males, which may be mediated by testosterone, which is also reduced in VIP KO males

(Lacombe et al., 2007). Physiologically, our data indicates that the VIP KO females have deficits in the expression and/or the phase of daily rhythms in spontaneous electrical activity (**Fig. 4.4**). VIP is critical for coupling SCN neurons, as mice deficient for the peptide or its receptor lose coherence and synchrony at the level of electrical firing (Aton et al., 2005; Brown et al., 2007) and gene expression (Harmar et al., 2002; Maywood et al., 2006; Hughes and Piggins, 2008; Ciarleglio et al., 2009; Dragich et al., 2010; Loh et al., 2011). Our finding that daytime SFR of SCN neurons is reduced in VIP-deficient females even in the presence of the GABA-blocker gabazine, suggests that even when GABA-dependent neuronal cross-talk is disabled acutely, the deficits remain. This is consistent with earlier work indicating that VIP signalling is a critical regulator of intrinsic membrane events in SCN neurons (Pakhotin et al., 2006; Kudo et al., 2013). Coupled with behavioural analysis our findings are consistent with a weakly rhythmic SCN in the female mutant mice. Alternatively, considering the antiphase rhythms observed in male VIP KO dSCN neurons (**Fig. 3.8**) and the much larger phase advance VIP KO males exhibit when released into constant conditions, female VIP KO dSCN neuronal rhythms may be similarly misaligned, but to a smaller degree, so that the time of examination may have occurred during the rhythm's inflection points and female dSCN output appeared non-rhythmic.

Finally, we assessed the molecular circadian clockwork by measuring PER2-driven bioluminescence in female VIP-deficient mice (**Fig. 4.5; Table 4.3**). At the level of the SCN, the PER2::LUC rhythms show reduced amplitude but a normal phase relationship to the prior LD cycle. With the exception of the pituitary, peripheral clocks mostly showed no change in amplitude, but their phases relative to each other and to the prior LD cycle were altered. These alterations in the timing of gene expression in peripheral oscillators were similar to those previously found in male VIP-deficient mice (Loh et al., 2011). Curiously, although the loss of VIP led to a phase advance of most of the peripheral oscillators (**Table 4.3**), the phasing of VIP KO ovaries was not different from WT (**Fig. 4.5**), suggesting that VIP is not necessary for the

circadian rhythm of PER2 expression in the ovary (Sellix and Menaker, 2010), and that the temporal gating of ovarian response to gonadotropins is unlikely to underlie ovulation deficits. The circadian phase of ovaries can be altered by gonadotropins (Yoshikawa et al., 2009), and is also dependent on estrous state (Nakamura et al., 2008a). By fixing our collection of PER2::LUC organs to proestrus, we may have picked an estrous state in which the phase of the circadian oscillator in the ovary is governed by circulating steroids. It is also important to note that the phase advance of the other peripheral oscillators is not due to a change in the intrinsic period of PER2 expression, which remains unaltered between WT and VIP KO tissues. Again, the gene expression data is best explained by a SCN clock whose output's phase is altered. These three lines of evidence for a disrupted SCN clock suggest a severe impact on the timing of SCN output signals. These include a dampening of the indirect AVP-kisspeptin route to the GnRH neurons and the loss of the direct VIP-GnRH relay, both of which ultimately result in a gross decrease in reproductive success.

One limitation of our study that we freely acknowledge is that using a whole-body knockout of VIP does not allow us to determine which of these deficits has the strongest impact on the observed sub-fertility of VIP KO females. The tripartite functions of VIP as a synchronizer between SCN neurons, its role as an SCN output signal to GnRH neurons, and its local role in ovarian follicular development cannot be distinguished in our model. Ideally, to distinguish the degree to which these varying functions of VIP affect reproduction, one would employ gene ablation targeted to specific organs or cell types, but a floxed-VIP mutation does not exist presently. Alternatively, one could use targeted rescue of VIP loss, for instance with viral constructs to restore VIP expression in SCN neurons. Nevertheless, our study reinforces the importance of VIP in female reproduction.

For the purposes of this study, the VIP-deficient female mice served as a model for circadian disruption caused by deficits in cellular communication rather than direct disruption of the molecular clockwork. In this sense, the present study serves to bring the females into the story being generated by a number of laboratories working with VIP and VIPR2 deficient mice. While in general the circadian phenotype observed with female mutants were similar to those gathered from males, there were also some interesting differences that highlight the importance of including both genders in our preclinical work (Clayton and Collins, 2014). In addition, there is good reason to be specifically interested in the role of VIP in the circadian regulation of female reproduction. VIP expressing neurons couple the SCN with GnRH neurons and alter their physiology. As previously described (Downs and Wise, 2009; Christian and Moenter, 2010), a decline in VIP has particular relevance to aging in women, where menopause and its corresponding index of symptoms have negative consequences on the quality of life for middle-aged women. In female rats, the beginnings of reproductive senescence are heralded by a decline in *Vip* expression in middle-age (Krajnak et al., 1998) that is correlated with a decline in the sensitivity of VIP-innervated GnRH neurons (Krajnak et al., 2001). When middle-aged female rats are treated with intracerebroventricular injections of VIP, the LH surge is restored to levels similar to young females (Sun et al., 2012). These findings suggest that reproductive aging may be due in part to hypothalamic changes as well as gonadal decline. Our findings that the absence of VIP has a greater impact on the SCN than the ovaries, supports the view that reproductive aging has a hypothalamic cause, and provides at least one mechanism (see Sellix, 2013 for discussion of others) by which circadian disruption can cause a decline in reproductive function.

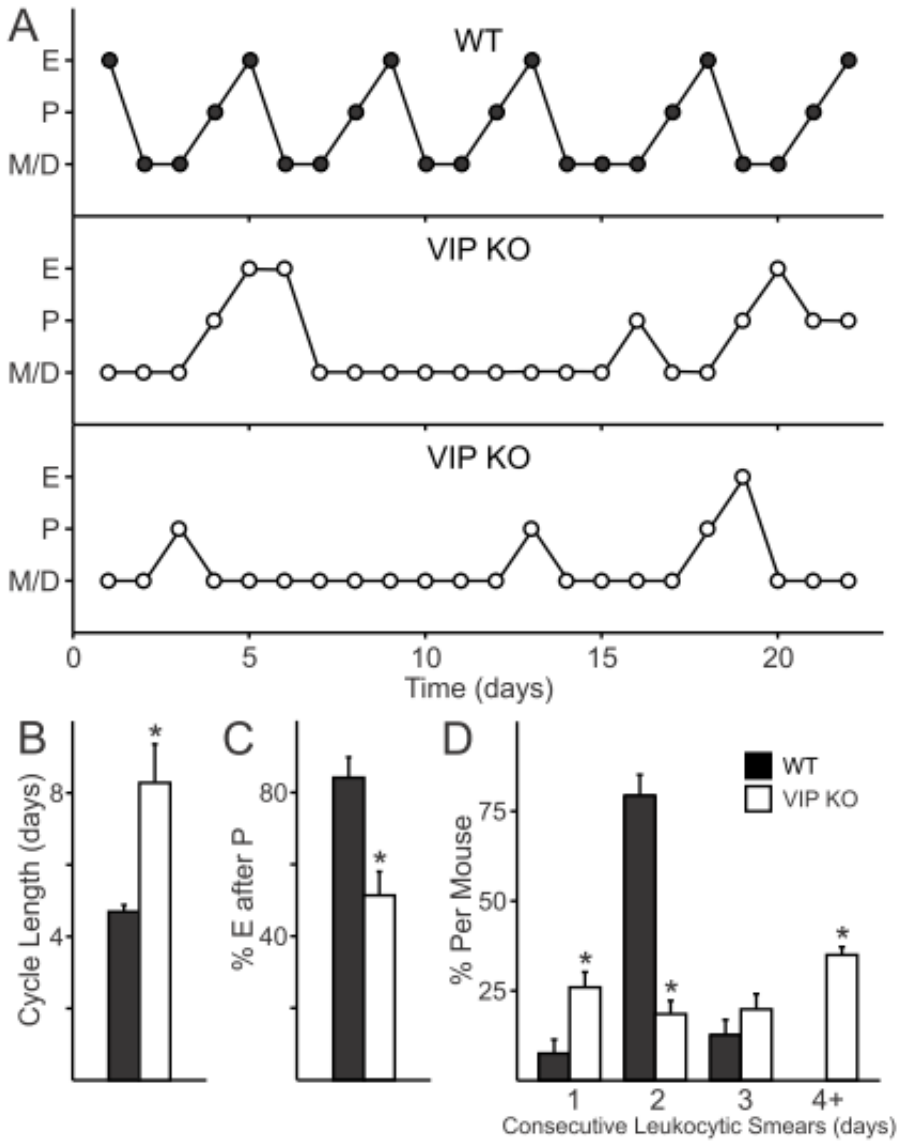

Figure. 4.1: Impact of VIP-deficiency on estrous cycles. **(A)** VIP-deficiency results in disrupted estrous cycles (middle and bottom) compared to the 4-5 day estrous cycles exhibited by WT females (top). P: proestrus, majority nucleated epithelial cells. E: oestrus, cornified cells. D/M: diestrus or metestrus, presence of leukocytic cells. **(B)** The average length of an estrous-to-estrous cycles in VIP-deficient mice is longer than in WT females (**P* < 0.05). **(C)** VIP-deficiency reduces the number of pro-estrous to estrous transitions. **(D)** The number of consecutive days in diestrus and metestrus increase with the loss of VIP (**P* < 0.05).

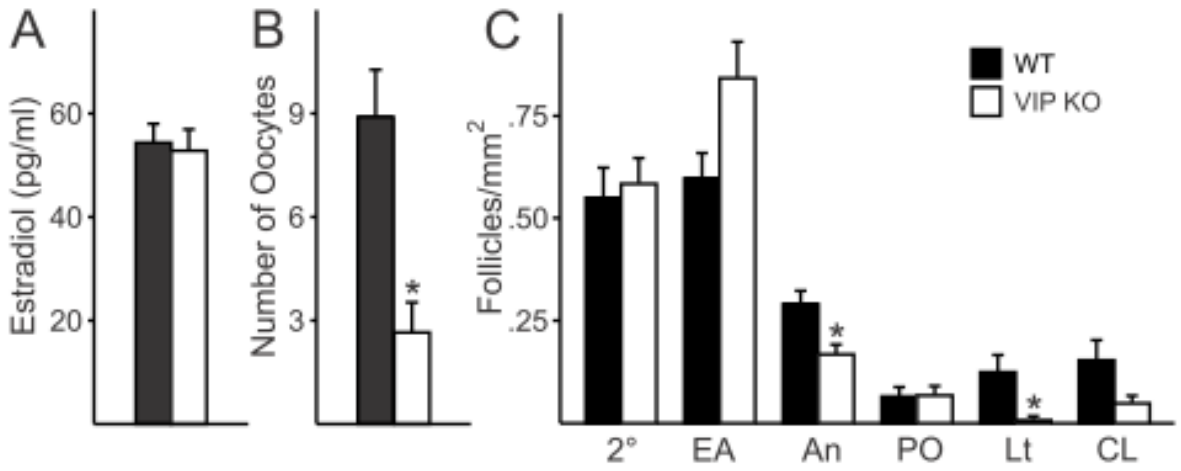

Figure 4.2: Impact of VIP-deficiency on circulating estradiol and ovulation in adult females. **(A)** The proestrus mid-day increase in serum estradiol is not affected by the loss of VIP in female mice. **(B)** The number of oocytes spontaneously released on the morning of oestrus is reduced in VIP KO oviducts compared to WT (**P* = 0.002). **(C)** The number of oocytes released in response to PMSG-hCG ovarian stimulation technique in hormone-primed female mice was not different between the genotypes.

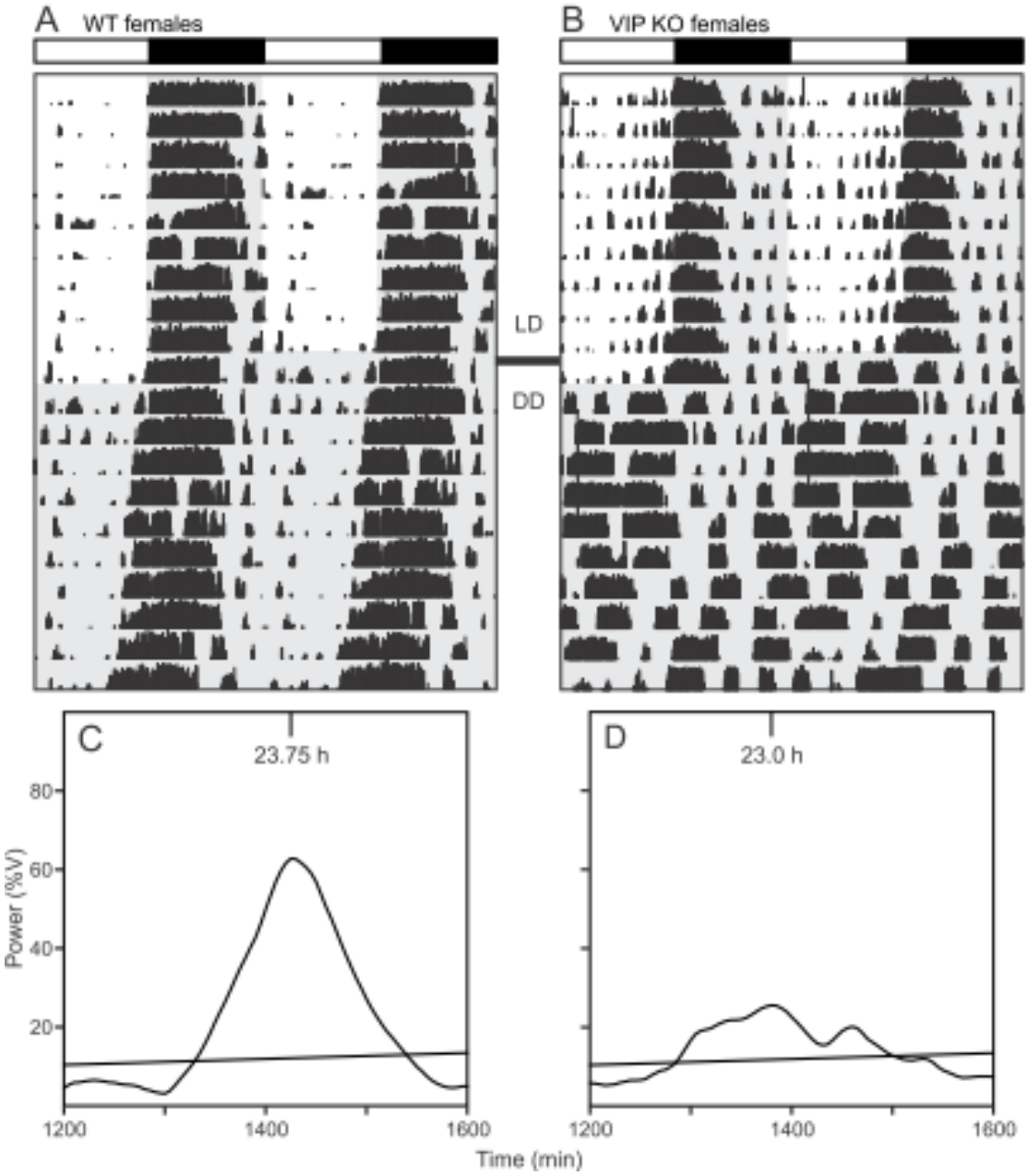

Figure 4.3: Representative actograms and periodograms of female WT **(A, C)** and VIP KO **(B, D)** mice under LD and DD conditions. **(A, C):** Wheel-running activity records are double plotted, gray shading on the actograms denotes lights off. **(B, D):** Plot of power of activity as a function of period (%V) under DD. The diagonal line represents 0.1% significance level.

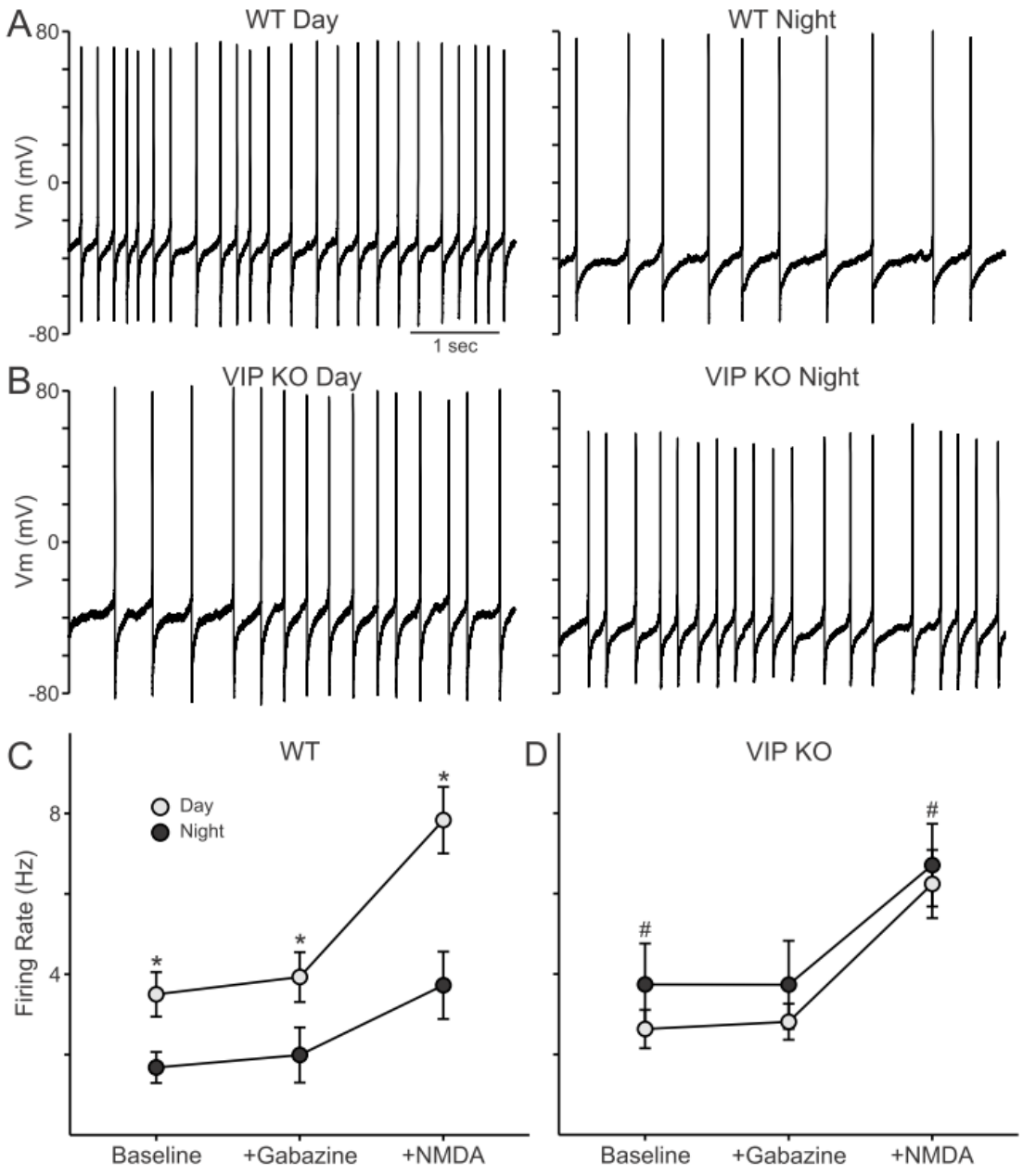

Figure 4.4: Reduced amplitude of spontaneous firing in VIP KO female SCN neurons. **(A, B)** Representative traces of spontaneous action potentials recorded during the day (left) and night (right) in WT **(A)** and VIP KO **(B)** dorsal SCN neurons. **(C)** WT (day *n* = 7, night *n* = 9) and **(D)** VIP KO (day *n* = 9, night *n* = 9) neuronal firing rate (Hz) population averages recorded under baseline conditions, in the presence of gabazine, and following NMDA treatment. Student's TTESTs determined a significant difference between day-time and night-time firing rates in WT (**P* < 0.05), not in VIP KO SCN. VIP KO firing rates were also found to be significantly different from WT ($^{\#}P$ < 0.05).

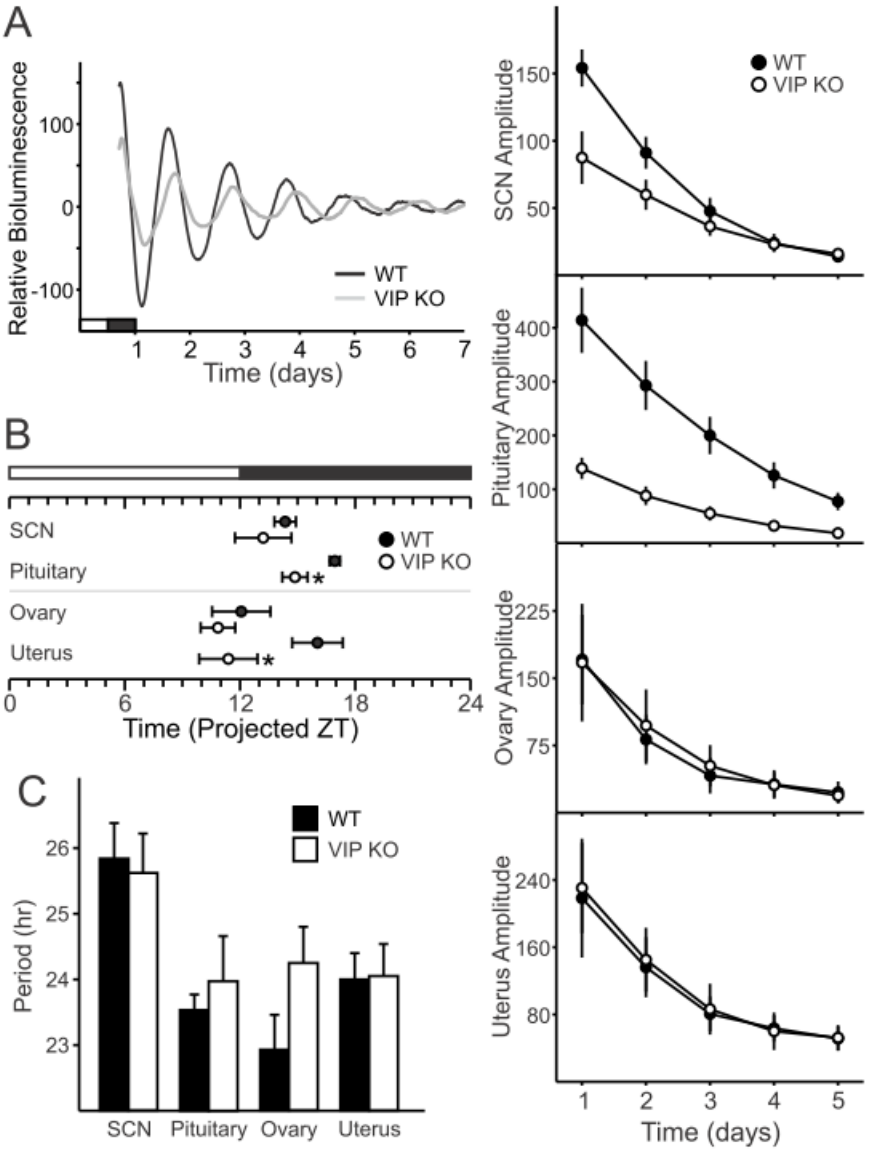

Figure 4.5: Impact of VIP-deficiency on the amplitude and phasing of PER2::LUC bioluminescence in female SCN and peripheral organs. **(A)** Representative bioluminescence rhythms from WT and VIP KO SCN *ex vivo* cultures. **(B)** Phase of peak PER2::LUC expression of pituitary and uterus are altered by VIP-deficiency relative to WT controls (**P* < 0.05). **(C)** The period of PER2::LUC bioluminescence is unaltered by the absence of VIP (*P* > 0.05). **(D)** Amplitude of PER2::LUC bioluminescence in SCN and pituitary are dependent on VIP (* *P* < 0.05), while the amplitude of the ovary and uterus are unaltered.

Part III. Circadian system dysfunction and neurodegenerative disease

Introduction

For many patients with chronic diseases of the nervous system, a good night's sleep is hard to find (Foley et al., 2004). It is increasingly evident that in neurodegenerative disorders such as Alzheimer's, Huntington's and Parkinson's diseases, sleep disruptions are common and occur early in the disease progression (McCurry et al., 2007; Morton, 2013; Willison et al., 2013). In some cases, prodromal sleep disturbance will occur years before the onset of dementia or motor symptoms characteristic of the specific disease in question (Iranzo et al., 2006; Julien et al., 2007). A number of possible mechanisms may underlie these sleep disturbances, but based on temporal aspects of patient sleep disturbances and animal model findings we propose that dysfunction of the circadian system is an integral contributing factor.

Focus on Huntington's disease

HD is caused by an expanded CAG trinucleotide repeat region in the gene encoding huntingtin (HTT) protein that translates into a long polyglutamine tract (Huntington et al., 1993). HD disease onset is typically in middle age, but this depends on the extent of the CAG repeat expansion and other genetic and environmental factors, so that symptoms can start quite young. The classical clinical features of HD are abnormal movements including both involuntary movements (chorea) and difficulty with motor coordination (Bonelli and Beal, 2012), which are associated with pathological and progressive neuronal cell loss in basal ganglia and cortex (Margolis et al., 2003; Schulte and Littleton, 2011). Although motor symptoms are requisite for the HD diagnosis, gene carriers typically exhibit early-onset non-motor symptoms including cognitive impairment that progresses to dementia, anxiety, apathy, personality changes, sleep disorders, depressed mood, and metabolic disorder (Lavin et al., 1981; Kremer et al., 1990; Petersén et al., 2005; Duff et al., 2007; Hinton et al., 2007; Wood et al., 2008; Paulsen et al.,

2008; Aziz et al., 2010a, 2010b; Peavy et al., 2010; Petersen et al., 2010; Vaccarino et al., 2011; Videnovic et al., 2014). These symptoms are likely related to alterations in hypothalamic, endocrine system, and cortical function (Duff et al., 2007; Soneson et al., 2010). Sleep disorders are extremely common in HD and have detrimental effects on daily functioning and quality of life for patients and their caregivers (Taylor and Bramble, 1997; Cuturic et al., 2009; Aziz et al., 2010b; Goodman et al., 2010, 2011; Morton, 2013). Due to the high prevalence of sleep disruptions in HD and because they often become apparent years before the onset of motor symptoms, an improved understanding of the mechanism underlying them has important implications for early diagnosis and treatment of gene carriers.

BACHD mouse model of HD

Previous work has shown that the R6/2 CAG150+ mouse model of HD exhibits a progressive and rapid breakdown of the circadian rest/activity cycle typified by loss of consolidated sleep, increased wakeful activity during the sleep phase, and more sleep during the active/waking phase (Morton et al., 2005; Pallier et al., 2007). No single mouse model can be expected to recapitulate all aspects of the human disease, so we sought to extend this work using the bacterial artificial chromosome (BAC) HD transgenic mouse – a sophisticated transgenic HD mouse model that expresses the entire human *Htt* gene and stable expression of 97 mixed CAA-CAG repeats in somatic and germline tissues under the control of human HD promoter (Gray et al., 2008).

The method of choice for screening mutations that influence the circadian system of small mammals is the monitoring of daily wheel-running activity. We examined the BACHD line using this method and found they exhibited low amplitude and fragmented rhythms in wheel running behavior under both a light/dark photic environment, and in constant darkness (Kudo et al.,

2011b). By young adulthood (3-6 mo), BACHD mice exhibit severe deficits in circadian rhythm fragmentation, rhythm power, and activity that further deteriorates with increasing age. The amplitude and coherence of behavioral rhythms progressively declines over the lifespan of both WT and BACHD mice, but this age-related decline occurs earlier in BACHD mice, with young BACHD mice exhibiting the circadian phenotype of an aged WT mouse. We also used video recordings to measure sleep distribution in BACHD mice, and although the effects of the human transgene were subtle, BACHD mice show significantly reduced sleep during the beginning of their rest phase. In other words, just like the human patient phenotype, BACHD mice show deficits in the onset of sleep.

Disrupted circadian regulation of the cardiovascular system in the BACHD mouse model

Poor cardiovascular health in additional to sleep related non-motor symptoms has been observed in HD patients. Alterations in autonomic tone that result in cardiac dysfunction are best evidenced by reductions in heart rate variability (HRV), a measure of variation in the beat-to-beat interval that reflects the dynamic balance of sympathetic and parasympathetic control of heart function. HRV normally displays a robust diurnal and circadian rhythm, but in BACHD mice day/night differences in HRV are lost and over 24 hours HRV is decreased. BACHD mice also show elevated resting phase heart rate and body temperature, and using electrocardiograph (ECG) we detected a loss of day/night differences in the PR interval (the time it takes for the cardiac electrical impulse to travel from the sinus node of the atria to the atrioventricular node). In BACHD mice, the PR interval was significantly elongated during the active period compared to WT mice, and implicates either aberrant autonomic system input to the cardiovascular system (Wallick et al., 1982; Carruthers et al., 1987) or deficits in the sensitivity of cardiomyocyte potassium handling (Akita et al., 1998). Consistent with the idea

that cardiac dysfunction is related to alterations in both branches of the autonomic nervous system, we found BACHD mice show a blunted baroreceptor reflex (Schroeder et al., 2011a). Decreases in HRV, alterations in the PR interval, and the inability to appropriately decrease heart rate and blood pressure during sleep, all support the hypothesis that autonomic function is compromised in BACHD mice and raises the possibility that circadian regulation of the autonomic nervous system is disrupted.

These findings in the BACHD mouse model are particularly relevant because similar decreases in HRV have also been reported in HD patients. Starting during the presymptomatic or early stages of HD, gene carriers show increased prevalence of reduced HRV relative to age-matched controls (Andrich et al., 2002; Kobal et al., 2010). Reduced HRV is generally considered an indication of poor cardiovascular health and a predictor for cardiovascular disease and mortality (Bigger et al., 1992; Buccelletti et al., 2009; Thayer et al., 2010). Considering cardiac failure is a leading cause of death among HD patients (Chiu and Alexander, 1982; Lanska et al., 1988), it is worth examining whether the loss of temporal control over autonomic output may be contributing to poor cardiovascular health in HD.

BACHD molecular clockwork may not be altered

To screen whether deficits in the molecular clockwork responsible for generating circadian oscillation underlies circadian deficits observed in BACHD mice, we examined PER2 expression in the SCN at peak and trough time-points, but found no differences in BACHD mice (Kudo et al., 2011b). These findings are inconsistent with prior work using the R6/2 line, suggesting behavioral impairments *are* accompanied by disordered circadian clock gene expression *in vivo* in the SCN, striatum, and liver (Pallier et al., 2007; Maywood et al., 2010). Due to the conflicting

findings between animal models, further work is required to definitively determine whether deficits in clock gene expression rhythms are a common phenotype in HD mouse models.

Reduced daytime firing rate of SCN neurons in BACHD mice during the early stages of HD progression

SCN neurons are spontaneously active and generate action potentials with peak firing rates during the day (Colwell, 2011) (**Fig. 5.0.1**). SCN rhythms in neuronal activity are believed to be necessary for regulating the autonomic nervous system and other physiological rhythms via a combination of direct neuronal and hormonal signaling pathways (Kalsbeek et al., 2006; Dibner et al., 2010). During the daytime, BACHD mouse SCN neurons showed significantly reduced spontaneous firing rates and an overall loss in firing rate rhythms (Kudo et al., 2011b). This critical finding is consistent with the hypothesis that reduced SCN output is part of the pathology responsible for circadian behavioral and physiological rhythm deficits observed in BACHD mice.

There are many ways to disrupt SCN function. The first potential mechanism by which mutant HTT may alter the function of the circadian system is by reducing the strength of inter-cellular coupling within the SCN circuit. Recent work in a variety of neurodevelopmental and psychiatric disorder mouse models have shown alterations in the balance between synaptic excitation and inhibition is related to specific disease states (Dani et al., 2005; Nelson and Turrigiano, 2008; Gogolla et al., 2009; Milnerwood and Raymond, 2010; Shepherd and Katz, 2011). In other mouse models of HD, similar pathophysiology is common. Increased inhibitory post-synaptic currents (IPSC) have been observed in cortex and striatum of R6/2 and YAC HD mouse models early in their disease progression, which are followed by late-stage decreases in spontaneous IPSC frequency (Cummings et al., 2009). Increased amplitude of spontaneous excitatory post-synaptic currents (EPSC) are seen at early stages in striatal medium spiny

neurons, and are followed by late stage decreases in spontaneous EPSC frequencies (Cepeda et al., 2003). These synaptic changes may underlie increased firing rates and decreased synchrony/coupling in both brain regions (Rebec et al., 2006; Miller et al., 2008; Walker et al., 2008), and similar alterations in synaptic transmission might explain disrupted SCN output we observed in the BACHD mouse.

A second possible mechanism for the loss of SCN firing rate rhythms may be alterations in the cell-autonomous pacemaking currents of BACHD SCN neurons. SCN spontaneous electrical activity is controlled by a set of currents that drive daily rhythms in action potentials that continue without synaptic input (Colwell, 2011) (**Fig. 5.0.1**). During the day, SCN neurons are relatively depolarized with a resting membrane potential (-50 to -55 mV) close to the threshold for generating an action potential (-45 mV). This relatively depolarized resting potential is the result of multiple cation currents that provide excitatory drive during the subjective day to which SCN neurons respond with sustained discharge for 4-6 hours without spike adaptation (de Jeu and Pennartz, 1997; Jackson et al., 2004; Kononenko et al., 2004). Additionally, prior work suggests that potassium (K^+) currents including fast delayed rectifier (FDR), A-type-K^+ current (I_A), and large-conductance Ca^{2+} activated K^+ (BK) currents are critical in the regulation of action potential dynamics and inter-spike intervals (**Fig. 5.0.2)**. Potentially, currents involved in regulating excitatory drive and/or those regulating action potential dynamics may underlie depressed daytime firing in BACHD neurons.

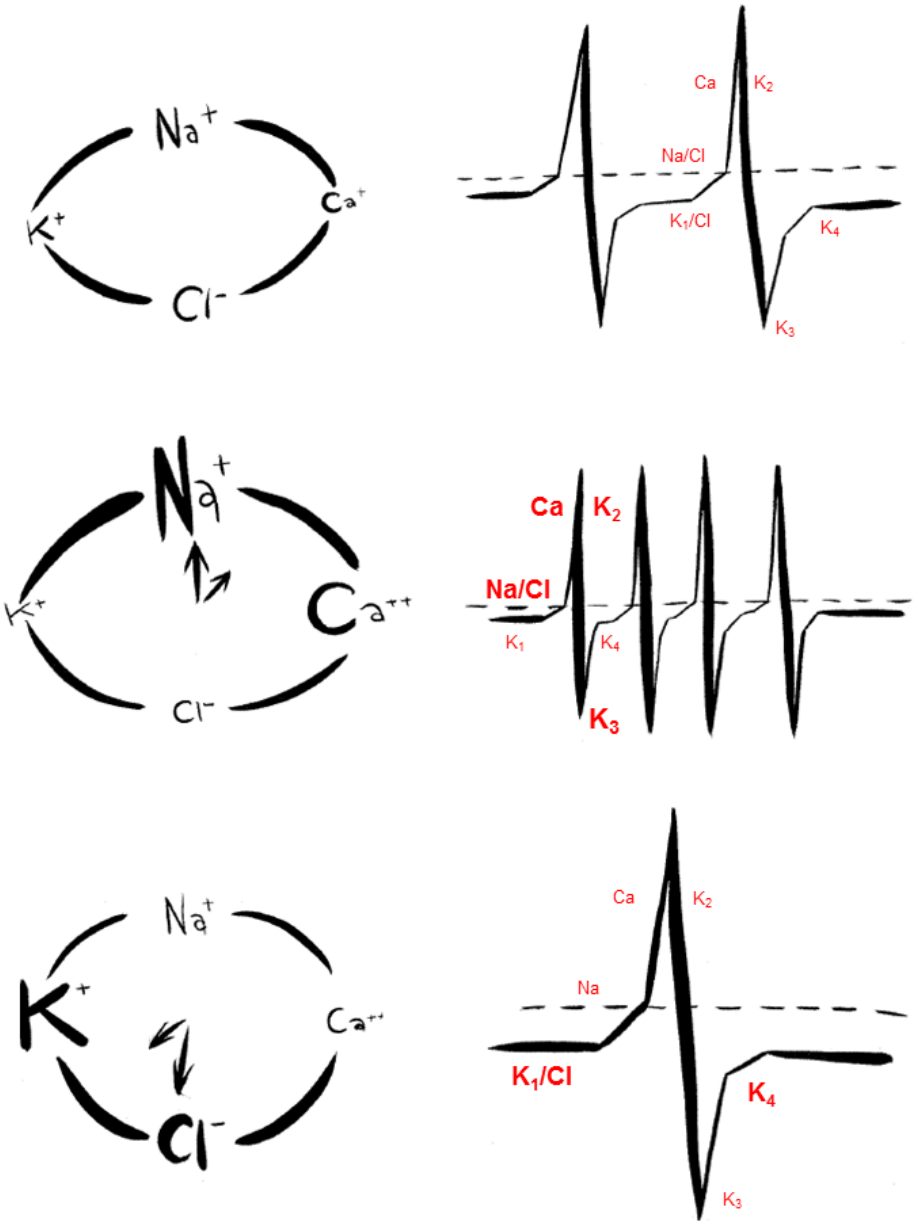

Figure 5.0.1: Ionic mechanisms of SCN neurons action potential generation. (Top) In an average neuron, inhibitory chloride and potassium currents K_1 (i.e. TEA sensitive) regulate inter-spike membrane potential. Excitatory chloride and persistent sodium currents depolarize membrane potential toward the action potential (AP) threshold (dotted line) where voltage-gated sodium and calcium currents are activated, initiating the depolarizing AP phase. Delayed activation of potassium currents K_2 (i.e. FDR, A-type) and K_3 (i.e. IbTX-insensitive), quickly re-hyperpolarize membrane potential, while K_4 (BK) currents regulate the duration of after-hyperpolarization. (Middle) During the daytime (ZT4-6), fast firing rates are mediated by relative increases in the currents regulating the rising and falling phase of the action potential, while during the night (bottom; ZT14-16), low firing rates are mediated by relative increases in the potassium currents (K_1 and K_2) that hyperpolarize membrane potential and increase after-hyperpolarization area following AP. Text size denote the relative contribution of currents.

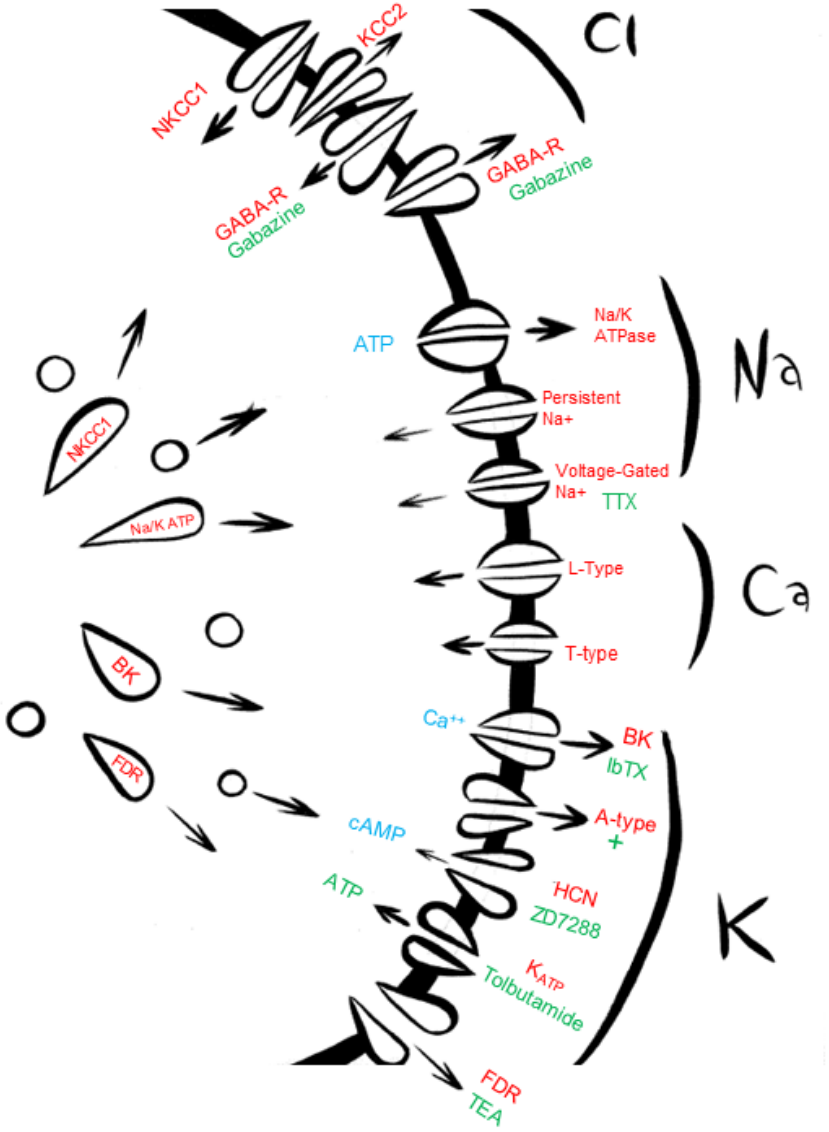

Figure 5.0.2: Ion channel regulation of action potential frequency in SCN neurons. Relative abundance of KCC2 and NKCC1 chloride symporters determine whether $GABA_A$-R chloride currents are excitatory or inhibitory. The $GABA_A$-R antagonist gabazine can be used to detect effects of GABA signaling on action potential frequency. Rhythms in ATP levels positively regulate Na^+/K^+ ATPase activity, thereby establishing a rhythmic electrochemical gradient needed to generate action potentials. Outward potassium currents, including BK, A-Type, and FDR are rhythmic in magnitude and can be identified using the current specific blockers iberiotoxin (IbTX), depolarization (+), and TEA respectively. HCN channel currents depolarize membrane potential in response to hyperpolarization via inward potassium and sodium currents and is positively regulated by cyclic nucleotides and can be blocked with ZD7288. K_{ATP} current hyperpolarizes membrane potential via an inwardly rectifying potassium current and is inhibited by intracellular ATP and the sulfonylurea tolbutamide. Current blockers (green text), current enhancers (blue text).

The subsequent chapters focus on understanding how mutant HTT alters the physiological properties of SCN neurons in the hope that a mechanistic understanding of the disrupted physiological output of BACHD SCN will aid in the development of interventions to treat circadian and sleep disruptions in HD patients and gene carriers. Successful therapies to treat sleep and circadian deficits in HD patients could vastly improve the quality of their lives and potentially even slow the progression of this incurable disease.

Chapter 5: Sex differences in circadian system dysfunction in the BACHD mouse model of Huntington's disease.

Huntington's disease (HD) is caused by a toxic gain of function mutation in the huntingtin gene (*HTT*) leading to progressive neuro-degeneration and dysfunction resulting in motor (chorea and dystonia), psychiatric (cognitive changes and depression), and other non-motor symptoms (sleep, hormonal, and metabolic) (Ross and Tabrizi, 2011). Generally, HD diagnosis is made sometime in the 4th or 5th decade, when a threshold of neurodegeneration in brain regions regulating movement is reached and characteristic motor symptoms emerge (DiFiglia et al., 1995; Ross and Tabrizi, 2011). Years before diagnosis, prodromal symptoms including disrupted sleep patterns, alterations in cognition, mood, and hormonal profiles are common, indicating the HD process is already well underway by the time diagnosis is made (Heuser et al., 1991; Marder et al., 2000; Petit et al., 2004; Morton et al., 2005; Duff et al., 2007; Aziz et al., 2009b, 2010b; van Duijn et al., 2010; Paulsen, 2011; Shirbin et al., 2013; Epping et al., 2013; Paulsen et al., 2013). Disrupted sleep, even in otherwise healthy individuals, can cause cognitive dysfunction, cardiovascular disease, metabolic dysfunction, affective disorder, gastrointestinal disturbance, and impaired immune system function (Moldofsky, 2001; Durmer et al., 2005; Wirz-Justice, 2006; Cohen et al., 2009; Mullington et al., 2009; Konturek et al., 2011; Besedovsky et al., 2012; Laermans et al., 2014; Leproult et al., 2014), all of which are also found in HD patients (Sorensen and Fenger, 1992; Morton et al., 2005; Paulsen and Conybeare, 2005; Paulsen et al., 2005, 2006, 2013; Duff et al., 2007; Aziz et al., 2010b; Peavy et al., 2010; Paulsen, 2011; Morton, 2013). The overlap of these symptoms raises the possibility that disrupted sleep is not only a symptom of HD, but that it triggers a host of health problems that feed forward into the HD pathological mechanism and accelerate disease progression. Promising evidence for this hypothesis includes a study of HD patients that found cognitive ability and functional capacity negatively correlated with sleep impairments, while depression

positively correlated with sleep impairments (Aziz et al., 2010b). Furthermore, a second study was able to delay cognitive decline in a mouse model of HD by pharmacologically imposing sleep (Pallier et al., 2007).

Identifying factors that mitigate sleep disruptions in HD will be essential for developing treatments to address it. Sex is one such factor, although its role in HD is unclear. Some epidemiological studies have found sex differences in HD age of onset, duration, or severity (Roos et al., 1991; Foroud et al., 1999; Pekmezovic et al., 2007; Zielonka et al., 2013), while others have not (Mattsson, 1974; Wexler, 2004). Sleep is a complex behavior regulated by multiple hypothalamic brain regions. The suprachiasmatic nucleus (SCN) regulates diurnal rhythms of sleep, while the lateral hypothalamus and magnocellular mammillary nucleus of the posterior hypothalamus regulate wakefulness (Saper et al., 2005). Post-mortem, patients' brains show specific patterns of cell loss within each of these key hypothalamic regions (Kremer et al., 1990; Timmers et al., 1996; Kassubek et al., 2004; Petersén et al., 2005; Björkqvist et al., 2006; Petersén and Björkqvist, 2006; Wamelen et al., 2013). How this atrophy relates to early sleep disruptions is unknown. The temporal characteristics of patient sleep complaints led us to further investigate the role of the SCN and circadian system in HD. The SCN contains a network of peptidergically distinct neurons that generate rhythms in electrical activity to orchestrate biological rhythms throughout the body using direct neural connections and paracrine factors (Reppert and Weaver, 2001; Schibler and Sassone-corsi, 2002; Lowrey and Takahashi, 2004; Tousson and Meissl, 2004; Schibler and Brown, 2005). The dynamics of SCN electrical activity rhythms are reflected at the behavioral and physiological level, with shorter periods in firing correlating with shorter periods in behavioral activity (Lehman et al., 1987; Ralph et al., 1990; Silver et al., 1996), and lower amplitude firing rate rhythms correlating with lower amplitude behavioral rhythms (Nakamura et al., 2011; Farajnia et al., 2012). Previously, we observed that SCN of BACHD male mice lost their ability to generate rhythmic electrical output, and this

correlated with reductions in behavioral and physiological rhythm amplitude, including, like in humans, a delayed sleep onset phenotype (Kudo et al., 2011b). Due to existing sex differences in human circadian rhythms, the prevalence of sleep disorders, and the severity of many neurodegenerative diseases (Wever, 1984; Ohayon, 2002; Czlonkowska et al., 2005; McCarthy et al., 2012; Smith and Dahodwala, 2014), we are interested in whether sex plays a role in the sleep disruptions reported for HD. Considering also that there are subtle sex differences in the circadian system of mice (Karatsoreos and Silver, 2007; Karatsoreos et al., 2007; Kuljis et al., 2013), we are testing the BACHD mouse model of HD for sex differences in behavioral rhythm abnormalities, as well as daytime SCN pathophysiology and pathology.

Materials and Methods

Animals and housing

All experimental protocols used in this study were approved by the UCLA Animal Research Committee, and followed guidelines and recommendations for animal use and welfare set by the UCLA Division of Laboratory Animal Medicine and National Institutes of Health. The mouse model of HD we employed in this study uses the bacterial artificial chromosome (BAC-)-mediated method to transgenically express the full length human mutant huntingtin gene encoding 97 glutamine repeats under the control of endogenous regulatory machinery (BACHD) (Gray et al., 2008). In our own breeding facility at UCLA, female BACHD dams backcrossed on a C57BL/6J background (minimum 12 generations), were bred with C57BL/6J (WT) males from The Jackson Laboratory (Bar Harbor, Maine), to obtain male and female offspring, either WT or heterozygous for the BACHD transgene. Genotyping was performed at 15 days of age by tail snips, and after weaning, naïve littermates were group housed by sex, until otherwise noted. Experiments testing behavioral rhythms, motor function, and body weight used WT and BACHD

mice from 3-7 months of age (n = 8, per group), while SCN physiology, and SCN anatomy focused on 3-month-old animals (n = 3 - 6, per group). All animals were housed in sound proof, humidity controlled chambers with controlled lighting conditions, using a 12 hour light, 12 hour dark cycle (12:12 LD, intensity 300 lux), unless otherwise noted. For all experiments, a light meter (BK precision, Yorba Linda, CA) was used to measure light-intensity (lux).

Rhythms in locomotor activity

Methods employed were as previously reported (Kuljis et al., 2013). Mice were individually housed in cages equipped with running wheels, and their voluntary wheel-running activity was recorded as revolutions (rev) per 3 minute intervals using a data acquisition system obtained from Mini Mitter Co. (Bend, OR). Diurnal rhythms in running wheel activity were assessed over 14 days, while animals were exposed to a 12:12 LD cycle, and circadian rhythms were assessed in constant darkness (DD) over the subsequent 10 days. To determine the effects of a phase delaying light treatment, a pulse of white light (100 lux, 10 min) was applied at Circadian time (CT) 16 after 10-14 days in DD. The resulting phase shift was calculated from the 10 days subsequent to the light pulse as previously described (Loh et al., 2013). All handling of mice in DD was performed with the aid of night vision goggles (FJW Industries, Palantine, IL).

Analysis of locomotor activity rhythms was as described (Loh et al., 2013). Briefly, we determined the period (hr) and power (%V, rhythm strength) by χ^2 periodogram analysis (Sokolove and Bushell, 1978). Periodogram-derived period estimates were confirmed using the slope of an eye-fitted line through behavioral onsets. Alpha was defined as the duration of the main activity bout from 10 days of activity, corrected for free-running period in DD. Fragmentation (bouts/day) and precision of day-to-day activity onset were determined using Clocklab (Actimetrics, Wilmette, IL). Fragmentation was defined by bouts/day, where a bout was

determined as 21 consecutive minutes of activity (maxgap setting of 21 min). Precision was determined by calculating the daily variation in onset from best-fit regression lines drawn through 10 days of activity, corrected for free-running period in DD. The phase shift following the phase delaying light treatment was determined by measuring the phase difference between best-fit regression lines drawn through the 10 days preceding and 10 days subsequent to the light treatment. Measurements were made by investigators blind to the experimental group and reported values are averaged between two independent determinations.

Statistically significant effects of sex and age on activity rhythm parameters within the BACHD line or genotype and age for BACHD and WT female mice, were tested using Two-Way ANOVA, with $P < 0.05$. When main or interaction effects were identified, significant genotype differences within sex and significant sex differences within genotype were identified post-hoc using Two-Tailed T-Tests, with $P < 0.05$ or the Holm-Sidak method for multiple pairwise comparisons.

Motor Testing

Rotarod testing was performed as previously described (Loh et al., 2013). Tests were performed during the early night under conditions of dim red light (<5 lux). Animals were trained for 5 trials (> 1 min rest interval between trials) on an accelerating rotarod apparatus (5 to 38 rpm, Ugo Basile, Varese, Italy). On the next day, mice were placed on the rotarod apparatus, and the latency to fall from the rotarod was recorded from 5 trials. An average of the 5 trials is reported. Significant effects of genotype, sex, and/or age on rotarod performance were tested using Three-Way ANOVA, with $P < 0.05$. When main or interaction effects were identified, significant genotypic differences within sex and age and significant sex differences within genotype and age were identified post-hoc, using Two-Tailed TTESTs, with $P < 0.05$

The challenge beam test, a modification of the beam walking test as first described by Fleming and colleagues (Fleming et al., 2004), was performed as previously described (Loh et al., 2013). Animals were trained to walk across the beam, from the widest to narrowest widths, to their home cages in the early night for 2 consecutive days (5 trials/day). On the day of testing, a wire grid (10 x 10 mm spacing) was overlaid onto the beam. Mice were recorded as they crossed the gridded beam, and videos were scored *post hoc* by two independent investigators for the number of steps taken and errors made per beam width. We considered an error to be when more than half of the foot in question fell below the grid. Averages of 5 testing trials are reported. Statistically significant effects of sex and age on challenge beam performance for BACHD mice were tested using Two-Way ANOVA, with $P < 0.05$. When main or interaction effects were identified, significant sex differences within age and significant age differences within sex were identified post-hoc using Two-Tailed TTESTs, with $P < 0.05$.

Body weight

A separate cohort of animals from the same colony was examined weekly for body weight from 2 to 7 months of age.

Electrophysiology

Methods for electrophysiology recordings were similar to those previously reported (Kuhlman and McMahon, 2004; Kudo et al., 2011b; Kuljis et al., 2013). Animals were briefly anesthetized with isoflurane before decapitation and brain removal at ZT2 and ZT11.5 for daytime (ZT4-6) and nighttime (ZT14-16) recordings respectively. After removal, brains were chilled in ice-cold slice solution (in mM: 26 $NaHCO_3$, 1.25 NaH_2PO_4, 10 glucose, 125 NaCl, 2

KCl, 1 $MgCl_2$, 1 $CaCl_2$; Sigma-Aldrich) for 5 minutes before trimming and slicing using a Leica VT1200S vibrotome (Nussloch, Germany). Two to three coronal slices (250 μm) containing the SCN were transferred into ice-cold artificial cerebrospinal fluid (ACSF) solution (in mM: 26 $NaHCO_3$, 1.25 NaH_2PO_4, 10 glucose, 125 NaCl, 3 KCl, 2 $MgCl_2$, 2 $CaCl_2$; Sigma-Aldrich), then incubated at 32°C for 30 minutes, before a final room temperature incubation for one hour. Slices were then placed into a recording chamber (PH-1, Warner Instruments, Hamden, CT) attached to the stage of a fixed upright DIC microscope (Olympus, Tokyo, Japan) and superfused continuously (2 ml/min) with room temperature ACSF. All solutions were adjusted for pH (7.20 - 7.40) and osmolarity (290 – 310) and aerated continually with 95% O_2/ 5% CO_2 for at least 15 minutes before use. Multiple slices containing the SCN were collected, but only mid-most SCN slices were used for recording because of its relatively discrete anatomical subdivisions (Yan et al., 2007). Mid-SCN was identified based on the morphology of the third-ventricle and optic chiasm, as well as SCN cell density. Dorsal SCN neurons, which have robust rhythms in electrical activity rhythms within the SCN in the absence of input (Jobst et al., 2004; Aton et al., 2006), were classified by their location just dorsal to the tip of the third ventricle within the mid-SCN slice.

Electrode micropipettes (3-7 MΩ) were used for whole cell patch clamp recordings. They were pulled from glass capillaries (WPI, Sarasota, FL) using a multistage puller (Sutter P-97, Novato, CA) and filled with standard internal solution (in mM: 112.5 K-gluconate, 4 NaCl, 17.5 KCl, 0.5 $CaCl_2$, 1 $MgCl_2$, 5 MgATP, 1 EGTA, 10 HEPES, 1 GTP, 0.1 Leupeptin, 10 Phosphocreatine; pH adjust to 7.2 using KOH and osmolarity adjusted to 290 using sucrose; Sigma-Aldrich). Single-cell recordings were made using the Axopatch 200B amplifier (Molecular Devices, Sunnyvale, CA) and monitored on-line with pCLAMP (Ver. 10, Molecular Devices). The amplifier's voltage-offset was used to cancel junction potentials between the micropipette's internal solution and the extracellular solution (ACSF). While in voltage-clamp mode (0 mV

holding), cells were approached with electrode micropipettes using slight positive-pressure , then by switching to negative-pressure and gradually lowering the holding potential to -70 mV, a high resistance seal (2-10 GΩ) was formed. A second pulse of negative pressure was used to break the membrane and enter whole-cell mode. While in voltage-clamp mode, membrane holding current, cell capacitance, and access resistance were tested using a 5mV step applied at 5 Hz from the -70 mV holding potential. Only cells with holding current between 0 and -20 pA, capacitance less than 20 pF, and access resistance less than 60 pA (typically 10 to 40 MΩ) were used. These parameters were monitored during the course of the experiment, and if they changed significantly, that cell's data was not included in analysis.

Following the formation of a high-resistance seal and going whole-cell, the amplifier mode was switched from voltage- to current-clamp, and baseline spontaneous firing rate (SFR) was recorded during the subsequent minute. No current injection was applied during SFR recordings. SFR was calculated using the total number of action potentials recorded during 1 minute and expressed as a rate in Hertz (Hz). Daytime SFRs for WT, BACHD, male and female mice were determined by averaging data from between 10 and 20 neurons collected from a minimum of 3 animals per group. Action potential (AP) properties were analyzed using ClampFit software's event detection feature (Ver. 10.4, Molecular Devices).

Resting membrane properties were examined in separate slices from SFR experiments. These slices were treated with TTX (1 μM; Tocris Bioscience, Minneapolis, MN) and gabazine (10 μM) to block action potential and GABAergic synaptic potentials, for at least 2 minutes before resting membrane properties were recorded. Multiple neuronal recordings were attempted per slice, and in between cells, drugs were washed off for 2-5 minutes, or long enough to partially unblock voltage gated sodium and GABA channels to partially restore action potential generation and facilitate discrimination of electrically active cells (neurons) from non-

electrically active cells (glia), both of which are present in the SCN. Previous studies have shown that Per1::GFP SCN neurons have circadian rhythms of input resistance, which underlie these neurons' circadian rhythms of membrane potential and thereby excitability (Kuhlman and McMahon, 2004). A similar protocol was used to examine the intrinsic excitability of SCN neurons of BACHD male and female neurons, but without the use of a fluorescent marker of gene expression to guide neuron selection. Similar to SFR experiments, after forming a high resistance seal and going into whole-cell mode in voltage-clamp (-70 mV), the amplifier was immediately switched to current-clamp mode. Each neuron reached a stable membrane potential typically within the first 10 seconds of the switch. The resting membrane potential (RMP) was recorded over the subsequent one to three minute period, and calculated as the average membrane potential during that time. Next, the neuron was treated to hyperpolarizing current steps (500 msec, -5 to -25 pA in 5 pA steps) three consecutive times. Resulting traces were filtered for electrical interference before analysis (harmonics 1:1, 119 cycles to average, auto-reference frequency). For each current injection step, peak hyperpolarization (using 5 smoothing points) was identified for each of the three replications and averaged. All other parameters (hyperpolarization peak time, area, and slope of the hyperpolarizing membrane response between 10 and 90%) were calculated from an average trace created using the three replications. Cells that weren't able to maintain steady membrane potential between current injection treatments were excluded from analysis.

Statistically significant effects of genotype and or sex on SFR, inter-spike membrane potential, and resting membrane potential were examined using Two-Way ANOVA, with $P < 0.05$. When main or interaction effects were identified, significant genotype differences within sex and significant sex differences within genotype were identified post-hoc using the Holm-Sidak method for multiple pairwise comparisons. Statistically significant effects of current injection, sex, and genotype on voltage responses were examined using Three-Way ANOVA,

with $P < 0.05$. When main or interaction effects were identified, significant genotype differences within sex and significant sex differences within genotype for each current step were identified post-hoc using Two-Tailed T-Test, with $P < 0.05$.

Anatomy

At 3 months of age animals were anesthetized in an isoflurane chamber between ZT 5 and 7, then perfused intracardially with 20 mL 0.9% saline in 0.1 M phosphate buffer (PB; pH 7.4) containing heparin (2 units/mL) and 40 mL 4% paraformaldehyde in 0.1 M PB. Brains were post-fixed overnight at 4 °C and then cryoprotected in 20% sucrose in 0.1 M PB overnight at 4 °C, before being flash frozen on CYRO-OCT Compound (Fisher Scientific) and sliced using a cryostat.

Brains used for VIP and AVP immunohistochemistry and cell counting were sliced coronally at 50 µm. Free-floating sections were washed with phosphate buffered saline (PBS) before 10 minute incubation with an endogenous peroxidase blocker (3% hydrogen peroxide, 10% methanol in PBS). Slices were washed again and incubated for at least one hour in a serum blocking solution (3% normal goat serum, 0.1% Triton X-100 in PBS) before a 48-hour incubation in primary antibody solution, containing either rabbit anti-VIP (1:2000, ImmunoStar; Hudson, WI, USA) or guinea pig anti-AVP (1:1000; ImmunoStar, Hudson, WI, USA) antibody in serum blocking solution. After primary antibody incubation, slices were washed, then incubated for 2 hours with the appropriate biotinylated goat secondary antibody (1:150; Vector Laboratories, Burlingame, CA, USA) in serum blocking solution. Slices were then treated with avidin-biotin complex (Vector Laboratories, Burlingame, CA, USA) for 45 minutes, and finally stained with nickel (II) chloride-enhanced diaminobenzidine (DAB; Sigma) for visualization. Slices underwent a final wash in tris-buffered saline, and were mounted on microscope slides

before cresyl violet counterstaining. Slices were then dehydrated in an alcohol series and xylenes, then cover-slipped with Depex mounting medium (Fisher Scientific).

Stereological analysis was performed by one experimenter using an AxioImager M2 ApoTome microscope (Zeiss), equipped with a motorized stage controlled by StereoInvestigator software (MicroBrightField Biosciences, Williston, VT, USA). The area of interest was defined as the entire SCN, which was outlined at 10x magnification using anatomical markers and cell density as guides. Due to the SCN's small area and the low number of VIP^+ or AVP^+ neurons in the SCN, stereological parameters were designed to cover the entire area of interest, and all immunopositive cell bodies were counted directly at 40x magnification under Köhler illumination. Statistically significant sex differences were examined using Mann-Whitney Rank Sum Test, with $P < 0.05$. Statistically significant effects of genotype and/or sex were examined using Two-Way ANOVA, with $P < 0.05$. All reported values are Means ± 95% C.I. of Mean.

Results

Delayed female BACHD mouse activity rhythm deterioration

Sex differences in BACHD mouse diurnal and circadian wheel running activity were examined at 3 and 6 months of age (**Fig. 5.1** and **Table 5.1**). Male and female BACHD mice displayed a similar age-related decline in diurnal (**Fig. 5.1E**) and circadian rhythm power. Activity levels in LD (**Fig. 5.1F**) and DD were protected in BACHD female mice at 3 months of age, but declined significantly by 6 months to levels similar to that of BACHD males. WT male mice have more precise wheel-running activity onsets (Iwahana et al., 2008; Kuljis et al., 2012). Unlike normal animals, at 3 months of age, BACHD mice do not display this sex difference, and while both sexes displayed age-related decreases in precision by 6 months, BACHD males

were more affected than females, so that male activity onsets in LD were significantly less precise than female's at 6 months of age (**Fig. 5.1G**) - a reversal of the normal sex difference. Notably, there was no sex difference in precision when animals were housed in DD. Similarly, both sexes showed age-related increases in activity fragmentation, but males again were more severely affected, so that by 6 months of age, BACHD male activity was significantly more fragmented than BACHD female activity (**Fig. 5.1H**). Previously we reported that the period of BACHD male mouse wheel running activity rhythms in DD was significantly longer than that of WT male controls (Kudo et al., 2011b). Here we also found BACHD male period lengths to be equally long to our previous report, and found that BACHD females had similar period lengthening at 3 months of age, but by 6 months of age BACHD females displayed age related period shortening so that their free-running activity rhythm period became significantly shorter than that of BAHCD males (**Fig. 5.1I**). Lastly, we observed that sex differences in photic phase shifting (Karatsoreos et al., 2011b; Kuljis et al., 2013) are also found in BACHD mice, with male BACHD mice exhibiting smaller magnitude phase shifts in response to CT16 light-pulse (LP) than females, but only at 3 months of age. By 6 months of age, BACHD females experienced age-related decreases in phase shift magnitude, and the sex difference observed at 3 months was lost (**Fig. 5.1J**).

The interaction of sex and the HD causing gene's effects on the circadian system are nuanced and age dependent. To fully understand how disease progression differs in females, we also compared BACHD female wheel-running activity rhythms to that of WT female littermate controls (**Fig. 5.2** and **Table 5.2**). Like males, BACHD female mice have reduced power rhythms in LD and DD relative to sex matched WT littermates, but unlike males, their activity levels were protected relative to WT female controls at 3 months of age. BACHD females did however exhibit significant activity reductions relative to WT females by 6 months of age, indicating that activity levels are protected only early in adulthood for BACHD females.

Additionally, the number of activity bouts was similar for WT and BACHD females at 3 months of age. Both genotypes' activity became more fragmented by 6 months, but BACHD females showed greater age-related fragmentation, so that BACHD female rhythms were significantly more fragmented than that of WT female controls. At 3-months-of-age, BACHD female free-running activity rhythm period length was longer than that of WT females; however, unlike BACHD male mice that maintain long period lengths throughout the first year of life (Kudo et al., 2011b), there was an interaction of age and genotype on female activity rhythm period length. BACHD females exhibited significant period shortening and WT female littermates exhibited slight, but non-significant period lengthening so that by 6 months of age their free-running periods were no longer different. Additionally, the precision of female rhythms and the magnitude of CT16 LP induced phase shifts were similar for BACHD and WT females, indicating a male specific factor disrupts light-entrainment properties in the BACHD male circadian system (**Fig. 5.3**).

Male and female SCN pathophysiology in BACHD mice

Previously, we found that male BACHD mouse SCN neurons fail to exhibit daily rhythms in electrical activity due to depressed daytime spontaneous firing rate (SFR) (Kudo et al., 2011b). Following up on this study, daytime SFR was examined in both sexes of BACHD mice to determine whether sex differences in wheel-running activity rhythms are related to the protection of SCN physiological properties (**Fig. 5.4**). Effects of genotype and sex on daytime SFR were tested using Two-Way ANOVA, and a significant effect of genotype ($F_{1, 64} = 24$, $P < 0.001$), but not sex ($F_{1, 64} = 0.183$, $P = 0.670$) nor interaction of genotype and sex ($F_{1, 64} = 3.315$, $P = 0.073$) was identified. Relative to WT controls, daytime SFR was depressed in both BACHD male (-3.8 ± 1.3 Hz, T = 4.38, $P < 0.001$) and BACHD female (-1.7 ± 1.0 Hz, T = 2.39, $P = 0.02$)

mouse SCN neurons (**Fig. 5.4B**). Although the interaction of sex and genotype on SFR approached but did not reach significance, this study may have been underpowered to detect subtle sex differences. Clues supporting this notion include the following, first, a sex difference in WT mouse SCN SFR has previously been shown (Kuljis et al., 2013), and although significant sex differences among WT control SFRs were not detected in this study, the data show a similar pattern, with WT female SFRs trending toward lower rates than that of WT males (-1.3 ± 1.3 Hz., T = 1.72, *P* = 0.09). Second, in contrast to the WT trend, BACHD female SFRs trended toward higher rates than that of BACHD males (+0.8 ± 1.0 Hz, T = 0.92, *P* = 0.36). Third, although an interaction of sex and genotype was not detected for SFR, it was detected for action potential (AP) amplitude, which is closely related to SFR. Generally, lower SFRs associate with larger AP amplitudes. So although WT female SFR was not significantly lower than WT male SFR, WT female AP amplitude *was* significantly larger (+18 ± 13 mV, T = 2.16, *P* = 0.04). Additionally, although BACHD female SFR was not significantly higher than BACHD male SFR, BACHD female AP amplitude *was* significantly lower than BACHD male AP amplitude (-20 ± 15 mV, 2.04, *P* < 0.05). We also examined a variety of other AP properties, but no additional effects of sex and genotype were identified (**Table 5.3**).

Finally, resting membrane properties were examined in electrically silent neurons using bath application of TTX (1 µM) to inhibit AP generation, and gabazine (10 µM) to silence synaptic activity. Under similar conditions, it has previously been shown that WT SCN neural excitability rhythms are regulated by daytime membrane depolarization related to the closure of potassium channels evident by increases in input resistance (Kuhlman and McMahon, 2004). Since daytime SFR is depressed in BACHD SCN neurons, we tested whether resting membrane potential was hyperpolarized and/or whether input resistance was decreased, as would be expected if depressed daytime SFR were related to dysregulation of the rhythmic potassium currents driving rhythms in intrinsic membrane potential in SCN neurons. However,

resting membrane potential was not hyperpolarized during the day in BACHD SCN (**Fig. 5.4D**, **Table 5.3**). Considering both BACHD sexes displayed depressed SFR and neither displayed differences in resting membrane potential, unexpectedly an interaction of genotype and sex on the voltage responses of SCN neurons to negative current step injections was detected using Three-Way ANOVA, although post-hoc pairwise comparisons failed to detect significant group differences for any given current injection step magnitude (**Fig. 5.4E + F**). The average voltage response to current injection for each group was used to calculate input resistance (**Table 5.3**), and consistent with the idea that more potassium channels are open at resting membrane potentials and inhibiting neural excitability, smaller input resistances were observed for BACHD female SCN neurons than for WT female SCN neurons (-0.6 ± 0.3 MΩ, T = 2.71, $P = 0.007$). Even though the greatest reduction in excitability was observed for BACHD male SCN neurons, they displayed slightly increased input resistances relative to WT male controls (+0.4 ± 0.2 MΩ, T = 2.10, $P = 0.04$). In the absence of significant membrane hyperpolarization, these changes are difficult to interpret, but considering they are relatively small compared to those seen across time in WT SCN neurons, they likely do not fully account for the reduced daytime SFR observed in BACHD SCN. In summary, both male and female BACHD SCN neurons show evidence of pathophysiology, but it cannot be accounted for by membrane hyperpolarization.

No change in AVP or VIP cell counts in the SCN of male and female BACHD mice

Since there is little evidence of pathophysiological mitigation underlying the delayed activity rhythm phenotype for BACHD females, we tested an alternative hypothesis. Reductions in the signaling peptides AVP and VIP can disrupt SCN circuit function (Harmar, 2003; Maywood et al., 2011) and physiological output rhythms (Li et al., 2009; Loh et al., 2011; Schroeder et al., 2011b). We predicted differential reductions in peptide expression between

male and female BACHD mice might underlie sex differences in behavioral rhythm deficits. We examined BACHD SCN for sex differences in the number of cell bodies immunoreactive for AVP (**Fig. 5.5A**). Although there was a trend for BACHD female SCN to contain more AVP^+ cell bodies (889 ± 198, n = 5) than BACHD male SCN (658 ± 283, n = 5), this difference was not significant (T = 19, *P* = 0.095). We also examined BACHD SCN for sex differences in the number of cell bodies immunoreactive for VIP (Fig. 3B). Male BACHD SCNs had similar VIP^+ cell counts (387 ± 70, n = 6) to BACHD females (427 ± 172, n = 5), and there was not a statistically significant sex difference (T = 33.0, *P* = 0.66). We also examined WT SCN AVP and VIP expression to see if there were normal sexual dimorphisms in peptide expression at this age in mice (**Fig. 5.6**). Male WT SCN had similar numbers of AVP^+ cell bodies (734 ± 291, n = 5) to female WT SCN (839 ± 171, n = 5; T = 23.00, *P* = 0.4), and WT male SCN VIP^+ cell counts (391 ± 152, n = 6) were also similar to WT female counts (411 ± 40, n = 5; T = 27.00, *P* = 0.7). Two-Way ANOVA, failed to detect an effect of genotype on AVP ($F_{1, 19} = 0.023$, *P* = 0.9) or VIP expression ($F_{1, 19} = 0.02$, *P* = 0.9). It also failed to detect an effect of sex on AVP ($F_{1, 19} = 3.75$, *P* = 0.07) or VIP expression ($F_{1, 19} = 0.43$, P = 0.5), and failed to detect interaction effects of genotype and sex on AVP ($F_{1, 19} = 0.53$, *P* = 0.5) or VIP expression ($F_{1, 19} = 0.05$, *P* = 0.8). If alterations in AVP and VIP expression are a component of SCN pathology in the BACHD mouse phenotype, it likely does not occur until later in disease progression.

Sex differences in motor coordination and body weight

The presentation of characteristic motor symptoms is requisite for the HD diagnosis (Ross and Tabrizi, 2011). To test whether BACHD mice exhibit analogous motor dysfunction, and whether there are sex differences in the onset, severity, or progression of this dysfunction, two motor coordination tests were performed at 3 and 6 months of age in male and female

BACHD mice. The first, called the challenge beam test (Loh et al., 2013) requires mice to traverse across 4 consecutively placed, increasingly narrow (1-4) beams covered in wire mesh that increasingly require balance, motor control, and motor coordination. As expected, all mice made more step errors on the narrower beams at both 3 and 6 months of age (**Fig. 5.7A** and **Table 5.4**). We also observed sex differences in performance at both ages. At 3 months of age, BACHD females made significantly fewer errors on the first and widest beam (-0.28 ± 0.06 errors, T = 3.04, *P* = 0.005), evidence that only gross motor control is protected for females. Additionally, age-related deterioration in motor control on the challenge beam test largely occurred only for females (Beam 1: +0.43 ± 0.21 errors, T = 4.70, *P* < 0.001; Beam 2: +0.88 ± 0.50 errors, T = 3.34, *P* = 0.002; Beam 3: +0.66 ± 0.53 errors, T = 2.39, *P* = 0.02; Beam 4: 0.99 ± 0.64, T = 2.45, *P* = 0.02). By 6 months, BACHD female step errors were on par with male's, except on the third beam for which BACHD females still performed significantly better than males (+0.84 ± 0.53 errors, T = 3.03, *P* = 0.005). This is also the only beam for which males had more step errors between 3 and 6 months of age (+1.39 ± 0.50 errors, T = 5.01, *P* < 0.001). We also examined the time it took animals to cross the challenging beams, but neither sex ($F_{1, 31}$ = 0.062, *P* = 0.8) nor age ($F_{1, 31}$ = 2.9, *P* = 0.1) had a statistically significant effect (**Fig. 5.7B**). In summary, performance on the challenge beam task showed age-related impairment for BACHD mice, occurring later for females.

We also used the rotarod to test for motor coordination deficits in BACHD animals relative to WT littermates in both sexes and found an interaction of genotype, sex, and age on performance (**Fig. 5.7C** and **Table 5.3**). First, compared to WT controls, BACHD rotarod performance was poorer at both 3 months (BACHD male -83 ± 50 sec., T = 2.69, *P* = 0.02; BACHD female -203 ± 30 sec., T = -2.66, *P* < 0.001) and 6 months of age (BACHD male -119 ± 28 sec., T = 7.50, *P* < 0.001; BACHD female -124 ± 67 sec., T = 2.79, *P* = 0.01). Previous studies did not detect sex differences among BACHD mouse performance using this test

(Menalled et al., 2009; Southwell et al., 2009). At 3 months, we too did not observe sex differences in the latencies to fall off rotarod for BACHD mice (BACHD female -4 ± 30 sec., T = 0.211, *P* = 0.8); however, while BACHD male mice exhibited age related decline in rotarod performance (-94 ± 28 sec., T = 3.88, *P* = 0.002), BACHD females did not (+60 ± 67 sec., T = -1.92, *P* = 0.08). At 6 months, BACHD female rotarod performance was significantly better than that of BACHD males (+149 ± 67 sec., T = -4.82, *P* < 0.001). Notably, WT female littermates also performed significantly better than WT males, but only at 3 months of age (WT female +115 ± 89 sec., T = -2.7, *P* = 0.02). Although there was no significant age-related change to WT rotarod performance (6 vs. 3 mo.: WT male +42 ± 63 sec., T = -1.21, *P* = 0.24; WT female -19 ± 81 sec., T = 0.375, *P* = 0.7), the sex difference did not persist at 6 months of age when WT males and females had similar latencies to fall (+54 ± 81 sec., T = -1.26, *P* = 0.23).

Multiple factors influence an animal's ability to perform a motor task in addition to the integrity of the cortico-striatal motor circuit. Different motor tests differentially require motor strength, maneuverability, balance, and motor learning. Some traits like body size, which are sexually dimorphic, influence these parameters. We examined body weights of male and female BACHD and WT control animals weekly, and found body weight does not fully account for the sex differences in motor coordination we observed in young WT mice or middle age BACHD mice (**Fig. 5.5D**). Effects of genotype, sex, and/or age on bodyweight were tested using Three-Way ANOVA and highly statistically significant main effects of genotype ($F_{1,880}$ = 208, *P* < 0.001), sex ($F_{1,880}$ = 471.0, *P* < 0.001), and age ($F_{19,880}$ = 11.58, *P* < 0.001) were found, as well as interaction effects of genotype and sex ($F_{1,880}$ = 17.95, *P* < 0.001) and sex and age ($F_{19,880}$ = 2.54, *P* < 0.001). WT males weighed more than females throughout early adulthood, but this difference in weight was greater at 6 months when there was no sex difference in rotarod performance (+11.2 ± 3.4 g, T = 9.31, *P* < 0.001), than at 3 months when WT females performed better on rotarod than males (+5.8 ± 1.8 g, T = 4.15, *P* < 0.001). BACHD mice are

obese, and in contrast to WT mice, variably show sex differences in body weight during the first 6 months of life. BACHD males weighed more on average than BACHD females from 9 to 15 weeks (+4.4 ± 2.7 g, T = 2.02, *P* = 0.04), but from 18-23 weeks of age, BACHD females experienced rapid weight gains so that they were of similar weight to BACHD males (-2.69 ± 5.1 g, T = 1.20, *P* = 0.23). This rapid weight gain for BACHD females ended before BACHD males stopped growing, so that after 24 weeks, BACHD males were again larger than BACHD females (+4.8 ± 4.5 g, T = 2.18, *P* = 0.03), albeit to a smaller degree than the weight differences observed among WT mice (+11.2 ± 3.4 g, T = 9.31, *P* < 0.001). Even though BACHD males weighed more than BACHD females at both 3 and 6 months of age, their rotarod performances were worse only at 6 months of age. Although BACHD and WT females weighed less than their male counterparts at both of the ages motor testing was conducted, they did not consistently perform better on motor challenges. Sex differences in performance were exhibited among WT animals only at 3 months of age, and among BACHD animals only at 6 months of age. Additionally, genotypic differences in weight alone cannot account for deficits in rotarod performance observed in BACHD animals. BACHD males weighed more than WT males only until 4 months of age (+5.1 ± 3.9 g, T = 2.20, *P* = 0.03), and BACHD females weighed as much as WT males from 2 to 6 months of age (-0.9 ± 3.4 g, T = 0.36, *P* = 0.7), but both BACHD sexes consistently performed worse on rotarod relative to WT males. Taken together, body-weight alone cannot account for the impaired motor coordination we observed in BACHD mice, nor for the sex difference in rotarod performance of young WT mice or aged BACHD mice.

Discussion

Sex differences in behavioral patterning and the circadian system are seen in many animals (Zucker and Stephan, 1973; Roper, 1976; Davis et al., 1983; Moe et al., 1991; Helfrich-

Förster, 2000; Lee et al., 2004; Roenneberg et al., 2007; Kuljis et al., 2013). In mice, SCN-regulated behavioral patterning characteristics, such as activity onsets, the closely-related free running activity rhythm period, activity offsets, activity rates, bouts and durations, sleep onsets, as well as light-induced behavioral rhythm phase shift magnitudes are regulated by gonadal hormones and/or sex chromosomes (Kopp et al., 2006; Paul et al., 2006; Karatsoreos et al., 2007; Iwahana et al., 2008; Blattner and Mahoney, 2012; Butler et al., 2012; Ehlen et al., 2013; Kuljis et al., 2013). The fact that many of these parameters also show sex differences in humans (Wever, 1984; Adan and Natale, 2002; Krishnan and Collop, 2006; Paul et al., 2008; Cain et al., 2010; Duffy et al., 2011), and are altered in individuals with HD (Fix et al., 2004; Morton et al., 2005; Aziz et al., 2009a; Goodman et al., 2010; Kalliolia et al., 2014), led us to investigate whether there are sex differences in circadian system dysfunction in a mouse carrying the human HD gene. We focused our investigation on the ages when the greatest decline in behavioral and physiological output rhythms occur in male BACHD mice (Kudo et al., 2011b). At the level of their behavioral output, BACHD male mice have more severe circadian system dysfunction than BACHD females (**Fig. 5.1**). At 6 months of age BACHD male activity onset times were more variable (**Fig. 5.1G**). BACHD males had impaired phase-shifts to light exposure at CT16 (**Fig. 5.1J**), the period of their free-running activity rhythm was abnormally longer (**Fig. 5.1I**), and their activity bouts were more fragmented than BACHD females (**Fig. 5.1H**). This circadian disruption also correlated with more severe motor dysfunction (**Fig. 5.4A** and **5.4C**).

The ability to align behavior to a predictably rhythmic environment is an important survival adaptation for predated animals like mice (Halle, 2000), and is conducive to maintaining a regular and productive work/life schedule for humans (Roenneberg et al., 2003; van der Vinne et al., 2015). Increased variability in activity onset times in LD (**Fig. 5.1G**), but not DD, indicate that BACHD males may have more severe deficits in their circadian system's ability to entrain to

rhythmic photic environments. This is also evidenced by the increased number of days they require to align behavior to phase shifts of environmental LD cycles, and the smaller magnitude phase shifts they display in response to an early subjective-evening light exposure relative to WT male controls (Kudo et al., 2011b) and BACHD females (**Fig. 5.1J**). Typically, WT male mice have more precise rhythms than females, but experience greater impairments following gonadectomy (Iwahana et al., 2008). Young gonadectomized WT mice display many of the same phenotypes as BACHD male mice, including reduced activity levels and rhythm amplitude, as well as reduced rhythm precision in LD (Karatsoreos et al., 2007; Kuljis et al., 2013). BACHD male mouse testosterone levels are unknown, but considering that human HD patients and other mouse models of HD exhibit reduced testosterone levels (Markianos et al., 2005; Papalexi et al., 2005; Van Raamsdonk et al., 2005), the highest levels of HTT are expressed in the brain and testes (Strong et al., 1993), and the noted disruptive effects mHTT has on testicular cells (Van Raamsdonk et al., 2007), it is possible deficits in entrainment of BACHD mice may be due to reduced testosterone levels. Notably however for humans, a relationship between disordered sleep and hypogonadism has not been identified (Wittert, 2014), raising the possibility there may be limited therapeutic potential of testosterone replacement for patients.

Alternatively, reduced precision of BACHD male activity rhythms may be related to the longer period of their free-running activity rhythms. If the internal biological timing drive were at odds with the powerful direct effects light has on mouse behavior, this might also explain the imprecision of BACHD male entrainment and decreased nocturnality. WT male mouse free-running activity rhythm periods typically lengthen with age (Possidente et al., 1995; Valentinuzzi et al., 1997), but WT female rhythms do not (Kopp et al., 2006). Unlike BACHD males, BACHD female free-running rhythms display period shortening from 3 to 6 months of age (**Fig. 5.1I**), which may facilitate a more stable nocturnal phase-angle of entrainment. The similarity of the

effects of aging on WT free running periods raises the possibility a similar mechanism prematurely underlies age-related changes to free-running periods we observed in BACHD mice.

Depressed daytime firing rates (**Fig. 5.42B**) are associated with a significant reduction in behavioral rhythm power for both sexes (**Table 5.2**). Part of the natural aging process results in reduced behavioral and physiological rhythm power, and increased behavioral fragmentation, which occurs prematurely in BACHD mice (Kudo et al., 2011b; Nakamura et al., 2011). In aged WT mice these phenotypes are associated with reduced sleep efficiency and reduced amplitude electrical output from SCN caused by the dysregulation of potassium currents active during the inter-spike interval (Farajnia et al., 2012). BACHD mice showed a similar loss in SCN electrical activity rhythms due to depressed daytime SCN electrical activity, but neither BACHD male or female SCN neurons show daytime membrane potential hyperpolarization (**Fig. 5.4C** and **5.4D**), suggesting rhythmic currents regulating inter-spike intervals rather than membrane potential may likely underlie their pathophysiology. Additional parallels to aging's effects on the circadian system include the persistence of clock gene expression rhythms in the SCN. While aged WT and BACHD mouse SCNs lose rhythms in electrical excitability, they both maintain rhythms in clock gene expression (Kudo et al., 2011b; Nakamura et al., 2011), suggesting the mechanisms disrupting rhythmic physiology of aged and BACHD mouse SCN neurons is likely post-translational in nature.

BACHD female activity rhythm dysfunction showed an intermediate phenotype relative to males (**Fig. 5.1**). Although there was a trend toward BACHD female daytime pathophysiology being less severe than BACHD male's (**Fig. 5.4B** and **Table 5.3**), a sex difference in BACHD SCN output was not found. One alternative explanation for the intermediate behavioral rhythm phenotype we observed in BACHD female mice was a differential loss of cells expressing the

peptide signaling molecules involved in intra-SCN function (Brancaccio et al., 2013; Maywood et al., 2013), photic entrainment (Hughes et al., 2004; Vosko et al., 2007; Dragich et al., 2010), and SCN-output (Vosko et al., 2007; Loh et al., 2011; Schroeder et al., 2011a). There was no evidence the number of cells expressing AVP or VIP is reduced in BACHD mice (**Fig. 5.5** and **5.6**), or evidence of sex difference in peptide expression during early adulthood for WT mice (**Fig. 5.6**). In humans, AVP and VIP loss occurs in the SCN during aging (Roozendaal et al., 1987; Zhou et al., 1995; Hofman et al., 1996; Hofman, 1997) and in HD (Wamelen et al., 2013). In rodents, sexual dimorphisms of *AVP* mRNA rhythms have not been reported, while *VIP mRNA* rhythms have been reported to be antiphase in males and females (Krajnak et al., 1998; Mahoney et al., 2009). It is unknown whether transcriptional rhythms in other rodent SCN correspond to changes in cell body numbers expressing these proteins in mice. Notably, we did not find a sex difference in AVP or VIP immunopositive cell numbers during mid-day in mice, leaving it open to a question of interpretation. If the number of VIP^+ cell bodies changes throughout the day, and this rhythm is different between males and females, it is possible VIP was assessed during the rising or falling phases of expression for males and females. Testing this possibility would require examination of many more time points. For humans, sex differences in AVP expression have not been detected (Swaab and Hofman, 1990), while sex differences for VIP vary depending on age (Zhou et al., 1995). It is believed similar patterns of peptide expression occurs in other mammals, as they do in humans (Cassone et al., 1988; Moore, 1993). The lack of sex differences in AVP expression for BACHD and WT mice is consistent with previous findings in humans and rats, while similar levels of VIP expression in BACHD and WT mice may alternatively be accounted for with two explanations. Either there are no sex differences in VIP expression at this age, or VIP levels are not sexually dimorphic during adulthood in mice. Lastly, although no peptide loss is detected in BACHD mouse SCN at three months of age, SCN pathology may occur at later stages of disease progression. It is clear

however, that sex differences in circadian system regulation of activity are not fully accounted for by sex differences in daytime SCN pathology or pathophysiology.

These findings suggest sex differences in mHTT disruption of other brain regions and/or peripheral tissues may underlie sex differences in activity patterning of BACHD mice. Activity levels are dramatically reduced for both BACHD mouse sexes, but are reduced earlier for BACHD males, indicating female-specific factors protect against activity level decline. The preoptic area of the hypothalamus plays a key role in regulating activity levels and is known to mediate estrogen-related increases in activity levels (Fahrbach et al., 1985), raising the possibility that female hormones may be activationally improving levels of BACHD female locomotor activity, or alternatively that mHTT disruption of activity level regulating neural circuits of the preoptic area is mitigated in BACHD females relative to BACHD males. Alternatively, mHTT disruption of cardiac and/or skeletal muscle may also reduce activity levels. We've previously shown that BACHD male mouse cardiovascular function is disrupted (Kudo et al., 2011b; Schroeder et al., 2011a), and although we can only speculate whether similar deterioration occurs for females, considering the protective effects of estrogens on cardiovascular disease (Murphy, 2011), it may be possible that mHTT disruption of muscle may be less severe for BACHD females. Circadian system dysfunction related activity level reductions, have previously been noted in a mouse model with disrupted core clock genes. This phenotype can be rescued by restoring the functionality of the circadian molecular network in skeletal muscle alone (McDearmon et al., 2006). Although there is little evidence that the circadian molecular network is disrupted in BACHD mouse tissues (Kudo et al., 2011b), mHTT may have downstream effects on the trafficking or posttranslational modifications of proteins regulated by clock genes in skeletal muscle, SCN, and/or the preoptic area to disrupt these tissues' functionality, and thus cause the deficits in activity levels we observe.

The obesity phenotype in the BACHD mouse is not typically experienced by human HD patients, but is evidence that mHTT disrupts the hypothalamic circuits and metabolic tissues regulating metabolic function, which *is* experienced by humans. Similar to previous observations (Menalled et al., 2009; Lundh et al., 2012; Baldo et al., 2014), we found BACHD mice display an obesity phenotype (**Fig. 5.7D**). BACHD female mice gain a higher percentage fat than BACHD males (Hult et al., 2011), and considering that BACHD males are significantly heavier than their WT littermates only until 4 months of age (**Fig. 5.7D**), it would be fair to say that the obesity phenotype is relatively worse for BACHD females. Alternatively, if higher body weight is protective in mice like it is in human HD patients (Myers et al., 1991), alterations in feeding and energy homeostasis exhibited by BACHD female mice, might be an adaptive compensation to the presence of mHTT related to their improved motor functionality and delayed circadian system dysfunction relative to BACHD males.

The idea that improving behavioral and physiological rhythmicity can delay HD symptom progression is compelling for many reasons, the most important of which is the benefit longer health-spans would have for HD gene carriers and their families. Along with previous studies showing an association of delayed HD progression with improved rhythms (Pallier et al., 2007; Aziz et al., 2010b), the sex differences in behavioral patterning and motor function found in this study provide further persuasive evidence in support of the idea that the maintenance of healthy behavioral and physiological rhythms slows disease progression in HD. The paucity of clear evidence for sex difference in the human HD phenotype, raises questions to the relevance of our findings for the human disease. It is possible there is an overly narrow focus of epidemiological studies on tracking motor symptoms, so that while the effects of mHtt on striatal and cortical circuits might occur at a similar rate for men and women, they may be slower/faster in other brain regions, such as those mediating non-motor HD symptoms. Additional studies testing for sex differences in prodromal non-motor phenotypes, such as those related to

circadian system function, will need to be conducted in order to definitively know whether there are sex differences in circadian system function or dysfunction for HD gene carriers. Considering that alterations to melatonin rhythms are amongst the earliest disease phenotypes exhibited by HD gene carriers (Kalliolia et al., 2014), it is worthwhile to examine. Alternatively, considering that HD is typically diagnosed at the end of a woman's child bearing years, circa-menopause when estrogen levels drop severely for women (Sherman et al., 1976), it may not be surprising more robust sex differences have not been observed in humans if they are mediated by estrogens.

Conclusion

Dysfunction in the circadian regulation of biological rhythms occurs early in the HD process and likely has negative health consequences that feed into the disease mechanism. Whether there are sex differences in sleep disruptions of HD gene carriers is unknown, but the observations outlined in this report are promising evidence that sex specific factors mitigate some aspects of circadian and motor dysfunction.

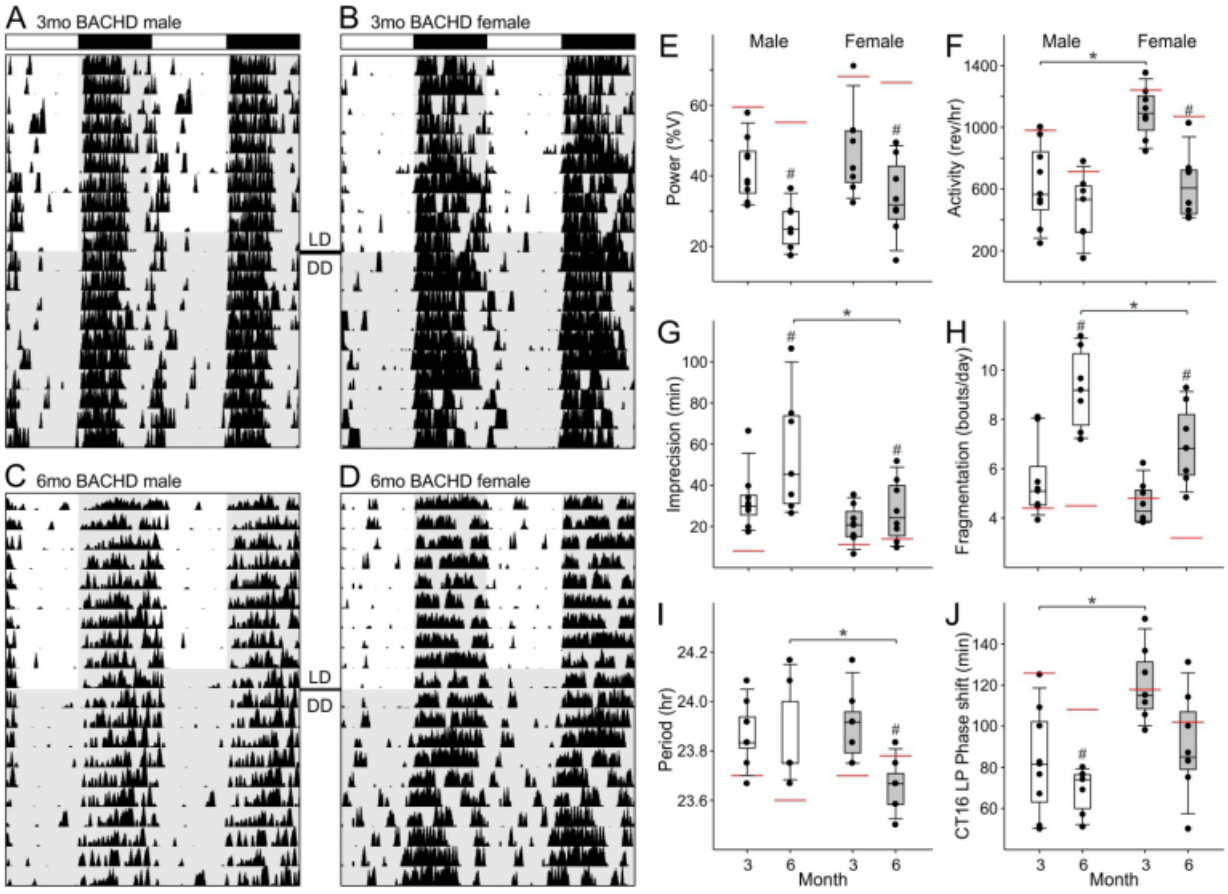

Figure 5.1: Delayed daily and circadian wheel running activity rhythm deterioration for BACHD females relative to BACHD males. **(A-D)** Representative double-plotted actograms of BACHD male and female wheel running activity during 10 days in 12:12 LD (300 lux) and 10 days in DD at 3 and 6 months of age. **(E-J)** Box plots representing first and third quartile (box), medians (middle line), and data range (whiskers) for male (white boxes) and female (grey boxes) BACHD mouse behavioral rhythm parameters recorded at 3 and 6 months of age in LD **(E-H)** or DD **(I+J).** Individual data points (black dots) and mean WT values for reference (red lines) are superimposed. Two-way ANOVA was used to detect significant effects of sex and/or age on BACHD mouse behavioral rhythm parameters. When main or interaction effects were identified, significant sex differences within age (*) or significant age differences within sex (#) were identified post-hoc, using the Holm-Sidak method for multiple pairwise comparisons, with $P < 0.05$. Rev/hr refer to wheel revolutions per hour.

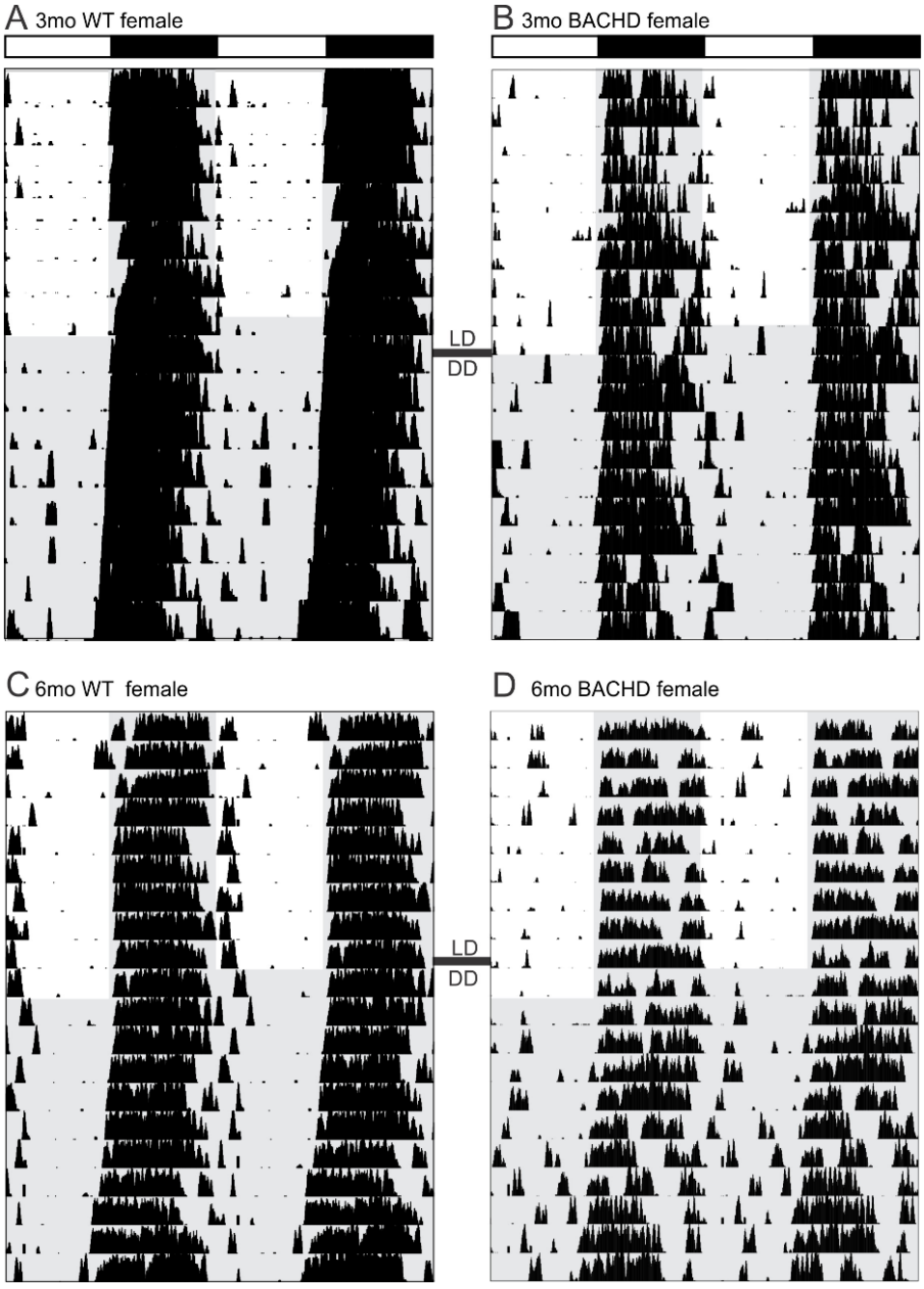

Figure 5.2: Early onset deficits in BACHD female mouse daily and circadian wheel running activity relative to WT littermate females. **(A-D)** Representative double-plotted actograms of WT female littermates and BACHD female wheel running activity during 10 days in 12:12 LD (300 lux) and 10 days in DD at 3 and 6 months of age.

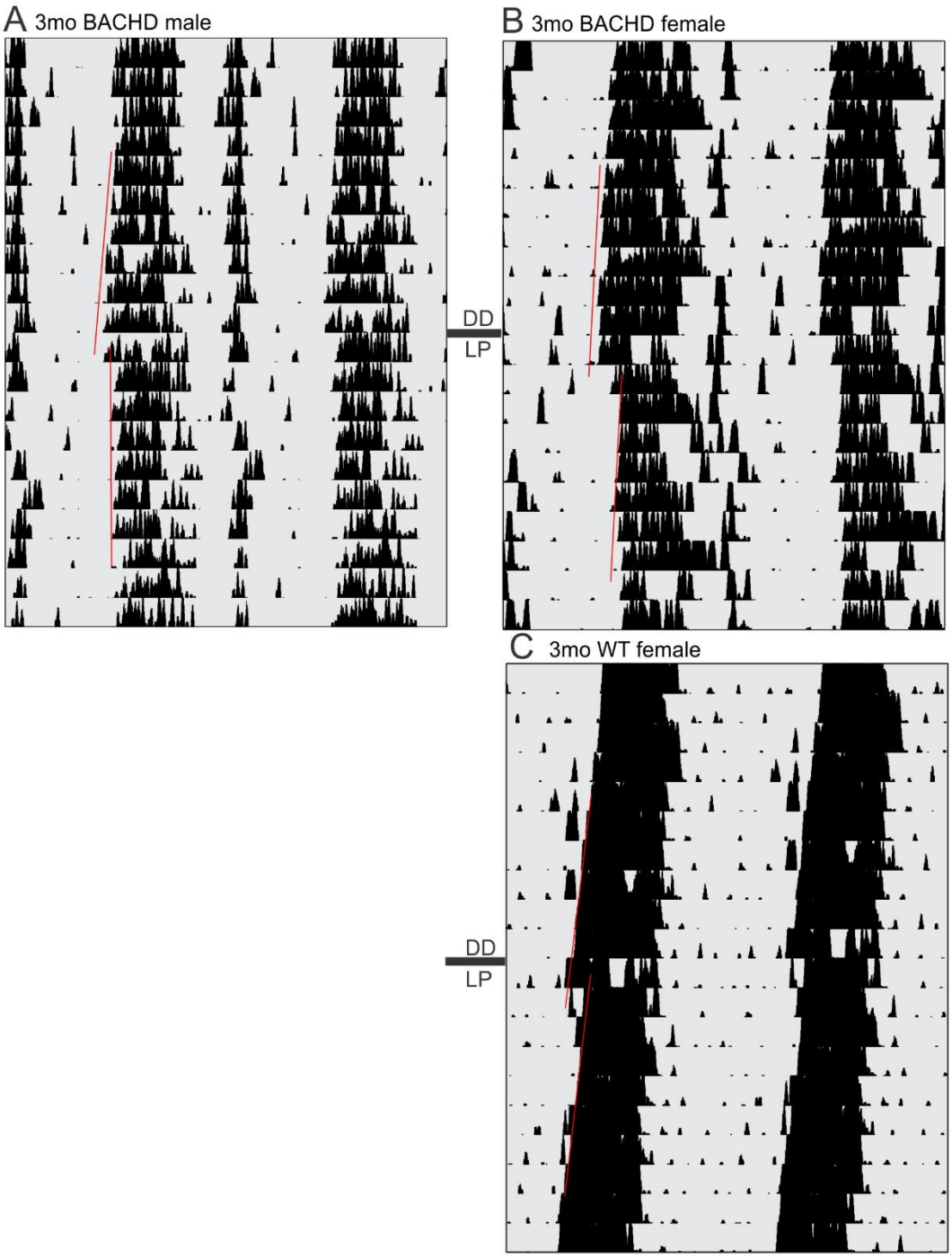

Figure 5.3: Sex difference in CT16 light-pulse induced phase shifts of locomotor activity at 3 months. Representative actograms of behavioral phase shifts in response to CT16 light-pulse, with activity onsets 10 days before and 10 days after light pulse presentation marked with a red line for a BACHD male **(A)**, BACHD female **(B)**, and WT female mouse **(C)**.

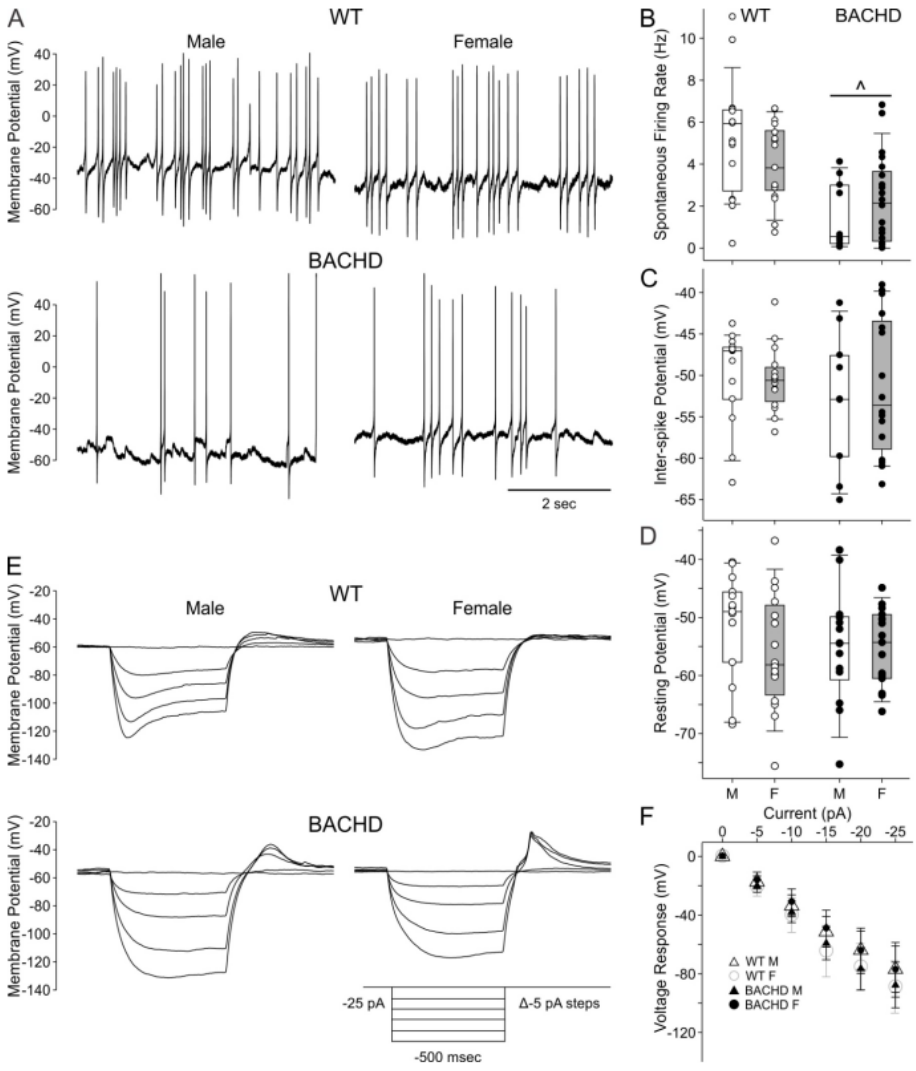

Figure 5.4: Depressed daytime SFR in male and female BACHD dSCN neurons but no hyperpolarization. **(A)** Representative traces of SCN neuron spontaneous electrical activity recorded during the day. **(B-D)** Box plots representing the first and third quartile (box), group medians (middle line) and data range (whiskers) of male (white boxes) and female (grey boxes) SCN neuron electrophysiological properties, with individual data points superimposed for WT (white dots) and BACHD (black dots) neurons. If Two-Way ANOVA identified effects of genotype and/or sex, then post-hoc multiple pairwise comparison testing using the Holm-Sidak method ($P < 0.05$) was used to identify significant group differences. Statistical analysis summarized in Table 2. **(B)** SFR is reduced during the daytime in BACHD SCN neurons. **(C)** Inter-spike membrane potential is not altered for BACHD neurons. **(D-F)** Resting membrane properties recorded in the presence of TTX (1µM) and gabazine (10µM) to silence synaptic and electrical activity. **(D)** No sex or genotype differences in membrane potential at rest. **(E)** Representative traces of SCN neuron membrane potential responses to progressively negative current step injections. **(F)** Baseline subtracted voltage responses are plotted for each group as means ± 95% CI of means. Three-Way ANOVA detected significant main effects of current injection and an interaction of sex and genotype on voltage responses, but post-hoc pairwise comparisons using Two-Tailed T-Test ($P < 0.05$) failed to detect significant voltage response magnitudes for any particular current injection magnitude.

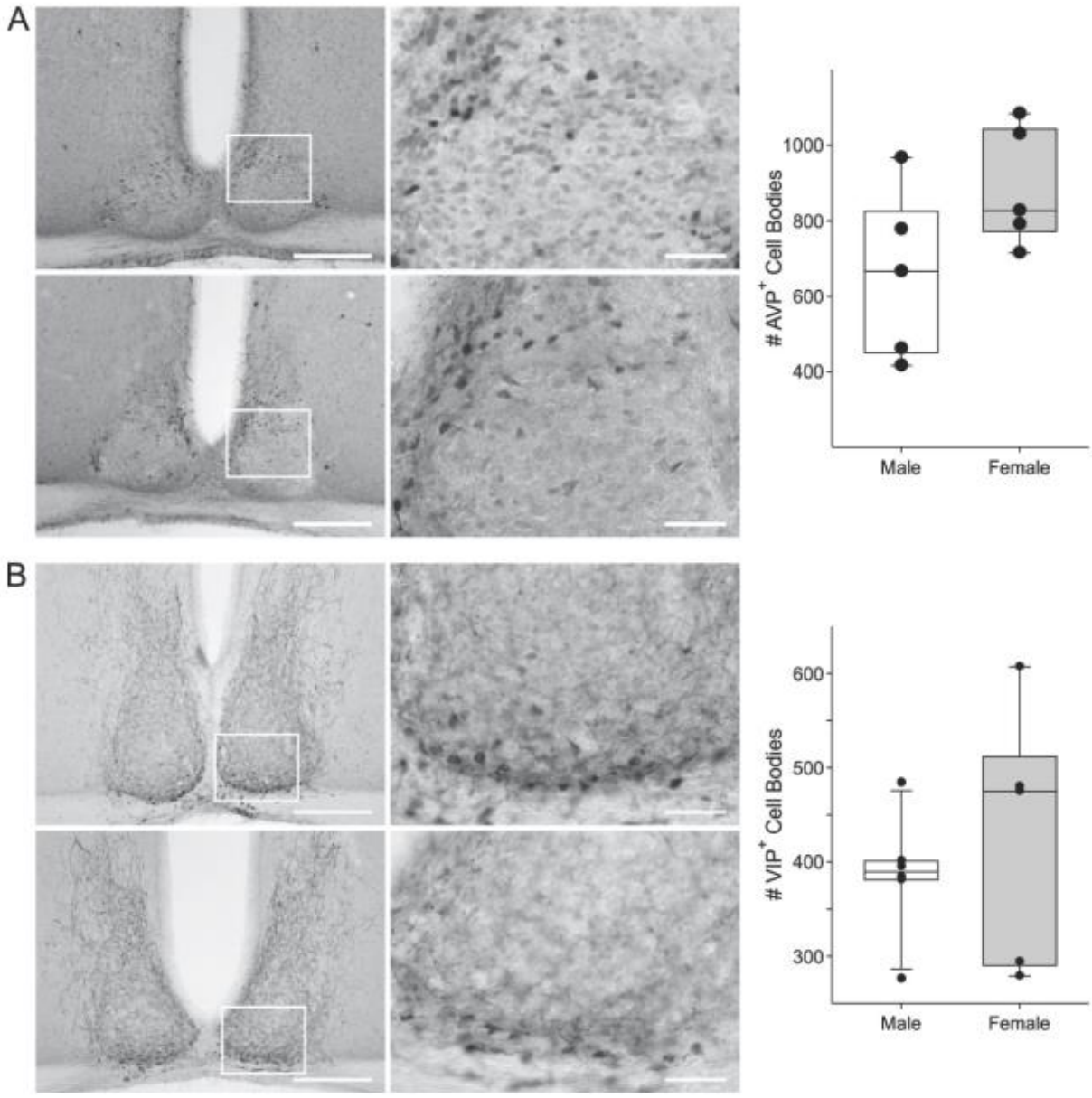

Figure 5.5: No sex difference in BACHD daytime SCN AVP$^+$ or VIP$^+$ cell counts. **(A)** Right panel shows representative images of male (top) and female (bottom) SCNs stained using AVP primary antibody. Boxed regions in 10x image (left, scale bar = 200µm) are magnified at 40x (right, scale bar = 40µm). Left panel shows box plots representing first and third quartile (box), group medians (middle line) and data range (whiskers) for group cell counts with individual data points superimposed. **(B)** Images of SCNs stained using VIP primary antibody (left panel) and corresponding cell counts (right panel) using the same organization and scale as in (A).

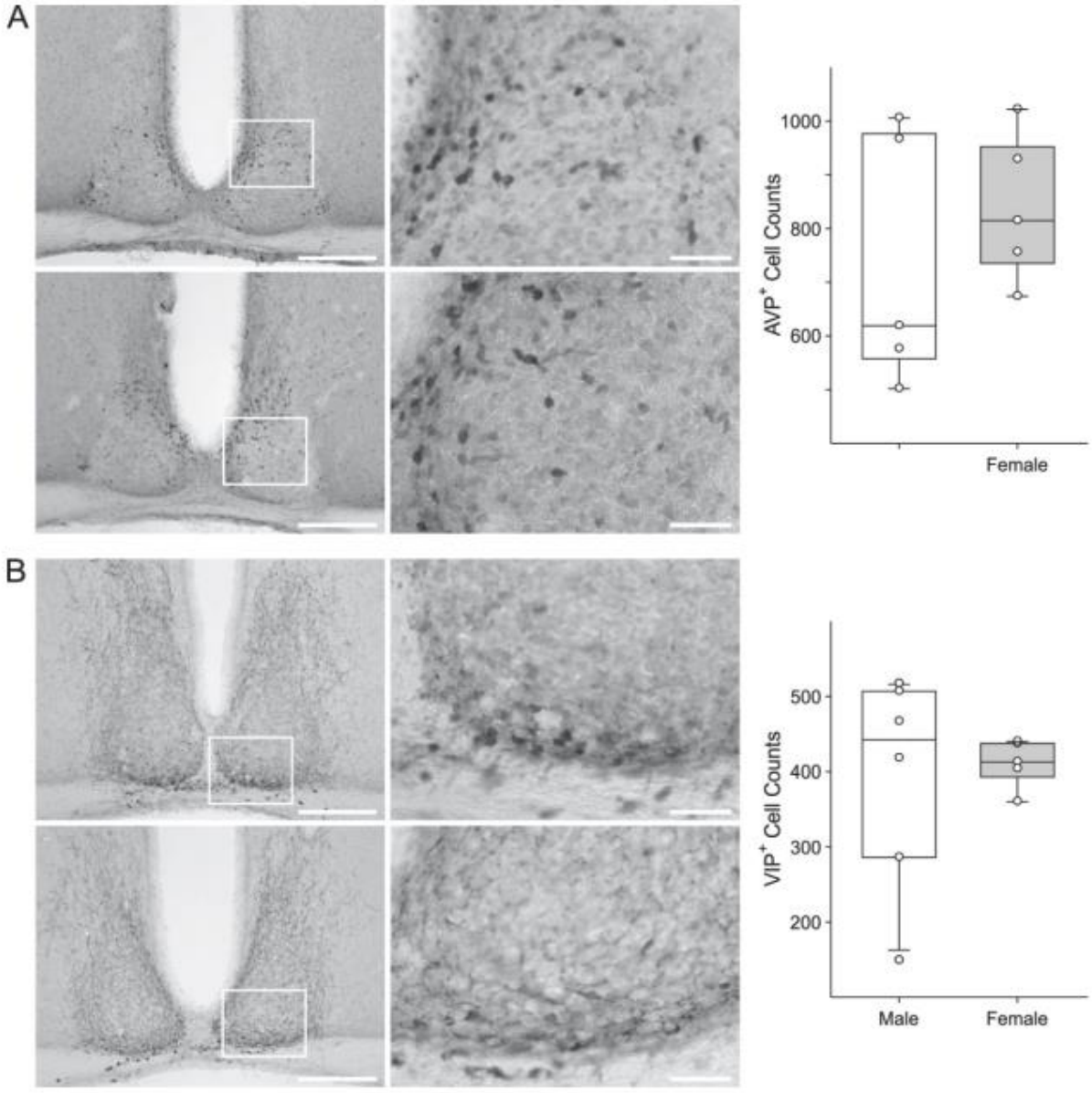

Figure 5.6: No sex difference in WT daytime SCN AVP⁺ or VIP⁺ cell counts. **(A)** Left panel shows representative images of male (top) and female (bottom) SCNs stained using AVP primary antibody. Boxed regions in 10x image (left, scale bar = 200µm) are magnified at 40x (right, scale bar = 40µm). Right panel shows box plots representing first and third quartile (box), group medians (middle line) and data range (whiskers) for group cell counts, with individual data points superimposed. **(B)** Images of SCNs stained using VIP primary antibody (left panel) and corresponding cell counts (right panel) using the same organization and scale as in (A).

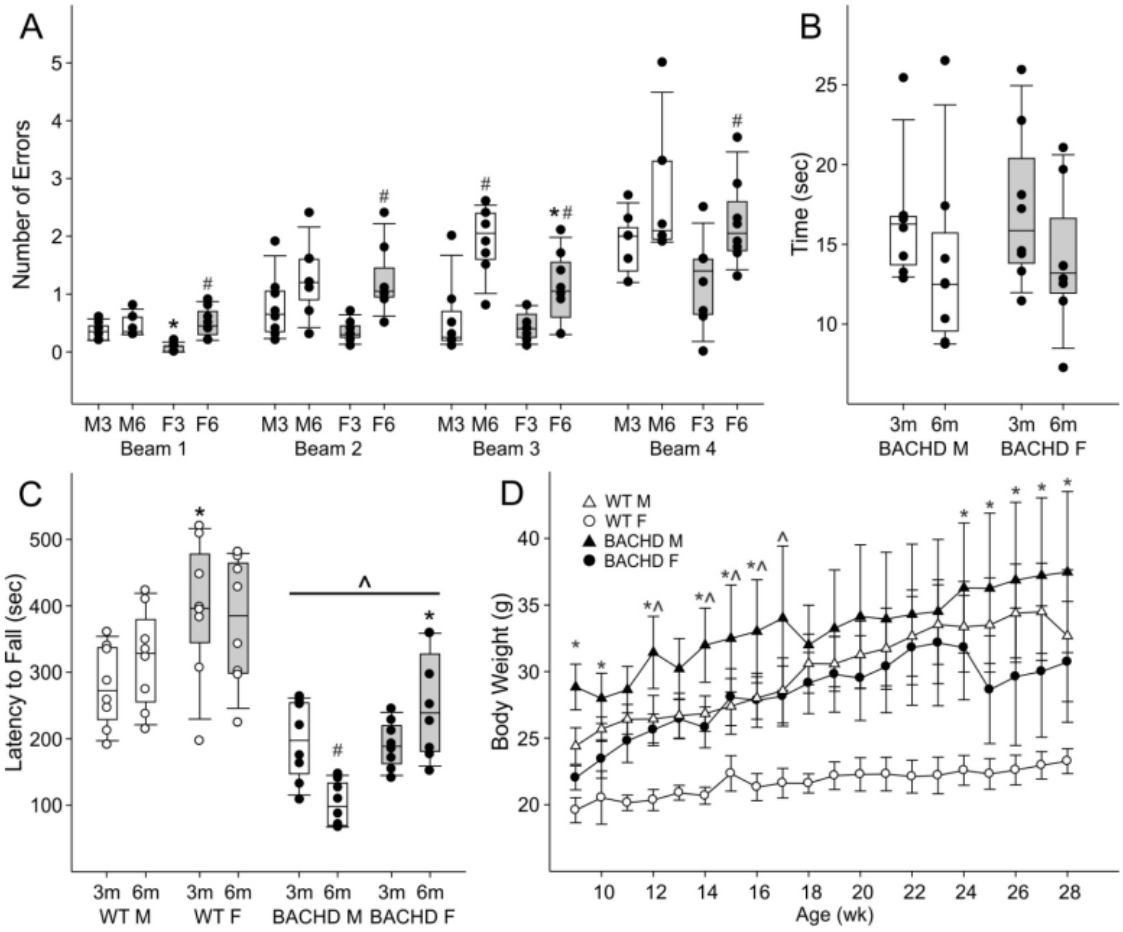

Figure 5.7: Sex differences in motor coordination and body weight. **(A-C)** Box plots represent first and third quartile (box), group medians (middle line) and data range (whiskers) of male (white boxes) and female (grey boxes) mice, with individual data points superimposed. **(A)** BACHD mouse step errors on progressively narrowing challenge beams (Beams 1-4). Two-Way ANOVA identified main effects of sex and age on step errors. Significant sex differences within age (*) and/or significant age differences within sex (#) for each beam were identified post-hoc, using the Holm-Sidak method for multiple pairwise comparisons, with $P < 0.05$. **(B)** Time to traverse all 4 challenging beams. **(C)** Rotarod latency to fall for WT (white dots) and BACHD (black dots) mice. Three-Way ANOVA identified main effects of genotype, and interactions of sex, age, and genotype on latency to fall. Significant genotype differences within age and sex (^), sex differences within genotype and age (*), and significant age differences within sex and genotype (#) on latency to fall were identified post-hoc, using the Holm-Sidak method for multiple pairwise comparisons, with $P < 0.05$. **(D)** Body weight of WT and BACHD mice. Three-Way ANOVA identified main effects of genotype, sex, and age, and interactions of genotype and sex, as well as sex and age on body weight. Post-hoc pairwise comparisons using the Holm-Sidak method identified that at all age points, WT females weighed less than BACHD females and WT males. Ages when significant differences in weight were detected between BACHD male and female mice (* $P < 0.05$), and BACHD male and WT male mice (^$P < 0.05$). Points represent means, while error bars are the 95% CI of means.

	Parameter	DF	Sex Effect F	Sex Effect P	Age Effect F	Age Effect P	Interaction F	Interaction P
LD	%V	31	3.49	NS	17.0	< 0.001	0.117	NS
	Activity (rev/hr)		15.7	< 0.001	16.3	< 0.001	4.22	0.049
	% Activity in Light		0.269	NS	0.0397	NS	7.74	0.01
	Alpha (min)		0.0365	NS	0.325	NS	0.157	NS
	Imprecision (min)		9.72	0.004	5.32	0.029	1.63	NS
	Fragmentation (bouts/day)		10.4	0.003	36.9	< 0.001	1.71	NS
	LD-DD Phase Angle (min)		1.50	NS	0.437	NS	0.0522	NS
DD	Period (hr)	31	2.32	NS	7.49	0.011	5.01	0.033
	% V		0.548	NS	29.4	< 0.001	0.0009	NS
	Activity (rev/hr)		17.2	< 0.001	28.8	< 0.001	6.75	0.015
	Alpha (min)		1.24	NS	0.0114	NS	0.814	NS
	Imprecision (min)		0.0109	NS	10.4	0.003	0.0199	NS
	Fragmentation (bouts/day)		2.13	NS	20.6	< 0.001	1.92	NS
	CT16 LP (min)		15.6	< 0.001	8.36	0.007	1.18	NS

	BACHD 3 months	Males	Females
LD	%V	41.7 ± 6.8	47.1 ± 10.3
	Activity (rev/hr)	627 ± 200	1093 ± 138***
	% Activity in Light	14.8 ± 8.2	23.3 ± 6.2
	Alpha (min)	727 ± 42	712 ± 57
	Imprecision (min)^	32.7 ± 11.0	21.0 ± 7.7
	Fragmentation (bouts/day)^	5.53 ± 1.15	4.58 ± 0.73
	LD-DD Phase Angle (min)	22.0 ± 23.8	10.5 ± 34.3
DD	Period (hr)	23.87 ± 0.10	23.91 ± 0.11
	% V	44.1 ± 7.5	46.5 ± 7.4
	Activity (rev/hr)^	681 ± 187	1187 ± 99***
	Alpha (min)^	643 ± 102	651 ± 64
	Imprecision (min)	12.6 ± 4.6	11.8 ± 4.7
	Fragmentation (bouts/day)^	5.74 ± 1.64	5.70 ± 1.08
	CT16 LP (min)	82.6 ± 19.4	119.9 ± 14.6**

**Sex p < 0.01, ***Sex p < 0.001, Mean ± 95% C.I. of Mean, Sex effects determined using Two-Tailed Ttest, or if ^Normality test failed, Mann-Whitney Rank Sum Test

	BACHD 6 months	Males	Females
LD	%V	25.9 ± 6.1~	33.7 ± 9.2~
	Activity (rev/hr)	474 ± 201	621 ± 178~
	% Activity in Light^	26.0 ± 12.5~	13.6 ± 8.5
	Alpha (min)^	731 ± 93	736 ± 41
	Imprecision (min)	55.5 ± 27.3~	27.5 ± 12.5~*
	Fragmentation (bouts/day)	9.22 ± 1.49~	6.95 ± 1.29~*
	LD-DD Phase Angle (min)	32.3± 24.4	15.5 ± 24.9
DD	Period (hr)^	23.85 ± 0.18	23.66 ± 0.09~*
	% V	27.8 ± 8.1~	29.9 ± 5.2~
	Activity (rev/hr)	474 ± 192	590 ± 205~
	Alpha (min)^	612 ± 134	690 ± 52
	Imprecision (min)^	23.1 ± 6.5~	23.2 ± 13.2~
	Fragmentation (bouts/day)	9.12 ± 0.83~	7.50 ± 1.39~*
	CT16 LP (min)	69.1 ± 10.2	90.4 ± 20.7~

*Sex p < 0.05, ~Age p < 0.01

Table 5.1: Sex differences in BACHD behavioral rhythms. Two-way ANOVA results testing effects of sex and/or age on BACHD mouse behavioral rhythm parameters (top). When main or interaction effects were identified, significant sex differences at 3 (middle) and 6 months (bottom) of age, as well as age differences within sex ($^{\#}$) were identified post-hoc using Two-Tailed T-Tests, or if the Normality test failed (^), the Mann-Whitney Rank Sum Test (*Sex, P < 0.05; **Sex, P < 0.01; *** Sex, P < 0.001; ~ Age, P < 0.01). Reported values are means ± 95% CI of means.

			Genotype effect		Age effect		Interaction	
	Parameter	DF	F	P	F	P	F	P
LD	%V	31	52.3	< 0.001	4.1	NS	2.46	NS
	Activity (rev/hr)		15.9	< 0.001	18.2	< 0.001	4.25	0.049
	% Activity in Light		3.73	NS	14.4	< 0.001	0.764	NS
	Alpha (min)		2.78	NS	0.436	NS	0.288	NS
	Imprecision (min)		11.01	0.003	1.598	NS	0.425	NS
	Fragmentation (bouts/day)		19.53	< 0.001	2.785	NS	25.6	< 0.001
	LD-DD Phase angle (min)		8.81	0.006	0.542	NS	1.485	NS
DD	Period (hr)	31	0.719	NS	3.302	< 0.001	15.981	< 0.001
	% V		42.3	< 0.001	8.232	0.008	3.232	NS
	Activity (rev/hr)		10.82	0.003	27.39	< 0.001	6.253	0.02
	Alpha (min)		2.163	NS	0.123	NS	1.09	NS
	Imprecision (min)		2.024	NS	3.74	NS	1.98	NS
	Fragmentation (bouts/day)		24.9	< 0.001	1.48	NS	8.49	0.007
	CT16 LP (min)		1.16	NS	9.87	0.004	0.193	NS

Females 3 Mo.		WT	BACHD
LD	%V	68.1 ± 7.5	47.1 ± 10.3$^{\#\#\#}$
	Activity (rev/hr)	1240 ± 210	1090 ± 140
	% Activity in Light	19.8 ± 11.3	23.3 ± 6.2
	Alpha (min)	690 ± 48	712 ± 24
	Imprecision (min)^	11.8 ± 4.7	21.0 ± 7.7
	Fragmentation (bouts/day)^	4.8 ± 0.5	4.6 ± 0.7
	LD-DD Phase angle (min)	-7.6 ± 19.1	10.5 ± 34.3
DD	Period (hr)	23.70 ± 0.11	23.90 ± 0.11$^{\#}$
	% V	63.2 ± 12.4	46.5 ± 7.4$^{\#\#}$
	Activity (rev/hr)^	1250 ± 260	1190 ± 100
	Alpha (min)^	639 ± 78	651 ± 64
	Imprecision (min)	11.7 ± 5.5	11.8 ± 4.7
	Fragmentation (bouts/day)^	4.8 ± 0.8	5.7 ± 1.1
	CT16 LP (min)	125 ± 23	120 ± 15

Females 6 mo.		WT	BACHD
LD	%V	66.4 ± 7.9	33.7 ± 9.2$^{\#\#\#\sim}$
	Activity (rev/hr)	1070 ± 170	620 ± 180$^{\#\#\#\sim}$
	% Activity in Light^	4.3 ± 2.8~	13.6 ± 8.5~
	Alpha (min)^	692 ± 39	736 ± 40.8
	Imprecision (min)	13.9 ± 4.9	27.5 ± 12.5$^{\#\#}$
	Fragmentation (bouts/day)	3.6 ± 0.6~	7.0 ± 1.3$^{\#\#\sim\sim}$
	LD-DD Phase angle (min)	-27.9 ± 6.5	15.5 ± 24.9$^{\#\#}$
DD	Period (hr)^	23.79 ± 0.10	23.66 ± 0.10$^{\sim\sim}$
	% V	59.4 ± 6.7	29.9 ± 5.2$^{\#\#\#\sim}$
	Activity (rev/hr)	1040 ± 130	590 ± 210$^{\#\#\#\sim}$
	Alpha (min)^	619 ± 69	690 ± 52
	Imprecision (min)^	13.5 ± 5.8	23.2 ± 13.2
	Fragmentation (bouts/day)	4.1 ± 0.7	7.5 ± 1.4$^{\#\#\sim}$
	CT16 LP (min)	103 ± 19	90.4 ± 20.7~

Table 5.2. : Deficits in BACHD female behavioral rhythm parameters relative to WT females. Two-way ANOVA results testing effects of genotype and/or age on female wheel-running activity rhythm parameters (top) with group means at 3 and 6 months below. When main or interaction effects were identified, significant genotypic differences at 3 (middle) and 6 months (bottom), as well as age differences within genotype ($^{\#}$) were identified post-hoc using the Holm-Sidak method for multiple pairwise comparisons (*Sex, $P < 0.05$; ** Sex, $P < 0.01$; ***Sex, $P < 0.001$; ~Age, $P < 0.01$). Reported values are means ± 95% CI of means.

	Genotype			Sex		Genotype x Sex	
Action Potential Properties	DOF	F	P	F	P	F	P
Spontaneous Firing Rate (Hz)	65	24.000	<0.001	0.183	NS	3.325	NS
Instantaneous Frequency (Hz)	47	14.400	< 0.001	0.827	NS	0.695	NS
Interevent Interval (msec)	49	10.194	0.003	0.858	NS	0.406	NS
Inter-Spike Membrane Potential (mV)	54	1.008	NS	0.073	NS	0.304	NS
Peak Amplitude (mV)	50	0.104	NS	0.005	NS	8.776	0.005
Time to Peak (msec)	50	4.159	0.047	1.337	NS	0.520	NS
Half-Amplitude (mV)	49	0.042	NS	0.034	NS	9.215	0.004
Time to Rise Half Amplitude (msec)	50	2.284	NS	0.406	NS	0.067	NS
Rise Tau (msec)	50	0.117	NS	0.002	NS	1.495	NS
Area (mV*msec)	49	0.401	NS	2.404	NS	0.377	NS
Half-Width (msec)	50	1.674	NS	0.570	NS	0.092	NS
Antipeak Amplitude (mV)	49	4.815	0.03	0.575	NS	0.028	NS
Time to Antipeak (msec)	49	1.362	NS	2.988	NS	0.140	NS
Time to Decay Half Amplitude (msec)	47	1.903	NS	0.537	NS	0.115	NS
Decay Time (msec)	49	1.575	NS	2.590	NS	0.297	NS
Decay Slope (mV/msec)	49	0.854	NS	0.709	NS	0.269	NS
Decay Tau (msec)	49	0.401	NS	2.404	NS	0.377	NS
Resting Membrane Properties							
Capacitance (pF)	55	2.823	NS	0.016	NS	0.076	NS
Resting Membrane Potential (mV)	59	0.431	NS	1.163	NS	0.979	NS
Input resistance (MΩ)	657	0.252	NS	0.021	NS	11.628	<0.001
Hyperpolarization Slope (mV/msec)	343	0.887	NS	2.310	NS	4.559	0.03
Hyperpolarization Area (mV/msec)	353	0.396	NS	1.475	NS	8.514	0.04
Hyperpolarization Peak Time (msec)	353	0.053	NS	3.422	NS	0.206	NS

	WT		BACHD	
Action Potential Properties	**Male** (n=19)	**Female** (n=17)	**Male** (n=10)	**Female** (n=20)
Spontaneous Firing Rate (Hz)	5.3 ± 1.3	4.0 ± 1.0	1.5 ± 1.1^^^	2.3 ± 1.0^^
Instantaneous Frequency (Hz)	4.8 ± 1.4	4.8 ± 1.0	2.1 ± 1.3^^	3.1 ± 1.4^
Interevent Interval (msec)	283 ± 127	230 ± 48	981 ± 889^^	696 ± 459
Inter-Spike Membrane Potential (mV)	-50.0 ± 3.3	-50.5 ± 2.2	-52.8 ± 5.7	-51.3 ± 4.5
Peak Amplitude (mV)	94.0 ± 12.5	112 ± 9.0*	114 ± 15.9^	95.5 ± 15.1*
Time to Peak (msec)	2.44 ± 0.18	2.22 ± 0.31	2.11 ± 0.35	2.06 ± 0.22
Half-Amplitude (mV)	47.2 ± 6.3	55.6 ± 4.5*	56.9 ± 7.8^	47.2 ± 8.0^*
Time to Rise Half Amplitude (msec)	0.74 ± 0.29	0.69 ± 0.22	0.58 ± 0.33	0.47 ± 0.24
Rise Tau (msec)	4.41 ± 1.84	5.87 ± 2.61	6.22 ± 4.36	4.85 ± 1.50
Area (mV*msec)	313 ± 42	354 ± 78	350 ± 84	306 ± 25
Half-Width (msec)	2.22 ± 061	2.22 ± 0.43	1.93 ± 0.63	2.14 ± 0.96
Antipeak Amplitude (mV)	9.4 ± 11.0	13.2 ± 12.0	21.1 ± 19.8	25.2 ± 8.7
Time to Antipeak (msec)	4.81 ± 0.31	4.12 ± 0.94	4.30 ± 0.67	3.85 ± 0.85
Time to Decay Half Amplitude (msec)	3.92 ± 0.40	3.66 ± 0.65	3.51 ± 0.98	3.41 ± 0.30
Decay Time (msec)	0.65 ± 0.33	0.59 ± 0.33	0.57 ± 0.43	0.25 ± 0.29
Decay Slope (mV/msec)	-32.9 ± 21.4	-40.7 ± 26.5	-41.9 ± 34.2	-10.5 ± 13.6
Decay Tau (msec)	16.1 ± 11.2	12.2 ± 12.0	17.9 ± 15.5	10.6 ± 7.2
Resting Membrane Properties	**Male** (n=16)	**Female** (n=17)	**Male** (n=17)	**Female** (n=14)
Capacitance (pF)	9.1 ± 1.4	9.0 ± 1.8	10.4 ± 2.1	10.7 ± 2.4
Resting Membrane Potential (mV)	-51.2 ± 4.9	-56.0 ± 5.3	-55.0 ± 5.6	-55.2 ± 3.7
Input resistance (MΩ)	2.7 ± 0.1	3.2 ± 0.1*	3.1 ± 0.14^	2.6 ± 0.2^^*
Hyperpolarization Slope (mV/msec)	-1.30 ± 0.23	-1.78 ± 0.32**	-1.46 ± 0.23	-1.37 ± 0.24^
Hyperpolarization Area (mV*msec)	-13220 ± 2130	-15570 ± 2470**	-14520 ± 2210	-13710 ± 2480^
Hyperpolarization Peak Time (msec)	804 ± 29	771 ± 25	794 ± 27	774 ± 32

Table 5.3: SCN neuron action potential and resting membrane properties. Two-way ANOVA results testing effects of genotype and sex on daytime action potential and resting membrane properties of WT and BACHD SCN neurons (top), with group means below. When main or interaction effects were identified, significant genotype differences within sex, and significant sex differences within genotype were identified post-hoc using the Holm-Sidak method for multiple pairwise comparisons (^Genotype within Sex, $P < 0.05$; ^^ Genotype within Sex, $P < 0.01$; ^^^Genotype within Sex, $P < 0.001$; *Sex within Genotype, $P < 0.05$; **Sex within Genotype, $P < 0.01$). Reported values are means ± 95% CI of means.

			Sex Effect		Age Effect		Interaction	
	Parameter	DF	F	P	F	P	F	P
Challenge Beam	Beam 1	31	3.10	NS	16.87	< 0.001	0.117	0.02
	Beam 2		1.56	NS	13.56	< 0.001	4.22	NS
	Beam 3		5.89	0.022	27.4	< 0.001	3.43	NS
	Beam 4		3.79	NS	9.98	0.004	0.09	NS
	Time		0.06	NS	2.9	NS	0.03	NS

3 Months	Parameter	Males	Females
Challenge Beam	Beam 1	0.35 ± 0.13	0.075 ± 0.059*
	Beam 2	0.78 ± 0.46	0.35 ± 0.16
	Beam 3	0.55 ± 0.53	0.44 ± 0.21
	Beam 4	1.88 ± 0.44	1.23 ± 0.65
	Time	16.5 ± 3.3	17.2 ± 4.1

6 Months	Parameter	Males	Females
Challenge Beam	Beam 1	0.45 ± 0.16	0.50 ± 0.21##
	Beam 2	1.26 ± 0.53	1.23 ± 0.50##
	Beam 3	1.94 ± 0.50#	1.10 ± 0.53#*
	Beam 4	2.70 ± 0.92	2.22 ± 0.64#
	Time	13.8 ± 4.9	14.0 ± 3.7

		Genotype		Sex		Age		Genotype x Sex		Genotype x Age		Sex x Age		Genotype x Sex x Age	
	DF	F	P	F	P	F	P	F	P	F	P	F	P	F	P
Rotorod	63	74.1	< 0.001	18.4	< 0.001	0.02	0.9	0.13	0.72	0.6	0.4	1.62	0.2	8.6	0.005

	WT		BACHD	
Rotorod	Male	Female	Male	Female
3 months	279 ± 52	394 ± 89**	196 ± 50^	191 ± 30^^
6 months	321 ± 63	375 ± 81	102 ± 28^^#	251 ± 67^***

Table 5.4: Sex and genotypic differences in motor coordination. Two-way ANOVA results used to detect significant effects of sex and age on challenge beam step errors (Top), Three-Way ANOVA results testing effects of genotype, sex and age on rotarod performance (Bottom), with group means below ANOVA results. When main or interaction effects were identified, significant sex differences within the 3 and 6 month age group were identified post-hoc using the Holm-Sidak method for multiple pairwise comparisons (^Genotype within Sex, $P < 0.05$; ^^Genotype within Sex, $P < 0.01$; ^^^Genotype within Sex, $P < 0.001$; *Sex within Genotype, $P < 0.05$; **Sex within Genotype, $P < 0.01$). Reported values are means ± 95% CI of means.

Chapter 6: Potassium current alterations associated with the loss of rhythmic output from SCN of the BACHD mouse model of Huntington's disease.

HD related neural degeneration within cortical and striatal tissues is thought to cause cognitive and motor deficits, while specific patterns of cell loss and alteration in neural circuit function within hypothalamic tissues are thought to underlie sleep and mood disruptions associated with the disease (Halliday et al., 1998; Li and Li, 2004; Gatchel and Zoghbi, 2005; Petersén et al., 2005; Paulsen et al., 2006; Petersén and Björkqvist, 2006; Wamelen et al., 2013). The onset of motor symptoms, which typically occurs in mid-life, is requisite for the HD diagnosis, and much effort has been spent to investigate the mechanisms underlying the striatal degeneration that cause them (Ross and Tabrizi, 2011). Non-motor symptoms often begin years before-hand and likely have insidious effects on gene carrier health spans (Paulsen and Conybeare, 2005; Pallier et al., 2007; Aziz et al., 2010b; Morton, 2013; Wamelen et al., 2013), but their mechanisms are relatively poorly understood. Temporal changes to gene carrier's activity, sleep, and melatonin rhythms raise the possibility that disruption to the circadian system is an early component of HD progression (Morton et al., 2005; Aziz et al., 2009a; Goodman et al., 2011; Morton, 2013; Kalliolia et al., 2014).

At the top of the circadian system hierarchy is the SCN, and under normal conditions its rhythmic output provides the temporal signals used by the rest of the brain and body to synchronize cellular oscillations in gene expression and adaptively phase those rhythms across multiple tissues and organ systems (Van Der Beek et al., 1997; Tousson and Meissl, 2004; Kalsbeek et al., 2006). SCN neurons are GABAergic interneurons whose unique patterns of GABA and peptidergic synaptic signaling and gap junction communication mediate its robustly rhythmic properties (Liu and Reppert, 2000; Shinohara et al., 2000; Colwell et al., 2003; Li et al., 2009; Lee et al., 2013). Subnuclear patterns of peptide expression, functional connections, and

rhythmic molecular and physiological properties can be used to further subdivide the SCN, with neurons in the dorsal region typically expressing larger amplitude clock protein and electrical activity rhythms (Brown and Piggins, 2009; Pauls et al., 2014), that provide a majority of the SCN's output signals (Kalsbeek et al., 2006, 2010). Neurons in the ventral region play a key role in adaptively phase aligning dSCN output rhythms to those of the environment. Although these ventral and dorsal subnuclear regions have different functions in the SCN, both are clearly needed to function properly (Yan et al., 2007; Loh et al., 2011; Maywood et al., 2011).

By 3 months of age, BACHD mice exhibit reduced amplitude activity rhythms, impaired sleep, and their SCN neurons lose their SFR rhythms due to depressed daytime rates (Kudo et al., 2011b). By 6 months, BACHD mice also show reduced body temperature and heart rate rhythms as well as deficits in their behavioral response to phase shifting light signals. The ionic mechanisms mediating dSCN neurons' electrical activity rhythms and vSCN neurons' photic gating properties are diverse, and to some degree vary between regions. In the absence of synaptic drive, SCN neurons' spontaneous firing rates (SFR) are high during the day and low at night, indicating SFR rhythms are an intrinsic property of individual SCN neurons (Webb et al., 2009). SFR rhythms are mediated by multiple ionic currents that interact to depolarize cell membrane potentials toward action potential thresholds during the day, hyperpolarize membrane potentials to silence them at night, and modulate firing patterns by regulating action potential width and after-hyperpolarization magnitude. The key ionic players regulating membrane potential include the persistent sodium (Jackson et al., 2004; Kononenko et al., 2004, 2008), Na^+/K^+ ATPase (Wang and Huang, 2004, 2006; Wang et al., 2012b), hyperpolarization-activated cyclic nucleotide gated (I_H) (Jiang et al., 1995; de Jeu and Pennartz, 1997; Notomi and Shigemoto, 2004; Atkinson et al., 2011), and large-conductance Ca^{2+} activated potassium (BK) currents (Cloues and Sather, 2003; Meredith et al., 2006; Pitts et al., 2006; Kent and Meredith, 2008). Currents that regulate firing patterns without significantly

contributing to membrane potential include the fast delayed rectifier (FDR) (Itri et al., 2005; Kudo et al., 2011a) and A-type potassium currents (Huang, 1993; Bouskila and Dudek, 1995; Alvado and Allen, 2008; Itri et al., 2010). Amongst both classes, many currents' magnitudes are rhythmic. For some, the rhythm is mediated by rhythmic expression of the protein subunits making up their ion channels (Panda et al., 2002; Lein et al., 2007), while for others, it is mediated by post-translational mechanisms. Notably, for vSCN neurons, both rhythmic expression of the NR2B NMDA-R subunit and its post-translational phosphorylation contribute to rhythms in activity-dependent calcium entry, which is an essential component in the mechanism mediating and gating photic-induced phase shifts of physiology and behavior (Colwell, 2001; Wang et al., 2008).

Following up on our earlier study that found loss of rhythmic SFR in BACHD SCN and deficits in photic responsiveness at the behavioral level in BACHD male mice, the aim of the current work seeks to identify pathophysiological mechanism(s) involved in impaired photic phase shifting and the loss of SFR rhythms by testing for alterations in the currents known to mediate photic phase shifts and regulate SCN SFR.

Materials and Methods

Animals and housing

The UCLA Animal Research Committee approved all experimental protocols used in this study, which followed guidelines and recommendations for animal use and welfare set by the UCLA Division of Laboratory Animal Medicine and National Institutes of Health. The mouse model of HD we employed for this study uses the bacterial artificial chromosome (BAC-)-mediated method to transgenically express the full length human mutant huntingtin gene

encoding 97 glutamine repeats under the control of endogenous regulatory machinery (BACHD) (Gray et al., 2008). Female BACHD dams backcrossed on a C57BL/6J background (minimum 12 generations) were bred with C57BL/6J (WT) males from The Jackson Laboratory (Bar Harbor, Maine) in our own breeding facility to obtain male and female offspring, either WT or heterozygous for the BACHD transgene. Only male mice were used in this study. Genotyping was performed at 15 days of age by tail snips, and after weaning, littermates were group housed, until otherwise noted. All animals were housed in sound proof, humidity controlled chambers with controlled lighting conditions, using a 12 hour light, 12 hour dark cycle (12:12 LD, intensity 300 lux) for at least two-weeks prior to experimentation. For all experiments, a light meter (BK precision, Yorba Linda, CA) was used to measure light-intensity (lux).

Acute slice preparation

Methods for electrophysiology recordings were similar to those previously reported (Kudo et al., 2011b; Kuljis et al., 2013). All animals were between 2.5 and 3.5 months of age, unless otherwise noted. For daytime (ZT4-6) and nighttime (ZT14-16) recordings, animals were briefly placed into a charged isoflurane chamber before decapitation and brain removal at ZT2 and ZT11.5 respectively. Brains were chilled in ice-cold slice solution (in mM: 26 $NaHCO_3$, 1.25 NaH_2PO_4, 10 glucose, 125 NaCl, 2 KCl, 1 $MgCl_2$, 1 $CaCl_2$; Sigma-Aldrich) before trimming and slicing using a Leica VT1200S vibrotome (Nussloch, Germany). Two to three coronal slices (250 µm) containing the SCN were transferred into ice-cold artificial cerebrospinal fluid (ACSF; in mM: 26 $NaHCO_3$, 1.25 NaH_2PO_4, 10 glucose, 125 NaCl, 3 KCl, 2 $MgCl_2$, 2 $CaCl_2$; Sigma-Aldrich), then incubated at 32°C for 30 minutes before a room temperature incubation for one hour. All solutions were adjusted for pH (7.20 - 7.40) and osmolarity (290 – 310), and aerated continually with 95% O_2/ 5% CO_2 for at least 15 minutes before use. Following room-

temperature incubation, slices were placed into a recording chamber (PH-1, Warner Instruments, Hamden, CT) attached to the stage of a fixed upright DIC microscope (Olympus, Tokyo, Japan) and superfused continuously (2 ml/min) with room temperature ACSF. The mid-SCN slice was identified based on third-ventricle and optic chiasm morphology, as well as SCN cell density and area as visualized under magnification. Each cell was determined to be within either ventral mid-SCN or dorsal mid-SCN by directly visualizing its location with reference to anatomical markers. Ventral SCN (vSCN) neurons were classified by their location immediately adjacent to, or in close proximity with the optic chiasm. They are most densely innervated by retinal input (Morin and Allen, 2006; Morin et al., 2006), and were tested for responsiveness to NMDA because of the important role NMDA receptor currents play in photic entrainment (Colwell et al., 1991; Wang et al., 2008). Dorsal SCN (dSCN) neurons were classified by their location just dorsal to the tip of third ventricle. They drive electrical activity rhythms within the SCN in the absence of input and were tested for rhythmic electrical activity, rhythmic resting membrane properties, daytime potassium current magnitude, and responsiveness to pharmacological treatments.

Whole-cell patch-clamp electrophysiology

Whole-cell patch-clamp recordings used electrode micropipettes (3-7 MΩ) pulled from glass capillaries (WPI, Sarasota, FL) using a multistage puller (Sutter P-97, Novato, CA) and were filled with standard internal solution (in mM: 112.5 K-gluconate, 4 NaCl, 17.5 KCl, 0.5 CaCl2, 1 MgCl2 , 5 MgATP, 1 EGTA, 10 HEPES, 1 GTP, 0.1 Leupeptin, 10 Phosphocreatine; pH adjust to 7.2 using KOH and osmolarity adjusted to 290 using sucrose; all chemicals from Sigma-Aldrich), unless otherwise specified. Single-cell recordings were made using the Axopatch 200B amplifier (Molecular Devices, Sunnyvale, CA) and monitored on-line with

pCLAMP (Ver. 10, Molecular Devices). The amplifier's voltage-offset was used to cancel the junction potential between the pipette's internal solution and the extracellular solution (ACSF). While in voltage-clamp mode (0 mV holding), cells were approached by electrode micropipettes, with slight positive-pressure to clear extracellular matrix. By switching to negative-pressure and gradually lowering the holding potential to -70 mV, a high resistance seal (2-10 GΩ) was formed. A second pulse of negative pressure was used to break the membrane and enter whole cell mode. Membrane holding current, cell capacitance, and access resistance were tested using a 5mV step applied at 5 Hz from the -70 mV holding potential. Cells with holding currents greater than 0 or less than -20 pA, capacitances greater than 20 pF, or access resistances greater than 60 MΩ (typically 10 to 40 MΩ) were excluded from analysis. These membrane parameters were monitored during the course of the experiment, and if they changed significantly, or if a cell was unable to decrease firing rate or re-hyperpolarize membrane potential following excitatory treatment, that cell's data was discarded. Pipette-resistance and series-resistance compensation was performed for all voltage-clamp recordings, unless otherwise noted.

Action potential frequency

Following the formation of a high-resistance seal and going whole-cell, the amplifier mode was switched from voltage- to current-clamp, and action potential frequency, here defined as spontaneous firing rate (SFR), was recorded during the subsequent minute without any current injection. SFR was calculated using the total number of action potentials recorded over 60 seconds, unless otherwise noted. Drug treatments were performed by dissolving gabazine (10 μM; Tocris Bioscience, Minneapolis, MN) and N-methyl-d-aspartate (NMDA, 25 μM; Tocris) in ACSF, and were delivered to the slice bath using a rapid gravity feed system. Slices were

treated with gabazine alone for at least 3-4 minutes, or until synaptic activity was abolished as determined by on-line monitoring of membrane activity. SFR was examined over the subsequent minute of gabazine treatment. Slices were then treated with NMDA in the presence of gabazine for two to three minutes, and NMDA SFRs recorded during the subsequent minute. Following NMDA treatment, slices were washed with ACSF for at least four minutes and monitored for the restoration of GABAergic synaptic activity and in the case of NMDA treatment, the re-hyperpolarization of membrane potential and/or reduction of SFR. For dSCN recordings, daytime and nighttime SFRs during gabazine and NMDA treatment were examined for WT and BACHD mice by averaging data from 15-20 cells for baseline and gabazine conditions, and at least 10 cells for NMDA treatment. For vSCN recordings, nighttime NMDA response was examined in slices obtained from both 3 and 6 month old animals in the presence of gabazine. Data for each group were collected from 10-13 neurons using a minimum of 3 animals per group. For both dSCN and vSCN recordings, action potential (AP) properties were analyzed using Clampfit Software (Ver 10.4, Molecular Devices) and MiniAnalysis (Ver. 6.0.3, Synaptosoft, Inc., Fort Lee, NJ). Effects of genotype and pharmacological treatments (gabazine and NMDA) on SFR were examined using Two-Way ANOVA, and when significant effects were detected ($P < 0.05$), post-hoc multiple pairwise comparison testing using the Holm-Sidak method was used to identify significant group differences ($P < 0.05$).

Resting Membrane Properties

Previous studies have shown that Per1::GFP SCN neurons show daily rhythms in multiple resting membrane properties (Kuhlman and McMahon, 2004). A similar protocol was used to examine the intrinsic excitability of SCN neurons in this study, but without the use of a fluorescent marker of gene expression to guide neuron selection. Resting membrane properties

of dSCN neurons were examined during the daytime and nighttime in slices treated for at least 2 minutes with TTX (1μM; Tocris Bioscience, Minneapolis, MN) and gabazine (10μM; Tocris Bioscience) to block action potential and GABAergic synaptic potentials. Multiple neuronal recordings were attempted per slice. Between cells within the same slice, drugs were washed off for 2-5 minutes, or long enough to partially unblock voltage gated and GABA channels. The partial restoration of action potentials allowed discrimination between neurons (electrically active cells) and glia (non-electrically active cells), both of which are found in the SCN. After forming a high resistance seal, going whole-cell, and obtaining membrane parameters for the selected neuron, the amplifier was switched from voltage-clamp to current-clamp mode. Cells typically reached a stable membrane potential within the first 10 seconds of the switch. Resting membrane potential was recorded over the subsequent one to three minute period and was calculated as the average membrane potential during that time. Neurons were then treated with increasingly hyperpolarizing current steps (500 msec, -5 to -25 pA in 5 pA steps). Each neuron was treated three times. Membrane voltage response traces were filtered for electrical interference before analysis (harmonics 1:1, 119 cycles to average, auto-reference frequency). For each replication, peak hyperpolarization (using 5 smoothing points) was examined for each current injection step, then averaged. For all other parameters, the average trace of the three replications was used to identify hyperpolarization peak time, area, and slope of the response between 10 and 90% of its value. Cells which weren't able to maintain steady membrane potential between current injection treatments were excluded from analysis. Two-Way ANOVA was used to identify effects of time and genotype on resting membrane potential and input resistance ($P < 0.05$). Three-Way ANOVA was used to identify effects of time, genotype, and magnitude of negative current injection on neuronal voltage responses ($P < 0.05$). When significant effects were detected, post-hoc multiple pairwise comparisons using the Holm-Sidak method were used to identify statistically significant group differences ($P < 0.05$).

Potassium currents

Potassium current magnitudes were examined in BACHD and WT littermate dSCN neurons during the daytime in voltage-clamp mode. After forming a high resistance seal, going whole-cell, and obtaining membrane parameters, cells were held at -70 mV before treatment with a voltage-step protocol to activate the specific current (protocol details below) twice per minute. After baseline current readings became stable for two consecutive minutes, either an inactivating voltage-step protocol, or a current-specific blocker was applied until further perfusion of blocker did not further reduce current magnitude. The subtraction of the baseline current from inactivation current, or current in the presence of pharmacological blocker was used to calculate the specific current's magnitude. When currents were blocked pharmacologically, cells were washed to confirm that current changes detected during toxin application were toxin specific. All current magnitudes were normalized to cell capacitance. Unless otherwise noted, Two-way ANOVA was used to detect effects of genotype and voltage step on normalized membrane currents ($P < 0.05$). When significant effects were detected, post-hoc multiple pairwise comparison testing using the Holm-Sidak method was used to identify significant group differences ($P < 0.05$).

Fast-delayed rectifier current (FDR) was examined using a similar protocol as published previously (Itri et al., 2005; Farajnia et al., 2012). FDR current was elicited by applying an inactivating -100 mV step (100 msec.) followed by an increasingly positive delta voltage step from -50 to 60 mV (10mV step, 400 msec. duration), after which membrane potential was returned to -100 mV (20 msec.). Control recording medium contained Cd^{++} (25 µM), TTX (1 µM), and gabazine (25 µM) dissolved in ACSF to block voltage-gated calcium, voltage-gated sodium, and $GABA_A$ channels. Control currents typically stabilized over 3 to 8 minutes. Cells were then treated for four minutes with tetra-ethyl ammonium (TEA; 1mM) to block the FDR current and

were then subjected to the same voltage-step protocol. TEA current was subtracted from control current to calculate FDR current magnitude. Control, TEA, and FDR (Control-TEA) currents were normalized to cell capacitance. Current magnitudes were examined both at the start (peak current during the first 90 msec. following capacitive current, using 11-smoothing points) and at the end of the voltage-step (mean current during the last 200 msec. of voltage step). Peak currents were not significantly different from mean currents at the end of the voltage-step, so current values reported in text and figures are mean normalized current at the end of the voltage-step. Traces used in figures were filtered for noise using Bessel (8-pole, 60 Hz) and Boxcar (99-smoothing points) filtering.

The A-type potassium current was examined using methods similar to those previously published (Itri et al., 2010; Farajnia et al., 2012; Granados-Fuentes et al., 2012). Whole-cell patch was formed in regular ACSF using an internal solution similar to the standard one described above except that it contained BAPTA (1mM) instead of EGTA because of its faster calcium-chelating ability. Between recordings, cell membrane potential was held at -70 mV. Due to the voltage sensitivity of the A-type potassium current, its magnitude was calculated as the difference between current responses to voltage-clamp steps from -40 mV to + 40 mV (Δ +10mV per step, 4 sec. each), after either an activating -90 mV, or an inactivating -30 mV pre-pulse step (200 msec.). A baseline reading was taken within one minute of entering whole-cell mode. Cells were then treated with gabazine (10μM), TTX (1μM), CdCl (100μM), and TEA (10mM) for 5 to 10 minutes to block the FDR and slow-delayed rectifier current before a final reading was taken. Both peak (peak current during first 600 msec. of voltage step) and tail currents (mean current during last 100 msec. of voltage-step) were examined. Not all SCN neurons express the A-type potassium current, so two sets of analyses were conducted. The first set examined current magnitudes of all SCN neurons tested, and the second set only examined cells displaying current responses with a characteristic A-shaped peak of the A-type

potassium current. Traces used in figures were filtered for noise using Boxcar filtering (99-smoothing points).

H-current (I_H) was examined using similar methods to those previously published (de Jeu and Pennartz, 1997), except that recordings were made in the presence of gabazine (10μM) and TTX (1μM) to inhibit electrical and synaptic activity in the slice. The presence of I_H was examined using both voltage- and current-clamp mode. For voltage-clamp recordings, cells were held at -70 mV. When tested, cell membrane potential was briefly stepped to -50mV (100 msec.) before an increasingly negative voltage step was applied to evoke I_H (-50 to -120 mV, Δ-10 mV step, 1000 msec.), after which membrane potential was returned to -50 mV (250 msec.). Before analysis, voltage-clamp traces were filtered for electrical interference (harmonics 1 to 6, cycle average 83 Hz, reference frequency 60 Hz.) using a Bessel filter (8-pole, 40 Hz. cutoff), due to a large amount of recording noise obscuring the small current magnitudes. I_H was quantified as the difference in current magnitude from the start of the hyperpolarizing voltage step (T1: between 80 and 110 msec. or between 230 and 260 msec.) to the end of the step (T2: 890 – 920 msec.). Two-way ANOVA was used to detect genotypic and/or voltage-step effects on currents at T1, and delta current at T2 for all voltage-clamp steps. Not all SCN neurons expressed I_H. The magnitudes of current responses specifically for neurons showing a current potentiation from T1 to T2 (Δ current > -0.1 pA) for the -110 mV step were tested for genotypic differences using a Two-Tailed TTEST ($P < 0.05$). Voltage-clamp traces for figures were subjected to additional low-pass Box Car filtering (99 smoothing points).

In current-clamp mode, I_H was tested by examining membrane voltage-responses to negative current injection. Before the start of current-clamp recordings, current was manually injected to bring membrane potential to -50 mV, or baseline. During the current-clamp protocol, 0 pA of additional current was applied from baseline (350 msec.), then an increasingly negative

current step was injected to evoke I_H (-7.5 to -52.5 pA, Δ -7.5 pA steps, 1000 msec.), before return to baseline (2650 msec). If current-step injection hyperpolarized membrane potential beyond -150 mV, the protocol was terminated to avoid damaging the cell. If a cell was not able to maintain baseline membrane potential, it was discarded from further analysis. Peak voltage hyperpolarization was examined for all current-injection steps. Current-injection steps that produced peak hyperpolarizing voltage-responses between -90 and -110 mV (physiologically relevant range that should illicit I_H if present) were selected for further analysis. If the peak occurred before the end of step, the difference in membrane potential from the peak to the end of the step (900-990 msec.) was calculated as the magnitude of the hyperpolarization-induced depolarizing sag. Magnitude of the current injection step required to bring the membrane potential into the relevant range, time of peak hyperpolarizing membrane potential response, and magnitude of the depolarizing sag were tested for genotypic differences using a Two-Tailed TTEST ($P < 0.05$). Depolarizing sag amplitudes were variable cell-to-cell, and were binned based on magnitude. The proportion of neurons expressing no sag, sags less than 5 mV, and sags greater than or equal to 5 mV was compared between genotypes using Chi2 test ($P < 0.05$).

Large-conductance potassium (Big-K or BK) currents were tested using methods similar to those previously published (Pitts et al., 2006). Recording conditions were the same as those described above, except that internal solution had a lower concentration of EGTA (0.5 mM) so as not to interfere with calcium activation of the BK current. In whole-cell mode, cells were voltage-clamped at -60 mV holding potential for 3 to 5 minutes. Next, the cell's membrane potential was clamped at -70 mV (100 msec.) to fully inactivate voltage-gated channels, and membrane potentials were moved from -100 to +80 mV (20mV steps, 180 msec.) to activate BK-currents before being returned to -70 mV (200 msec.). Current magnitude was examined during the last 20 to 30 msec. of each voltage step. Baseline currents were measured twice per

minute until they were stable across three trials. Cells were then treated with iberiotoxin (IbTX, 100nM; Sigma) for 5 to 8 minutes to block BK currents. Current magnitude was tested every minute, and IbTX treatment was terminated when no further reduction of currents were detected. Cells were then washed for 10 to 30 minutes to either partially or fully restore current magnitudes back to baseline levels.

The ATP-sensitive potassium channel (K_{ATP}) is inhibited by intracellular ATP and the sulfonylurea tolbutamide (Edwards and Weston, 1993). Its activation causes membrane hyperpolarization and reduced excitability of hypothalamic neurons (Parsons and Hirasawa, 2010). Immediately after entering whole-cell mode and recording membrane properties, baseline current magnitudes were examined by clamping membrane potential from -140 mV to 80 mV (20 mV steps, 180 msec. duration). Cells were perfused with gabazine (10μM), TTX (1μM), CdCl (100μM), and 0.1% dimethyl-sulfoxide (DMSO). Then current magnitudes were tested every minute until stable for at least two minutes (typically 5-8 minutes). Tolbutamide (1mM in 0.1% DMSO; Sigma-Aldrich) was added for 5 minutes and membrane currents were tested every minute thereafter until they remained stable over two minutes (typically 7-9 minutes). Current magnitudes were examined during the last 40 msec. of the current step. Normal internal solution was used for K_{ATP} current experiments and therefore, intracellular ATP levels were likely clamped at high levels for all neurons. Baseline currents, stabilized control currents, tolbutamide treated currents, and the magnitude of the K_{ATP} current (stabilized control – tolbutamide) was examined.

SFR rescue experiments

Daytime SFR was examined in dSCN neurons from BACHD animals and in a subset of WT neurons with low SFR for effects of pharmacological agents targeting either potassium currents (tolbutamide, IbTX, and ZD7288), or intracellular second messenger pathways (L-name, 8-bromo-cGMP, 8-bromo-cAMP, and forskolin/phosphodiesterase inhibitor 3-isobutyl-1-methylxanthine (FS/IBMX). Typically, baseline SFR was recorded over 5 minutes, then the specific drug was applied over 10-15 minutes and SFR was re-examined. Cells were then washed for 15 to 30 minutes and SFR examined a last time for washout effects. Most recordings were performed using the cell-attached recording (CAR) method to avoid the confounding effects of internal solution diffusion into the intracellular milieu, but in some cases both recording conditions were used for comparison. Voltage responses recorded in current-clamp mode using CAR and whole-cell (WC) recording methods were used to calculate SFR. Effects of drug treatment both during treatment and following washout were tested relative to baseline SFR using Paired TTESTs. All drugs were prepared in ddH_20 at 1:1000 concentration (except tolbutamide which was prepared in DMSO) and aliquots frozen at -20°C until the day of experimentation when they were dissolved into ACSF at the final concentrations noted in text and figures. Baseline SFR was recorded in equal concentrations of drug vehicle.

BACHD and WT littermate daytime SFR was examined in dSCN neurons for effects of depolarizing current injection. After going whole-cell in voltage-clamp mode, SFR was examined in current-clamp mode over 1 minute. Cells were then injected with positive current steps (0 to 25 pA, Δ5 pA steps, 1 sec. duration) and effects on SFR were examined. SFR was calculated as the average number of action potentials recorded during the positive current injection step. Paired TTESTs were used to detect effects of positive-current injection steps on SFRs and intern-spike membrane potentials (ISMP) relative to the previous current injection step.

CT16 light-pulse

At 6 months of age, BACHD and WT littermate animals (n = 4) were singly housed with running wheels for two weeks in 12:12LD, then released into constant darkness for a minimum of 5 days to determine free-running locomotor rhythm period, which was used to calculate circadian time 16 (CT16), or 4 circadian hours following activity onset. At CT16 each animal was exposed to 10 minutes of 100 lux light. Fifty minutes later, animals were anesthetized with isoflurane and perfused intracardially with 20 mL 0.9% saline in 0.1 M phosphate buffer (PBS; pH 7.4) containing heparin (2 units/mL), followed by 40 mL 4% paraformaldehyde in 0.1 M PB (4% PFA). Brains were post-fixed in 4% PFA overnight at 4 °C, then cryoprotected in 20% sucrose in 0.1 M PB overnight at 4 °C. Brains were then flash frozen on CYRO-OCT Compound (Fisher Scientific, Pittsburgh, PA) and sliced using a cryostat (20 µm thick sections). Immunohistochemistry was performed on free-floating sections from mid-SCN. Sections were washed with PBS before and after endogenous peroxidase quenching (3%H_2O_2 and 10%MeOH in PBS), then protein blocked for 1 hour (3% normal goat serum, 0.1% TritonX-100), before overnight 4°C incubation with cFos antibody (1:10,000; Millipore, Danvers, MA). Sections were washed with PBS and incubated with biotinylated goat anti-rabbit antibody (1:200) for 2 hours before being washed with PBS again, and dipped in AB solution (Vector Laboratories, Burlingame, CA) for 45 minutes. Slices were then washed with tris-buffered saline (TBS; 0.1M), and placed for 5.5 minutes in filtered 0.05% 3,3'-diaminobenzidine (Sigma-Aldrich, St. Louis, MO) containing 1:800 dilution of 1.3% H_2O_2. A final TBS wash was then performed, and slices mounted on slides. Mounted sections were dried overnight and cover-slipped using DEPEX (Fisher Scientific). FOS^+ cells were counted twice by blind volunteers, and averaged across the 4 mid-most SCN slices. Genotypic differences in cFOS induction were assessed using the Mann-Whitney Rank Sum Test.

All reported values are means ± 95% CI. Significance levels for all statistical procedures were set at $P < 0.05$.

RESULTS

Light-input

By 6 months of age, male BACHD mice exhibited smaller magnitude phase shifts in response to CT16 light-pulse and took longer to re-entrain to phase shifts of their photic environmental rhythm (Kudo et al., 2011b). To test whether defects in light-entrainment at the behavioral level are related to deficits in the light-input pathway at the level of the SCN neuron, two experiments were conducted. First, we tested the ability of synaptically isolated vSCN neurons to respond to acute application of NMDA (25μM). Previous studies have shown that NMDA-R currents are essential for SCN-mediated photic phase shifts (Colwell et al., 1991; Wang et al., 2008), and a growing body of evidence indicates NMDA-R signaling is altered in the HD brain (Li, 2003; Fan and Raymond, 2007). We hypothesized that if alterations to NMDA-R currents in BACHD vSCN neurons underlie deficits in behavioral entrainment, NMDA-induced SFR increases at night would be impaired.

Effects of NMDA on vSCN neuron SFR were examined at both 3 and 6 months of age in WT and BACHD brain slices. Three-Way ANOVA was performed to test for statistically significant effects of genotype, age, and NMDA treatment on SFR (**Fig. 6.1A**). Significant main effects of age ($F_{1,95} = 7.9$, $P = 0.006$) and NMDA treatment ($F_{1,95} = 44.3$, $P < 0.001$) were found, but not a main effect of genotype ($F_{1,95} = 0.2$, $P = 0.7$), nor interaction effects of genotype and age ($F_{1,95} = 2.6$, P = 0.1), genotype and treatment ($F_{1,95} = 3.5$, $P = 0.07$), age and treatment ($F_{1,95} = 0.06$, P = 0.8), or genotype, age and treatment ($F_{1,95} = 0.7$, $P = 0.4$) on SFR were identified.

Pairwise multiple comparisons using the Holm-Sidak method found that average firing rates of vSCN neurons decreased from 3 to 6 months (-0.95 ± 0.6 Hz., t = 2.8, *P* = 0.006), and post-hoc Paired TTESTs found that NMDA treatment caused significant increases in SFR for WT vSCN neurons both at 3 months (+1.3 ± 0.4 Hz., n = 10, t = -7.4, *P* < 0.001) and 6 months of age (+2.0 ± 0.6 Hz., n = 13, t = -7.1, *P* < 0.001). No deficits in BACHD vSCN neuronal responses were detected either at 3 months (+3.1 ± 1.0 Hz, n = 12, t = -7.0, *P* < 0.001) or 6 months of age (+2.7 ± 1.4 Hz, n = 13, t = -4.2, *P* = 0.001) (**Fig. 6.1B**). There were however genotype-specific differences in the effects NMDA treatment had on action potential (AP) properties at 6 months of age. Following NMDA application BACHD vSCN neuronal APs exhibited reduced peaks, larger and longer widths, slower and smaller after-hyperpolarizations, and slower decays (**Table 6.1**). Taken together, these findings indicate that when BACHD mice exhibit behavioral deficits in photic re-entrainment, at the physiological level, NMDA still potently excites BACHD vSCN neurons, but different effects of NMDA on BACHD AP properties indicate NMDA-activated currents are likely altered in BACHD mice. These changes may affect the mechanism whereby SCN electrical events are transduced into phase shifts of gene expression rhythms and the onset of wheel-running activity.

To test the ability of light-input to upregulate SCN gene expression, we examined whether light at night would induce SCN immediate early gene *cFos* expression (**Fig. 6.1C**), an effect thought to play a causal role in the phase shifting of the circadian system by light (Albrecht, 2012). A low intensity (100 lux) light-pulse was presented in the early subjective evening (CT16) to 6 month old BACHD and WT littermate mice, and cFOS induction was examined 60 minutes later. Using immunohistochemical techniques, we found robust cFOS induction within 60 minutes in SCN for both WT (71 ± 26 cells, n = 4) and BACHD (60 ± 21 cells, n = 4) animals, but no significant genotypic difference was detected (Mann-Whitney Rank Sum Test, T = 23, *P* = 0.2) (**Fig. 6.1D**). These findings indicate the retina is able to communicate

light-signals to the SCN of BACHD mice. The mechanism underlying behavioral deficits in photic phase shift re-entrainment lies within the SCN circuit, and/or the ability of the SCN to communicate temporal signals effectively to downstream targets.

SFR, GABA, and membrane potential rhythms

Previously we found that BACHD SCN neurons lose their rhythm in electrical activity due to depression of daytime spontaneous firing rates (SFR) (Kudo et al., 2011b). Here we re-examined this finding, and again found that at baseline (**Fig. 6.2A**), WT dSCN neurons have fast SFRs during the day (5.3 ± 1.2 Hz.) and low SFRs during the night (3.6 ± 1.1 Hz), while BACHD dSCN neurons have low SFRs both during the day (1.8 ± 0.7 Hz.) and night (2.4 ± 1.0 Hz.). The SCN is a GABAergic neuronal network and alterations in its circuit properties may have caused excess inhibitory tone.

Extending our earlier findings, we tested whether depressed SFRs were a property of the BACHD SCN circuit or a cell-autonomous deficit by examining SFR rhythms in the presence of the $GABA_A$-R antagonist gabazine (10μM) (**Fig. 6.2B**). Gabazine treated WT dSCN neurons still showed fast SFRs during the day (6.8 ± 1.8 Hz.) and low SFRs at night (4.1 ± 1.3 Hz.). Gabazine treated BACHD neurons still had low SFRs during both the day (1.7 ± 0.7 Hz.) and night (2.0 ± 1.0 Hz.). Three-Way ANOVA was performed to identify significant effects of genotype, time, and/or gabazine treatment on SFR of dSCN neurons. Significant interaction effects of genotype and time ($F_{1,129}$ = 13.8, P < 0.001) were found, as well as main effects of genotype ($F_{1,129}$ = 67, P < 0.001) and time ($F_{1,129}$ = 5.5, P = 0.02), but not of treatment ($F_{1,139}$ = 1.3, P = 0.3), and no interaction effects of genotype and treatment ($F_{1,129}$ = 3.0, P = 0.1), time and treatment ($F_{1,129}$ = 0.8, P = 0.4), nor for genotype, time and treatment ($F_{1,129}$ = 0.2, P = 0.7). Post-hoc multiple pairwise comparison testing using the Holm-Sidak method identified that SFR

was significantly higher during the day than night for WT dSCN neurons (+2.2 ± 1.1 Hz., t = 4.1, $P < 0.001$), but not significantly different between the day and night for BACHD dSCN neurons (-0.5 ± 1.0 Hz., t = 1.0, $P = 0.3$). Additionally, regardless of gabazine treatment, BACHD SFRs were lower than that of WT, both during the day (-4.3 ± 0.7 Hz, t = 8.7, $P < 0.001$) and night (-1.6 ± 1.0 Hz, t = 3.1, $P = 0.003$). Fisher Exact Test was used to identify whether the proportion of neurons that responded to gabazine with increased SFR (indicative of GABA inhibition) or decreased SFR (indicative of GABA excitation), varied based on time of day within genotype or between genotypes within time of day. A higher proportion of WT dSCN neurons exhibited GABA-inhibitory responses during the day (11/13) than at night (6/14, $P < 0.05$), while BACHD dSCN neurons exhibited no more GABA-inhibitory responses during the day (11/20) than during the night (6/16, $P = 0.3$). Additionally, BACHD neurons exhibited no higher proportion of GABA-inhibitory responses relative to WT either during the day ($P = 0.1$) or night ($P = 1.0$).

We also tested a variety of AP properties for effects of genotype, time and/or gabazine treatment using Three-Way ANOVA (**Table 6.2**). Post-hoc comparison testing identified that BACHD APs had larger areas, slower rise times, and slower decay times relative to WT APs. We also found a main effect of genotype ($F_{1, 104} = 11$, $P = 0.001$) on inter-spike membrane potential. BACHD dSCN neuron inter-spike membrane potentials were significantly hyperpolarized during the day (-4.4 ± 1.4 mV, t = 3.3, $P = 0.001$). Using the Fisher Exact Test, we determined gabazine treatment depolarized WT during the day (12/12) and night at similar rates (10/14, $P = 0.1$). BACHD dSCN neurons also had similar rates of depolarization during the day (6/12) and night (10/12, $P = 0.2$), but relative to WT, they exhibited a reduced proportion of depolarizing responses to gabazine during the day ($P = 0.01$) and not the night ($P = 0.7$). These findings indicate that if anything, GABA has reduced inhibitory effects on BACHD dSCN neurons, and we conclude that hyperpolarization of its inter-spike membrane potential and reduced SFRs are not synaptically mediated.

Inter-spike membrane potential hyperpolarization hints at the possibility that rhythmic regulation of excitatory drive at the level of the individual neuron may be altered in BACHD dSCN neurons. Previously it was shown that rhythmic resting membrane potential is a component of the physiological mechanism mediating SFR rhythms in dSCN neurons, and is regulated by rhythmic potassium conductances near resting membrane potentials that can be evidenced as changes to input resistance (Kuhlman and McMahon, 2004). To test whether deficits in resting membrane properties are a part of the mechanism that underlies the loss of rhythmic electrical output in BACHD dSCN, we tested for rhythms in cell capacitance, resting membrane potential, and input resistance in the presence of the voltage gated sodium channel blocker TTX and the $GABA_A$-R antagonist gabazine. Two-Way ANOVA was used to test for effects of genotype and/or time on cellular capacitance and resting membrane potential, while Three-Way ANOVA was used to test for effects of genotype, time, and/or hyperpolarizing current injection magnitude on membrane voltage responses, which were also used to calculate input resistance.

Cell capacitance, or a cell's ability to act as a capacitor, is directly related to its surface area, and was tested using a small voltage step pulse in voltage-clamp mode (**Fig. 6.3A**). We found there was a main effect of genotype on cell capacitance ($F_{1, 118} = 14.7$, $P < 0.001$), but not of time ($F_{1, 118} = 0.7$, $P = 0.4$), nor an interaction effect of genotype and time ($F_{1, 118} = 2.3$, $P = 0.1$). Post-hoc multiple pairwise comparisons using the Holm-Sidak method found that although capacitance was not rhythmic for either BACHD neurons (Day +1.3 ± 1.4 pF, t = 1.7, $P = 0.4$) or WT neurons (Day -0.39 ± 0.44 pF, t = 0.5, $P = 0.6$), BACHD neuron capacitance was significantly larger than that of WT neurons during the day (+3.1 ± 1.4 pF, t = 4.5, $P < 0.001$), and not at night (+1.3 ± 1.4 pF, t = 1.4, $P = 0.2$). Resting membrane potential, showed a main effect of time ($F_{1, 129} = 7.0$, $P = 0.009$), but not of genotype ($F_{1, 129} = 0.2$, $P = 0.7$), nor an interaction of genotype and time ($F_{1, 129} = 0.9$, $P = 0.4$). Post-hoc pairwise comparison testing

using the Holm-Sidak method found WT dSCN neurons exhibited rhythmic resting membrane potentials. Their daytime potentials were more depolarized than nighttime potentials (Day -49.9 ± 2.8, Night -55.5 ± 3.5, t = 2.5, P = 0.01). BACHD dSCN neurons lost this rhythm in resting membrane potential, so that daytime and nighttime potentials were not significantly different (Day -51.7 ± 3.3 mV, Night -54.6 ± 3.1 mV, t = 1.2, P = 0.2). Additionally, resting membrane potentials displayed an intermediate level in BACHD neurons, so that they were not significantly different from WT neurons either during the day (-2.2 ± 2.8 mV, t = 1.1, *P* = 0.3) or night (+0.9 ± 3.1 mV, t = 0.3, *P* = 0.7).

Next, we tested membrane potential responses to negative current injection to measure for rhythms in input resistance (**Fig. 6.3C**). Main effects of genotype ($F_{1, 736} = 4.7$, $P = 0.03$), time ($F_{1, 736} = 5.7$, $P = 0.02$), and current ($F_{5, 736} = 280$, $P < 0.001$), and an interaction effect of genotype and time were identified ($F_{1, 736} = 4.4$, $P = 0.04$). Non-significant interaction effects include genotype and current ($F_{5, 736} = 0.4$, $P = 0.8$), time and current ($F_{5, 736} = 0.7$, $P = 0.6$), and genotype, time and current ($F_{5, 736} = 0.4$. $P = 0.9$). Post-hoc pairwise comparison of voltage response magnitudes using Two-Tailed TTESTs for each current injection step indicated that although voltage responses trended toward larger values in WT dSCN neurons during the daytime for each step, they were only significantly larger for the largest negative current injection step (-25pA step Day -15.4 ± 5.4 mV, t = 2.1, *P* = 0.04) (**Fig. 6.3D** top). Post-hoc pairwise comparison testing using the Holm-Sidak method found that WT neurons exhibited significantly greater voltage responses than BACHD neurons during the day (-6.3 ± 1.3 mV, t = 3.2, *P* = 0.002; night: +0.11 ± 1.4 mV, t = 0.05, *P* = 1.0). However, they were not significantly different for any specific current injection step including the largest (-25 pA WT -9 ± 10 mV, t = -1.1, *P* = 0.3).The average voltage response was used to calculate input resistance. WT dSCN neuronal input resistance was rhythmic (Day 3.1 ± 0.1 MΩ, Night 2.7 ± 0.1 MΩ, t = 3.2, *P* =

0.001), and this rhythm was lost in BACHD dSCN neurons (Day 2.7 ± 0.1 MΩ, Night 2.7 ± 0.1 MΩ, t = 0.2, $P = 0.8$).

Notably, the selected trace examples showing membrane potential responses to negative current injection displayed hyperpolarization induced depolarization *following* current step injection only for WT neurons. The presence of this response was visually assessed for all recordings to determine whether the proportion of neurons exhibiting this response was altered in BACHD SCN. Although it was slightly more common in WT neurons (day: 24/45; night: 13/23) than for BACHD's (day: 14/31; night: 14/28), the proportion of neurons exhibiting these responses did not significantly vary by time of day for WT (Chi2 = 0.04, $P = 0.8$) or BACHD neurons (Chi2 = 0.01, $P = 0.9$), nor did it vary by genotype either during the day (Chi2 = 0.4, $P = 0.5$) or night (Chi2 = 0.2, $P = 0.7$). Voltage-response traces were selected to emphasize the different magnitudes of WT day/night voltage responses. Many neurons also showed depolarization *during* the hyperpolarizing current injection (as seen in WT nighttime trace), which is consistent with HCN channel current tested more directly later.

BACHD dSCN neurons displayed a wide-range of resting membrane potentials. An additional experiment was conducted to test whether voltage responses would differ if baseline membrane potentials were standardized. All neurons' membrane potentials were brought to a -50 mV baseline using manual current injection, then the same negative current injection steps were performed and peak voltage responses were examined for effects of genotype and/or current using Two-Way ANOVA. Main effects of genotype ($F_{1, 200} = 7.7$, $P = 0.006$) and current were found ($F_{5, 200} = 51$, $P < 0.001$) without interaction effects ($F_{5, 200} = 0.5$, $P = 0.7$). Although there was an even greater difference in the mean voltage responses between WT and BACHD neurons (WT -9.3 ± 2.5 mV, t = 2.8, $P = 0.006$), no significant genotypic differences were

identified for any particular current injection step, including the largest (-25 pA WT – 11.8 ± 11 mV, t = 1.4, *P* = 0.2).

In summary, the loss of rhythmic SFR in BACHD dSCN neurons is associated with the loss of rhythmic resting membrane potential and input resistance, depressed daytime SFR and hyperpolarized daytime inter-spike membrane potentials. However, no significant hyperpolarization of resting membrane potential was detected, indicating membrane potential alone cannot account for the reduced electrical activity we observed in BACHD dSCN. Another potential mechanism underlying BACHD dSCN daytime SFR depression includes alterations to potassium currents regulating inter-spike timing.

Potassium currents altered during the daytime in BACHD dSCN

Multiple potassium currents could alter spiking rates, but not significantly affect resting membrane potentials, including the FDR, A-type-potassium, BK, and hyperpolarization induced potassium (I_H) currents. The next step in characterizing pathophysiology of SCN in the BACHD model, focuses on determining whether these currents were altered specifically during the daytime, when the greatest effects on SFR were observed.

First, to test the possibility that HCN channel mediated hyperpolarization-induced currents (I_H) are altered in the BACHD SCN, the magnitude and prevalence of I_H in dSCN neurons was compared between BACHD and WT littermates using both voltage- and current-clamp recording methods (**Fig. 6.4**). In voltage-clamp mode, cellular membrane potential was held at -50 mV, then moved to increasingly negative voltages using voltage-clamp steps long enough in duration to activate I_H (~1 sec) (**Fig. 6.4A**). The difference in the magnitude of outward currents at the beginning of the voltage step (T1) versus the end (T2), was quantified

as the magnitude of I_H and reported as the delta T2 current (**Fig. 6.4B**). The current magnitude at T1 and the delta T2 current was tested for effects of genotype and voltage-step magnitude using Two-Way ANOVA. Main effects of genotype ($F_{1, 831} = 52$, $P < 0.001$) and voltage ($F_{7, 831} = 48$, $P < 0.001$) were identified for T1 current, but no interaction of genotype and voltage ($F_{7, 831} = 1.5$, $P = 0.1$). Main effects of genotype ($F_{1, 831} = 6.7$, $P = 0.01$) and voltage ($F_{7, 831} = 6.4$, $P < 0.001$) were also found for T2 delta current, without interaction effects of genotype and voltage ($F_{7, 831} = 0.8$, $P = 0.6$). Post-hoc pairwise comparisons of T1 current magnitudes at each voltage step using the Holm-Sidak method found significant genotypic differences from -80 mV (WT -0.69 ± 0.4 pA/pF, t = 2.3, $P = 0.02$) through -120 mV voltage steps (WT – 1.35 ± 0.4 pA/pF, t = 4.4, $P < 0.001$) (**Fig. 6.4B** top), while delta T2 current was only significantly larger in WT neurons for the -110 mV step (-0.15 ± 0.06, t = 2.5, $P = 0.01$) and the -120 mV step (-0.12 ± 0.06, t = 2.0, $P = 0.04$).

We also examined the effects negative current injection had on membrane potential in current clamp mode (**Fig. 6.4C**). Cell membrane potential was manually clamped at -50 mV, and negative current injection steps were applied. Traces for which peak hyperpolarization reached between the -90 to -110 mV range, were examined further for the presence of a depolarizing sag during the current step. Depolarizing sag magnitude was quantified as the difference in membrane potential from peak hyperpolarization to the membrane potential at the end of the current injection step. Across all current-clamp recordings, WT neurons exhibited larger magnitude depolarizing sags than BACHD neurons (+ 2.0 ± 1.7 mV, t = 2.2, $P = 0.03$). Notably, the magnitude of the current-injection step required to bring membrane potential within the -90 to -110 mV range did not differ (WT -2.4 ± 3.9 pA, t = -1.2, $P = 0.2$), nor did the time of the hyperpolarization peak based on genotype (WT -71 ± 85 msec., t = -1.6, $P = 0.1$). It became clear however that for both genotypes, cell-to-cell, there was a considerable variety in the magnitude of voltage sags (**Fig. 6.4C**). We also examined whether the proportion of neurons

showing no sag, a small sag (< 5 mV), or large sags (≥ 5 mV) differed between genotypes, and found that a significantly reduced proportion of BACHD neurons displayed voltage sags (Chi2 = 6.5, $P = 0.04$). Fewer BACHD neurons expressed I_H, raising the possibility that the magnitude of the current may or may not be altered among neurons that do express it. To test this possibility, we compared delta T2 currents with magnitudes greater than -0.1 pA during the -110 mV voltage step. The T1 current for these recordings was still larger in WT neurons (-1.8 ± 0.9 pA/pF, t = -3.7, $P < 0.001$), but the genotypic difference in the delta T2 current was lost (-0.19 ± 0.58 pA/pF, t = -1.8, $P = 0.07$), indicating that although a reduced proportion of BACHD neurons express I_H current for cells that do express it, the magnitude was not altered.

The nuanced differences in the I_H are likely insufficient to account for the robust decrease in daytime SFR observed in BACHD neurons, so we examined additional potassium currents regulating SFR. FDR current magnitude was calculated as the difference in current evoked by a series of voltage-clamp steps, before and after the application of the FDR antagonist TEA (**Fig. 6.5A**). Two-Way ANOVA was used to identify significant effects of genotype and voltage-step magnitude on control currents, TEA insensitive currents, and FDR currents (Control – TEA) (**Fig. 6.5B**). For control currents, main effects of genotype ($F_{1, 755} = 4.1$, $P = 0.04$) and voltage ($F_{11, 755} = 113$, $P < 0.001$) were found, but no interaction effect of genotype and voltage ($F_{11, 755} = 0.3$, $P = 1.0$). Although BACHD neurons tended toward expressing larger control currents than WT neurons (60 mV step BACHD +18 ± 18 pA/pF, t = 1.6, $P = 0.1$), post-hoc testing failed to detect significant genotypic differences in current magnitudes for any particular voltage step. For TEA currents, a main effect of voltage ($F_{11, 754} = 105$, $P < 0.001$) was identified, but no effect of genotype ($F_{1, 754} = 3.2$, $P = 0.08$) or interaction of genotype and voltage ($F_{11, 751} = 0.2$, $P = 1.0$). Similarly for FDR currents, a main effect of voltage ($F_{11, 754} = 57$, $P < 0.001$) was identified, but not of genotype ($F_{1, 754} = 0.4$, $P = 0.5$) or the interaction of genotype and voltage ($F_{11, 754} = 0.1$, $P = 1.0$). Peak FDR currents are very similar for WT (67 ±

12 pA/pF) and BACHD neurons (63 ± 17 pA/pF), and we conclude FDR current is not altered in BACHD dSCN neurons.

The third current examined was the voltage-gated A-type potassium current. Its magnitude was calculated as the difference in current responses evoked by a series of voltage steps after an activating pre-pulse step to -100 mV and an inactivating pre-pulse step at -30 mV (**Fig. 6.6A**). About two-thirds of all WT and BACHD neurons tested exhibited the characteristic shape of the A-type potassium current, so two sets of analysis were conducted. One examined the current magnitudes of all neurons tested, while the second focused only on neurons exhibiting the characteristic A-type shape of the A-type potassium current. For both sets of analyses, Two-Way ANOVA was used to identify effects of genotype and voltage step magnitude on peak and tail currents. For the analysis examining all neurons (WT, n = 33; BACHD, n = 27), a main effect of voltage ($F_{8, 548} = 31$, $P < 0.001$) on peak current was identified, but no effect of genotype ($F_{1, 548} = 0.8$, $P = 0.4$) or an interaction of genotype and voltage ($F_{8, 548} = 0.02$, $P = 1.0$). For tail currents, a main effect of genotype ($F_{1, 548} = 7$, $P = 0.008$) and voltage ($F_{8, 18} = 18$, $P < 0.001$) was found, but no interaction effects of genotype and voltage ($F_{8, 548} = 0.5$, $P = 0.8$); however, post-hoc multiple pairwise comparison testing using the Holm-Sidak method failed to detect any significant difference in tail current magnitudes for any particular voltage-step. The second set of analysis focused only on neurons displaying current responses with the characteristic A-shape of the A-type potassium current (**Fig. 6.6B**). A main effect of voltage on peak current magnitude was identified for cells expressing A-type potassium currents ($F_{8, 350} = 31$, $P < 0.001$), but no effect of genotype ($F_{1, 350} = 2.4$, $P = 0.1$) or interaction effects of genotype and voltage were found ($F_{8, 350} = 0.2$, $P = 1.0$). For tail currents however, a main effect of genotype ($F_{1, 350} = 28$, $P < 0.001$) and voltage were found ($F_{8, 350} = 12$, $P < 0.001$), as well as a significant interaction of genotype and voltage ($F_{8, 350} = 2.3$, $P = 0.02$). Post-hoc multiple pairwise comparison testing using the Holm-Sidak method determined that tail currents for BACHD

neurons were not sensitive to the magnitude of the voltage-clamp step, and were significantly smaller than that of WT neurons for all positive voltage steps. On average WT neurons' tail currents were larger than those of BACHD neurons (+2.5 to 4.5 ± 0.3 pA/pF, t = 5.3, $P < 0.001$).

The fourth current examined was the BK current, which is sensitive to both voltage and intracellular calcium levels. Due to the effects of APs on intracellular calcium levels, this set of recordings was not performed in the presence of TTX. The magnitude of current responses to a series of voltage-steps were examined under control conditions and following application of the BK channel blocker IbTX. BK current was calculated as the difference between control currents and those recorded during IbTX treatment (**Fig. 6.7A**). Two-way ANOVA was used to test for effects of genotype and/or voltage step on the magnitude of control, IbTX insensitive, and IbTX sensitive currents. For control currents, a significant main effect of genotype ($F_{1, 399} = 6.9$, $P = 0.009$) and voltage were detected ($F_{9, 399} = 113$, $P < 0.001$), but not an interaction effect of genotype and voltage ($F_{9, 399} = 1.6$, $P = 0.1$). Post-hoc multiple pairwise comparison testing using the Holm-Sidak method determined that control current magnitudes were significantly greater in BACHD than WT neurons at 60 mV (+38 ± 11 pA/pF, t = 2.6, $P = 0.01$) and 80 mV voltage-steps (+52 ± 11 pA/pF, t = 3.5, $P < 0.001$). For IbTX insensitive currents, a main effect of voltage ($F_{9, 399} = 81$, $P < 0.001$) was found, but not for genotype ($F_{1, 399} = 2.3$, $P = 0.1$) or genotype and voltage interaction effects ($F_{9, 399} = 0.6$, $P = 0.8$). For the BK current, significant main effects of genotype ($F_{1, 399} = 8.9$, $P = 0.003$), voltage ($F_{9, 399} = 52$, $P < 0.001$), and interaction effects of genotype and voltage ($F_{9, 399} = 2.1$, $P = 0.03$) were found. Post-hoc multiple pairwise comparison testing using the Holm-Sidak method determined that BACHD neurons exhibited significantly greater BK current magnitudes at 60 mV (+21 ± 5 pA/pF, t = 3.1, $P = 0.002$) and 80 mV holding potential than WT neurons (+25 ± 5 pA/pF, t = 3.7, $P < 0.001$) (**Fig. 6.7B**).

We also examined a fifth current - the ATP-regulated potassium (K_{ATP}) current, which regulates excitability. Although this current is inhibited by intracellular ATP, these recordings were performed using regular internal solution, which contains ATP, in order to determine whether under similar conditions as those used when measuring daytime SFR, alterations in K_{ATP} could be detected in BACHD dSCN neurons. The magnitude of currents evoked using a series of voltage steps was tested immediately after going whole-cell (before pipette internal solution had time to diffuse intracellularly), following stabilization under control recording conditions, and following treatment with the K_{ATP} current blocker tolbutamide. K_{ATP} current was calculated as the difference between control and tolbutamide treated current responses (**Fig. 6.8A**). Two-Way ANOVA was used to test for effects of genotype and/or voltage step on the magnitude of current responses before stabilization, under control conditions, following tolbutamide treatment, and for K_{ATP} currents. For the first reading prior to stabilization, a main effect of voltage ($F_{11, 251} = 77$, $P < 0.001$) on currents were found, but not of genotype ($F_{1, 251} = 2.5$, $P = 0.1$) or interaction effects of genotype and voltage ($F_{11, 251} = 0.7$, $P = 0.7$). Under control recording conditions following current stabilization (**Fig. 6.8B**), again a significant main effect of voltage on current magnitudes was identified ($F_{11, 251} = 55$, $P < 0.001$), but not a main effect of genotype ($F_{1, 251} = 3.2$, $P = 0.08$) or an interaction effect of genotype and voltage ($F_{11, 251} = 0.6$, $P = 0.8$). Post-hoc multiple pairwise comparison testing using the Holm-Sidak method, found that the magnitude of the current response to 80 mV holding potential was significantly greater in BACHD neurons than it was for WT neurons (+37 ± 31 pA/pF , t = 2.1, $P = 0.04$). Similarly, following tolbutamide treatment, main effects of voltage on current magnitudes were found ($F_{11, 228} = 39$, $P < 0.001$), but no main effects of genotype ($F_{1, 251} = 2.9$, $P = 0.09$) or interaction effects of genotype and voltage ($F_{11, 228} = 0.6$, $P = 0.6$), while post-hoc pairwise multiple comparisons using the Holm-Sidak method identified that BACHD current responses were again significantly larger for the 80 mV holding potential (+42 ± 31 pA/pF, t = 2.1, $P = 0.04$). For K_{ATP} currents,

voltage had a significant main effect ($F_{11, 251} = 2.9$, $P = 0.001$), but no main effects of genotype ($F_{1, 251} = 0.001$, $P = 1.0$) or interaction effects of genotype and voltage ($F_{11, 251} = 0.005$, $P = 1.0$). Confidence intervals for peak K_{ATP} current magnitudes of WT (26 ± 46 pA/pF) and BACHD neurons (25 ± 25 pA/pF) include 0 pA/pF, indicating tolbutamide treatment did not have a significant effect on currents. This is likely due to the fact that K_{ATP} currents were maximally inhibited by recording conditions (ATP-containing pipette internal solution). Although no genotypic differences in current magnitudes were identified immediately after going whole-cell before pipette internal solution had time to diffuse into the cell, this is still an inconclusive test.

In summary, daytime BACHD dSCN neurons have smaller magnitude A-type potassium tail currents and larger magnitude BK current at depolarized potentials. Additionally, while the magnitude of the FDR current and I_H are not altered, a smaller proportion of BACHD neurons express I_H. Finally, although no genotypic differences were detected for K_{ATP} currents, if this were a part of the pathophysiological mechanism, the recording conditions would have obscured it. Taken together, depressed daytime SFR is associated with small changes in a number of potassium currents regulating SFR in SCN.

SFR rescue: potassium current targets

To test whether manipulating altered potassium currents could pharmacologically rescue depressed SFR in BACHD dSCN neurons or a subset of low SFR WT dSCN neurons, a series of experiments was conducted. In the first experiment (**Fig. 6.9A**), SFR was examined under baseline conditions over 5 minutes (WT 3.1 ± 0.8 Hz, BACHD 2.4 ± 1.7 Hz.), then slices were treated with the K_{ATP} current blocker tolbutamide for 15 minutes. A significant increase in AP frequency was detected for both WT and BACHD neurons (WT +1.1 ± 0.9 Hz, T = -2.61, $P = 0.024$; BACHD +1.0 ± 0.4 Hz, T = -5.18, $P < 0.001$). Following treatment, slices were washed

for 15 minutes and AP frequency returned to baseline levels (WT -0.3 ± 1.2 Hz, T = -1.87, *P* = 0.09; BACHD -0.4 ± 1.2 Hz, T = -1.37, *P* = 0.21). Although we weren't able to detect genotypic differences in K_{ATP} currents using our standard whole-cell recording procedure, using cell-attached recording (CAR) methods we found this current's inhibition using tolbutamide increased SFR for both BACHD and WT, indicating that K_{ATP} regulates SFR in SCN.

Next, using a low concentration of IbTX (50nM), we tested whether partial blockage of BK currents could increase SFR (**Fig. 6.9B**). A small increase in BK current magnitudes was detected in BACHD dSCN neurons, so a lower concentration of IbTX was applied to reduce BK current. AP frequency was examined under baseline conditions for 5 minutes (WT 3.8 ± 1.2 Hz, BACHD 2.3 ± 0.7 Hz.), then slices were treated with IbTX (50nM) for 10 minutes and changes to AP frequency were examined. Overall, neither WT or BACHD neurons' SFRs significantly responded to treatment, although WT neurons trended toward lower rates, while BACHD neurons trended toward higher rates (WT -0.3 ± 0.5 Hz., T = 1.25, *P* = 0.23; BACHD +0.2 ± 0.3 Hz., T = -1.24, *P* = 0.24). Following treatment, slices were washed for 30 minutes and AP frequency examined again for drug washout effects, but again, although there was a trend toward IbTX treatment causing small increases in SFR for BACHD neurons even after washout, this effect was not statistically significant (WT -0.4 ± 1.5 Hz., T = -0.70, *P* = 0.50; BACHD +0.5 ± 0.5 Hz., T = -1.77, *P* = 0.10), indicating that acute manipulations of BK currents does not rescue reduced SFR for BACHD neurons.

Finally, considering that a reduced proportion of BACHD dSCN neurons expressed the I_H current, we tested whether application of the I_H current blocker ZD7288 could phenocopy reduced daytime SFR in WT neurons (**Fig. 6.9C**). Using the whole-cell (WC) recording method to assess effects on fast SFR (n = 10) and the CAR method to assess effects on a subset of WT neurons with lower SFRs (n = 14), SFR was first assessed under baseline conditions over 5

minutes (CAR 3.6 ± 0.7 Hz, WC 6.7 ± 4.7 Hz.). Slices were then treated with I_H blocker ZD7288 (10 μM) for 5 minutes, and although there was a trend toward increased firing rates in the presence of ZD7288, these effects were not statistically significant (CAR +0.2 ± 0.8 Hz, T = -0.53. *P* = 0.61; WC +0.1 ± 1.5 Hz, T = -0.14, *P* = 0.90). Following treatment, slices were washed for 5 minutes and SFR was examined for drug washout effects. A significant increase in AP frequency relative to baseline rates was detected for CAR but not WC recordings (CAR +0.9 ± 0.7 Hz, T = -2.55, *P* = 0.02; WC +1.3 ± 1.3 Hz, T = -1.51, *P* = 0.17). Reducing I_H did not reduce SFR in WT neurons with high SFR, which is consistent with previous studies (de Jeu and Pennartz, 1997). It did however slightly increase rates for neurons with low SFRs after washout, which was unexpected because this current is excitatory, and blocking excitatory currents usually results in reduced action potential frequencies.

SFR rescue: cyclic nucleotides

Some ion channel's activity is modulated by cyclic nucleotides and other second messenger pathways (Ko et al., 2009; Colwell, 2011). For instance, I_H is gated by intracellular cyclic nucleotide levels (He et al., 2014) and cyclic nucleotide regulated kinases modify activity of BK channels (Kyle and Braun, 2014). Considering also that cyclic nucleotide levels are altered in the HD brain (Bollen and Prickaerts, 2012), we next tested whether manipulating levels of intracellular cyclic nucleotides and other 2nd messengers pharmacologically could acutely increase SFR for BACHD neurons and a subset of WT neurons with low SFR. The nitric oxide/cGMP and adenylate cyclase/cAMP pathways were targeted as both play important roles in regulating SCN electrical activity (Prosser et al., 1989; An et al., 2011; Atkinson et al., 2011).

The first second messenger tested was nitric oxide using the inducible nitric oxide synthase inhibitor, L-name (**Fig. 6.10A**). AP frequency was examined under baseline conditions

for 5 minutes (WT 2.5 ± 1.5 Hz, BACHD 3.2 ± 1.3 Hz), then slices were treated for 15 minutes with L-name, and SFR was examined for changes. Although a subset of cells responded to L-name with faster SFRs, overall the trend toward higher SFRs was not statistically significant for either BACHD or WT neurons (WT +0.5 ± 1.0 Hz, Paired TTEST, $T = 0.17$, $P = 0.87$; BACHD +0.6 ± 1.3 Hz, $T = 0.14$, $P = 0.89$). Following treatment, slices were washed for 30 minutes, and AP frequency examined to test for after-effects of drug treatment, but again, no significant difference in SFR was detected (WT +0.3 ± 1.1 Hz, T = 0.41, $P = 0.69$; BACHD +0.3 ± 0.6 Hz., T = 0.58, $P = 0.58$).

Nitric oxide functions in neurons by regulating cGMP levels (Shen and Johnson, 2010). Although inhibition of nitric oxide synthase was not able to increase firing rates, perhaps increasing levels of cGMP might, so we tested whether the cGMP cell permeable analog 8-bromo-cGMP could acutely raise SFRs (**Fig. 6.10B**). AP frequency was examined under baseline conditions for 5 minutes (WT 3.1 ± 0.4 Hz, BACHD 2.1 ± 1.8 Hz.), then slices were treated for 15 minutes with the 8-bromo-cGMP and AP frequency was examined for changes. SCN neurons tended to respond to 8-bromo-cGMP with decreased SFR, but overall there was no significant effect of treatment (WT -0.3 ± 0.7 Hz, T = 1.11, P = 0.33; BACHD -0.5 Hz. ± 1.2 Hz, T = 1.14, $P = 0.31$). Slices were washed for 30 minutes and SFR examined for after-effects of drug treatment, but again SFRs were on par with baseline rates and no significant effect on SFR was found (WT -0.5 ± 1.2 Hz., T = 1.18, $P = 0.30$; BACHD -0.8 ± 1.5 Hz., T = 1.34, $P = 0.24$).

The second pathway we tested was the adenylate cyclase/cAMP second messenger system. The activation of adenylate cyclase and downstream increases of intracellular cAMP are known to have an important role in the regulation rhythms of electrical activity within the SCN (Welsh et al., 2010; An et al., 2011; Atkinson et al., 2011). We tested whether acute

manipulation of this pathway could alter SFRs. We first treated cells with the cell permeable cAMP analog, 8-bromo-cAMP (**Fig. 6.10C**). AP frequency was examined under baseline conditions for 5 minutes (WT 2.3 ± 0.6 Hz, BACHD 1.9 ± 1.6 Hz.), then slices were treated for 15 minutes with 8-bromo-cAMP, and AP frequency was examined for changes. Some neurons with low starting SFR responded with increases in SFR, but most cells either did not respond or responded with decreased SFR so that overall, there was no statistically significant effect of 8-bromo-cAMP treatment (WT -0.4 ± 0.5 Hz., T = 1.8, *P* = 0.13; BACHD -0.3 Hz. ± 0.7 Hz., T = 0.34, *P* = 0.35). Following treatment, slices were washed for 30 minutes, and AP frequency was tested again for after-effects of treatment. Again no significant changes in SFR were detected (WT -0.3 ± 0.6 Hz, T = 1.24, *P* = 0.26; BACHD -0.6 ± 1.0 Hz, T = 1.50, *P* = 0.19).

Finally, we examined whether acute treatment with the adenylate cyclase activator forskolin (FS, 20μM) and phosphodiesterase inhibitor 3-isobutyl-1-methylxanthine (IBMX, 500μM) could increase SFR for BACHD neurons specifically, using either the CAR or WC recording methods (**Fig. 6.10D**). AP frequency was examined under baseline conditions over 2 minutes (CAR 3.1 ± 0.5 Hz, WC 1.3 ± 1.0 Hz.), then slices were treated for 10 minutes with FS and IBMX, and changes in AP frequency were examined. There was a promising trend toward increased SFRs using the CAR method, but overall FS/IBMX did not have a statistically significant effect on SFRs using either recording method (CAR +0.4 ± 0.5 Hz, T = -2.0, *P* = 0.07; WC -0.1 Hz. ± 1.3 Hz, T = 0.20, *P* = 0.85). Following treatment, slices were washed for 10 minutes, and AP frequency was re-examined to test for after-effects of drug treatment. No significant changes in SFR from baseline rates were detected (CAR -0.4 ± 1.3 Hz, T = 0.68, *P* = 0.52; WC -0.1 ± 1.4 Hz, T = 0.14, *P* = 0.89). Overall acute drug applications manipulating levels of cyclic nucleotides did not have significant effects on SFR in BACHD dSCN neurons, and failed to rescue depressed daytime SFRs; however, adenylate cyclase activation had a

promising effect on SFR, raising the possibility that a longer application and/or time-interval for assessment of SFR may be warranted.

SFR rescue: excitation

Although targeting K_{ATP} currents slightly increased SFR and there were indications targeting cAMP levels might increase SFR in BACHD dSCN, the lack of a clear rescue for depressed dSCN SFR using acute drug treatment was evident. Although a significant hyperpolarization of resting membrane potential was not detected for BACHD dSCN neurons, a small but significant hyperpolarization of the inter-spike membrane potential was detected, so for the last two last-experiments, we revisited the possibility that reduced excitatory drive underlies reduced SFR in BACHD dSCN neurons by testing their responsiveness to direct and pharmacological excitation. For the first experiment, positive current was directly injected into WT and BACHD neurons (**Fig. 6.11**). For all WT and BACHD neurons examined, progressively larger current injection steps (0 to 25 pA, Δ5 pA steps, 1 minute duration) caused significant increases in inter-spike membrane potential relative to the previous current step. WT neurons, which already had fast SFRs, did not respond to further membrane depolarization with further increases in SFR. Larger magnitude current injection steps were associated with reduced SFR (**Fig. 6.11A**). In contrast, for BACHD neurons, membrane depolarization significantly increased neural SFRs for the first three positive current injection steps relative to each previous step (5 < 10 < 15 pA), and all current injection steps significantly increased SFRs relative to baseline (**Fig. 6.11B**). Remarkably, direct current injection successfully restored SFRs of BACHD neurons to the levels of WT neurons.

Next, we tested whether pharmacological excitation could similarly restore SFRs. NMDA treatment was applied during both the day and night to synaptically isolated WT and BACHD

dSCN neurons (**Fig. 6.12**). Two-Way ANOVA was used to detect effects of genotype and/or time of treatment on SFR and inter-spike membrane potential changes induced by NMDA treatment. No main effects of genotype ($F_{1, 40} = 0.06$, $P = 0.8$) or time ($F_{1, 40} = 2.5$, $P = 0.1$), nor interaction effects of genotype and time were detected for NMDA-induced changes to SFR ($F_{1, 40} = 2.4$, $P = 0.1$). Both BACHD and WT neuron's SFRs increased to a similar degree following NMDA treatment (WT +2.7 ± 0.9 Hz, BACHD +3.0 ± 1.0 Hz). For NMDA-induced changes to inter-spike membrane potentials, there were no main effects of genotype ($F_{1, 36} = 0.007$, $P = 0.9$) or time ($F_{1, 36} = 2.3$, $P = 0.1$), but there was an interaction of genotype and time ($F_{1, 36} = 8.1$, $P = 0.007$). Post-hoc multiple pairwise comparisons testing using the Holm-Sidak method, found that following NMDA treatment, WT neurons did not depolarize during the daytime (-0.8 ± 1.1 mV), but did at night (+4.7 ± 1.3 mV, t = 3.2, $P = 0.003$). In contrast, BACHD neurons significantly depolarized during both the day (+2.9 ± 1.3 mV) and night (+1.2 ± 1.3 mV, t = 0.9, $P = 0.4$). Additionally, during the day, the magnitude of BACHD neurons' inter-spike membrane potential depolarization was significantly greater than that of WT neurons (+3.7 ± 1.3 mV, t = 2.2, $P = 0.04$), but not at night when they were comparable between genotypes (BACHD -3.5 ± 3.5 mV, t = 1.9, $P = 0.07$). The variable effects of NMDA application to WT and BACHD neurons during the daytime led us to also test for effects of genotype and/or NMDA treatment on absolute SFRs specifically during the daytime using Two-Way ANOVA. Highly significant main effects of genotype ($F_{1, 54} = 26$, $P < 0.001$) and treatment ($F_{1, 54} = 8.6$, $P = 0.005$) were found, but no interaction effects of genotype and treatment ($F_{1, 54} = 0.1$, $P = 0.8$). Post-hoc multiple pairwise comparison testing using the Holm-Sidak method found that although NMDA treatment was associated with significantly higher SFRs in BACHD neurons (baseline: 1.7 ± 0.6 Hz., NMDA: 4.7 ± 0.9 Hz., t = 2.8, $P = 0.01$), this was not true for WT neurons (baseline: 6.8 ± 0.8, NMDA: 9.3 ± 0.9, t = 2.2, $P = 0.07$). Additionally, although NMDA treatment significantly increased

BACHD neuron SFRs, their rates still were not on par with WT's in the presence of NMDA (BACHD -4.5 ± 0.9 Hz., t = 3.7, $P < 0.001$).

Taken together with findings from current injection experiments, NMDA effects on SFR and inter-spike membrane potential indicate that WT neurons may be maximally depolarized and/or firing at maximal rates during the daytime. NMDA treatment does not further depolarize WT inter-spike membrane potentials or induce significant increases in SFR during the daytime. While the positive current injection depolarized WT neurons membrane potential, it decreased SFRs by increasing AP failure rates. In contrast, BACHD neurons' SFRs and inter-spike membrane potentials increased both during the day and night in response to NMDA. This indicates either the gating of excitatory input to the SCN may be disrupted in BACHD SCN, and/or NMDA responsiveness at both times of day is simply due to the fact that BACHD neuron SFRs start out at lower rates and are more hyperpolarized, and therefore not constricted by the same ceiling effects of excitation as WT SFRs. Overall, the responsiveness of BACHD dSCN neurons to excitation is a promising finding that indicates manipulating the timing of SCN excitatory inputs to occur specifically during the day may be therapeutically useful for improving circadian system function.

Discussion

The inability to get a restful night's sleep for HD patients has a significant impact on the quality of life for both patients and their caregivers (Taylor and Bramble, 1997). Taking into account the negative impact sleep disruption has on mental, cognitive, and physical health (Foster and Wulff, 2005; Rüger and Scheer, 2009; Castanon-Cervantes et al., 2010), understanding the mechanisms underlying HD related sleep disruption may have important implications for improving gene carrier health-spans. Temporal aspects of patient sleep and

physiological rhythms implicate dysfunction of the circadian system (Morton et al., 2005; Aziz et al., 2009a; Goodman et al., 2010, 2011; Kalliolia et al., 2014; Videnovic et al., 2014). Multiple animal models of HD recapitulate this dysfunction (Morton et al., 2005; Goodman et al., 2010; Maywood et al., 2010; Kudo et al., 2011b; Loh et al., 2013). Focusing on the BACHD mouse model, we followed up on our earlier study characterizing their age-related decline in behavioral and physiological rhythms (Kudo et al., 2011b) by testing multiple ionic mechanisms to account for alterations in photic responsiveness of BACHD behavioral rhythms and the loss of electrical activity rhythms of BACHD SCN neurons.

The SCN typically generates robust rhythms in electrical activity that entrain to photic environmental rhythms using a mechanism involving NMDA-R activation and induction of gene transcription (Colwell et al., 1991; Morin and Allen, 2006; Wang et al., 2008). We examined the light-input pathway to the SCN by testing SCN neuron's responsiveness to excitation by NMDA and a light-pulse's ability to induce gene transcription at 6 months of age -- when male BACHD mice exhibit smaller magnitude phase shifts in response to CT16 light-pulse and take longer to re-entrain to photic environmental rhythm phase shifts (Kudo et al., 2011b). On the physiological level NMDA still potently excites BACHD vSCN neurons, and at the molecular level, CT16 light-pulse still induces cFOS expression in BACHD mid-SCN (**Fig. 6.1**). Based on these findings, we conclude light-signals are successfully reaching BACHD SCN from the retina, but a trend toward less cFOS induction in BACHD SCN and NMDA treatment's aberrant effects on BACHD AP peaks, widths, after-hyperpolarization, and decay properties suggest subtle changes in the BACHD light-input pathway (**Fig.6.1** and **Table 6.1**). The lack of clear deficits favor alternative explanations to account for aberrant photic entrainment of BACHD behavioral rhythms, including disruption of communication between retinorecipient and dorsal output SCN neurons, the possibility that deficits in rhythmic SCN output obscure subtle changes light has on its phase, and/or deficits in extra-SCN tissue's responsiveness to SCN signals.

Previously we found that BACHD SCN neurons lose their rhythms in electrical activity due to depression of daytime SFR that correlates with elevated daytime activity, body temperature, and heart rate (Kudo et al., 2011b). Extending our earlier findings, we sought to identify the ionic mechanisms underlying depressed daytime SFR and the subsequent loss of electrical activity rhythms in BACHD dSCN. Our first hypothesis was that enhanced GABA signaling within the GABAergic SCN circuit inhibited electrical activity of BACHD SCN neurons, but treatment with the $GABA_A$-R antagonist gabazine has no effect on BACHD dSCN SFR (**Fig. 6.2**), indicating that rather than being an aberrant property of the SCN circuit, depressed SFR is a cell-autonomous property of individual BACHD SCN neurons. At the level of the individual SCN cell, the interplay of multiple ionic currents regulates daily rhythms in SFR. These currents can be broadly categorized into two classes - those regulating resting membrane potential rhythms and those regulating AP dynamics and rates. Hints that both classes of currents are disrupted in BACHD dSCN include the daytime hyperpolarization of inter-spike membrane potentials and slower AP re-hyperpolarization dynamics (**Table 6.2**).

First we examined membrane potential regulating currents. Previous studies have shown that night-time hyperpolarization of *Per1*::GFP neurons in SCN is associated with reduced input resistance and increased potassium conductance that regulate nighttime hyperpolarization of resting membrane potential (Kuhlman and McMahon, 2004). Similarly we find WT littermate dSCN neurons have a rhythm in resting membrane potential and input resistance, with daytime depolarization associated with increased input resistance and nighttime hyperpolarization associated with decreases in input resistance (**Fig. 6.3**). Notably, the magnitude of the rhythm detected in the current study is smaller than the one previously reported, likely due to the fact that selection of cells in the current study was limited to anatomical markers, while the previous work used fluorescent markers of clock protein expression to guide neuron selection. Surprisingly, even though daytime inter-spike membrane

potentials are hyperpolarized in BACHD dSCN neurons, resting membrane potentials are no different than those of WT neurons either during the day or night (**Fig.6.3**). Additionally, no day/night rhythm in resting membrane potential or input resistance is seen among BACHD neurons, but relative to WT neurons, they show a small decrease in input resistance during the day. Why this is not associated with hyperpolarization of resting membrane potential is unclear, but one possibility is that reduced excitability of BACHD dSCN neurons may be related to deficits in the dynamic interplay of the ionic currents that regulate membrane potential and those that regulate AP properties. This is supported by our observation that inter-spike membrane hyperpolarization of BACHD dSCN neurons is lost when electrical activity is silenced.

Multiple potassium currents that alter spiking rates and have little or no effects on resting membrane potentials are expressed in SCN (Colwell, 2011). Focusing on the daytime when the greatest effects on SFR were observed, BACHD dSCN neurons show small alterations in multiple currents. First, the proportion of neurons expressing I_H currents and I_H-type voltage responses to hyperpolarizing current injection is reduced. Similar to previous reports, we found a majority of WT SCN neurons express large depolarizing sags in response to negative current injection (Kim and Dudek, 1993; Akasu and Shoji, 1994; Cloues and Sather, 2003), but only about a third of BACHD neurons do (**Fig. 6.4**). I_H is an excitatory current regulated by cyclic nucleotides and cAMP levels (Akasu and Shoji, 1994; He et al., 2014), and its reduction in BACHD SCN is consistent with reduced excitatory drive, and raises the possibility that mHTT affects cyclic nucleotide levels. Although acute inhibition of I_H current using ZD7288 does not contribute to fast daytime SFRs of WT neurons (**Fig. 6.9C**)(Cloues and Sather, 2003; Atkinson et al., 2011), sustained I_H blockade compromises molecular pacemaking and AP firing (Atkinson et al., 2011). Under pathological conditions such as in BACHD SCN, the reduction of its expression across the SCN circuit may significantly alter how cells respond to prolonged inhibition and play a significant role in daytime SFR depression and the loss of SFR rhythms.

Acute manipulations of cyclic nucleotide levels using 8-bromo-cAMP, 8-bromo-cGMP, L-name, and FS/IBMX failed to increase low SFR in SCN. Multiple explanations can account for the inability of cyclic nucleotides to acutely increase BACHD dSCN SFR, including the limited duration of treatment (< 1 hr), and the possibility that the reduction of I_H current expressing cells in BACHD dSCN is due to the dysregulation of HCN channel expression rather than at the level of cyclic nucleotide gating of HCN channels.

Next, we found that the BK current was larger in BACHD dSCN neurons during the daytime (**Fig. 6.7**). This is consistent with the reduction in daytime SCN SFR associated with the enhancement of BK currents, and increased SCN SFR associated with the loss of BK channels previously reported (Meredith et al., 2006; Montgomery and Meredith, 2012). BK channels are typically open during action potential repolarization and after-hyperpolarization phases, which is consistent with the longer times BACHD dSCN neuron APs take to rehyperpolarize (**Table 6.2**). Additionally, enhanced BK currents in BACHD SCN raise the possibility that either the pattern of BK channel subunit expression, subunit post-translational modifications, and/or calcium levels are altered in BACHD SCN. BK currents were targeted pharmacologically using a low concentration of the BK channel blocker IbTX in an attempt to rescue BACHD SFR. Although some neuron's SFRs increase in response to IbTX treatment, others were inhibited, and overall our attempts at reducing BK currents failed to have significant effects on SFR (**Fig. 6.9**).

In contrast, although we were not able to reliably detect genotypic differences in the K_{ATP} current, its pharmacological inhibition did acutely increase SFRs for BACHD and WT dSCN neurons (**Fig. 6.9**). The K_{ATP} channel is uncharacterized in the SCN, but is expressed by neurons throughout the nervous system, including glucose sensing neurons of the hypothalamus, feeding and wake promoting orexinergic neurons, and dopaminergic neurons of the midbrain (Liss et al., 1999; Burdakov et al., 2005; Parsons and Hirasawa, 2010). The K_{ATP}

current is inhibited by intracellular ATP levels, and for some neurons it is activated in response to low blood glucose levels during fasting for the purpose of stimulating feeding behavior, while in other neurons when energetic levels become unfavorable for sustained neural activity such as in the case of metabolic stress, it hyperpolarizes membrane potential to silence neurons. For many neurons, the activation of K_{ATP} currents is an adaptive function to prevent excitotoxic neuronal damage and can even be pharmacologically manipulated to prevent neurodegeneration (Virgili et al., 2013). The significant excitatory effects of the K_{ATP} channel blocker tolbutamide on SCN neurons indicate K_{ATP} current regulates SCN neuron SFR and warrants further more detailed examination.

Aged mice exhibit lengthening of behavioral rhythm periods, reductions to activity and physiological rhythm amplitudes, and activity fragmentation similar to those of young BACHD mice (Valentinuzzi et al., 1997; Nakamura et al., 2011). Aged SCN also exhibits a similar reduction in the amplitude of SFR rhythms (Nakamura et al., 2011; Farajnia et al., 2012). We predicted that premature alterations to the same currents underlying the loss of SFR rhythm amplitude in aged SCN would be altered in BACHD SCN and found remarkable similarities (Farajnia et al., 2012). Reduced daytime SFRs are common for aged SCN neurons, and like BACHD neurons, they are not associated with significant resting membrane potential hyperpolarization. Additionally, both aged and BACHD dSCN neurons exhibit reduced A-type current during the day (**Fig. 6.6**). We also examined FDR current magnitude because of the known effects it has in regulating fast daytime SFRs in SCN (Kudo et al., 2011a), but like for aged SCN (Farajnia et al., 2012), significant alterations in daytime FDR currents are not associated with reduced SFR in BACHD dSCN (**Fig. 6.5**). Unlike aged SCN neurons which have reduced cell capacitances relative to young neurons, BACHD dSCN neurons have significantly larger cell capacitances than WT littermates (**Fig. 6.3**). The two phenotypes of aged and BACHD SCN dysfunction, further diverge in their nighttime profiles. Aged SCN neurons

exhibit significant night time resting membrane potential depolarization and increased SFRs, which we did not observe in BACHD dSCN neurons (Farajnia et al., 2012). Nevertheless, the overlap in daytime pathophysiology of aged and BACHD SCN neurons raises the possibility that a similar mechanism underlying reduced daytime SFR is at play in aged and BACHD SCN.

Although BACHD dSCN neurons' SFR is depressed during the daytime, it increases in response to direct current injection and pharmacological excitation. In contrast, WT neurons are firing close to their maximal rates during the daytime and exhibit a ceiling effect to additional daytime excitation. Excitation with NMDA for BACHD neurons causes significant depolarization inter-spike membrane potentials and increases in SFRs both during the day and night. These findings indicate that timing SCN excitatory stimuli to occur specifically during the day and inhibitory stimuli to occur at night, may be therapeutically useful for improving circadian system function in the BACHD mouse. Promising evidence of the therapeutic benefits of imposing such temporal structures has already been shown using short duration bright light exposure, scheduled voluntary wheel running, and timed administration of $GABA_A$-R agonists using a different mouse model of HD (Pallier et al., 2007; Cuesta et al., 2014). An important caveat for the use of drugs potentiating or inhibiting $GABA_A$-R currents is that NKCC1 and KCC2 Cl^+ symporters are rhythmically expressed, and their relative abundances dynamically regulate whether GABA signaling is inhibitory or excitatory (Choi et al., 2008; Haam et al., 2012). Additionally, GABA effects on the SCN circuit may be affected by sex, other genetic factors such as mHTT, and change based on environmental factors (Kim et al., 2011; Kuljis et al., 2013). Other potential interventions, including the timing of meals and nighttime melatonin treatment, should also be considered for their effects on regulating SCN activity. Ultimately, the findings outlined in this study should be used to inform the development of pharmacological and behavioral interventions for the treatment of circadian rhythm abnormalities associated with HD. The overlap of circadian dysfunction phenotypes associated with HD, other neurodegenerative

disorders, and ageing (Kuljis et al., 2012) raises the possibility that similar interventions may be useful for treating circadian disruption for a diverse patient population.

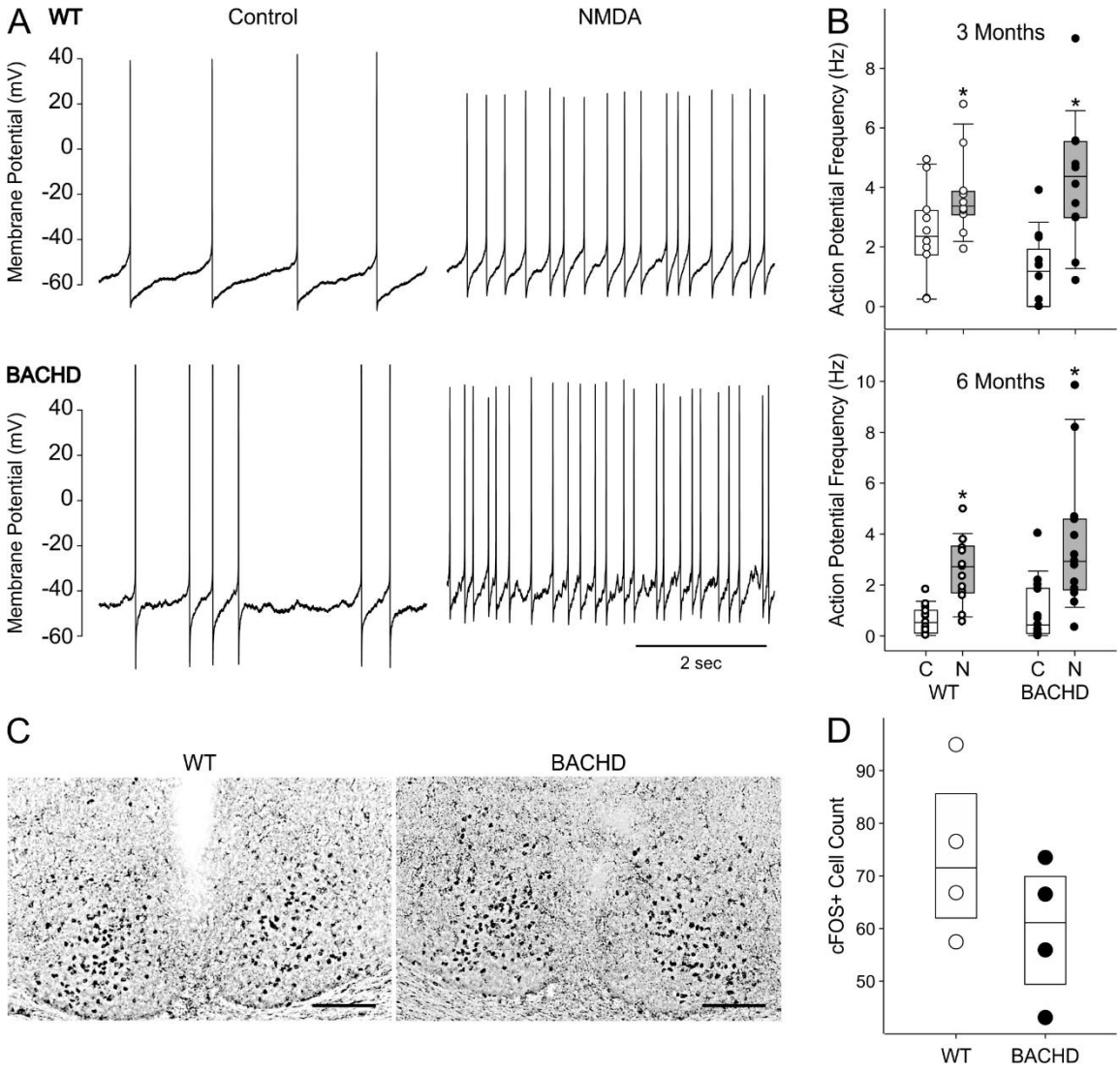

Figure 6.1: SCN light-input pathway. **(A)** Individual traces of a synaptically isolated vSCN neuron's electrical activity recorded during the night in current clamp mode under control conditions (10 µM gabazine) and following application of NMDA (25 µM) using acute slice cultures harvested from 6 month old WT (top) and BACHD (bottom) mice. **(B)** Box plots showing the 25th and 75th percentile (box), medians (center line), and data range (whiskers), with individual data points of neuronal action potential frequencies overlaid for both recording conditions (C = control, N = NMDA). Effects of NMDA were examined at 3 and 6 months of age for WT (white dots; 3 months, n =10; 6 months, n = 13) and BACHD vSCN neurons (black dots; 3 moths, n = 12; 6 months, n = 13). Paired TTEST, *P < 0.05. **(C)** Representative images of cFOS immunoreactivity in mid-SCN slices taken from 6 month old WT (left) and BACHD (right) mice. Scale bar (100 µm). **(D)** Box plots showing 25th and 7th percentile (box) and median (center line) of cFOS^{+} cell counts induced by CT16 light-pulse for 6 month old WT (white dots, n = 4) and BACHD mice (black dots, n = 4).

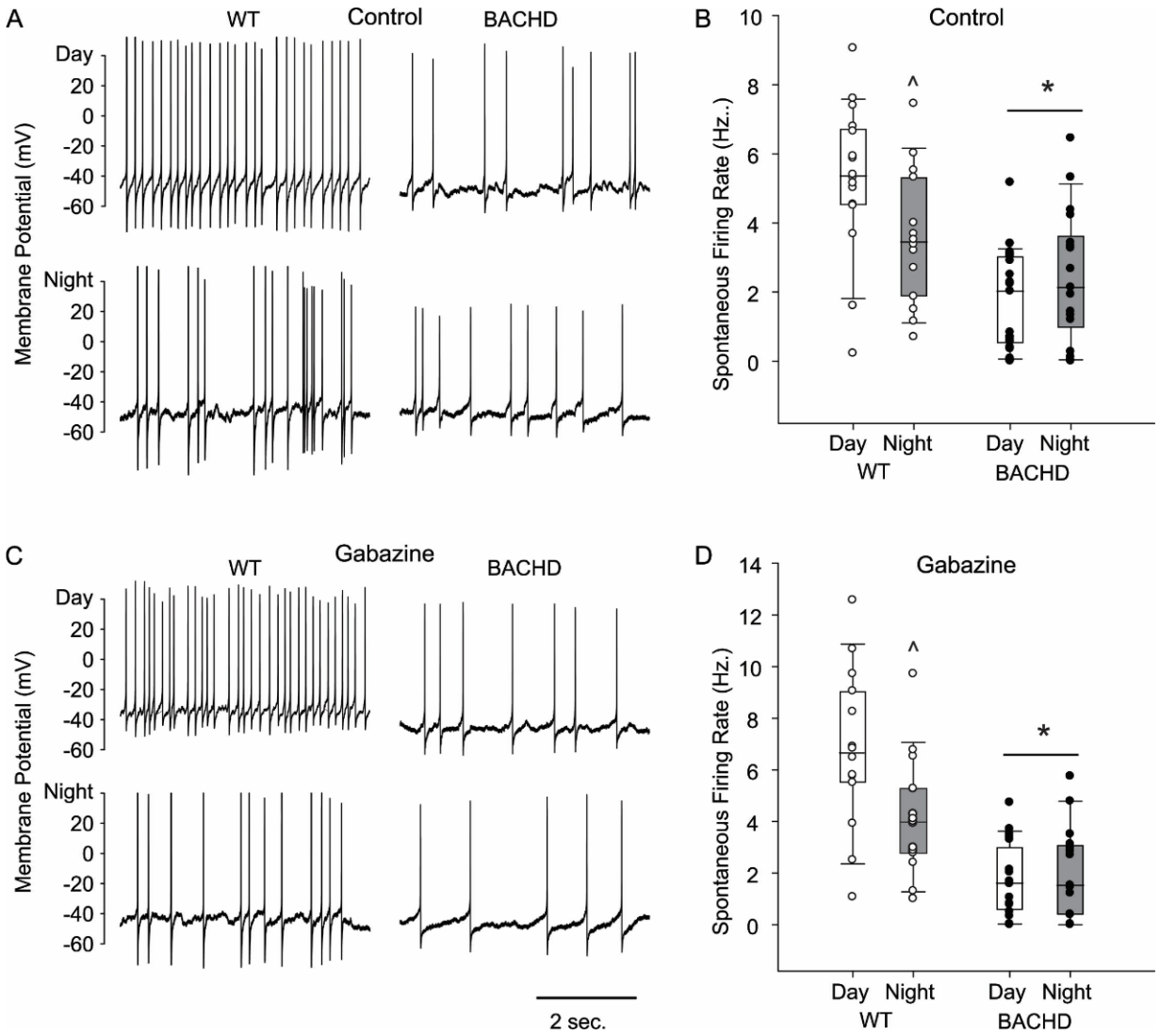

Figure 6.2: Depressed daytime SFR in BACHD dSCN is not mediated by GABA. **(A)** Representative traces of dSCN neuron spontaneous firing rates (SFR) under control conditions (ACSF) recorded during the day (top) and night (bottom) from WT (left) and BACHD (right) mouse brain slices harvested at 3 months of age. **(B)** Box plots showing the 25th and 75th percentile (box), medians (center line), and data range (whiskers) of day (white box) and night (dark gray box) WT (white dots; Day, n =16; Night, n =14) and BACHD dSCN neurons SFR (black dots; Day, n = 21; Night, n =17). **(C)** Traces showing SFR following $GABA_A$-R antagonism with gabazine (10 µM) using the same organization as in part A. **(D)** Box plots of SFR recorded in the presence of gabazine for WT (Day, n = 14; Night, n = 14) and BACHD neurons (Day, n = 21; Night, n = 17) using the same organization as in part B.

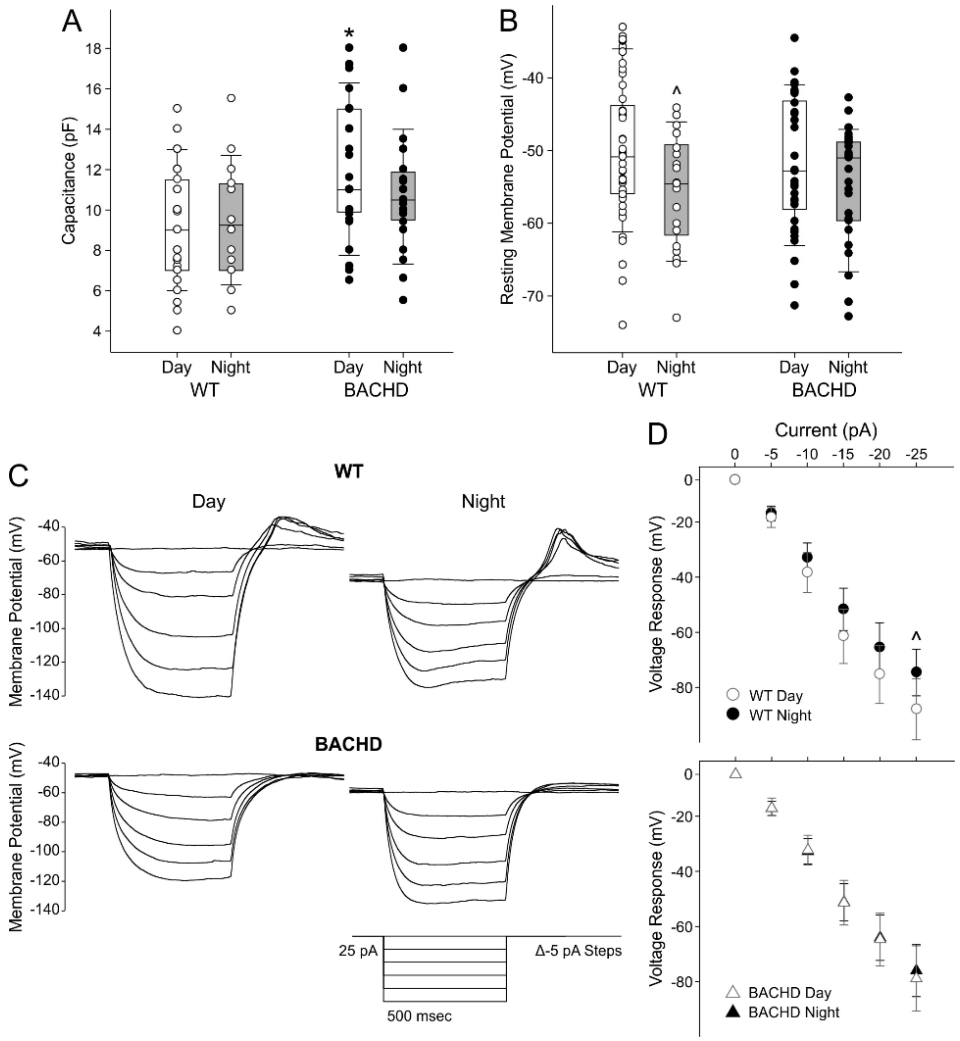

Figure 6.3: BACHD dSCN neurons lose day/night rhythms in resting membrane potential and input resistance. **(A)** Box plots showing the 25th and 75th percentile (box), medians (center line), and data range (whiskers) of dSCN neuron capacitances recorded during the day (white box) and night (dark gray box) for WT neurons (white dots; Day, n = 46; Night, n = 18) and BACHD neurons (black dots; Day, n = 34; Night, n = 23). Following Two-Way ANOVA, post-hoc multiple pairwise comparison testing using the Holm-Sidak method found a significant difference between WT and BACHD daytime capacitances (**P* < 0.001). **(B)** Box and dot plots with the same organization as in part A, representing dSCN neuron resting membrane potential. Following Two-Way ANOVA, post-hoc multiple pairwise comparison testing using the Holm-Sidak method determined that WT neuron resting membrane potentials are significantly more hyperpolarized at night than during the day (^*P* = 0.01). **(C)** Trace examples of WT (top) and BACHD (bottom) neurons' responses to negative current injection during the day (left) and night (right). **(D)** Voltage responses to negative current injection for WT neurons (top, circles) recorded during the day (n = 45) and night (n = 23), as well as BACHD neurons (bottom, triangles) recorded during the day (n = 31) and night (n = 28). Symbols and error bars represent mean ± 95% CI of means. Following Three-Way ANOVA, post-hoc multiple comparison testing using Two-Tailed TTESTs of voltage responses at each current magnitude identified significantly smaller voltage responses for WT neurons at night (^*P* = 0.04).

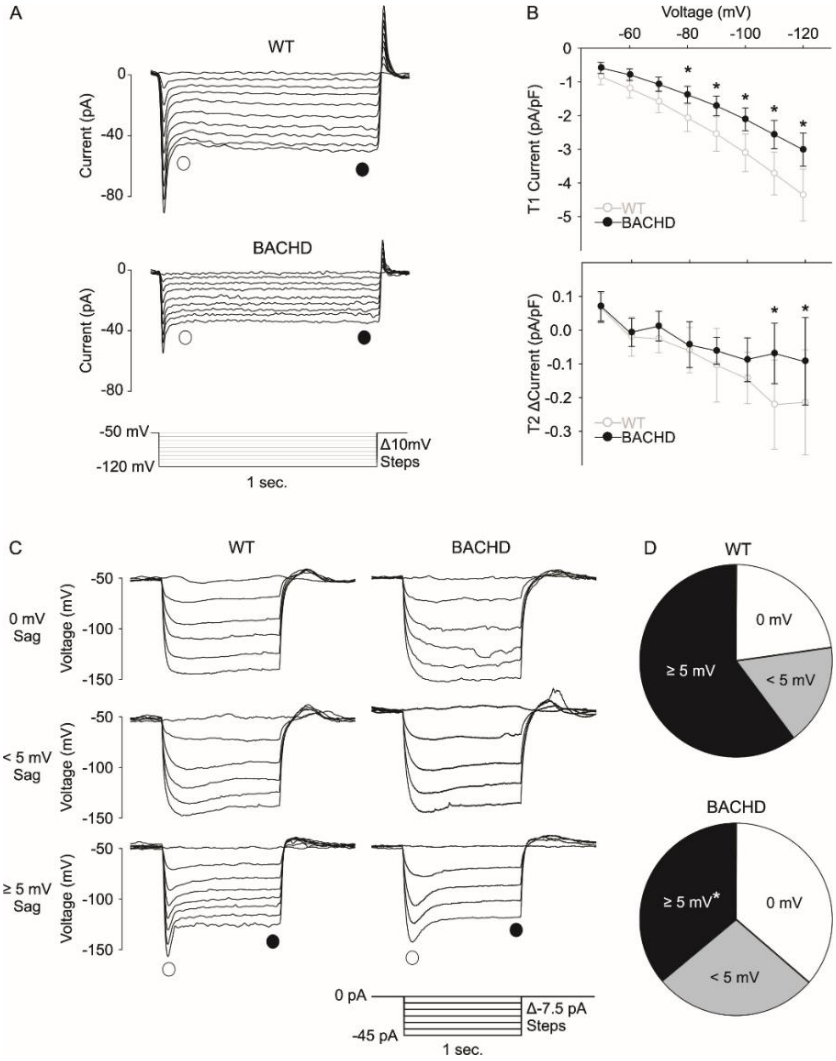

Figure 6.4: Reduced proportion of BACHD dSCN neurons exhibit I_H during the daytime. **(A)** Representative traces of WT (top) and BACHD (bottom) dSCN neuron current responses to increasingly negative voltage-clamp steps recorded in voltage-clamp mode during the daytime. T1 current = ○. T2 current = ●. **(B)** Summary of normalized T1 current magnitudes (top) and delta T2 current magnitudes (bottom) to various voltage-clamp steps for WT (white/gray, n = 56) and BACHD neurons (black, n = 48). Symbols and error bars represent means ± 95% CI of means. Following Two-Way ANOVA, post-hoc multiple pairwise comparison testing using the Holm-Sidak method identified voltage-steps that evoked significantly different current responses between WT and BACHD neurons (*P < 0.05). **(C)** Trace examples of WT (left) and BACHD (right) neuron membrane potential responses to negative current injection recorded in current-clamp mode. Neurons in both genotypes displayed 0 mV depolarizing sags (top), < 5 mV depolarizing sags (middle), and ≥ 5 mV depolarizing sags. Peak hyperpolarization responses (○). Membrane potential sag at the end of the current step (●). **(D)** Pie charts representing the proportion of WT (top, n = 56) and BACHD neurons (bottom, n = 48) that displayed no depolarizing sags (0 mV, white), small depolarizing sags (< 5 mV, gray), or large depolarizing sags (≥ 5 mV, black) during current injection steps that hyperpolarized membrane potential to between -90 and -110 mV. Chi2 test was used to identify significantly different ratios of voltage responses between BACHD and WT neurons (*P < 0.05).

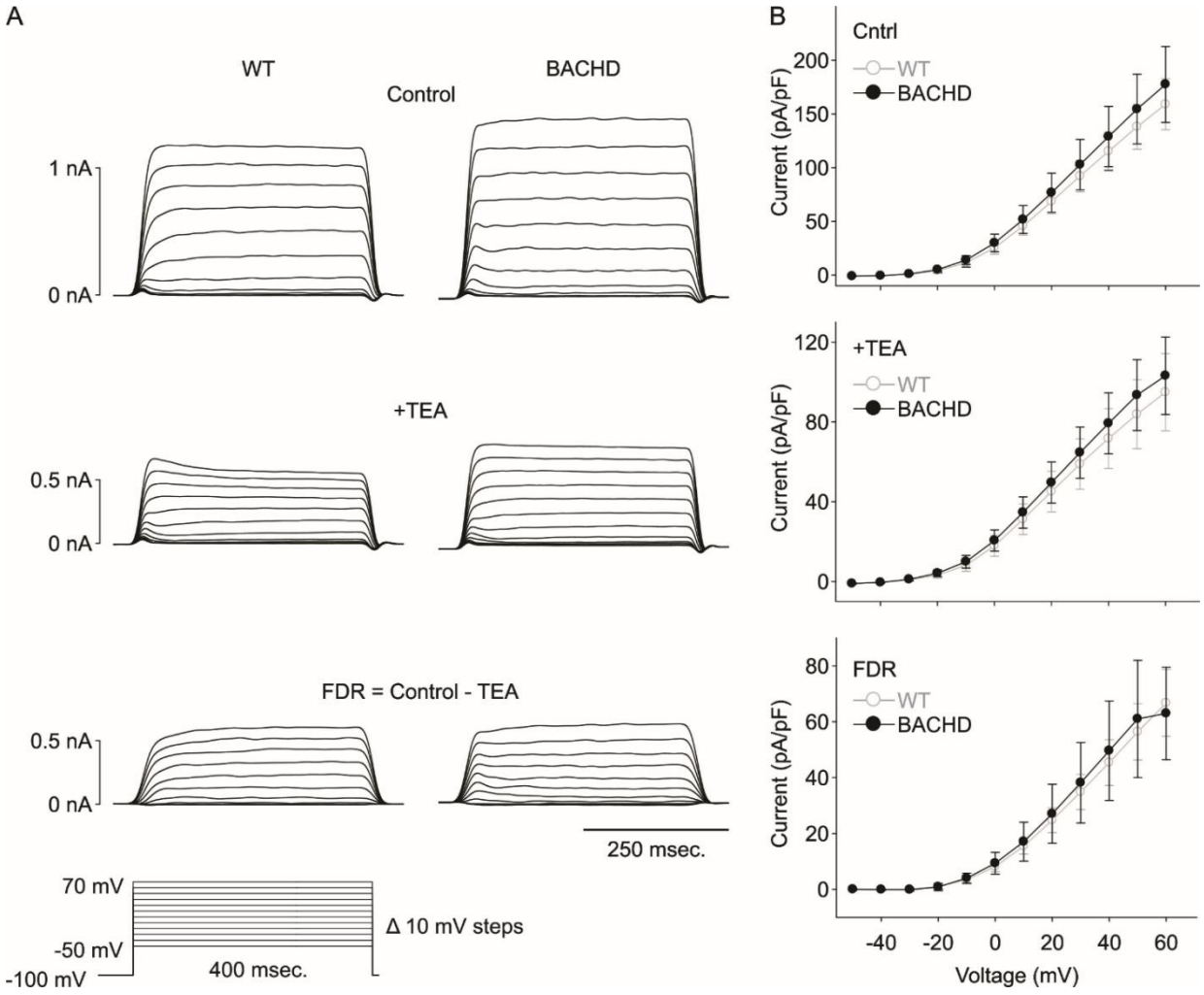

Figure 6.5: No alteration in FDR current during the daytime in BACHD dSCN neurons. **(A)** Trace examples of a WT (left) and BACHD neuron's (right) current responses to voltage clamp steps under control conditions (top) or in the presence of TEA (1mM; middle). FDR current is the subtraction current of TEA currents from control currents (bottom). **(B)** Summary of normalized current magnitudes under control conditions (top), in the presence of TEA (middle), and for the FDR current at various voltage-clamp steps for WT (white/gray, n = 28) and BACHD neurons (black, n = 35). Symbols and error bars represent means ± 95% CI of means. Two-Way ANOVA was used to identify significant effects of genotype and/or voltage step magnitude on evoked currents ($P < 0.05$). All depolarizing steps cause significant increases in current, but the magnitude of currents were not significantly different between genotypes.

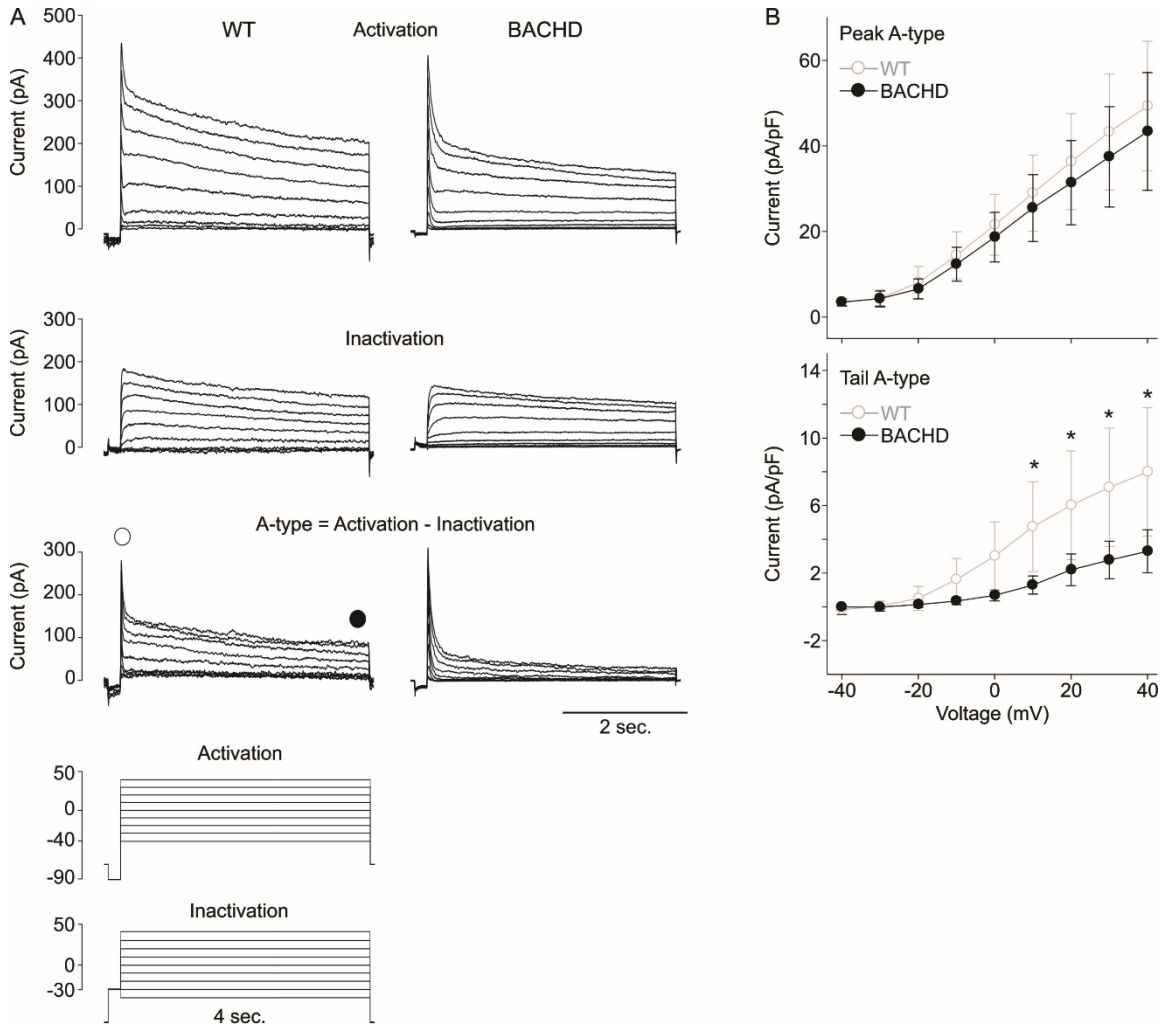

Figure 6.6: A-type potassium current is reduced during the daytime in BACHD dSCN neurons. **(A)** Trace examples of a WT (left) and BACHD neuron's (right) current responses to voltage clamp steps following an activating pre-pulse step to -90 mV (top) or an inactivating pre-pulse step to -30 mV (middle). A-type potassium current is the subtraction current of activation currents from inactivation currents (bottom). Peak (○) and tail current responses (●). **(B)** Summary of normalized peak (top) and tail (bottom) A-type potassium current magnitudes at various voltage-clamp steps for WT (white/gray, n = 21) and BACHD neurons (black, n = 18). Symbols and error bars represent means ± 95% CI of means. Following Two-Way ANOVA, post-hoc multiple pairwise comparison testing identified significant genotypic differences for each voltage step in tail current magnitudes (**P* < 0.001).

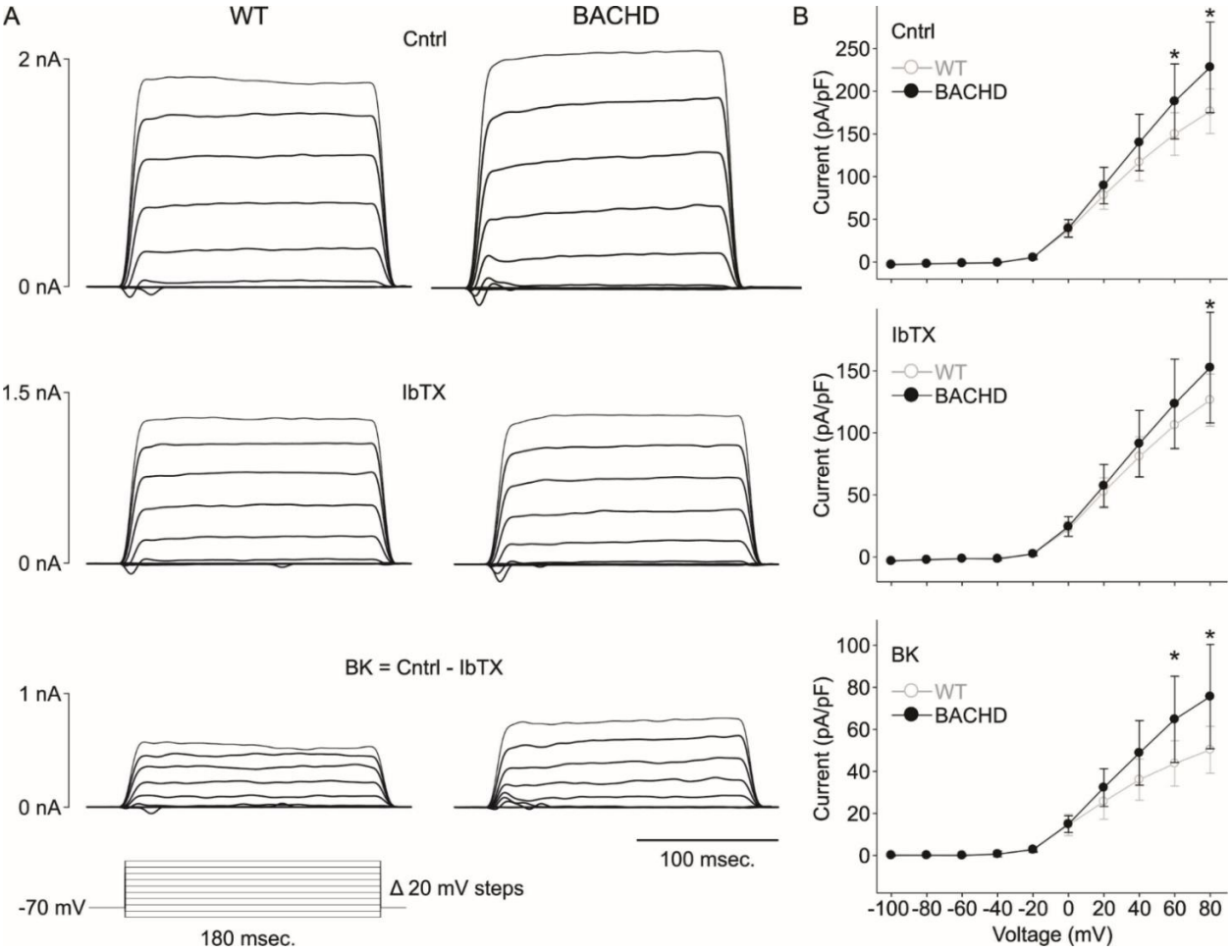

Figure 6.7: BK current is enhanced during the daytime in BACHD dSCN neurons. **(A)** Trace examples of a WT (left) and BACHD neuron's (right) current responses to voltage clamp steps under control conditions (top) or in the presence of IbTX (100nM; middle). BK current is the subtraction current of IbTX currents from control currents (bottom). **(B)** Summary of normalized current magnitudes under control conditions (top), in the presence of IbTX (middle), and for the BK current at various voltage-clamp steps for WT (white/gray, n = 18) and BACHD neurons (black, n = 22). Symbols and error bars represent means ± 95% CI of means. Following Two-Way ANOVA, post-hoc multiple pairwise comparison testing using the Holm-Sidak method identified voltage steps for which current magnitudes were significantly different between BACHD and WT neurons (*$P < 0.01$).

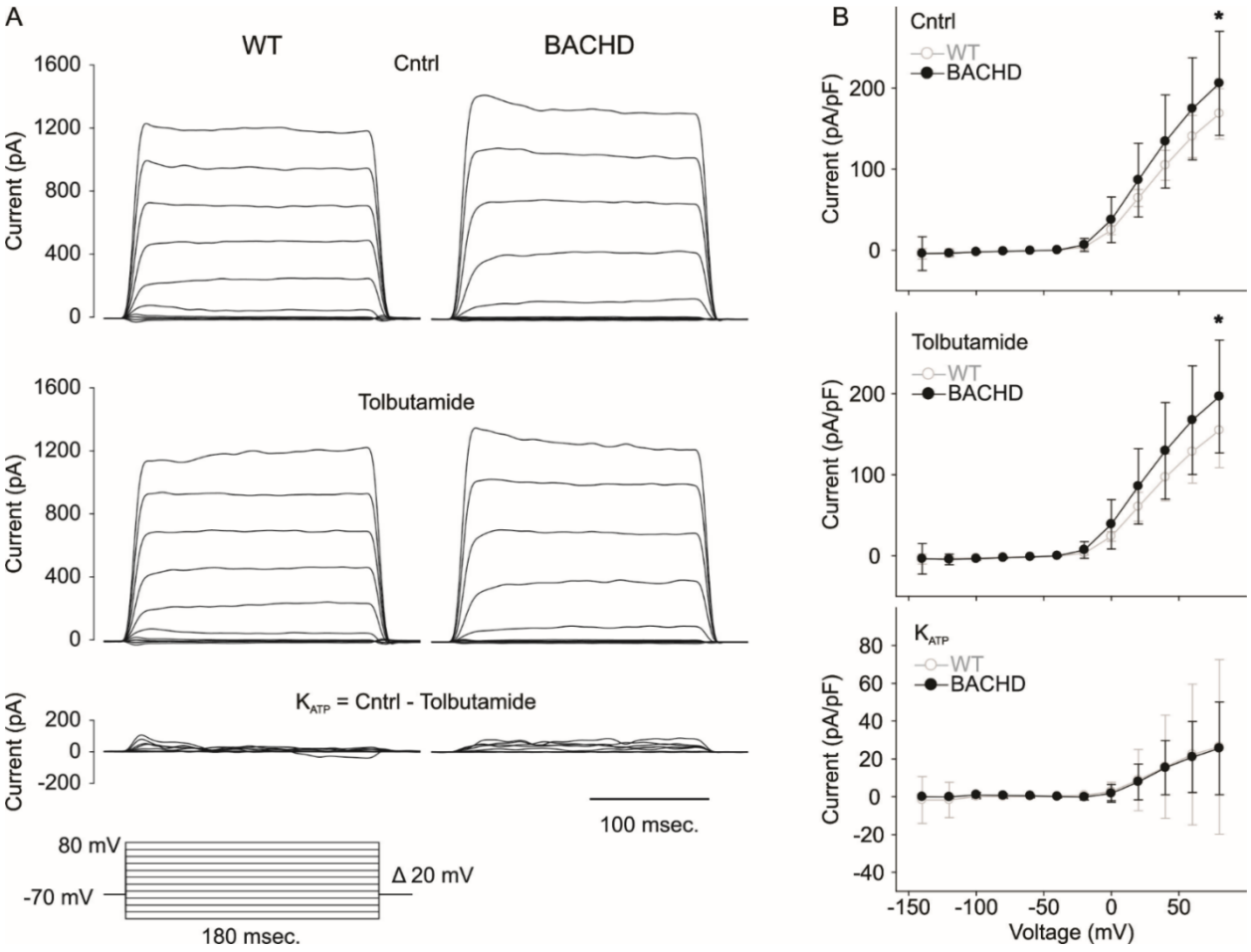

Figure 6.8: When intracellular ATP levels are clamped, K_{ATP} current is not altered during the daytime in BACHD dSCN neurons. **(A)** Trace examples of a WT (left) and BACHD neuron's (right) current responses to membrane potential voltage clamp steps under control conditions (top) or in the presence of tolbutamide (1mM; middle). K_{ATP} current is the subtraction current of tolbutamide currents from control currents (bottom). **(B)** Summary of normalized current magnitudes under control conditions (top), in the presence of tolbutamide (middle), and for the K_{ATP} current at various voltage-clamp steps for WT (white/gray, n = 12) and BACHD neurons (black, n = 11). Symbols and error bars represent means ± 95% C.I. of means. Following Two-Way ANOVA, post-hoc multiple pairwise multiple pairwise comparison testing using the Holm-Sidak method identified voltage steps for which current magnitudes were significantly different between BACHD and WT neurons (*P < 0.01).

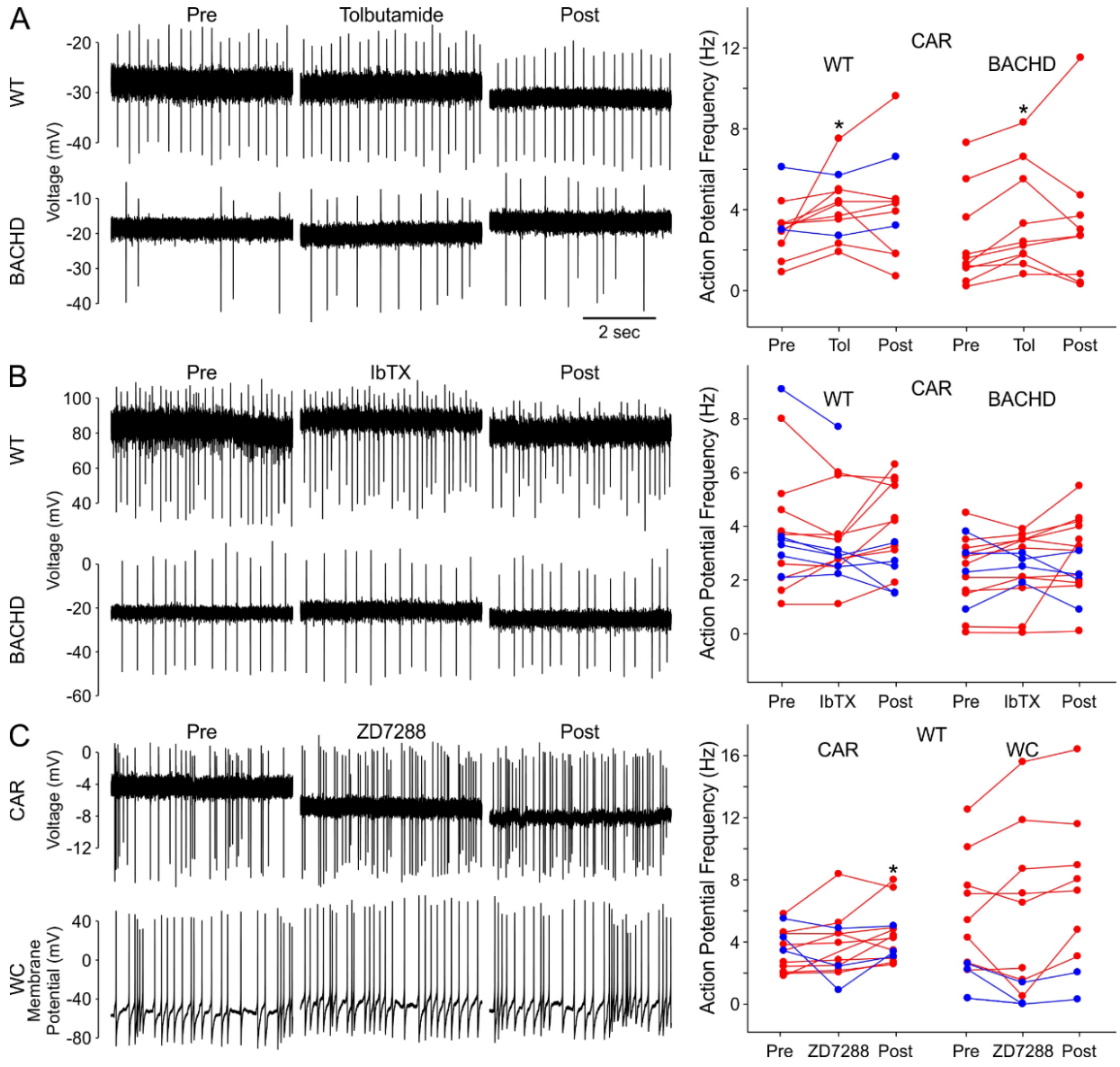

Figure 6.9: Pharmacological agents targeting potassium currents can in some cases acutely increase daytime dSCN SFR. Example traces showing treatments effects on daytime electrical activity for an individual neurons before, during and after treatment (left), and summaries of AP frequencies for all neurons examined (right). Recordings were made using cell-attached recording (CAR) method unless otherwise notes. **(A)** Tolbutamide (1 mM) effects on WT neurons selected for low SFR (n = 12) and BACHD neurons (n = 10). **(B)** IbTX (50 nM) effects on WT (n = 15) and BACHD neurons (n = 15). **(C)** I_H blocker ZD7288 (10 μM) effects on WT neurons tested using either CAR (top, n = 14) or whole-cell (WC, bottom, n = 10) recording method. Individual cells displaying overall increases in AP frequency are visualized in red, and cells displaying overall decreases in AP frequency are visualized in blue. For each genotype or recording method, Paired TTESTs were used to identify significant effects of each potassium current blocker on neural action potential frequency during or after treatment relative to baseline (*$P < 0.05$).

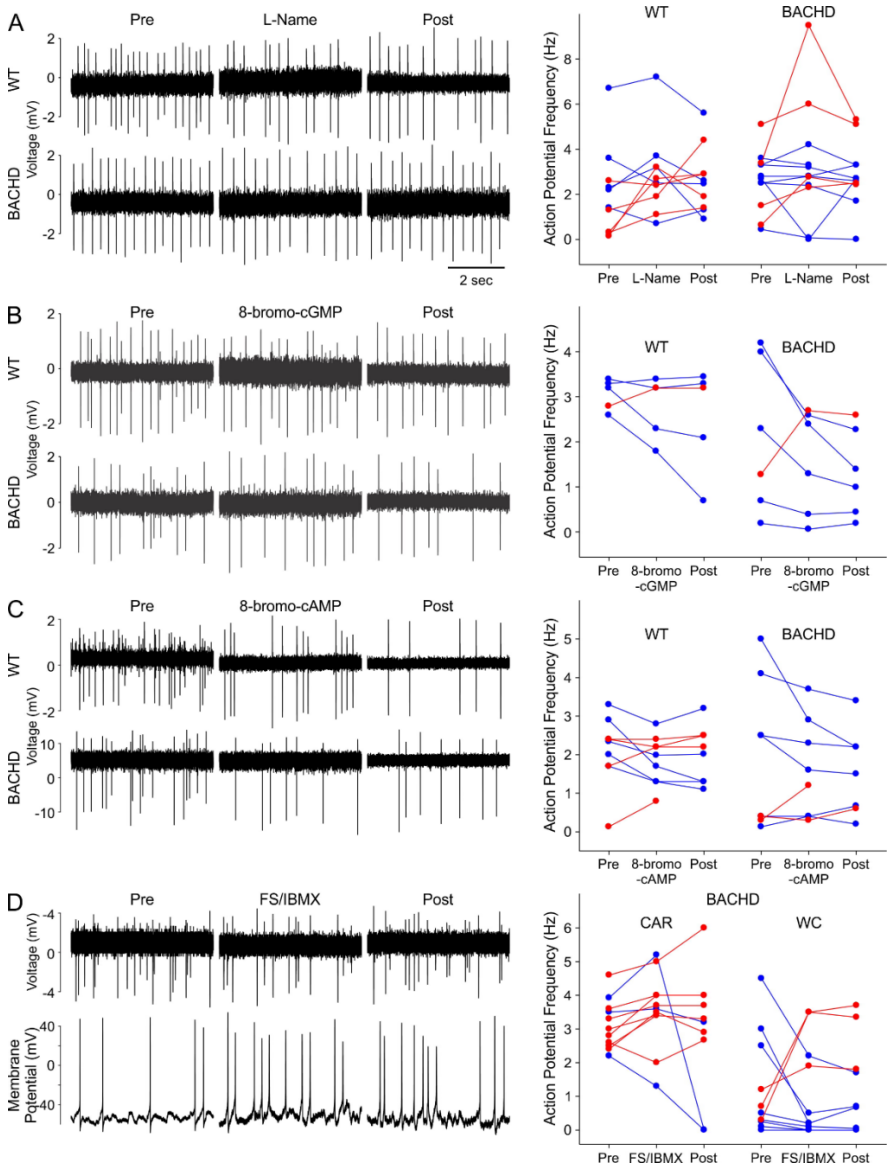

Figure 6.10: Acute treatment with pharmacological agents targeting second-messenger pathways do not rescue depressed daytime SFR in BACHD dSCN neurons. Example traces showing treatments effects on daytime electrical activity on individual neurons before, during and after treatment (left), and summaries of AP frequencies for all neurons examined (right). Recordings made using cell-attached recording (CAR) method unless otherwise noted. **(A)** L-Name (100μM) treatment effects on WT neurons selected for low SFR (n = 12) and BACHD neurons (n = 13). **(B)** 8-bromo-cGMP (10μM) effects on WT neurons selected for low SFR (n = 5) and BACHD neurons (n = 6). **(C)** 8-bromo-cAMP (10μM) effects on WT neurons selected for low SFR (n = 7) and BACHD neurons (n = 8). **(D)** FS/IBMX (20/500μM) effects BACHD neurons recorded using the CAR (top, n =11) or whole-cell (WC, bottom, n = 12) recording method (bottom). Individual cells displaying overall increases in AP frequency are visualized in red, and cells displaying overall decreases in AP frequency are visualized in blue. For each genotype or recording method, Paired TTESTs were used to identify significant effects of each potassium current blocker on neural action potential frequency during or after treatment relative to baseline (*$P < 0.05$).

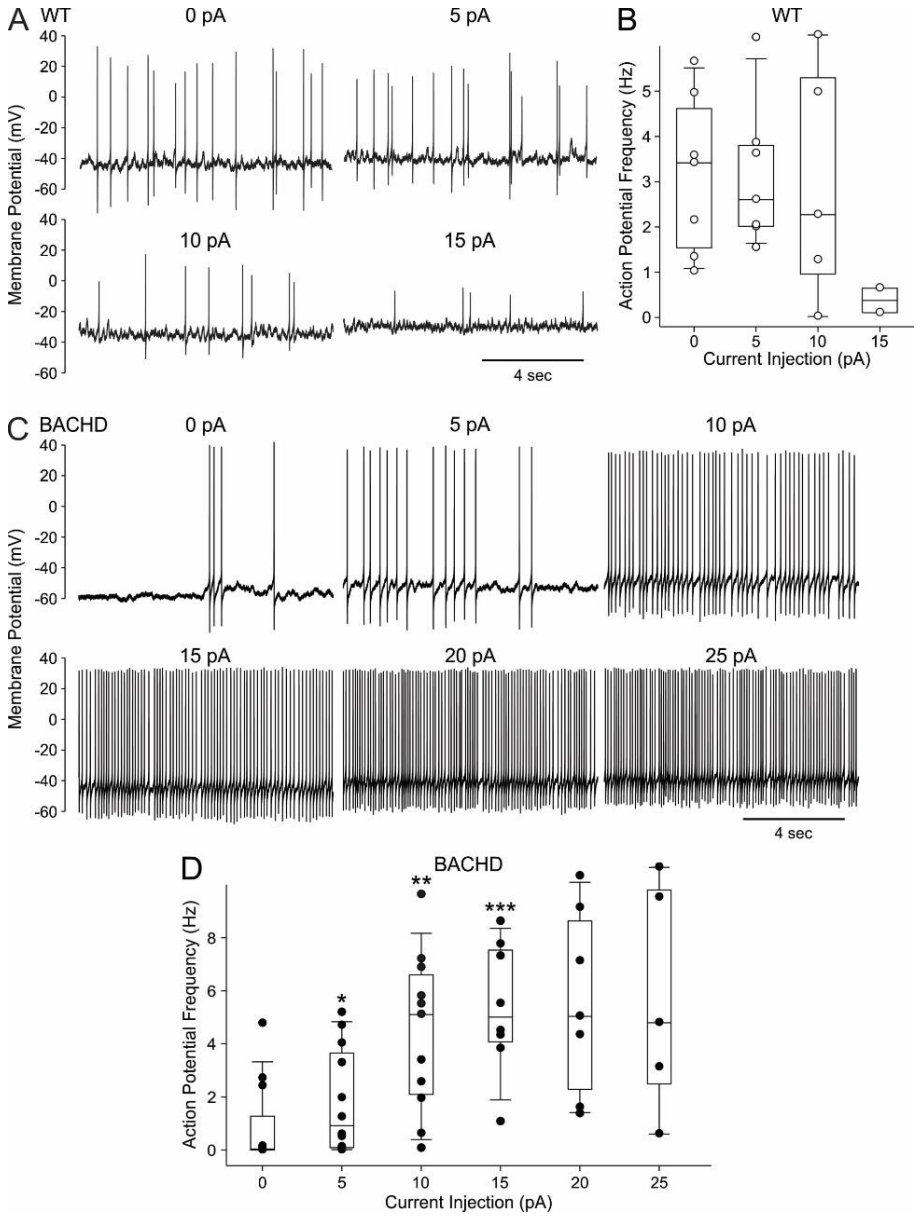

Figure 6.11: Direct current injection rescues depressed daytime SFR of BACHD dSCN neurons. **(A)** Trace example showing effects of positive current injection on membrane potential and electrical activity of a WT dSCN neuron. **(B)** Summary of positive current injection effects on WT neuron (n =7) action potential (AP) frequency. **(C)** Trace example showing effects of positive current injection on membrane potential and electrical activity of a BACHD dSCN neuron. **(D)** Summary of positive current injection effects on BACHD neuron (n = 12) AP frequency. Paired TTESTs were used to detect significant changes to inter-spike membrane potential and AP frequency caused by positive current injection relative to the previous current injection step. All positive current steps caused significant depolarization of inter-spike membrane potential. Significant increases to SFR caused by positive current injection relative to the previous current injection step (*P < 0.01).

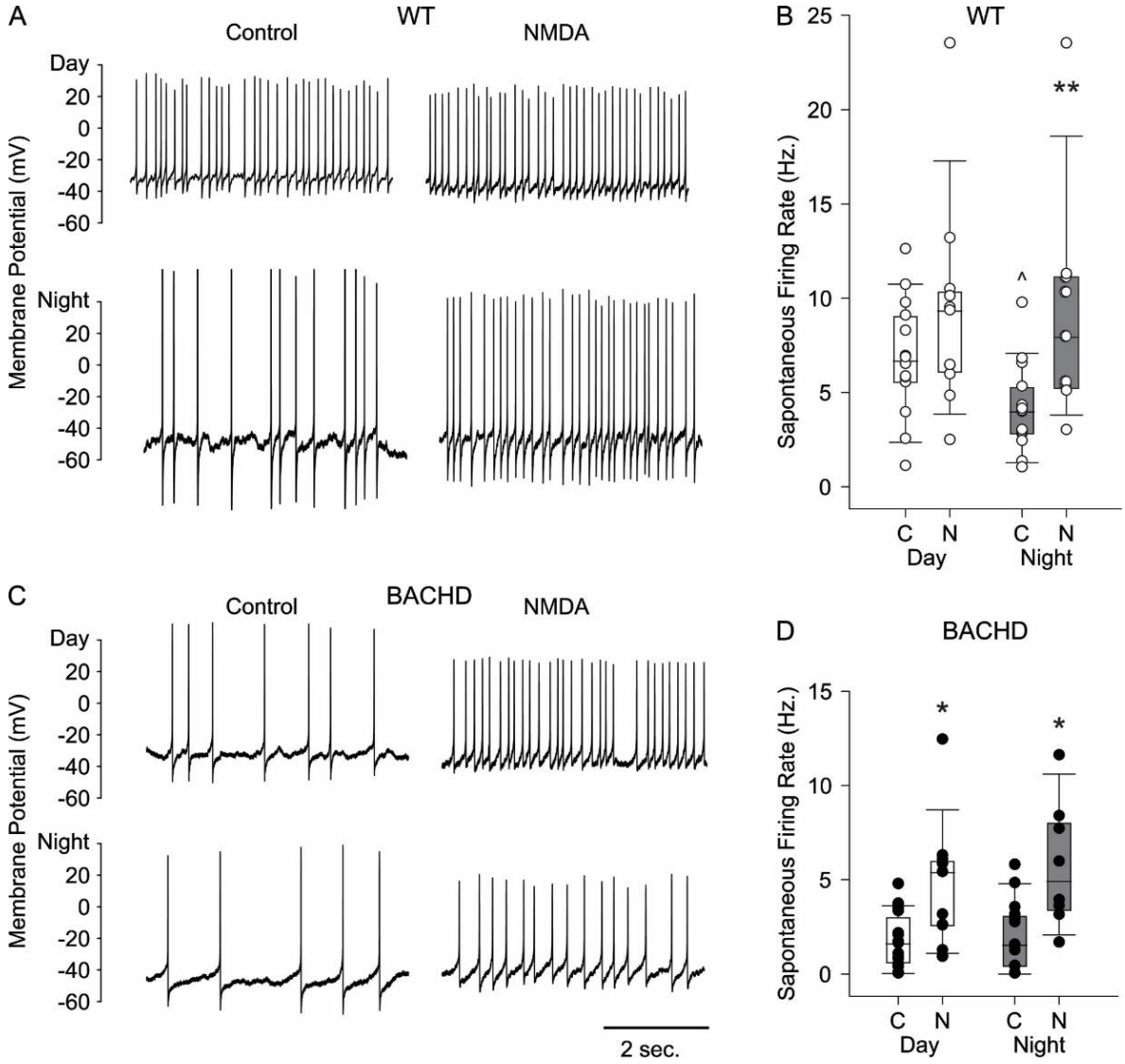

Figure 6.12: NMDA excitation rescues depressed daytime SFR of BACHD dSCN neurons. **(A)** Example traces of a synaptically isolated WT neuron's electrical activity recorded under baseline conditions (10 µM gabazine, left) and following NMDA application (25 µM, right) recorded during the daytime (top) or nighttime (bottom) using the whole-cell recording method in current-clamp mode. **(B)** Box plots showing the 25th and 75th percentile (box), medians (center line), and data range (whiskers) of WT dSCN neuron SFRs recorded during the day (white boxes, n = 10) and night (dark gray boxes, n = 9) under control conditions (C) and following NMDA application (N). **(C)** Example traces of a synaptically isolated BACHD neuron's electrical activity recorded under baseline conditions (10 µM gabazine, left) and following NMDA application (25 µM, right) recorded during the daytime (top) and nighttime (bottom) using the whole-cell recording method in current-clamp mode. **(D)** Box plots showing the 25th and 75th percentile (box), medians (center line), and data range (whiskers) of BACHD dSCN neuron SFRs recorded during the day (white boxes, n = 9) and night (dark gray boxes, n = 8) under control conditions (C) and following NMDA application (N).

	Genotype		Treatment		Genotype x Treatment	
3 Months	F	P	F	P	F	P
Peak (mV)	1.23	NS	4.53	0.04	0.09	NS
Rise 10 -90% (msec)	0.39	NS	11.6	0.002	0.56	NS
Positive Area (mV)	0.38	NS	2.20	NS	0.55	NS
Half-Width (msec)	2.89	NS	9.98	0.003	2.00	NS
Slope (mV/msec.)	0.044	NS	0.08	NS	0.57	NS
Peak to After-Hyperpolarization Peak (msec)	3.96	NS	6.67	0.01	1.71	NS
Threshold (mV)	1.30	NS	0.28	NS	0.47	NS
Width (msec)	0.51	NS	1.53	NS	0.20	NS
After-Hyperpolarization Area (mV*msec)	0.33	NS	5.90	0.02	2.08	NS
After-Hyperpolarization Peak (mV)	0.38	NS	7.65	0.009	0.39	NS
Decay (mV/msec)	3.05	NS	6.49	0.02	1.76	NS
6 Months						
Peak (mV)	0.79	NS	10.6	0.003	0.022	NS
Rise 10 -90% (msec)	0.81	NS	31.2	< 0.001	0.58	NS
Positive Area (mV)	3.3	NS	1.93	NS	2.67	NS
Half-Width (msec)	0.63	NS	13.6	< 0.001	0.45	NS
Slope (mV/msec)	0.84	NS	0.34	NS	0.35	NS
Peak to After-Hyperpolarization Peak (msec)	3.54	NS	17.4	< 0.001	2.96	NS
Threshold (mV)	0.011	NS	0.006	NS	0.65	NS
Width (msec)	3.74	NS	5.57	0.02	1.16	NS
After-Hyperpolarization Area (mV*msec)	1.87	NS	5.43	0.03	0.10	NS
After-Hyperpolarization Peak (mV)	5.48	0.03	16.5	< 0.001	0.104	NS
Decay (mV/msec)	5.29	0.03	13.6	< 0.001	2.63	NS

	WT		BACHD	
3 Months	Cntrl	NMDA	Cntrl	NMDA
Peak (mV)	61.5 ± 4.9	52.6 ± 4.9	57.6 ± 5.2	45.8 ± 4.3
Rise 10 -90% (msec)	2.8 ± 0.3	3.6 ± 0.3	2.8 ± 0.3	4.0 ± 0.3**
Positive Area (mV)	206 ± 15	218 ± 15	204 ± 16	238 ± 13
Half-Width (msec.)	3.3 ± 0.4	4.0 ± 0.4	3.4 ± 0.5	5.3 ± 0.4**#
Slope (mV/msec)	1.7 ± 0.2	1.6 ± 0.2	1.5 ± 0.2	1.7 ± 0.2
Peak to After-Hyperpolarization Peak (msec)	3.5 ± 1.0	4.8 ± 1.0	4.2 ± 1.1	8.1 ± 0.9**#
Threshold (mV)	8.3 ± 0.9	8.5 ± 0.9	7.9 ± 1.0	6.8 ± 0.8
Width (msec)	3.2 ± 0.2	3.4 ± 0.2	3.2 ± 0.3	3.7 ± 0.2
After-Hyperpolarization Area (mV*msec)	-3360 ± 420	-2960 ± 420	-3720 ± 440	-2140 ± 360**
After-Hyperpolarization Peak (mV)	-22.2 ± 2.8	-16.2 ± 2.8	-22.2 ± 3.0	-12.8 ± 2.4
Decay (mV/msec.)	1.2 ± 0.3	1.6 ± 0.3	1.3 ± 0.3	2.5 ± 0.3**#
6 Months				
Peak (mV)	65.9 ± 5.1	49.2 ± 6.2	70.2 ± 4.6	53.0 ± 4.2**
Rise 10 -90% (msec)	2.6 ± 0.2	3.7 ± 0.3**	2.2 ± 0.2	3.7 ± 0.2***
Positive Area (mV)	192 ± 12	189 ± 14	194 ± 11	230 ± 10
Half-Width (msec)	2.8 ± 0.3	3.6 ± 0.3	2.8 ± 0.3	4.0 ± 0.2***
Slope (mV/msec)	1.3 ± 3.0	1.3 ± 3.6	2.3 ± 2.7	5.8 ± 2.5
Peak to After-Hyperpolarization Peak (msec)	3.0 ± 0.3	3.8 ± 0.4	3.1 ± 0.3	5.0 ± 0.3***#
Threshold (mV)	8.5 ± 0.9	7.7 ± 1.1	7.7 ± 0.8	8.3 ± 0.7
Width (msec)	2.8 ± 0.2	3.1 ± 0.3	3.0 ± 0.2	3.7 ± 0.2**#
After-Hyperpolarization Area (mV*msec)	-5070 ± 540	-6970 ± 670	-4490 ± 490	-3050 ± 450*
After-Hyperpolarization Peak (mV)	-38.2 ± 2.8	-27.5 ± 3.5*	-32.4 ± 2.6	-19.9 ± 2.4**
Decay (mV/msec)	0.90 ± 0.12	1.15 ± 0.15	0.98 ± 0.11	1.62 ± 0.10***#

Table 6.1: BACHD vSCN AP properties show age related changes following NMDA treatment. (Top) Two-Way ANOVA results examining the effects of genotype and NMDA treatment on AP properties of a subset of neurons with stable AP properties, with significance levels set at $P < 0.05$. Group means ± 95% CI of means (below). vSCN AP properties under control conditions (10µM gabazine) and in the presence of NDMA (25µM) recorded from acute brain slices harvested from WT mice at 3 (n = 10) and 6 months of age (n = 9), as well as BACHD mice at 3 (n =10) and 6 months of age (n = 11). When Two-Way ANOVA identified significant effects, post-hoc multiple pairwise comparison testing using the Holm-Sidak method identified group differences within genotype and age between treatment conditions (* $P < 0.05$, ** $P < 0.01$, *** $P < 0.001$), and between genotype within age and treatment condition ($^{\#}P < 0.05$).

		WT		BACHD		Genotype		Time		Treatment		Genotype x Time		Genotype x Treatment		Time x Treatment		Genotype x Time x Treatment	
AP Property	Treatment	Day	Night	Day	Night	F	P	F	P	F	P	F	P	F	P	F	P	F	P
Instantaneous Frequency	Cntrl	5.4 ± 1.5	3.9 ± 1.1^	2.1 ± 1.1$^{\#}$	2.6 ± 1.3	50.1	<0.001	2.83	NS	0.61	NS	10.5	0.002	3.13	NS	0.28	NS	0.807	NS
	GabZ	7.2 ± 2.1	4.4 ± 1.3	1.5 ± 0.8$^{\#\#**}$	1.6 ± 1.0$^{\#*}$														
Interevent Interval	Cntrl	418 ± 471	353 ± 152	2850 ± 3390	1180 ± 1480	7.6	NS	2.48	NS	0.87	NS	2.55	NS	0.39	NS	0.054	NS	0.005	NS
	GabZ	195 ± 97	283 ± 90	1950 ± 2030	570 ± 370														
Baseline	Cntrl	-46.5 ± 3.4	-43.6 ± 3.5	-46.0 ± 5.0	-44.2 ± 5.3	3.84	NS	0.036	NS	3.54	NS	0.53	NS	0.04	NS	0.097	NS	0.34	NS
	GabZ	-39.6 ± 4.3	-42.0 ± 3.8	-45.7 ± 3.8	-43.1 ± 3.2														
Peak Amplitude	Cntrl	101 ± 9	90 ± 13	97 ± 15	94 ± 12	0.94	NS	1.53	NS	0.44	NS	0.5^{-5}	NS	1.18	NS	0.22	NS	1.1	NS
	GabZ	88 ± 14	89 ± 13	100 ± 13	93 ± 16														
Half-Amplitude	Cntrl	51 ± 4	45 ± 6	48 ± 7	47 ± 6	0.94	NS	1.53	NS	0.44	NS	0.5^{-5}	NS	1.18	NS	0.22	NS	1.07	NS
	GabZ	44 ± 7	44 ± 6	50 ± 7	47 ± 8														
Area	Cntrl	200 ± 11	181 ± 16	219 ± 15$^{\#}$	199 ± 35	7.07	0.009	5.4	0.02	2.89	NS	0.363	NS	0.006	NS	0.23	NS	0.32	NS
	GabZ	205 ± 13	200 ± 17	231 ± 19$^{\#}$	210 ± 33														
Half-Width	Cntrl	2.1 ± 0.2	1.5 ± 0.5^	2.4 ± 0.4	1.7 ± 0.7	1.6	NS	3.97	0.049	0.03	NS	0.213	NS	0.007	NS	2.06	NS	0.0422	NS
	GabZ	1.8 ± 0.7	1.8 ± 0.6	2.2 ± 0.6	1.9 ± 0.7														
Rise Tau	Cntrl	2.9 ± 1.4	3.2 ± 1.5	3.9 ± 1.5	2.5 ± 1.0	0.15	NS	1.42	NS	0.3	NS	3.02	NS	0.014	NS	0.0058	NS	0.0075	NS
	GabZ	2.7 ± 1.4	2.9 ± 1.5	3.6 ± 1.7	2.4 ± 0.9														
Time to Peak	Cntrl	1.5 ± 0.1	1.5 ± 0.2	1.8 ± 0.2$^{\#\#}$	1.5 ± 0.2	3.97	0.049	3.25	NS	1.39	NS	3.3	NS	0.51	NS	0.16	NS	0.75	NS
	GabZ	1.6 ± 0.2	1.6 ± 0.2	1.8 ± 0.2	1.6 ± 0.2														
Time to Decay Half Amplitude	Cntrl	2.5 ± 0.2	2.4 ± 0.2	3.0 ± 0.3$^{\#\#}$	2.7 ± 0.4	6.29	0.014	3.59	NS	5.03	0.03	0.54	NS	2.7	NS	0.32	NS	0.072	NS
	GabZ	2.9 ± 0.4	2.8 ± 0.3*	3.0 ± 0.4	2.8 ± 0.4														
Antipeak Amplitude	Cntrl	19.6 ± 8.9	18.6 ± 7.0	9.7 ± 9.9	21.0 ± 10.2	2.83	NS	2.13	NS	1.7	NS	4.03	0.048	0.13	NS	0.13	NS	0.028	NS
	GabZ	24.9 ± 9.1	22.8 ± 5.2	13.9 ± 11.6	22.2 ± 8.1														
Time to Antipeak	Cntrl	2.9 ± 0.4	3.0 ± 0.5	3.8 ± 0.4$^{\#\#}$	3.1 ± 0.5	4.1	0.047	2.2	NS	2.45	NS	5.7	0.02	2.27	NS	0.24	NS	0.29	NS
	GabZ	3.3 ± 0.4	3.5 ± 0.5	3.7 ± 0.4	3.3 ± 0.5														
Decay Tau	Cntrl	1.5 ± 0.3	1.3 ± 0.2	2.4 ± 0.5$^{\#\#}$	2.3 ± 1.7	9.75	0.002	0.089	NS	0.33	NS	0.3^{-5}	NS	0.33	NS	0.003	NS	0.009	NS
	GabZ	1.5 ± 0.3	1.4 ± 0.2	2.8 ± 1.6	2.7 ± 2.2														
Peak	Cntrl	82.4 ± 5.8	74.9 ± 4.8	75.0 ± 5.2	69.9 ± 5.8	1.52	NS	0.47	NS	0.85	NS	0.024	NS	0.21	NS	1.02	NS	0.23	NS
	GabZ	71.8 ± 5.5	75.4 ± 4.8	71.3 ± 4.4	70.2 ± 5.2														
Rise	Cntrl	3.1 ± 0.3	3.2 ± 0.2	3.2 ± 0.2	3.2 ± 0.3	0.314	NS	0.12	NS	6.33	0.01	0.016	NS	0.14	NS	0.21	NS	0.024	NS
	GabZ	3.6 ± 0.2*	3.4 ± 0.2*	3.7 ± 0.2*	3.6 ± 0.2*														
Positive Area	Cntrl	339 ± 20	299 ± 16	319 ± 18	305 ± 20	0.16	NS	3.4	NS	5.6	0.02	0.41	NS	0.021	NS	0.076	NS	0.119	NS
	GabZ	360 ± 19*	336 ± 16*	352 ± 15*	336 ± 18*														
Slope	Cntrl	1.8 ± 0.4	1.9 ± 0.3	1.9 ± 0.3	2.3 ± 0.4	0.2	NS	1.6	NS	1.32	NS	0.5^{-5}	NS	0.405	NS	0.006	NS	0.26	NS
	GabZ	2.1 ± 0.3	2.4 ± 0.3	2.1 ± 0.3	2.3 ± 0.3														
Width	Cntrl	4.9 ± 0.3	4.6 ± 0.3	5.0 ± 0.3	5.1 ± 0.3	1.53	NS	1.61	NS	9.6	0.003	1.2	NS	0.12	NS	0.67	NS	0.0041	NS
	GabZ	5.7 ± 0.3*	5.1 ± 0.3	5.7 ± 0.2*	5.5 ± 0.3														
After-Hyperpolarization Area	Cntrl	-9650 ± 740	-9170 ± 600	-9960 ± 660	-9170 ± 740	0.29	NS	0.122	NS	1.74	NS	1.3	NS	0.04	NS	1.03	NS	0.63	NS
	GabZ	-8100 ± 690	-9310 ± 600	-9640 ± 560	-8750 ± 660														
After-Hyperpolarization Peak	Cntrl	-38.1 ± 4.1	-38.8 ± 3.4	-34.7 ± 3.7	-35.2 ± 4.1	0.562	NS	0.5	NS	1.46	NS	0.015	NS	0.34	NS	0.29	NS	0.018	NS
	GabZ	-31.8 ± 3.9	-35.8 ± 3.4	-32.0 ± 3.1	-34.7 ± 3.7														
Decay	Cntrl	1.5 ± 0.2	1.4 ± 0.1	1.9 ± 0.2	1.6 ± 0.2	2.95	NS	2.21	NS	2.35	NS	0.14	NS	1.97	NS	0.0016	NS	0.49	NS
	GabZ	1.8 ± 0.2	1.7 ± 0.1	1.8 ± 0.1	1.7 ± 0.2														

Table 6.2: BACHD dSCN AP properties are largely unaltered at 3 months of age. AP property values in WT and BACHD columns are group means ± 95% CI of means either under control conditions or in the presence of gabazine (10μM) for a subset of the neurons examined in Fig. 6.2. Two-Way ANOVA results examining the effects of genotype, time, and gabazine treatment for each AP property with significance levels set at $P < 0.05$ (right). When significant effects were found, post-hoc multiple pairwise comparison testing using the Holm-Sidak method identified significant group differences, which are noted next to group means: effects of gabazine treatment within genotype and recording time ($^{*}P < 0.05$), effects of genotype within recording condition and time ($^{\#}P < 0.05$, $^{\#\#}P < 0.01$). WT control (Day, n = 13; Night, n = 14), BACHD control (Day, n = 13; Night, n = 12), WT gabazine (Day, n = 12; Night, n = 14), BACHD gabazine (Day: n = 11; Night: n = 12).

EPILOGUE

Circadian system coordination of rhythmic behavior and physiology is mediated by a hierarchical system of molecular oscillations and neural and humoral signals that are orchestrated by rhythmic output from the SCN. The SCN's ability to generate this output is related to pacemaking properties of individual SCN neurons and their unique properties when combined as a circuit. SCN physiological properties are rhythmically regulated by the circadian molecular network, which drives expression of the ion channel protein subunit and molecules that regulate those ion channel's currents (**Fig. E1**). When functioning properly, robust molecular and electrical activity oscillations in SCN are able to respond to changes in photic environmental rhythms, in order to mediate adaptive phase alignment of internal biological rhythms with external environmental rhythms. Light plays an important role in mediating this phenomenon because on Earth, over billions of years of evolution, sunlight has mediated highly predictable daily and seasonal changes in environmental resource availability. Millions of years of evolution in mammals fine-tuned the mechanism by which biological rhythms align to the solar cycle, with different species evolving diverse temporal niches and seasonal adaptations to provide them with survival advantage. Humans are diurnal mammals, but over the last 100 years, the increased prevalence of industrial work schedules and increased affordability of electric light has within a few generations significantly altered the rhythms of daily life for humans (Foster and Roenneberg, 2008). Social demands for a 24 hour society are increasingly in conflict with the intrinsic rhythms of the individual, and research examining the effects of jet travel across time zones, shift-work, and competition between social and professional demands have revealed a host of negative health consequences associated with circadian system disruption (Schernhammer et al., 2006; Stevens, 2006; Navara and Nelson, 2007; Karatsoreos et al., 2011a; Pan et al., 2011). Understanding how and why this happens is critical for the well-being of humanity in the post-modern era.

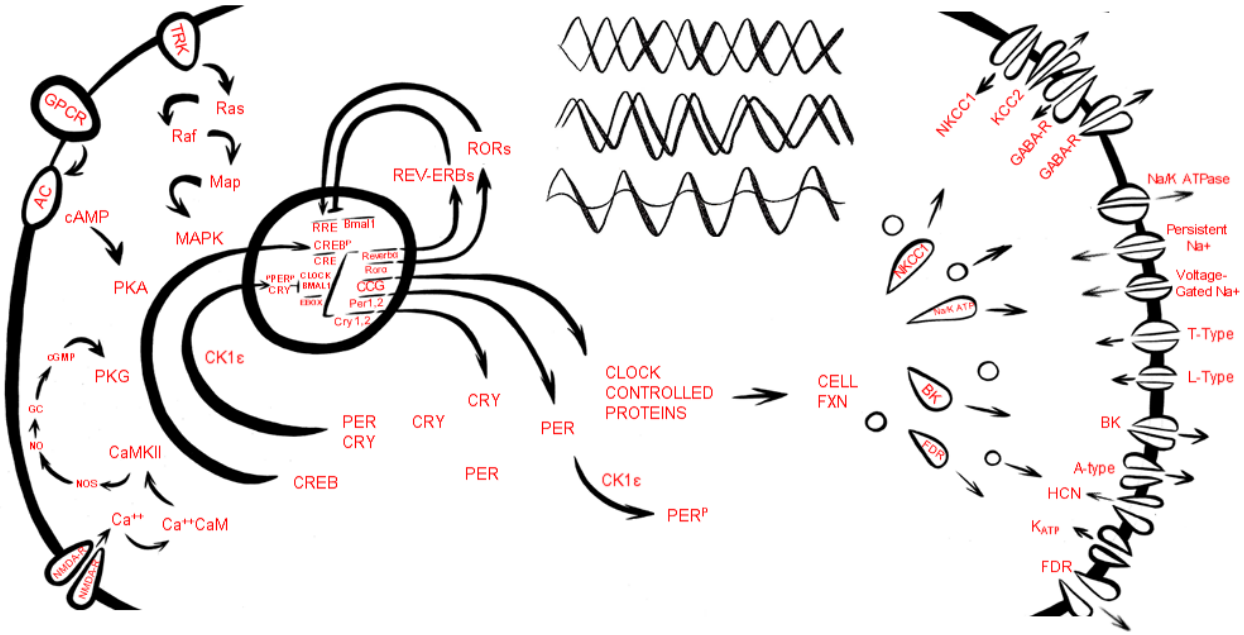

Figure E.1: Circadian regulation of SCN neural activity. Rhythmic clock gene expression drives rhythms in clock controlled protein availability within cells. In SCN neurons, rhythmic transcription of ion channel subunits regulating ionic flux regulate rhythms in electrical activity that can be modified by TRK, GPCR, and NMDA-R activation. In the absence of VIP/VPAC2-R signaling alterations in AC activation alter the rhythm of intrinsic SFRs so that they are antiphase in VIP KO males and either have an altered phase, or no rhythm in females. This is associated with deficits in SCN responsivity to light-input and disrupts circadian regulation of the estrous cycle. Chloride symporters KCC2 excretes chloride (Cl) and NKCC1 imports it, to regulate whether GABA signaling is inhibitory or excitatory. In WT mice, sex differences in GABA-R antagonism effects on SFR are consistent with enhanced GABA inhibitory drive within the female SCN circuit which may result in a less tightly coupled SCN that is more susceptible to environmental perturbations. Enhanced daytime Na/K ATPase, voltage gated sodium channels currents, and calcium currents regulate increased excitatory drive during the daytime, while BK, A-type, HCN, FDR and possibly K_{ATP} currents regulate the inter-spike interval. In BACHD mice alterations in BK, A-type, and H-type potassium currents are associated with the loss of rhythmic electrical activity, and decreased amplitude behavioral and physiological rhythms. Figure summarized from (Brown and Piggins, 2007; Colwell, 2011).

To address this problem on a mechanistic level, we examined the circadian systems of multiple mouse models predisposed to circadian disruption in order to determine how SCN physiological properties are related to behavioral and physiological states.

Women have increased rates of insomnia symptoms (Ohayon, 2002; Grandner et al., 2012), so first we tested whether the circadian system of the common laboratory mouse exhibits potentially related sex differences (Chapter 2). There were remarkably few sex differences in circadian behavior and molecular expression, but we found subtle differences in the circadian regulation of activity duration which may be regulated by sex chromosome compliment. The greater prevalence of GABA-inhibitory responses and the increased damping rate of SCN molecular rhythms in culture suggests that the reduced coupling strength of SCN cellular oscillators may underlie the larger spread of activity across the day and predispose the female circadian system to disruption by environmental perturbations.

Using the VIP KO mouse model, we tested the role of VIP signaling on SCN's responsiveness to light input and circadian regulation of female reproductive rhythms (Chapters 3 and 4). Previously VIP KO mice have been shown to exhibit deficits in their ability to entrain to light (Colwell et al., 2003; Dragich et al., 2010), while their SCN exhibit altered circuit dynamics and molecular rhythms (Brancaccio et al., 2013; Pauls et al., 2014). First, we found that at the physiological level, retinal input signals excite retinorecipient neurons in the SCN, but unlike in WT animals, VIP KO SCN light-induced excitability dissipates faster and does not spread to dorsal output regions. This was associated with the altered phasing of intrinsic electrical activity rhythms of VIP KO dSCN neurons, that are likely related to the large phase advance VIP KO animals exhibit relative to WT mice when released into constant conditions (Colwell et al., 2003). These findings indicate intrinsic electrical activity rhythms within the SCN regulate its photic responsiveness. Female VIP KO SCN electrical activity rhythms were examined at the

same phases of their environmental light-dark cycle, but did not exhibit the same antiphase relationship as VIP KO male SCN neurons did relative to sex-matched WT controls. Instead, we observed a non-rhythmic intermediate SFR phenotype in VIP KO female SCN that may be related to a less severe phase difference relative to WT females. It is an appealing hypothesis considering female VIP KO animals exhibit smaller phase shifts when released into constant conditions relative to VIP KO males. The mechanism mediating this sex difference is unknown, but regardless of whether VIP KO female SCN output is arrhythmic or just altered in phase, it is clear that the aberrant timing of VIP KO female circadian output is associated with disrupted phasing of peripheral tissue clock gene expression and dysregulation of reproductive rhythms resulting in reduced fertility. These findings provide important evidence that circadian regulation of the hypothalamic pituitary gonadal axis is integral for reproductive success, and considering that environmental circadian disruption reduces fertility in animal models and humans (Summa et al., 2012; Gamble et al., 2013), it may be a public health issue warranting intervention and education.

Neurodegenerative diseases are also commonly associated with altered sleep/wake cycles (Kuljis et al., 2012), and considering the negative impact disrupted sleep has on otherwise healthy individuals, it may feed forward into the neurodegenerative disease mechanisms increasing the rate of functional loss. Focusing on the BACHD mouse model of HD, we tested for sex differences in circadian system dysfunction and multiple pathophysiological mechanisms for disrupted SCN electrical activity previously reported in males (Chapter 5 and 6). We found BACHD female activity level deficits and behavioral fragmentation were less severe relative to BACHD males, and that mitigation of their circadian system's dysfunction was associated with delayed motor coordination deterioration. These findings provide exciting evidence that circadian regulation of behavioral rhythms is negatively correlated with disease progression, and raise the possibility that sex differences in BACHD mouse circadian dysfunction may be related

to neuroprotective effects of estrogens, and/or sex differences in activational gonadal hormone effects on the circadian system. These findings also emphasize the importance of balancing sex in clinical study designs, as females may have different rates of disease progression and may respond differently to therapeutic interventions.

Focusing on BACHD male mice, who exhibit greater deficits in circadian system dysfunction early in life, we tested multiple mechanistic hypotheses to account for the depressed daytime SFR and the loss of rhythmic electrical output observed in BACHD SCN of both sexes (Chapter 6). First, we determined decreased SCN electrical activity in BACHD dSCN neurons was not due to enhanced GABA inhibition, but *is* associated with alterations in the intrinsic membrane currents that regulate SCN neuron's pacemaking properties. During the daytime, BACHD SCN neurons exhibit similar changes to those of aged mice. Although direct and pharmacological excitation acutely increases BACHD dSCN depressed SFR, we were unable to rescue SFR by targeting individual potassium currents. Reduced daytime SFR may be due to the additive effects of subtle alterations across multiple currents, or mHTT related disruption of those currents is not acutely reversible. The mechanism whereby mHTT disrupts SCN potassium currents and SFR rhythms is unknown. SCN electrical activity may be disrupted by impaired mitochondrial function resulting in insufficient ATP production and/or increased oxidative stress. Similar effects have been observed in other neural circuits (Correia et al., 2012; Schapira, 2012), and many studies indicate mutant huntingtin aggregation disrupts mitochondrial trafficking (Trushina et al., 2004) and increases reactive oxygen species (ROS) production via decreased complex I-dependent mitochondrial respiration (Shimohata et al., 2000; Sugars et al., 2004).

Membrane repolarization following action potential generation is energetically demanding, and insufficient ATP availability may disrupt an individual neuron's ability to maintain a favorable

ionic concentration gradient for generating fast AP frequencies. Insufficient ATP levels may also be depressing BACHD SCN SFR by increasing the inhibitory K_{ATP} current. Although the K_{ATP} current has not been characterized in the SCN, we found its acute inhibition with tolbutamide increases SFR in both WT and BACHD neurons. Alternatively, decreased electrical activity may be related to mutant HTT-driven increases in oxidative damage in SCN. Oxidative stress damages a range of cellular processes, and potassium channels are particularly sensitive to its effects (Sesti et al., 2010; Cotella et al., 2012). If oxidative damage to potassium channels contributes to BACHD SCN pathophysiology, it would likely not be acutely reversible, but raises the possibility that long-term treatment with antioxidants or other interventions aimed at improving mitochondrial efficiency, may restore potassium channel function pending damaged protein turnover. Future examination of mitochondrial efficiency and oxidative stress in BACHD SCN will provide important insights into the mechanism underlying altered potassium currents and depressed daytime SFR.

References

Abraham U, Granada AE, Westermark PO, Heine M, Kramer A, Herzel H (2010) Coupling governs entrainment range of circadian clocks. Mol Syst Biol 6:438.

Abrahamson EE, Moore RY (2001) Suprachiasmatic nucleus in the mouse: retinal innervation, intrinsic organization and efferent projections. Brain Res 916:172–191.

Adan A, Natale V (2002) Gender differences in morningness-eveningness preference. Chronobiol Int 19:709–720.

Ahmed C, Dees W, Ojeda S (1986) The immature rat ovary is innervated by vasoactive intestinal peptide (VIP)-containing fibers and responds to VIP with steroid secretion. Endocrinology 118:1682–1689.

Akasu T, Shoji S (1994) cAMP-dependent inward rectifier current in neurons of the rat suprachiasmatic nucleus. Pflugers Arch 429:117–125.

Akhtar R a., Reddy AB, Maywood ES, Clayton JD, King VM, Smith AG, Gant TW, Hastings MH, Kyriacou CP (2002) Circadian cycling of the mouse liver transcriptome, as revealed by cDNA microarray, is driven by the suprachiasmatic nucleus. Curr Biol 12:540–550.

Akita M, Kuwahara M, Tsubone H, Sugano S (1998) ECG changes during furosemide-induced hypokalemia in the rat. J Electrocardiol 31:45–49.

Albers HE, Elliott H (1981) Gonadal hormones organize and modulate the circadian system of the rat Gonadal hormones organize circadian system of the rat and modulate the. Am J Physiol Regul Integr Comp Physiol 241:R62–R66.

Albers HE, Liou SY, Stopa EG, Zoeller RT (1991) Interaction of colocalized neuropeptides: functional significance in the circadian timing system. J Neurosci 11:846–851.

Albrecht U (2012) Timing to Perfection: The Biology of Central and Peripheral Circadian Clocks. Neuron 74:246–260.

Albrecht U, Sun ZS, Eichele G, Lee CC (1997) A differential response of two putative mammalian circadian regulators, mper1 and mper2, to light. Cell 91:1055–1064.

Ali T, Choe J, Awab A, Wagener TL, Orr WC (2013) Sleep, immunity and inflammation in gastrointestinal disorders. World J Gastroenterol 19:9231–9239.

Alvado L, Allen CN (2008) Tetraethylammonium (TEA) increases the inactivation time constant of the transient K+ current in suprachiasmatic nucleus neurons. Brain Res 1221:24–29.

Alvarez JD, Hansen A, Ord T, Bebas P, Chappell PE, Giebultowicz JM, Williams C, Moss S, Sehgal A (2008) The circadian clock protein BMAL1 is necessary for fertility and proper testosterone production in mice. J Biol Rhythms 23:26–36.

An S, Irwin RP, Allen CN, Tsai C, Herzog ED (2011) Vasoactive intestinal polypeptide requires parallel changes in adenylate cyclase and phospholipase C to entrain circadian rhythms to a predictable phase. J Neurophysiol 105:2289–2296.

An S, Tsai C, Ronecker J, Bayly A, Herzog ED (2012) Spatiotemporal distribution of vasoactive intestinal polypeptide receptor 2 in mouse suprachiasmatic nucleus. J Comp Neurol 520:2730–2741.

Andrich J, Schmitz T, Saft C, Postert T, Kraus P, Epplen JT, Przuntek H, Agelink MW (2002) Autonomic nervous system function in Huntington's disease. J Neurol Neurosurg Psychiatry 72:726–731.

Antle MC, Silver R (2005) Orchestrating time: arrangements of the brain circadian clock. Trends Neurosci 28:145–151.

Antle MC, Smith VM, Sterniczuk R, Yamakawa GR, Rakai BD (2009) Physiological responses of the circadian clock to acute light exposure at night. Rev Endocr Metab Disord 10:279–291.

Antoch MP, Kondratov R V. (2010) Circadian proteins and genotoxic stress response. Circ Res 106:68–78.
Arnold AP, Chen X (2009) What does the “four core genotypes” mouse model tell us about sex differences in the brain and other tissues? Front Neuroendocrinol 30:1–9.
Artinian LR, Ding JM, Gillette MU (2001) Carbon monoxide and nitric oxide: interacting messengers in muscarinic signaling to the brain’s circadian clock. Exp Neurol 171:293–300.
Atkinson SE, Maywood ES, Chesham JE, Wozny C, Colwell CS, Hastings MH, Williams SR, Michael H, Williams SR, Hastings MH, Williams SR (2011) Cyclic AMP Signaling Control of Action Potential Firing Rate and Molecular Circadian Pacemaking in the Suprachiasmatic Nucleus. J Biol Rhythms 26:210–220.
Aton SJ, Colwell CS, Harmar AJ, Waschek J, Herzog ED (2005) Vasoactive intestinal polypeptide mediates circadian rhythmicity and synchrony in mammalian clock neurons. Nat Neurosci 8:476–483.
Aton SJ, Huettner JE, Straume M, Herzog ED (2006) GABA and Gi/o differentially control circadian rhythms and synchrony in clock neurons. Proc Natl Acad Sci U S A 103:19188–19193.
Aziz N a., Pijl H, Frölich M, Schröder-Van Der Elst JP, van der Bent C, Roelfsema F, Roos R a C (2010a) Growth hormone and ghrelin secretion are associated with clinical severity in Huntington’s disease. Eur J Neurol 17:280–288.
Aziz NA, Anguelova G V, Marinus J, Lammers GJ, Roos R a C (2010b) Sleep and circadian rhythm alterations correlate with depression and cognitive impairment in Huntington’s disease. Parkinsonism Relat Disord 16:345–350.
Aziz NA, Pijl H, Frölich M, Schröder-van der Elst JP, van der Bent C, Roelfsema F, Roos R a C (2009a) Delayed onset of the diurnal melatonin rise in patients with Huntington’s disease. J Neurol 256:1961–1965.
Aziz NA, Pijl H, Frölich M, van der Graaf a WM, Roelfsema F, Roos R a C (2009b) Increased hypothalamic-pituitary-adrenal axis activity in Huntington’s disease. J Clin Endocrinol Metab 94:1223–1228.
Bae K, Jin X, Maywood ES, Hastings MH, Reppert SM, Weaver DR (2001) Differential functions of mPer1, mPer2, and mPer3 in the SCN Circadian Clock. Neuron 30:525–536.
Baggs JE, Hogenesch JB (2010) Genomics and systems approaches in the mammalian circadian clock. Curr Opin Genet Dev 20:581–587.
Baldo B, Cheong RY, Petersén Å (2014) Effects of deletion of mutant huntingtin in steroidogenic factor 1 neurons on the psychiatric and metabolic phenotype in the BACHD mouse model of Huntington disease. PLoS One 9:e107691.
Barbacka-Surowiak G, Surowiak J, Stokłosowa S (2003) The involvement of suprachiasmatic nuclei in the regulation of estrous cycles in rodents. Reprod Biol 3:99–129.
Beaver LM, Gvakharia BO, Vollintine TS, Hege DM, Stanewsky R, Giebultowicz JM (2002) Loss of circadian clock function decreases reproductive fitness in males of Drosophila melanogaster. Proc Natl Acad Sci U S A 99:2134–2139.
Beery, Annaliese K, Zucker I (2011) Sex Bias in Neuroscience and Biomedical Research. Neurosci Biobehav Rev 35:565–572.
Berson DM, Dunn F a, Takao M (2002) Phototransduction by retinal ganglion cells that set the circadian clock. Science 295:1070–1073.
Besedovsky L, Lange T, Born J (2012) Sleep and immune function. Pflugers Arch 463:121–137.
Bhattacharya A, Vavra V, Svobodova I, Bendova Z, Vereb G, Zemkova H (2013) Potentiation of inhibitory synaptic transmission by extracellular ATP in rat suprachiasmatic nuclei. J Neurosci 33:8035–8044.

Bigger JT, Fleiss JL, Steinman RC, Rolnitzky LM, Kleiger RE, Rottman JN (1992) Frequency domain measures of heart period variability and mortality after myocardial infarction. Circulation 85:164–171.
Björkqvist M, Petersén A, Bacos K, Isaacs J, Norlén P, Gil J, Popovic N, Sundler F, Bates GP, Tabrizi SJ, Brundin P, Mulder H (2006) Progressive alterations in the hypothalamic-pituitary-adrenal axis in the R6/2 transgenic mouse model of Huntington's disease. Hum Mol Genet 15:1713–1721.
Blattner MS, Mahoney MM (2012) Circadian parameters are altered in two strains of mice with transgenic modifications of estrogen receptor subtype 1. Genes Brain Behav 11:828–836.
Bollen E, Prickaerts J (2012) Phosphodiesterases in neurodegenerative disorders. IUBMB Life 64:965–970.
Bonelli R, Beal M (2012) Huntington's disease. Handb Clin Neurol 106:507–526.
Bouskila Y, Dudek FE (1995) A rapidly activating type of outward rectifier K+ current and A-current in rat suprachiasmatic nucleus neurones. J Physiol 488 (Pt 2:339–350.
Brancaccio M, Maywood ES, Chesham JE, Loudon ASI, Hastings MH (2013) A Gq-Ca2+ axis controls circuit-level encoding of circadian time in the suprachiasmatic nucleus. Neuron 78:714–728.
Branchey M, Branchey L, Nadler RD (1971) Effects of estrogen and progesterone on sleep patterns of female rats. Physiol Behav 6:743–746.
Brown TM, Colwell CS, Waschek J a, Piggins HD (2007) Disrupted neuronal activity rhythms in the suprachiasmatic nuclei of vasoactive intestinal polypeptide-deficient mice. J Neurophysiol 97:2553–2558.
Brown TM, Piggins HD (2007) Electrophysiology of the suprachiasmatic circadian clock. Prog Neurobiol 82:229–255.
Brown TM, Piggins HD (2009) Spatiotemporal Heterogeneity in the Electrical Activity of Suprachiasmatic Nuclei Neurons and their Response to Photoperiod. J Biol Rhythms 24:44–54.
Brown TM, Wynne J, Piggins HD, Lucas RJ (2011) Multiple hypothalamic cell populations encoding distinct visual information. J Physiol 589:1173–1194.
Buccelletti E, Gilardi E, Scaini E, Galiuto L, Persiani R, Biondi A, Basile F, Silveri N (2009) Heart rate variability and myocardial infarction: systematic literature review and metanalysis. Eur Rev Med Pharmacol Sci 13:299–307.
Burdakov D, Luckman SM, Verkhratsky A (2005) Glucose-sensing neurons of the hypothalamus. Philos Trans R Soc Lond B Biol Sci 360:2227–2235.
Busino L, Bassermann F, Maiolica A, Lee C, Nolan PM, Godinho SIH, Draetta GF, Pagano M (2007) SCFFbxl3 controls the oscillation of the circadian clock by directing the degradation of cryptochrome proteins. Science 316:900–904.
Butler MP, Karatsoreos IN, LeSauter J, Silver R (2012) Dose-dependent effects of androgens on the circadian timing system and its response to light. Endocrinology 153:2344–2352.
Cain SW, Dennison CF, Zeitzer JM, Guzik AM, Khalsa SBS, Santhi N, Schoen MW, Czeisler C a, Duffy JF (2010) Sex differences in phase angle of entrainment and melatonin amplitude in humans. J Biol Rhythms 25:288–296.
Caligioni CS (2009) Assessing reproductive status/stages in mice. Curr Protoc Neurosci:1–8.
Carruthers SG, Mccall B, Cordell BA, Wu R (1987) Relationships between heart rate and PR interval during physio- logical and pharmacological interventions. Br J Clin Pharmacol 23:259–265.
Cassone VM, Joan C, Moore RY (1988) Comparative Anatomy of the Mammalian Hypothalamic Suprachiasmatic Nucleus. J Biol Chem 3:71–91.

Castanon-Cervantes O, Wu M, Ehlen JC, Paul K, Gamble KL, Johnson RL, Besing RC, Menaker M, Gewirtz AT, Davidson AJ (2010) Dysregulation of inflammatory responses by chronic circadian disruption. J Immunol 185:5796–5805.
Cecconi S, Rossi G, Barberi M, Scaldaferri L, Canipari R (2004) Effect of pituitary adenylate cyclase-activating polypeptide and vasoactive intestinal polypeptide on mouse preantral follicle development in vitro. Endocrinology 145:2071–2079.
Cepeda C, Hurst RS, Calvert CR, Herna E, Nguyen OK, Jocoy E, Christian LJ, Ariano MA, Levine MS (2003) Transient and Progressive Electrophysiological Alterations in the Corticostriatal Pathway in a Mouse Model of Huntington ' s Disease. J Neurosci 23:961–969.
Chen G, van den Pol a N (1998) Presynaptic GABAB autoreceptor modulation of P/Q-type calcium channels and GABA release in rat suprachiasmatic nucleus neurons. J Neurosci 18:1913–1922.
Chen N, Li Y, Wang W, Ma Y, Yang D, Zhang Q (2012) Vasoactive Intestinal Peptide Can Promote the Development of Neonatal Rat Primordial Follicles During In Vitro Culture. Biol Reprod 88:12–12.
Cheng MY, Bullock CM, Li C, Lee AG, Bermak JC, Belluzzi J, Weaver DR, Leslie FM, Zhou Q-Y (2002) Prokineticin 2 transmits the behavioural circadian rhythm of the suprachiasmatic nucleus. Nature 417:405–410.
Chiu E, Alexander L (1982) Causes of death in Huntington's disease. Med J Aust 1:153.
Choi HJ, Lee CJ, Schroeder A, Kim YIYS, Jung SH, Kim JS, Kim DY, Son EJ, Han HC, Hong SK, Colwell CS, Kim YIYS (2008) Excitatory actions of GABA in the suprachiasmatic nucleus. J Neurosci 28:5450–5459.
Christian CA, Mobley JL, Moenter SM (2005) Diurnal and estradiol-dependent changes in gonadotropin-releasing hormone neuron firing activity. Proc Natl Acad Sci U S A 102:15682–15687.
Christian CA., Moenter SM (2008) Vasoactive intestinal polypeptide can excite gonadotropin-releasing hormone neurons in a manner dependent on estradiol and gated by time of day. Endocrinology 149:3130–3136.
Christian CA., Moenter SM (2010) The neurobiology of preovulatory and estradiol-induced gonadotropin- releasing hormone surges. Endocr Rev 31:544–577.
Ciarleglio CM, Gamble KL, Axley JC, Strauss BR, Cohen JY, Colwell CS, McMahon DG (2009) Population encoding by circadian clock neurons organizes circadian behavior. J Neurosci 29:1670–1676.
Clarke A, Pörtner HO (2010) Temperature, metabolic power and the evolution of endothermy. Biol Rev 85:703–727.
Clayton J, Collins F (2014) Policy: NIH to balance sex in cell and animal studies. Nature 509:282–283.
Cloues RK, Sather W a (2003) Afterhyperpolarization regulates firing rate in neurons of the suprachiasmatic nucleus. J Neurosci 23:1593–1604.
Cohen S, Doyle WJ, Alper CM, Janicki-Deverts D, Turner RB (2009) Sleep habits and susceptibility to the common cold. Arch Intern Med 169:62–67.
Colvin G, Whitmoyer D, Sawyer C (1969) Circadian sleep-wakefulness patterns in rats after ovariectomy and treatment with estrogen. Exp Neurol 25:616–625.
Colwell CS (2001) NMDA-evoked calcium transients and currents in the suprachiasmatic nucleus: gating by the circadian system. Eur J Neurosci 13:1420–1428.
Colwell CS (2011) Linking neural activity and molecular oscillations in the SCN. Nat Rev Neurosci 12:553–569.
Colwell CS, Foster RG, Menaker M (1991) NMDA receptor antagonists block the effects of light on circadian behavior in the mouse. Brain Res 554:105–110.

Colwell CS, Michel S, Itri J, Rodriguez W, Tam J, Lelievre V, Hu Z, Liu X, Waschek J a (2003) Disrupted circadian rhythms in VIP- and PHI-deficient mice. Am J Physiol Regul Integr Comp Physiol 285:R939–R949.
Colwell CS, Michel S, Itri J, Rodriguez W, Tam J, Lelièvre V, Hu Z, Waschek J a, Lelie V, Hu Z, Waschek J a, Lelièvre V, Hu Z, Waschek J a (2004) Selective deficits in the circadian light response in mice lacking PACAP. Am J Physiol Regul Integr Comp Physiol 287:R1194–R1201.
Colwell CS, Ralph MR, Menaker M (1990) Do NMDA receptors mediate the effects of light on circadian behavior? Brain Res 523:117–120.
Coogan AN, Piggins HD (2004) MAP kinases in the mammalian circadian system--key regulators of clock function. J Neurochem 90:769–775.
Correia SC, Santos RX, Perry G, Zhu X, Moreira PI (2012) Chapter 16: Mitochondrial importance in ALzheimer's, Huntington's, and Parkinson's siseases:205–221.
Cotella D, Hernandez-Enriquez B, Wu X, Li R, Pan Z, Leveille J, Link CD, Oddo S, Sesti F (2012) Toxic Role of K+ Channel Oxidation in Mammalian Brain. J Neurosci 32:4133–4144.
Crumbley C, Wang Y, Kojetin DJ, Burris TP (2010) Characterization of the core mammalian clock component, NPAS2, as a REV-ERBalpha/RORalpha target gene. J Biol Chem 285:35386–35392.
Cuesta M, Aungier J, Morton a J (2014) Behavioral therapy reverses circadian deficits in a transgenic mouse model of Huntington's disease. Neurobiol Dis 63:85–91.
Cummings DM, André VM, Uzgil BO, Gee SM, Fisher YE, Cepeda C, Levine MS (2009) Alterations in cortical excitation and inhibition in genetic mouse models of Huntington's disease. J Neurosci 29:10371–10386.
Cunha-Reis D, Sebastião AM, Wirkner K, Illes P, Ribeiro JA (2004) VIP enhances both pre- and postsynaptic GABAergic transmission to hippocampal interneurones leading to increased excitatory synaptic transmission to CA1 pyramidal cells. Br J Pharmacol 143:733–744.
Cuturic M, Abramson RK, Vallini D, Frank EM, Shamsnia M (2009) Sleep patterns in patients with Huntington's disease and their unaffected first-degree relatives: a brief report. Behav Sleep Med 7:245–254.
Czeisler C, Richardson G, JC Z, Moore-Ede M, Weitzman E (1981) Entrainment of human circadian rhythms by light-dark cycles: a reassessment. Photochem Photobiol 34:239–247.
Czlonkowska A, Ciesielska A, Gromadzka G, Kurkowska-Jastrzebska I (2005) Estrogen and cytokines production - the possible cause of gender differences in neurological diseases. Curr Pharmacol Des 11:1017–1030.
Dani VS, Chang Q, Maffei A, Turrigiano GG, Jaenisch R, Nelson SB (2005) Reduced cortical activity due to a shift in the balance between excitation and inhibition in a mouse model of Rett syndrome. Proc Natl Acad Sci U S A 102:12560–12565.
Davis FC, Darrow JM, Menaker M (1983) Sex differences in the circadian control of hamster wheel-running activity. Am J Physiol Regul Integr Comp Physiol:R93–R105.
De Jeu MT, Pennartz CM (1997) Functional characterization of the H-current in SCN neurons in subjective day and night: a whole-cell patch-clamp study in acutely prepared brain slices. Brain Res 767:72–80.
de la HO, de la Iglesia H, Meyer J, Carpino Jr. A, Schwartz W, De La HO, de la Iglesia H, Meyer J, Carpino Jr. A, Schwartz W (2000) Antiphase Oscillation of the Left and Right Suprachiasmatic Nuclei. Science (80-) 290:799–801.
de la Iglesia HO, Schwartz WJ (2006) Minireview: Timely ovulation: Circadian regulation of the female hypothalamo-pituitary-gonadal axis. Endocrinology 147:1148–1153.
Deboer T, Vansteensel MJ, Détári L, Meijer JH (2003) Sleep states alter activity of suprachiasmatic nucleus neurons. Nat Neurosci 6:1086–1090.

Dibner C, Schibler U, Albrecht U (2010) The mammalian circadian timing system: organization and coordination of central and peripheral clocks.
Dickmeis T (2009) Glucocorticoids and the circadian clock. J Endocrinol 200:3–22.
DiFiglia M, Sapp E, Chase K, Schwarz C, Meloni a, Young C, Martin E, Vonsattel JP, Carraway R, Reeves S a (1995) Huntingtin is a cytoplasmic protein associated with vesicles in human and rat brain neurons. Neuron 14:1075–1081.
Ding JM, Faiman LE, Hurst WJ, Kuriashkina LR, Gillette MU (1997) Resetting the biological clock: mediation of nocturnal CREB phosphorylation via light, glutamate, and nitric oxide. J Neurosci 17:667–675.
Dolatshad H, Campbell E a, O'Hara L, Maywood ES, Hastings MH, Johnson MH (2006) Developmental and reproductive performance in circadian mutant mice. Hum Reprod 21:68–79.
Downs J, Wise PM (2009) The role of the brain in female reproductive aging. Mol Cell Endocrinol 299:32–38.
Dragich JM, Loh DH, Wang LM, Vosko AM, Kudo T, Nakamura TJ, Odom IH, Tateyama S, Hagopian A, Waschek J a, Colwell CS (2010) The role of the neuropeptides PACAP and VIP in the photic regulation of gene expression in the suprachiasmatic nucleus. Eur J Neurosci 31:864–875.
Drouyer E, Rieux C, Hut R a, Cooper HM (2007) Responses of suprachiasmatic nucleus neurons to light and dark adaptation: relative contributions of melanopsin and rod-cone inputs. J Neurosci 27:9623–9631.
Duff K, Paulsen JS, Beglinger LJ, Langbehn DR, Stout JC (2007) Psychiatric symptoms in Huntington's disease before diagnosis: the predict-HD study. Biol Psychiatry 62:1341–1346.
Duffy JF, Cain SW, Chang A-M, Phillips AJK, Münch MY, Gronfier C, Wyatt JK, Dijk D-J, Wright KP, Czeisler C a (2011) Sex difference in the near-24-hour intrinsic period of the human circadian timing system. Proc Natl Acad Sci U S A 108 Suppl :15602–15608.
Duong H a, Robles MS, Knutti D, Weitz CJ (2011) A molecular mechanism for circadian clock negative feedback. Science 332:1436–1439.
Durmer JS, Ph D, Dinges DF, Ph D (2005) Neurocognitive Consequences of Sleep deprivation. Semin Neurol 25:117–129.
Edwards G, Weston AH (1993) The pharmacology of ATP-sensitive potassium channels. Annu Rev Pharmacol Toxicol 33:597–637.
Ehlen JC, Hesse S, Pinckney L, Paul KN (2013) Sex chromosomes regulate nighttime sleep propensity during recovery from sleep loss in mice. PLoS One 8:e62205.
Endo a, Watanabe T (1989) Effects of non-24-hour days on reproductive efficacy and embryonic development in mice. Gamete Res 22:435–441.
Epping E a. et al. (2013) Characterization of depression in prodromal Huntington disease in the neurobiological predictors of HD (PREDICT-HD) study. J Psychiatr Res 47:1423–1431.
Everett J, Sawyer C (1950) A 24-hour periodicity in the "LH-release apparatus" of female rats, disclosed by barbiturate sedation. Endocrinology 47:198–218.
Fahrbach S, Meisel R, Pfaff D (1985) Preoptic implants of estradiol increase wheel running but not the open field activity of female rats. Physiol Behavrior 35:985–992.
Fan MMY, Raymond L a (2007) N-methyl-D-aspartate (NMDA) receptor function and excitotoxicity in Huntington's disease. Prog Neurobiol 81:272–293.
Farajnia S, Michel S, Deboer T, Vanderleest HT, Houben T, Rohling JHT, Ramkisoensing A, Yasenkov R, Meijer JH (2012) Evidence for neuronal desynchrony in the aged suprachiasmatic nucleus clock. J Neurosci 32:5891–5899.

Field MD, Maywood ES, O'Brien J a, Weaver DR, Reppert SM, Hastings MH (2000) Analysis of clock proteins in mouse SCN demonstrates phylogenetic divergence of the circadian clockwork and resetting mechanisms. Neuron 25:437–447.
Fix C, Jordan C, Cano P, Walker WH (2004) Testosterone activates mitogen-activated protein kinase and the cAMP response element binding protein transcription factor in Sertoli cells. Proc Natl Acad Sci U S A 101:10919–10924.
Flaws J, DeSanti A, Tilly K, Javid R, Kugu K, Johnson A, Hirshfield A, Tilly J (1995) Vasoactive intestinal peptide-mediated suppression of apoptosis in the ovary: potential mechanisms of action and evidence of a conserved antiatretogenic role through evolution. Endocrinology 136:4351–4359.
Fleming SM, Salcedo J, Fernagut P-O, Rockenstein E, Masliah E, Levine MS, Chesselet M-F (2004) Early and progressive sensorimotor anomalies in mice overexpressing wild-type human alpha-synuclein. J Neurosci 24:9434–9440.
Foley D, Ancoli-Israel S, Britz P, Walsh J (2004) Sleep disturbances and chronic disease in older adults: Results of the 2003 National Sleep Foundation Sleep in America Survey. J Psychosom Res 56:497–502.
Foroud T, Gray J, Ivashina J, Conneally PM (1999) Differences in duration of Huntington's disease based on age at onset. J Neurol Neurosurg Psychiatry 66:52–56.
Foster RG, Roenneberg T (2008) Human responses to the geophysical daily, annual and lunar cycles. Curr Biol 18:R784–R794.
Foster RG, Wulff K (2005) The rhythm of rest and excess. Nat Rev Neurosci 6:407–414.
Freeman GM, Herzog ED (n.d.) (personal communication).
Gallego M, Virshup DM (2007) Post-translational modifications regulate the ticking of the circadian clock. Nat Rev Mol Cell Biol 8:139–148.
Gamble KL, Allen GC, Zhou T, McMahon DG (2007) Gastrin-releasing peptide mediates light-like resetting of the suprachiasmatic nucleus circadian pacemaker through cAMP response element-binding protein and Per1 activation. J Neurosci 27:12078–12087.
Gamble KL, Kudo T, Colwell CS, McMahon DG (2011) Gastrin-releasing peptide modulates fast delayed rectifier potassium current in Per1-expressing SCN neurons. J Biol Rhythms 26:99–106.
Gamble KL, Resuehr D, Johnson CH (2013) Shift work and circadian dysregulation of reproduction. Front Endocrinol (Lausanne) 4:1–9.
Gatchel JR, Zoghbi HY (2005) Diseases of unstable repeat expansion: mechanisms and common principles. Nat Rev Genet 6:743–755.
Gau D, Lemberger T, Von Gall C, Kretz O, Le Minh N, Gass P, Schmid W, Schibler U, Korf HW, Schütz G (2002) Phosphorylation of CREB Ser142 regulates light-induced phase shifts of the circadian clock. Neuron 34:245–253.
Gavrila a M, Robinson B, Hoy J, Stewart J, Bhargava a, Amir S (2008) Double-stranded RNA-mediated suppression of Period2 expression in the suprachiasmatic nucleus disrupts circadian locomotor activity in rats. Neuroscience 154:409–414.
Gekakis N, Staknis D, Nguyen H, Davis FC, Wilsbacher L, King D, Takahashi JS, Weitz C (1998) Role of the CLOCK Protein in the Mammalian Circadian Mechanism. Science (80-) 280:1564–1569.
Gerhold LM, Rosewell KL, Wise PM (2005) Suppression of vasoactive intestinal polypeptide in the suprachiasmatic nucleus leads to aging-like alterations in cAMP rhythms and activation of gonadotropin-releasing hormone neurons. J Neurosci 25:62–67.
Goel N, Rao H, Durmer JS, Dinges DF (2009) Neurocognitive consequences of sleep deprivation. Semin Neurol 29:320–339.

Gogolla N, Leblanc JJ, Quast KB, Südhof TC, Fagiolini M, Hensch TK (2009) Common circuit defect of excitatory-inhibitory balance in mouse models of autism. J Neurodev Disord 1:172–181.
Golombek D a, Rosenstein RE (2010) Physiology of Circadian Entrainment. Physiol Rev 90:1063–1102.
Goodman AOG, Morton AJ, Barker RA (2010) Identifying sleep disturbances in Huntington ' s disease using a simple disease-focused questionnaire. PLoS Curr HD:1–16.
Goodman AOG, Rogers L, Pilsworth S, McAllister CJ, Shneerson JM, Morton a J, Barker R a (2011) Asymptomatic sleep abnormalities are a common early feature in patients with Huntington's disease. Curr Neurol Neurosci Rep 11:211–217.
Granados-Fuentes D, Norris AJ, Carrasquillo Y, Nerbonne JM, Herzog ED (2012) I(A) channels encoded by Kv1.4 and Kv4.2 regulate neuronal firing in the suprachiasmatic nucleus and circadian rhythms in locomotor activity. J Neurosci 32:10045–10052.
Grandner M a, Jackson NJ, Pigeon WR, Gooneratne NS, Patel NP (2012) State and regional prevalence of sleep disturbance and daytime fatigue. J Clin Sleep Med 8:77–86.
Gray G, Söderstein P, Tallentire D, JM D (1978) Effects of lesions in various structures of the suprachiasmatic-preoptic region on LH regulation and sexual behavior in female rats. Neuroendocrinology 25:174–191.
Gray M, Shirasaki DI, Cepeda C, André VM, Wilburn B, Lu X-H, Tao J, Yamazaki I, Li S-H, Sun YE, Li X-J, Levine MS, Yang XW (2008) Full-length human mutant huntingtin with a stable polyglutamine repeat can elicit progressive and selective neuropathogenesis in BACHD mice. J Neurosci 28:6182–6195.
Haam J, Popescu IR, Morton L a, Halmos KC, Teruyama R, Ueta Y, Tasker JG (2012) GABA is excitatory in adult vasopressinergic neuroendocrine cells. J Neurosci 32:572–582.
Halle S (2000) Ecological Relevance of Daily Activity Patterns. In: Activity Patterns in Small Mammals, pp 67–90.
Halliday GM, McRitchie D a, Macdonald V, Double KL, Trent RJ, McCusker E (1998) Regional specificity of brain atrophy in Huntington's disease. Exp Neurol 154:663–672.
Hamada T, Antle MC, Silver R, Antle ÃMC, Silver R (2004) Temporal and spatial expression patterns of canonical clock genes and clock-controlled genes in the suprachiasmatic nucleus. Eur J Neurosci 19:1741–1748.
Han S, Yu FH, Schwartz MD, Linton JD, Bosma MM, Hurley JB, Catterall W a., de la Iglesia HO (2012) NaV1.1 channels are critical for intercellular communication in the suprachiasmatic nucleus and for normal circadian rhythms. Proc Natl Acad Sci 109:E368–E377.
Hannibal J, Brabet P, Fahrenkrug J (2008) Mice lacking the PACAP type I receptor have impaired photic entrainment and negative masking. Am J Physiol Regul Integr Comp Physiol 295:R2050–R2058.
Hannibal J, Hsiung HM, Fahrenkrug J (2011) Temporal phasing of locomotor activity, heart rate rhythmicity, and core body temperature is disrupted in VIP receptor 2-deficient mice. Am J Physiol Regul Integr Comp Physiol 300:R519–R530.
Hardeland R, Coto-Montes A, Poeggeler B (2003) Circadian rhythms, oxidative stress, and antioxidative defense mechanisms. Chronobiol Int 20:921–962.
Harmar AJ (2003) An Essential Role for Peptidergic Signalling in the Control of Circadian Rhythms in the Suprachiasmatic Nuclei. J Neuroendocrinol 15:335–338
Harmar AJ, Marston HM, Shen S, Spratt C, West KM, Sheward WJ, Morrison CF, Dorin JR, Piggins HD, Reubi JC, Kelly JS, Maywood ES, Hastings MH (2002) The VPAC2 receptor is essential for circadian function in the mouse suprachiasmatic nuclei. Cell 109:497–508.
Harms E, Kivimäe S, Young MW, Saez L (2004) Posttranscriptional and posttranslational regulation of clock genes. J Biol Rhythms 19:361–373.

Harney J, Scarbrough K, Rosewell K, Wise P (1996) In vivo antisense antagonism of vasoactive intestinal peptide in the suprachiasmatic nuclei causes aging-like changes in the estradiol-induced luteinizing hormone and prolactin surges. Endocrinology 137:3696–3701.
Hattar S, Liao H, Takao M, Berson D, Yau K (2002) Melanopsin-containing retinal ganglion cells: architecture, projections, and intrinsic photosensitivity. Science (80-) 295:1065–1070.
He C, Chen F, Li B, Hu Z (2014) Neurophysiology of HCN channels: From cellular functions to multiple regulations. Prog Neurobiol 112:1–23.
Helfrich-Förster C (2000) Differential control of morning and evening components in the activity rhythm of Drosophila melanogaster--sex-specific differences suggest a different quality of activity. J Biol Rhythms 15:135–154.
Herbison a E, Moenter SM (2011) Depolarising and hyperpolarising actions of GABA(A) receptor activation on gonadotrophin-releasing hormone neurones: towards an emerging consensus. J Neuroendocrinol 23:557–569.
Hermes MLHJ, Kolaj M, Doroshenko P, Coderre E, Renaud LP (2009) Effects of VPAC2 receptor activation on membrane excitability and GABAergic transmission in subparaventricular zone neurons targeted by suprachiasmatic nucleus. J Neurophysiol 102:1834–1842.
Heuser IJ, Chase TN, Mouradian MM (1991) The limbic-hypothalamic-pituitary-adrenal axis in Huntington's disease. Biol Psychiatry 30:943–952.
Hinton SC, Paulsen JS, Hoffmann RG, Reynolds NC, Zimbelman JL, Rao SM (2007) Motor timing variability increases in preclinical Huntington's disease patients as estimated onset of motor symptoms approaches. J Int Neuropsychol Soc 13:539–543.
Hofman M a (1997) Lifespan changes in the human hypothalamus. Exp Gerontol 32:559–575.
Hofman M a, Zhou JN, Swaab DF (1996) No evidence for a diurnal vasoactive intestinal polypeptide (VIP) rhythm in the human suprachiasmatic nucleus. Brain Res 722:78–82.
Hogenesch JB, Gu YZ, Jain S, Bradfield C a (1998) The basic-helix-loop-helix-PAS orphan MOP3 forms transcriptionally active complexes with circadian and hypoxia factors. Proc Natl Acad Sci U S A 95:5474–5479.
Hogenesch JB, Panda S, Kay S, Takahashi JS (2003) Circadian transcriptional output in the SCN and liver of the mouse. Novartis Found Symp 253:171–180; discussion 52–55, 102–109, 180–183.
Horvath TL, Cela V, Van Der Beek EM (1998) Gender-specific apposition between vasoactive intestinal peptide -containing axons and gonadotrophin-releasing hormone -producing neurons in the rat. Brain Res 795:277–281.
Huang RC (1993) Sodium and calcium currents in acutely dissociated neurons from rat suprachiasmatic nucleus. J Neurophysiol 70:1692–1703.
Huang W, Ramsey KM, Marcheva B, Bass J (2011) Circadian rhythms, sleep, and metabolism. J Clin Invest 121:2133–2141.
Hughes a TL, Piggins HD (2008) Behavioral responses of Vipr2-/- mice to light. J Biol Rhythms 23:211–219.
Hughes AT, Fahey B, Cutler DJ, Coogan AN, Piggins HD (2004) Aberrant gating of photic input to the suprachiasmatic circadian pacemaker of mice lacking the VPAC2 receptor. J Neurosci 24:3522–3526].
Hult S, Soylu R, Björklund T, Belgardt BF, Mauer J, Brüning JC, Kirik D, Petersén Å (2011) Mutant huntingtin causes metabolic imbalance by disruption of hypothalamic neurocircuits. Cell Metab 13:428–439.
Huntington T et al. (1993) A novel gene containing a trinucleotide repeat that is expanded and unstable on Huntington's disease chromosomes. The Huntington's Disease Collaborative Research Group. Cell 72:971–983.

Ibata Y, Takahashi Y, Okamura H, Kawakami F, Terubayashi H, Kubo T, Yanaihara N (1989) Vasoactive intestinal peptide (VIP)-like immunoreactive neurons located in the rat suprachiasmatic nucleus receive a direct retinal projection. Neurosci Lett 97:1–5.
Iranzo A, Molinuevo JL, Santamaría J, Serradell M, Martí MJ, Valldeoriola F, Tolosa E (2006) Rapid-eye-movement sleep behaviour disorder as an early marker for a neurodegenerative disorder: a descriptive study. Lancet Neurol 5:572–577.
Irwin RP, Allen CN (2007) Calcium response to retinohypothalamic tract synaptic transmission in suprachiasmatic nucleus neurons. J Neurosci 27:11748–11757.
Itil T, Cora R, Akpinar S, Herrmann W, Patterson C (1974) “Psychotropic” action of sex hormones: computerized EEG in establishing the immediate CNS effects of steroid hormones. Curr Ther Res Clin Exp 16:1147–1170.
Itri J, Michel S, Waschek JA, Colwell CS (2004) Circadian Rhythm in Inhibitory Synaptic Transmission in the Mouse Suprachiasmatic Nucleus. J Neurophysiol 92:311–319.
Itri JN, Vosko AM, Schroeder A, Dragich JM, Michel S, Colwell CS (2010) Circadian regulation of a-type potassium currents in the suprachiasmatic nucleus. J Neurophysiol 103:632–640.
Itri JNJ, Vansteensel MMJ, Meijer JJH, Colwell CCS, Michel S, Vansteensel MMJ, Meijer JJH, Colwell CCS (2005) Fast delayed rectifier potassium current is required for circadian neural activity. Nat Neurosci 8:650–656.
Iwahana E, Karatsoreos I, Shibata S, Silver R (2008) Gonadectomy reveals sex differences in circadian rhythms and suprachiasmatic nucleus androgen receptors in mice. Horm Behav 53:422–430.
Jackson AC, Yao GL, Bean BP (2004) Mechanism of spontaneous firing in dorsomedial suprachiasmatic nucleus neurons. J Neurosci 24:7985–7998.
Jagannath A, Butler R, Godinho SIH, Couch Y, Brown L a, Vasudevan SR, Flanagan KC, Anthony D, Churchill GC, Wood MJ a, Steiner G, Ebeling M, Hossbach M, Wettstein JG, Duffield GE, Gatti S, Hankins MW, Foster RG, Peirson SN (2013) The CRTC1-SIK1 pathway regulates entrainment of the circadian clock. Cell 154:1100–1111.
Jeftinija S, Murase K, Nedeljkov V, Randic M (1982) Vasoactive intestinal polypeptide excites mammalian dorsal horn neurons both in vivo and in vitro. Brain Res 243:158–164.
Jiang ZG, Nelson CS, Allen CN (1995) Melatonin activates an outward current and inhibits Ih in rat suprachiasmatic nucleus neurons. Brain Res 687:125–132.
Julien CL, Thompson JC, Wild S, Yardumian P, Snowden JS, Turner G, Craufurd D (2007) Psychiatric disorders in preclinical Huntington’s disease. J Neurol Neurosurg Psychiatry 78:939–943.
Kalliolia E, Silajdžić E, Nambron R, Hill NR, Doshi A, Frost C, Watt H, Hindmarsh P, Björkqvist M, Warner TT (2014) Plasma melatonin is reduced in Huntington’s disease. Mov Disord 29:1511–1515.
Kalsbeek a, Fliers E, Hofman M a, Swaab DF, Buijs RM (2010) Vasopressin and the output of the hypothalamic biological clock. J Neuroendocrinol 22:362–372.
Kalsbeek A, Palm IF, La Fleur SE, Scheer FAJL, Perreau-Lenz S, Ruiter M, Kreier F, Cailotto C, Buijs RM (2006) SCN outputs and the hypothalamic balance of life. J Biol Rhythms 21:458–469.
Karatsoreos IN, Bhagat S, Bloss EB, Morrison JH, McEwen BS (2011a) Disruption of circadian clocks has ramifications for metabolism, brain, and behavior. Proc Natl Acad Sci U S A 108:1657–1662.
Karatsoreos IN, Butler MP, Lesauter J, Silver R (2011b) Androgens modulate structure and function of the suprachiasmatic nucleus brain clock. Endocrinology 152:1970–1978.
Karatsoreos IN, Silver R (2007) Minireview: The neuroendocrinology of the suprachiasmatic nucleus as a conductor of body time in mammals. Endocrinology 148:5640–5647.

Karatsoreos IN, Wang A, Sasanian J, Silver R (2007) A role for androgens in regulating circadian behavior and the suprachiasmatic nucleus. Endocrinology 148:5487–5495.
Kassubek J, Juengling FD, Kioschies T, Henkel K, Karitzky J, Kramer B, Ecker D, Andrich J, Saft C, Kraus P, Aschoff AJ, Ludolph AC, Landwehrmeyer GB (2004) Topography of cerebral atrophy in early Huntington's disease: a voxel based morphometric MRI study. J Neurol Neurosurg 7:213–220.
Kelly M, Qiu J (2010) Estrogen Signaling in Hypothalamic Circuits Controling Reproduction. Brain Res 1364:44–52.
Kennaway DJ, Boden MJ, Voultsios A (2004) Reproductive performance in female Clock delta 19 mutant mice David. Reprod Fertil Dev 16:801–810.
Kent J, Meredith AL (2008) BK channels regulate spontaneous action potential rhythmicity in the suprachiasmatic nucleus. PLoS One 3:e3884.
Khalsa SBS, Jewett ME, Cajochen C, Czeisler C a (2003) A phase response curve to single bright light pulses in human subjects. J Physiol 549:945–952.
Kim DY, Choi HJ, Kim JS, Kim YS, Jeong DU, Shin HC, Kim MJ, Han HC, Hong SK, Kim YI (2005) Voltage-gated calcium channels play crucial roles in the glutamate-induced phase shifts of the rat suprachiasmatic circadian clock. Eur J Neurosci 21:1215–1222.
Kim JS, Kim W Bin, Kim YIYSY-B, Lee Y, Kim YIYSY-B, Shen F-Y, Lee SW, Park D, Choi H-J, Hur J, Park JJ, Han HC, Colwell CS, Cho Y-W, Kim YIYSY-B (2011) Chronic hyperosmotic stress converts GABAergic inhibition into excitation in vasopressin and oxytocin neurons in the rat. J Neurosci 31:13312–13322.
Kim YI, Dudek FE (1993) Membrane properties of rat suprachiasmatic nucleus neurons receiving optic nerve input. J Physiol 464:229–243.
Kiss J, Csáki Á, Csaba Z, Halász B (2008) Synaptic contacts of vesicular glutamate transporter 2 fibres on chemically identified neurons of the hypothalamic suprachiasmatic nucleus of the rat. Eur J Neurosci 28:1760–1774.
Ko GY-P, Shi L, Ko ML (2009) Circadian regulation of ion channels and their functions. J Neurochem 110:1150–1169.
Kobal J, Melik Z, Cankar K, Bajrovic FF, Meglic B, Peterlin B, Zaletel M (2010) Autonomic dysfunction in presymptomatic and early symptomatic Huntington's disease. Acta Neurol Scand 121:392–399.
Koch JM, Hagenauer MH, Lee TM (2009) The response of Per1 to light in the suprachiasmatic nucleus of the diurnal degu (Octodon degus). Chronobiol Int 26:1263–1271.
Koehl M, Battle S, Meerlo P (2006) Sex differences in sleep: the response to sleep deprivation and restraint stress in mice. Sleep 29:1224–1231.
Kondratov R V., Kondratova A a., Gorbacheva VY, Vykhovanets O V., Antoch MP (2006) Early aging and age-related pathologies in mice deficient in BMAL1, the core component of the circadian clock. Genes Dev 20:1868–1873.
Kononenko NI, Honma S, Dudek FE, Honma K-I (2008) On the role of calcium and potassium currents in circadian modulation of firing rate in rat suprachiasmatic nucleus neurons: multielectrode dish analysis. Neurosci Res 62:51–57.
Kononenko NI, Shao L-R, Dudek FE (2004) Riluzole-sensitive slowly inactivating sodium current in rat suprachiasmatic nucleus neurons. J Neurophysiol 91:710–718.
Konturek P, Brzozowski T, Konturek S (2011) Gut clock: implication of circadian rhythms in the gastrointestinal tract. J Physiol Pharmacol 62:139–150.
Kopp C, Ressel V, Wigger E, Tobler I (2006) Influence of estrus cycle and ageing on activity patterns in two inbred mouse strains. Behav Brain Res 167:165–174.
Kornhauser J, Mayo K, Takahashi J (1996) Light, immediate-early genes, and circadian rhythms. Behav Genet 26:221–240.

Kornmann B, Schaad O, Bujard H, Takahashi JS, Schibler U (2007) System-driven and oscillator-dependent circadian transcription in mice with a conditionally active liver clock. PLoS Biol 5:e34.
Kowalewski MP, Dyson MT, Boos A, Stocco DM (2010) Vasoactive intestinal peptide (VIP)-mediated expression and function of steroidogenic acute regulatory protein (StAR) in granulosa cells. Mol Cell Endocrinol 328:93–103.
Krajnak K, Kashon ML, Rosewell KL, Wise PM (1998) Sex differences in the daily rhythm of vasoactive intestinal polypeptide but not arginine vasopressin messenger ribonucleic acid in the suprachiasmatic nuclei. Endocrinology 139:4189–4196.
Krajnak K, Rosewell KL, Wise PM (2001) Fos-induction in gonadotropin-releasing hormone neurons receiving vasoactive intestinal polypeptide innervation is reduced in middle-aged female rats. Biol Reprod 64:1160–1164.
Kremer HP., Roos RAC, Dingjan G, Marani E, Bots (1990) Atrophy of the hypothalamic lateral tuberal nucleus in Huntington's disease. J Neuropathol Exp Neurol 49:371–382.
Kriegsfeld LJ, Leak RK, Yackulic CB, LeSauter J, Silver R (2004) Organization of suprachiasmatic nucleus projections in Syrian hamsters (Mesocricetus auratus): an anterograde and retrograde analysis. J Comp Neurol 468:361–379.
Kriegsfeld LJ, Silver R, Gore a. C, Crews D (2002) Vasoactive intestinal polypeptide contacts on gonadotropin-releasing hormone neurones increase following puberty in female rats. J Neuroendocrinol 14:685–690.
Krishnan V, Collop N a (2006) Gender differences in sleep disorders. Curr Opin Pulm Med 12:383–389.
Kudo T, Loh DH, Kuljis D, Constance C, Colwell CS (2011a) Fast delayed rectifier potassium current: critical for input and output of the circadian system. J Neurosci 31:2746–2755.
Kudo T, Schroeder A, Loh DH, Kuljis D, Jordan MC, Roos KP, Colwell CS (2011b) Dysfunctions in circadian behavior and physiology in mouse models of Huntington's disease. Exp Neurol 228:80–90.
Kudo T, Tahara Y, Gamble KL, McMahon DG, Block GD, Colwell CS (2013) Vasoactive intestinal peptide produces long-lasting changes in neural activity in the suprachiasmatic nucleus. J Neurophysiol 110:1097–1106.
Kuhlman SJ, McMahon DG (2004) Rhythmic regulation of membrane potential and potassium current persists in SCN neurons in the absence of environmental input. Eur J Neurosci 20:1113–1117.
Kuhlman SJ, Silver R, Le Sauter J, Bult-Ito A, McMahon DG (2003) Phase resetting light pulses induce Per1 and persistent spike activity in a subpopulation of biological clock neurons. J Neurosci 23:1441–1450.
Kuljis D a, Loh DH, Truong D, Vosko AM, Ong ML, McClusky R, Arnold AP, Colwell CS (2013) Gonadal- and sex-chromosome-dependent sex differences in the circadian system. Endocrinology 154:1501–1512.
Kuljis D, Schroeder AM, Kudo T, Loh DH, Willison DL, Colwell CS (2012) Sleep and circadian dysfunction in neurodegenerative disorders: insights from a mouse model of Huntington's disease. Minerva Pneumol 51:93–106.
Kume K, Zylka MJ, Sriram S, Shearman LP, Weaver DR, Jin X, Maywood ES, Hastings MH, Reppert SM (1999) mCRY1 and mCRY2 are essential components of the negative limb of the circadian clock feedback loop. Cell 98:193–205.
Kyle BD, Braun AP (2014) The regulation of BK channel activity by pre- and post-translational modifications. Front Physiol 5:1–10.
Lacombe A, Lelievre V, Roselli CE, Muller JM, Waschek J a., Vilain E (2007) Lack of vasoactive intestinal peptide reduces testosterone levels and reproductive aging in mouse testis. J Endocrinol 194:153–160.

Laermans J, Broers C, Beckers K, Vancleef L, Steensels S, Thijs T, Tack J, Depoortere I (2014) Shifting the circadian rhythm of feeding in mice induces gastrointestinal, metabolic and immune alterations which are influenced by ghrelin and the core clock gene bmal1. PLoS One 9:e110176.
Lange T, Dimitrov S, Born J (2010) Effects of sleep and circadian rhythm on the human immune system. Ann N Y Acad Sci 1193:48–59.
Lanska D, Lanska M, Lavine L, Schoenberg B (1988) Conditions associated with Huntington's disease at death. A case-control study. Arch Neurol 45:878–880.
Lavin PJ, Bone I, Sheridan P (1981) Studies of hypothalamic function in Huntington's chorea. J Neurol Neurosurg Psychiatry 44:414–418.
Lee C, Etchegaray JP, Cagampang FR, Loudon a S, Reppert SM (2001) Posttranslational mechanisms regulate the mammalian circadian clock. Cell 107:855–867.
Lee JE, Zamdborg L, Southey BR, Atkins N, Mitchell JW, Li M, Gillette MU, Kelleher NL, Sweedler J V (2013) Quantitative peptidomics for discovery of circadian-related peptides from the rat suprachiasmatic nucleus. J Proteome Res 12:585–593.
Lee S-H, Cox CL (2006) Excitatory actions of vasoactive intestinal peptide on mouse thalamocortical neurons are mediated by VPAC2 receptors. J Neurophysiol 96:858–871.
Lee TM, Hummer D, Jechura T, Mahonery, Megan M (2004) Pubertal development of sex differences in circadian function: an animal model. Ann NY Acad Sci:262–275.
Legan S, Coon G, Karsch F (1975) Role of estrogen as initiator of daily LH surges in the ovariectomized rat. Endocrinology 96:50–56.
Lehman M, Silver R, Gladstone W, Kahn R, Gibson M, Bittman E (1987) Circadian rhythmicity restored by neural transplant. Immunocytochemical characterization of the graft and its integration with the host brain. J Neurosci 7:1626–1638.
Lein ES et al. (2007) Genome-wide atlas of gene expression in the adult mouse brain. Nature 445:168–176.
Leproult R, Holmbäck U, Van Cauter E (2014) Circadian misalignment augments markers of insulin resistance and inflammation, independently of sleep loss. Diabetes 63:1860–1869.
Lesauter J, Silver R, Cloues R, Witkovsky P (2011) Light exposure induces short- and long-term changes in the excitability of retinorecipient neurons in suprachiasmatic nucleus. J Neurophysiol 106:576–588.
Li J-D, Burton KJ, Zhang C, Hu S-B, Zhou Q-Y (2009) Vasopressin receptor V1a regulates circadian rhythms of locomotor activity and expression of clock-controlled genes in the suprachiasmatic nuclei. Am J Physiol Regul Integr Comp Physiol 296:R824–R830.
Li L (2003) Role of NR2B-type NMDA receptors in selective neurodegeneration in Huntington disease. Neurobiol Aging 24:1113–1121.
Li SH, Li XJ (2004) Huntingtin-protein interactions and the pathogenesis of Huntington's disease. Trends Genet 20:146–154.
Liss B, Bruns R, Roeper J (1999) Alternative sulfonylurea receptor expression defines metabolic sensitivity of K-ATP channels in dopaminergic midbrain neurons. EMBO J 18:833–846.
Liu C, Reppert SM (2000) GABA synchronizes clock cells within the suprachiasmatic circadian clock. Neuron 25:123–128.
Loh DH, Abad C, Colwell CS, Waschek J a. (2008) Vasoactive intestinal peptide is critical for circadian regulation of glucocorticoids. Neuroendocrinology 88:246–255.
Loh DH, Dragich JM, Kudo T, Schroeder AM, Nakamura TJ, Waschek J a, Block GD, Colwell CS (2011) Effects of vasoactive intestinal peptide genotype on circadian gene expression in the suprachiasmatic nucleus and peripheral organs. J Biol Rhythms 26:200–209.
Loh DH, Kudo T, Truong D, Wu Y, Colwell CS (2013) The Q175 mouse model of Huntington's disease shows gene dosage- and age-related decline in circadian rhythms of activity and sleep. PLoS One 8:e69993.

Lowrey PL, Takahashi JS (2004) Mammalian circadian biology: elucidating genome-wide levels of temporal organization. Annu Rev Genomics Hum Genet 5:407–441.
Lucas R, Lall G, Allen A, Brown T (2012) How rod, cone, and melanopsin photoreceptors come together to enlighten the mammalian circadian clock. Prog Brain Res 199:1–18.
Lucassen E a, van Diepen HC, Houben T, Michel S, Colwell CS, Meijer JH (2012) Role of vasoactive intestinal peptide in seasonal encoding by the suprachiasmatic nucleus clock. Eur J Neurosci 35:1466–1474.
Lundh SH, Soylu R, Petersén A (2012) Expression of mutant huntingtin in leptin receptor-expressing neurons does not control the metabolic and psychiatric phenotype of the BACHD mouse. PLoS One 7:e51168.
Lundkvist GB, Kristensson K, Hill RH (2002) The Suprachiasmatic Nucleus Exhibits Diurnal Variations in Spontaneous Excitatory Postsynaptic Activity. J Biol Rhythms 17:40–51.
Mahoney MM (2010) Shift work, jet lag, and female reproduction. Int J Endocrinol 2010:813764.
Mahoney MM, Ramanathan C, Hagenauer MH, Thompson RC, Smale L, Lee T, Ramanathan, Hagenauer, Thompson, Smale, Lee (2009) Daily rhythms and sex differences in vasoactive intestinal polypeptide, VIPR2 receptor, and arginine vasopressin mRNA in the suprachasmatic nucleus of diurnal rodent, arvicanthis niloticus. Eur J Neurosci 30:1537–1543.
Malven P, Sawyer C (1966) Sleeping patterns in female guinea pigs; effects of sex hormones. Exp Neurol 15:229–239.
Marder K, Zhao H, Myers RH, Cudkowicz M, Kayson EM, Kieburtz, K. MD M, Orme CB, Paulsen J, Penney JBJ, Siemers E, Shoulson I, Group HS (2000) Rate of functional decline in Huntington's disease. Neurology 54:452.
Margolis RL, Ross CA, Huntington B (2003) Diagnosis of Huntington Disease. Clin Chem 49:1726–1732.
Markianos M, Panas M, Kalfakis N, Vassilopoulos D (2005) Plasma testosterone in male patients with Huntington's disease: relations to severity of illness and dementia. Ann Neurol 57:520–525.
Mattsson B (1974) Huntington's Chorea in Sweden. Acta Psychuatrica Scand.
Maywood ES, Chesham JE, O'Brien J a, Hastings MH (2011) A diversity of paracrine signals sustains molecular circadian cycling in suprachiasmatic nucleus circuits. Proc Natl Acad Sci U S A 108:14306–14311.
Maywood ES, Drynan L, Chesham JE, Edwards MD, Dardente H, Fustin J-M, Hazlerigg DG, O'Neill JS, Codner GF, Smyllie NJ, Brancaccio M, Hastings MH (2013) Analysis of core circadian feedback loop in suprachiasmatic nucleus of mCry1-luc transgenic reporter mouse. Proc Natl Acad Sci U S A 110:9547–9552.
Maywood ES, Fraenkel E, McAllister CJ, Wood N, Reddy AB, Hastings MH, Morton a J (2010) Disruption of peripheral circadian timekeeping in a mouse model of Huntington's disease and its restoration by temporally scheduled feeding. J Neurosci 30:10199–10204.
Maywood ES, Reddy AB, Wong GKY, O'Neill JS, O'Brien J a., McMahon DG, Harmar AJ, Okamura H, Hastings MH (2006) Synchronization and maintenance of timekeeping in suprachiasmatic circadian clock cells by neuropeptidergic signaling. Curr Biol 16:599–605.
McCarthy MM, Arnold AP, Ball GF, Blaustein JD, De Vries GJ (2012) Sex differences in the brain: the not so inconvenient truth. J Neurosci 32:2241–2247.
Mccarthy MM, Perrot-sinal TS, Auger AP, Sickel MJ (2002) Neuroplasticity, Development, and Steroid Hormone Action. CRC Press LLC.
McClung C a (2007) Circadian genes, rhythms and the biology of mood disorders. Pharmacol Ther 114:222–232.

McCurry SM, Logsdon RG, Teri L, Vitiello M V. (2007) Sleep disturbances in caregivers of persons with dementia: Contributing factors and treatment implications. Sleep Med Rev 11:143–153.
McDearmon EL, Patel KN, Ko CH, Walisser J a, Schook AC, Chong JL, Wilsbacher LD, Song EJ, Hong H-K, Bradfield C a, Takahashi JS (2006) Dissecting the functions of the mammalian clock protein BMAL1 by tissue-specific rescue in mice. Science 314:1304–1308.
Meijer JH, Schaap J, Watanabe K, Albus H (1997) Multiunit activity recordings in the suprachiasmatic nuclei: in vivo versus in vitro models. Brain Res 753:322–327.
Meijer JH, Watanabe K, Schaap J, Albus H, Détári L (1998) Light responsiveness of the suprachiasmatic nucleus: long-term multiunit and single-unit recordings in freely moving rats. J Neurosci 18:9078–9087.
Menalled L et al. (2009) Systematic behavioral evaluation of Huntington's disease transgenic and knock-in mouse models. Neurobiol Dis 35:319–336.
Meredith AL, Wiler SW, Miller BH, Takahashi JS, Fodor A a, Ruby NF, Aldrich RW (2006) BK calcium-activated potassium channels regulate circadian behavioral rhythms and pacemaker output. Nat Neurosci 9:1041–1049.
Michel S, Itri J, Han JH, Gniotczynski K, Colwell CS (2006) Regulation of glutamatergic signalling by PACAP in the mammalian suprachiasmatic nucleus. BMC Neurosci 7:15.
Michel S, Marek R, vanderLeest HT, vanSteensel MJ, Schwartz WJ, Colwell CS, Meijer JH (2013) Mechanism of bilateral communication in the suprachiasmatic nucleus. Eur J Neurosci 37:964–971.
Miller BH, Olson SL, Turek FW, Levine JE, Horton TH, Takahashi JS, Chase C (2004) Estrous Cyclicity and Maintenance of Pregnancy. 14:1367–1373.
Miller BR, Walker AG, Shah AS, Barton SJ, Rebec G V. (2008) Dysregulated information processing by medium spiny neurons in striatum of freely behaving mouse models of Huntington's disease. J Neurophysiol 100:2205–2216.
Milnerwood AJ, Raymond L a. (2010) Early synaptic pathophysiology in neurodegeneration: Insights from Huntington's disease. Trends Neurosci 33:513–523.
Mittag M, Wagner V (2003) The circadian clock of the unicellular eukaryotic model organism Chlamydomonas reinhardtii. Biol Chem 384:689–695.
Moe K, Prinz P, Vitiello M, Marks A, Larsen L (1991) Healthy elderly women and men have different entrained circadian temperature rhythms. J Am Geriatr Soc 39:383–387.
Mohawk J a, Takahashi JS (2011) Cell autonomy and synchrony of suprachiasmatic nucleus circadian oscillators. Trends Neurosci 34:349–358.
Mohawk J a., Green CB, Takahashi JS (2012) Central and Peripheral Circadian Clocks in Mammals. Annu Rev Neurosci 35:445–462.
Moldofsky H (2001) Sleep and pain. Sleep Med Rev 5:385–396.
Mong J, Baker F, Mahoney M, Paul K, Schwartz M, Semba K, Silver R (2011) Sleep, rhythms, and the endocrine brain: influence of sex and gonadal hormones. J Neurosci 31:16107–16116.
Montgomery JR, Meredith AL (2012) Genetic activation of BK currents in vivo generates bidirectional effects on neuronal excitability. Proc Natl Acad Sci U S A 109:18997–19002.
Moore R (1993) Organization of the primate circadian system. J Biol Rhythms 8:S3–S9.
Morin L, Fitzgerald K, Zucker I (1977) Estradiol shortens the period of hamster circadian rhythms. Science (80-) 96:305–307.
Morin LP, Allen CN (2006) The circadian visual system, 2005. Brain Res Rev 51:1–60.
Morin LP, Shivers K-Y, Blanchard JH, Muscat L (2006) Complex organization of mouse and rat suprachiasmatic nucleus. Neuroscience 137:1285–1297.

Moriya T, Horikawa K, Akiyama M, Shibata S (2000) Correlative association between N-methyl-D-aspartate receptor-mediated expression of period genes in the suprachiasmatic nucleus and phase shifts in behavior with photic entrainment of clock in hamsters. Mol Pharmacol 58:1554–1562.
Morton a J, Wood NI, Hastings MH, Hurelbrink C, Barker R a, Maywood ES (2005) Disintegration of the sleep-wake cycle and circadian timing in Huntington's disease. J Neurosci 25:157–163.
Morton AJ (2013) Circadian and sleep disorder in Huntington's disease. Exp Neurol 243:34–44.
Mosko S, RY M (1979) Neonatal ablation of the suprachiasmatic nucleus. Effects on the development of the pituitary-gonadal axis in the female rat. Neuroendocrinology 29:350–361.
Mullington JJM, Haack MM, Toth M, Serrador JM, Meier-Ewert HK (2009) Cardiovascular, inflammatory and metabolic consequences of sleep deprivation. Prog Cardiovasc Dis 51:294–302.
Mure LS, Rieux C, Hattar S, Cooper HM, Claude U, Lyon B, De C (2007) Melanopsin-dependent nonvisual responses: evidence for photopigment bistability in vivo. J Biol Rhythm 22:411–424.
Murphy E (2011) Estrogen signaling and cardiovascular disease. Circ Res 109:687–696.
Myers RH, Sax DS, Koroshetz WJ, Mastromauro C, Cupples LA, Kiely DK, Pettengill FK, Bird ED (1991) Factors associated with slow progression in Huntington's disease. Arch Neurol 48:800–804.
Nakamura TJ, Fujimura K, Ebihara S, Shinohara K (2004) Light response of the neuronal firing activity in the suprachiasmatic nucleus of mice. Neurosci Lett 371:244–248.
Nakamura TJ, Nakamura W, Yamazaki S, Kudo T, Cutler T, Colwell CS, Block GD (2011) Age-related decline in circadian output. J Neurosci 31:10201–10205.
Nakamura TJ, Sellix MT, Menaker M, Block GD (2008a) Estrogen directly modulates circadian rhythms of PER2 expression in the uterus. Am J Physiol Endocrinol Metab 295:E1025–E1031.
Nakamura W, Yamazaki S, Nakamura TJ, Shirakawa T, Block GD, Takumi T (2008b) In Vivo Monitoring of Circadian Timing in Freely Moving Mice. Curr Biol 18:381–385.
Nakamura W, Yamazaki S, Takasu NN, Mishima K, Block GD (2005) Differential response of Period 1 expression within the suprachiasmatic nucleus. J Neurosci 25:5481–5487.
Navara KJ, Nelson RJ (2007) The dark side of light at night: Physiological, epidemiological, and ecological consequences. J Pineal Res 43:215–224.
Nelson SB, Turrigiano GG (2008) Strength through Diversity. Neuron 60:477–482.
Nguyen T-V V, Yao M, Pike CJ (2005) Androgens activate mitogen-activated protein kinase signaling: role in neuroprotection. J Neurochem 94:1639–1651.
Nielsen HS, Hannibal J, Fahrenkrug J (2002) Vasoactive intestinal polypeptide induces per1 and per2 gene expression in the rat suprachiasmatic nucleus late at night. Eur J Neurosci 15:570–574.
Notomi T, Shigemoto R (2004) Immunohistochemical Localization of Ih Channel Subunits, HCN1-4, in the Rat Brain. J Comp Neurol 471:241–276.
Nunez a a, Stephan FK (1977) The effects of hypothalamic knife cuts on drinking rhythms and the estrus cycle of the rat. Behav Biol 20:224–234.
O'Neill JS, Maywood ES, Chesham JE, Takahashi JS, Hastings MH, Neill JSO, Maywood ES, Chesham JE, Takahashi JS, Hastings MH, O'Neill JS, Maywood ES, Chesham JE, Takahashi JS, Hastings MH (2008) cAMP-Dependent Signalling as a Core Component of the Mammalian Circadian Pacemaker. Science (80-) 320:949–953.
Ohayon MM (2002) Epidemiology of insomnia: what we know and what we still need to learn. Sleep Med Rev 6:97–111.

Pakhotin P, Harmar AJ, Verkhratsky A, Piggins H (2006) VIP receptors control excitability of suprachiasmatic nuclei neurones. Pflugers Arch Eur J Physiol 452:7–15.
Pallier PN, Maywood ES, Zheng Z, Chesham JE, Inyushkin AN, Dyball R, Hastings MH, Morton a J (2007) Pharmacological imposition of sleep slows cognitive decline and reverses dysregulation of circadian gene expression in a transgenic mouse model of Huntington's disease. J Neurosci 27:7869–7878.
Pan A, Schernhammer ES, Sun Q, Hu FB (2011) Rotating Night Shift Work and Risk of Type 2 Diabetes: Two Prospective Cohort Studies in Women Groop L, ed. PLoS Med 8:e1001141.
Panda S, Antoch MP, Miller BH, Su AI, Schook AB, Straume M, Schultz PG, Kay S a, Takahashi JS, Hogenesch JB (2002) Coordinated transcription of key pathways in the mouse by the circadian clock. Cell 109:307–320.
Papalexi E, Persson A, Björkqvist M, Petersén A, Woodman B, Bates GP, Sundler F, Mulder H, Brundin P, Popovic N (2005) Reduction of GnRH and infertility in the R6/2 mouse model of Huntington's disease. Eur J Neurosci 22:1541–1546.
Parsons MP, Hirasawa M (2010) ATP-sensitive potassium channel-mediated lactate effect on orexin neurons: implications for brain energetics during arousal. J Neurosci 30:8061–8070.
Paul KN, Dugovic C, Turek FW, Laposky AD (2006) Diurnal sex differences in the sleep-wake cycle of mice are dependent on gonadal function. Sleep 29:1211–1223.
Paul KN, Turek FW, Kryger MH (2008) Influence of sex on sleep regulatory mechanisms. J Womens Health (Larchmt) 17:1201–1208.
Pauls S, Foley NC, Foley DK, LeSauter J, Hastings MH, Maywood ES, Silver R (2014) Differential contributions of intra-cellular and inter-cellular mechanisms to the spatial and temporal architecture of the suprachiasmatic nucleus circadian circuitry in wild-type, cryptochrome-null and vasoactive intestinal peptide receptor 2-null mutant. Eur J Neurosci 40:2528–2540.
Paulsen J, Conybeare R (2005) Cognitive changes in Huntington's disease. Adv Neurol 96:209–225.
Paulsen J, Nehl C, Hoth K, Kanz J, Benjamin M, Conybeare R, McDowell B, Turner B (2005) Depression and stages of Huntington's disease. J Neuropsychiatry Clin Neurosci 17:496–502.
Paulsen JS (2011) Cognitive impairment in Huntington disease: Diagnosis and treatment. Curr Neurol Neurosci Rep 11:474–483.
Paulsen JS, Langbehn DR, Stout JC, Aylward E, Ross C a, Nance M, Guttman M, Johnson S, MacDonald M, Beglinger LJ, Duff K, Kayson E, Biglan K, Shoulson I, Oakes D, Hayden M (2008) Detection of Huntington's disease decades before diagnosis: the Predict-HD study. J Neurol Neurosurg Psychiatry 79:874–880.
Paulsen JS, Magnotta V a, Mikos AE, Paulson HL, Penziner E, Andreasen NC, Nopoulos PC (2006) Brain structure in preclinical Huntington's disease. Biol Psychiatry 59:57–63 A.
Paulsen JS, Smith MM, Long JD (2013) Cognitive decline in prodromal Huntington Disease: implications for clinical trials. J Neurol Neurosurg Psychiatry 84:1233–1239.
Pawelzik H, Dodt H, Zieglgänsberger W (1992) Actions of vasoactive intestinal polypeptide (VIP) on neocortical neurons of the rat in vitro. Neurosci Lett 147:167–170.
Peavy GM, Jacobson MW, Goldstein JL, Hamilton JM, Kane A, Gamst AC, Lessig SL, Lee JC, Corey-Bloom J (2010) Cognitive and functional decline in Huntington's disease: dementia criteria revisited. Mov Disord 25:1163–1169.
Pekmezovic T, Svetel M, Maric J, Dujmovic-Basuroski I, Dragasevic N, Keckarevic M, Romac S, Kostic VS (2007) Survival of Huntington's disease patients in Serbia: longer survival in female patients. Eur J Epidemiol 22:523–526.

Pennartz CM a, Hamstra R, Geurtsen a. MS (2001) Enhanced NMDA receptor activity in retinal inputs to the rat suprachiasmatic nucleus during the subjective night. J Physiol 532:181–194.
Perrot-Sinal TS, Davis AM, Gregerson KA, Kao JPY, Carthy MMMC (2001) Mediated Calcium Signaling in Neonatal Hypothalamic Neurons *. Endocrinology 142:2238–2243.
Petersén A, Björkqvist M (2006) Hypothalamic-endocrine aspects in Huntington's disease. Eur J Neurosci 24:961–967.
Petersén A, Gil J, Maat-Schieman MLC, Björkqvist M, Tanila H, Araújo IM, Smith R, Popovic N, Wierup N, Norlén P, Li J-Y, Roos R a C, Sundler F, Mulder H, Brundin P (2005) Orexin loss in Huntington's disease. Hum Mol Genet 14:39–47.
Petersen RC, Donohue MC, Gamst a C, Harvey DJ, Jack CR, Jagust WJ, Toga a W (2010) Alzheimer ' s Disease Neuroimaging Initiative (ADNI) Clinical characterization. Neurology 74:201–209.
Petit D, Gagnon J-F, Fantini ML, Ferini-Strambi L, Montplaisir J (2004) Sleep and quantitative EEG in neurodegenerative disorders. J Psychosom Res 56:487–496.
Piggins HD, Antle MC, Rusak B (1995) Neuropeptides Phase Shift the Mammalian Circadian Pacemaker. J Neurosci 15:5612–5622.
Pittendrigh C, Daan S (1976) A Functional Analysis of Circadian Pacemakers in Nocturnal Rodents. V. Pacemaker Structure: A Clock for All Seasons. Jounral Comp Phsyiology 106:333–355.
Pittendrigh CS (1960) Circadian Rhythms and the Circadian Organization of Living Systems Circadian Rhythms and the Circadian Organization of Living Systems. Most:159–184.
Pitts GR, Ohta H, McMahon DG (2006) Daily rhythmicity of large-conductance Ca2+ -activated K+ currents in suprachiasmatic nucleus neurons. Brain Res 1071:54–62.
Possidente B, McEldowney S, Pabon A (1995) Aging lengthens circadian period for wheel-running activity in C57BL mice. Physiol Behav 57:575–579.
Preitner N, Damiola F, Zakany J, Duboule D, Albrecht U, Schibler U (2002) The Orphan Nuclear Receptor REV-ERB Controls Circadian Transcription within the Positive Limb of the Mammalian Circadian Oscillator University of Geneva University of Geneva. 110:251–260.
Prosser R a, McArthur a J, Gillette MU (1989) cGMP induces phase shifts of a mammalian circadian pacemaker at night, in antiphase to cAMP effects. Proc Natl Acad Sci U S A 86:6812–6815.
Ralph M, Foster R, Davis F, Menaker M (1990) Transplanted suprachiasmatic nucleus determines circadian period. Science (80) 247:975–978.
Ratajczak CK, Boehle KL, Muglia LJ (2009) Impaired steroidogenesis and implantation failure in Bmal1 -/-mice. Endocrinology 150:1879–1885.
Rebec G V, Conroy SK, Barton SJ (2006) Hyperactive striatal neurons in symptomatic Huntington R6/2 mice: variations with behavioral state and repeated ascorbate treatment. Neuroscience 137:327–336.
Reed HE, Meyer-Spasche A, Cutler DJ, Coen CW, Piggins HD (2001) Vasoactive intestinal polypeptide (VIP) phase-shifts the rat suprachiasmatic nucleus clock in vitro. Eur J Neurosci 13:839–843.
Reppert SM, Weaver DR (2001) Molecular analysis of mammalian circadian rhythms. Annu Rev Physiol.
Robertson J, Clifton D, de la Iglesia H, Steiner R, Kauffman A (2009) Circadian regulation of Kiss1 neurons: implications for timing the preovulatory gonadotropin-releasing hormone/luteinizing hormone surge. Endocrinology 150:3664–3671.
Roenneberg T, Kuehnle T, Juda M, Kantermann T, Allebrandt K, Gordijn M, Merrow M (2007) Epidemiology of the human circadian clock. Sleep Med Rev 11:429–438.

Roenneberg T, Wirz-Justice A, Merrow M (2003) Life between Clocks: Daily Temporal Patterns of Human Chronotypes. J Biol Rhythms 18:80–90.
Roos RAC, Vlis MV Der, Hermans J, Elshove HM, Moll AC (1991) Age at onset in Huntington ' s disease : effect of line of inheritance and patient ' s sex. :515–519.
Roozendaal B, van Gool W a., Swaab DF, Hoogendijk JE, Mirmiran M (1987) Changes in vasopressin cells of the rat suprachiasmatic nucleus with aging. Brain Res 409:259–264.
Roper TJTJ (1976) Sex differences in circadian wheel running rhythms in the mongolian gerbil. Physiol Behav 17:549–551.
Ross C a, Tabrizi SJ (2011) Huntington's disease: from molecular pathogenesis to clinical treatment. Lancet Neurol 10:83–98.
Rüger M, Scheer F a JL (2009) Effects of circadian disruption on the cardiometabolic system. Rev Endocr Metab Disord 10:245–260.
Saper CB, Scammell TE, Lu J (2005) Hypothalamic regulation of sleep and circadian rhythms. Nature 437:1257–1263.
Sato F, Kawamoto T, Fujimoto K, Noshiro M, Honda KK, Honma S, Honma K, Kato Y (2004) Functional analysis of the basic helix-loop-helix transcription factor DEC1 in circadian regulation. Interaction with BMAL1. Eur J Biochem 271:4409–4419.
Schaap J, Meijer JH (2001) Opposing effects of behavioural activity and light on neurons of the suprachiasmatic nucleus. Eur J Neurosci 13:1955–1962.
Schapira AH V (2012) Mitochondrial diseases. Lancet 379:1825–1834.
Schernhammer ES, Kroenke CH, Laden F, Hankinson SE (2006) Night work and risk of breast cancer. Epidemiology 17:108–111.
Schibler U, Brown SA (2005) Enlightening the adrenal gland. Cell Metab 2:277–278.
Schibler U, Sassone-corsi P (2002) A web of circadian pacemakers. Cell 111:919–922.
Schopf JW, Kudryavtsev AB, Czaja AD, Tripathi AB (2007) Evidence of Archean life: Stromatolites and microfossils. Precambrian Res 158:141–155.
Schroeder A, Loh D, Jordan M, Roos K, Colwell C (2011a) Baroreceptor reflex dysfunction in the BACHD mouse model of Huntington's disease. PLoS Curr 4:RRN1266.
Schroeder A, Loh DH, Jordan MC, Roos KP, Colwell CS (2011b) Circadian regulation of cardiovascular function: a role for vasoactive intestinal peptide. Am J Physiol Heart Circ Physiol 300:H241–H250.
Schulte J, Littleton JT (2011) The biological functin of the Huntingtin proteina and its relevance to Huntington's disease pathology. Curr Trends Neurol 5:65–78.
Sellix MT (2013) Clocks underneath: The role of peripheral clocks in the timing of female reproductive physiology. Front Endocrinol (Lausanne) 4:1–6.
Sellix MT, Menaker M (2010) Circadian clocks in the ovary. Trends Endocrinol Metab 21:628–636.
Sesti F, Liu S, Cai SQ (2010) Oxidation of potassium channels by ROS: a general mechanism of aging and neurodegeneration? Trends Cell Biol 20:45–51.
Shearman LP, Zylka MJ, Weaver DR, Kolakowski LF, Reppert SM (1997) Two period homologs: circadian expression and photic regulation in the suprachiasmatic nuclei. Neuron 19:1261–1269 Available at: http://www.ncbi.nlm.nih.gov/pubmed/9427249.
Shen K-Z, Johnson SW (2010) Ca2+ influx through NMDA-gated channels activates ATP-sensitive K+ currents through a nitric oxide-cGMP pathway in subthalamic neurons. J Neurosci 30:1882–1893.
Shepherd GMG, Katz DM (2011) Synaptic microcircuit dysfunction in genetic models of neurodevelopmental disorders: Focus on Mecp2 and Met. Curr Opin Neurobiol 21:827–833.

Sherman B, West J, Korenman S (1976) The menopausal transition: analysis of LH, FSH, estradiol, and progesterone concentrations during menstrual cycles of older women. J Clin Endocrinol Metab 42:629–636.
Shibata S, Oomura Y, Hattori K, Kita H (1984) Responses of suprachiasmatic nucleus neurons to optic nerve stimulation in rat hypothalamic slice preparation. Brain Res 302:83–89.
Shigeyoshi Y, Taguchi K, Yamamoto S, Takekida S, Yan L, Tei H, Moriya T, Shibata S, Loros J, Dunlap J, Okamura H (1997) Light-Induced Resetting of a Mammalian Circadian Clock Is Associated with Rapid Induction of the. Cell 91:1043–1053.
Shimohata T, Onodera O, Tsuji S (2000) Interaction of expanded polyglutamine stretches with nuclear transcription factors leads to aberrant transcriptional regulation in polyglutamine diseases. Neuropathology 20:326–333.
Shinohara K, Funabashi T, Mitushima D, Kimura F (2000) Effects of gap junction blocker on vasopressin and vasoactive intestinal polypeptide rhythms in the rat suprachiasmatic nucleus in vitro. Neurosci Res 38:43–47.
Shirbin C a, Chua P, Churchyard A, Lowndes G, Hannan AJ, Pang TY, Chiu E, Stout JC (2013) Cortisol and depression in pre-diagnosed and early stage Huntington's disease. Psychoneuroendocrinology 38:2439–2447.
Siepka SM, Yoo S-H, Park J, Lee C, Takahashi JS (2007) Genetics and neurobiology of circadian clocks in mammals. Cold Spring Harb Symp Quant Biol 72:251–259.
Silver R, LeSauter J, Tresco P, Lehman M (1996) A diffusible coupling signal from the transplanted suprachiasmatic nucleus controlling circadian locomotor rhythms. Nature 382:810–813.
Smarr BL, Morris E, De La Iglesia HO (2012) The dorsomedial suprachiasmatic nucleus times circadian expression of Kiss1 and the luteinizing hormone surge. Endocrinology 153:2839–2850.
Smith KM, Dahodwala N (2014) Sex differences in Parkinson's disease and other movement disorders. Exp Neurol 259:44–56.
Smith M, Jiennes L, Wise P (2000) Localization of the VIP2 receptor protein on GnRH neurons in the female rat. Endocrinology 141:4317–4320.
Sokolove PG, Bushell WN (1978) The chi square periodogram: Its utility for analysis of circadian rhythms. J Theor Biol 72:131–160.
Soneson C, Fontes M, Zhou Y, Denisov V, Paulsen JS, Kirik D, Petersén Å (2010) Early changes in the hypothalamic region in prodromal Huntington disease revealed by MRI analysis. Neurobiol Dis 40:531–543.
Sorensen SA, Fenger K (1992) Causes of death in patients with Huntington' s disease and in unaffected first degree relatives. J Med Genet 29:911–914.
Southwell AL, Ko J, Patterson PH (2009) Intrabody gene therapy ameliorates motor, cognitive, and neuropathological symptoms in multiple mouse models of Huntington's disease. J Neurosci 29:13589–13602.
Spencer JL, Waters EM, Romeo RD, Wood GE, Milner TA, Mcewen BS, College B, York N (2008) Uncovering the Mechanisms of Estrogen Effects on Hippocampal Function. Front Neuroendocrinol 29:219–237.
Stevens RG (2006) Artificial lighting in the industrialized world: Circadian disruption and breast cancer. Cancer Causes Control 17:501–507.
Storch K-F, Lipan O, Leykin I, Viswanathan N, Davis FC, Wong WH, Weitz CJ (2002) Extensive and divergent circadian gene expression in liver and heart. Nature 417:78–83.
Strong T, Tagle D, Valdes J, Elmer L, Boehm K, Swaroop M, Kaatz K, Collins F, Albin R (1993) Widespread expression of the human and rat Huntington's disease gene in brain and nonneural tissues. Nat Genet Genet 5:259–265.

Sugars KL, Brown R, Cook LJ, Swartz J, Rubinsztein DC (2004) Decreased cAMP response element-mediated transcription: an early event in exon 1 and full-length cell models of Huntington's disease that contributes to polyglutamine pathogenesis. J Biol Chem 279:4988–4999.
Summa KC, Vitaterna MH, Turek FW (2012) Environmental perturbation of the circadian clock disrupts pregnancy in the mouse. PLoS One 7:e37668.
Sun Y, Shu J, Kyei K, Neal-Perry GS (2012) Intracerebroventricular infusion of vasoactive intestinal peptide rescues the luteinizing hormone surge in middle-aged female rats. Front Endocrinol (Lausanne) 3:1–9.
Sun ZS, Albrecht U, Zhuchenko O, Bailey J, Eichele G, Lee CC (1997) RIGUI, a putative mammalian ortholog of the Drosophila period gene. Cell 90:1003–1011.
Swaab D (2004) Sexual differentiation of the human brain: relevance for gender identity, transsexualism and sexual orientation. Gynecol Endocrinol 19:301–312.
Swaab DF, Hofman M a. (1990) An enlarged suprachiasmatic nucleus in homosexual men. Brain Res 537:141–148.
Takahashi JS, Menaker M (1980) Interaction of estradiol and progesterone: effects on circadian locomotor rhythm of female golden hamsters. Am J Physiol 239:R497–R504.
Takahata S, Sogawa K, Kobayashi A, Ema M, Mimura J, Ozaki N, Fujii-kuriyama Y (1998) Transcriptionally Active Heterodimer Formation of an Arnt-like PAS Protein, Arnt3, with HIF-1a, HLF, and Clock. Biochem Biophys Res Commun 794:789–794.
Taylor N, Bramble D (1997) Psychological consequences of road traffic accidents in children and adolescents. Br J Psychiatry 171:393.
Thayer JF, Yamamoto SS, Brosschot JF (2010) The relationship of autonomic imbalance, heart rate variability and cardiovascular disease risk factors. Int J Cardiol 141:122–131.
Thresher RJ, Vitaterna MH, Miyamoto Y, Kazantsev a, Hsu DS, Petit C, Selby CP, Dawut L, Smithies O, Takahashi JS, Sancar a (1998) Role of mouse cryptochrome blue-light photoreceptor in circadian photoresponses. Science 282:1490–1494.
Timmers HJLM, Swaab DF, van de Nes J a. P, Kremer HPH (1996) Somatostatin 1–12 immunoreactivity is decreased in the hypothalamic lateral tuberal nucleus of Huntington's disease patients. Brain Res 728:141–148.
Tousson E, Meissl H (2004) Suprachiasmatic nuclei grafts restore the circadian rhythm in the paraventricular nucleus of the hypothalamus. J Neurosci 24:2983–2988.
Travnickova-Bendova Z, Cermakian N, Reppert SM, Sassone-Corsi P (2002) Bimodal regulation of mPeriod promoters by CREB-dependent signaling and CLOCK/BMAL1 activity. Proc Natl Acad Sci U S A 99:7728–7733.
Trushina E et al. (2004) Mutant Huntingtin Impairs Axonal Trafficking in Mammalian Neurons In Vivo and In Vitro Mutant Huntingtin Impairs Axonal Trafficking in Mammalian Neurons In Vivo and In Vitro. Mol Cell Biol 24:8195.
Tu DC, Zhang D, Demas J, Slutsky EB, Provencio I, Holy TE, Van Gelder RN (2005) Physiologic diversity and development of intrinsically photosensitive retinal ganglion cells. Neuron 48:987–999.
Turek F, Swann J, Earnest D (1984) Role of the circadian system in reproductive phenomena. Recent Prog Horm Res 40:143–183.
Vaccarino AL, Sills T, Anderson K, Borowsky B, Craufurd D, Giuliano J, Goodman L, Guttman M, Kupchak P, Ho AK, Paulsen JS, Stout JC, van Kammen DP, Evans K (2011) Assessment of cognitive symptoms in prodromal and early Huntington disease. PLoS Curr.
Valentinuzzi VS, Scarbrough K, Takahashi JS, Turek FW (1997) Effects of aging on the circadian rhythm of wheel-running activity in C57BL/6 mice. Am J Physiol 273:R1957–R1964.

Van den Pol a N (1980) The hypothalamic suprachiasmatic nucleus of rat: intrinsic anatomy. J Comp Neurol 191:661–702.
Van Der Beek EM, Horvath TL, Wiegant VM, Van Hurk R Den, Buijs RM (1997) Evidence for a direct neuronal pathway from the suprachiasmatic nucleus to the gonadotropin-releasing hormone system: Combined tracing and light and electron microscopic immunocytochemical studies. J Comp Neurol 384:569–579.
Van der Horst GT, Muijtjens M, Kobayashi K, Takano R, Kanno S, Takao M, de Wit J, Verkerk a, Eker a P, van Leenen D, Buijs R, Bootsma D, Hoeijmakers JH, Yasui a (1999) Mammalian Cry1 and Cry2 are essential for maintenance of circadian rhythms. Nature 398:627–630.
Van der Vinne V, Zerbini G, Siersema A, Pieper A, Merrow M, Hut R a., Roenneberg T, Kantermann T (2015) Timing of Examinations Affects School Performance Differently in Early and Late Chronotypes. J Biol Rhythms 30:53–60.
Van Diepen HC, Ramkisoensing A, Peirson SN, Foster RG, Meijer JH (2013) Irradiance encoding in the suprachiasmatic nuclei by rod and cone photoreceptors. FASEB J 27:4204–4212.
Van Duijn E, Selis M a., Giltay EJ, Zitman FG, Roos R a C, van Pelt H, van der Mast RC (2010) Hypothalamic-pituitary-adrenal axis functioning in Huntington's disease mutation carriers compared with mutation-negative first-degree controls. Brain Res Bull 83:232–237.
Van Raamsdonk JM, Murphy Z, Selva DM, Hamidizadeh R, Pearson J, Petersén A, Björkqvist M, Muir C, Mackenzie IR, Hammond GL, Vogl a W, Hayden MR, Leavitt BR (2007) Testicular degeneration in Huntington disease. Neurobiol Dis 26:512–520.
Van Raamsdonk JM, Pearson J, Rogers D a, Bissada N, Vogl a W, Hayden MR, Leavitt BR (2005) Loss of wild-type huntingtin influences motor dysfunction and survival in the YAC128 mouse model of Huntington disease. Hum Mol Genet 14:1379–1392.
Vida B, Deli L, Hrabovszky E, Kalamatianos T, Caraty a., Coen CW, Liposits Z, Kalló I (2010) Evidence for suprachiasmatic vasopressin neurones innervating kisspeptin neurones in the rostral periventricular area of the mouse brain: Regulation by oestrogen. J Neuroendocrinol 22:1032–1039.
Videnovic A, Noble C, Reid KJ, Peng J, Turek FW, Marconi A, Rademaker AW, Simuni T, Zadikoff C, Zee PC (2014) Circadian Melatonin Rhythm and Excessive Daytime Sleepiness in Parkinson Disease. JAMA Neurol 02114:1–7.
Vieira E, Marroquí L, Figueroa ALC, Merino B, Fernandez-Ruiz R, Nadal A, Burris TP, Gomis R, Quesada I (2013) Involvement of the Clock Gene Rev-erb alpha in the Regulation of Glucagon Secretion in Pancreatic Alpha-Cells. PLoS One 8.
Virgili N, Mancera P, Wappenhans B, Sorrosal G, Biber K, Pugliese M, Espinosa-Parrilla JF (2013) KATP Channel Opener Diazoxide Prevents Neurodegeneration: A New Mechanism of Action via Antioxidative Pathway Activation. PLoS One 8:e75189.
Vosko AM, Schroeder A, Loh DH, Colwell CS (2007) Vasoactive intestinal peptide and the mammalian circadian system. Gen Comp Endocrinol 152:165–175.
Walker AG, Miller BR, Fritsch JN, Barton SJ, Rebec G V (2008) Altered information processing in the prefrontal cortex of Huntington's disease mouse models. J Neurosci 28:8973–8982.
Wallick DW, Martin PJ, Masuda Y, Levy MN (1982) Effects of autonomic activity and changes in heart rate on atrioventricular conduction. Am J Physiol 243:H523–H527.
Wamelen DJ Van, Aziz NA, Anink JJ, Steenhoven R Van, Angeloni D, Fraschini F, Jockers R, Roos RAC, Swaab DF (2013) Suprachiasmatic Nucleus Neuropeptide Expression in Patients with Huntington ' s Disease. Sleep 36:117–125.
Wang H-Y, Huang R-C (2004) Diurnal modulation of the Na+/K+-ATPase and spontaneous firing in the rat retinorecipient clock neurons. J Neurophysiol 92:2295–2301.

Wang LM-C, Schroeder AM, Loh DH, Smith D, Kin K, Han J, Michel S, Hummer D, Ehlen J, Albers H, Colwell CS (2008) Role for the NR2B subunit of the NMDA receptor in mediating light input to the circadian system. Eur J Neurosci 27:1771–1779.
Wang TA, Yu Y V, Govindaiah G, Ye X, Artinian L, Colweman TP, Sweedler JV, Cox CL, Gillette MU (2012a) Circadian rhythm of redox state regulates excitability in suprachiasmatic nucleus neurons. Science (80-) 337:839–842.
Wang Y-C, Huang R-C (2006) Effects of sodium pump activity on spontaneous firing in neurons of the rat suprachiasmatic nucleus. J Neurophysiol 96:109–118 Available at: http://www.ncbi.nlm.nih.gov/pubmed/16467417 [Accessed March 17, 2014].
Wang Y-C, Yang J-J, Huang R-C (2012b) Intracellular Na(+) and metabolic modulation of Na/K pump and excitability in the rat suprachiasmatic nucleus neurons. J Neurophysiol 108:2024–2032.
Ward DR, Dear FM, Ward I a., Anderson SI, Spergel DJ, Smith P a., Ebling FJP (2009) Innervation of gonadotropin-releasing hormone neurons by peptidergic neurons conveying circadian or energy balance information in the mouse. PLoS One 4:1–9.
Warren EJ, Allen CN, Brown RL, Robinson DW (2003) Intrinsic light responses of retinal ganglion cells projecting to the circadian system. Eur J Neurosci 17:1727–1735.
Watanabe K, Vanecek J, Yamaoka S (2000) In vitro entrainment of the circadian rhythm of vasopressin-releasing cells in suprachiasmatic nucleus by vasoactive intestinal polypeptide. Brain Res 877:361–366.
Webb AB, Angelo N, Huettner JE, Herzog ED (2009) Intrinsic, nondeterministic circadian rhythm generation in identified mammalian neurons. Proc Natl Acad Sci U S A 106:16493–16498.
Weber M, Lauterburg T, Tobler I, Burgunder JM (2004) Circadian patterns of neurotransmitter related gene expression in motor regions of the rat brain. Neurosci Lett 358:17–20.
Welsh DK, Takahashi JS, Kay S a (2010) Suprachiasmatic nucleus: cell autonomy and network properties. Annu Rev Physiol 72:551–577.
Wever R a (1984) Sex differences in human circadian rhythms: intrinsic periods and sleep fractions. Experientia 40:1226–1234.
Wexler NS (2004) Venezuelan kindreds reveal that genetic and environmental factors modulate Huntington's disease age of onset. Proceedings from the National Academy of Sciences of the United States of America 101(10): 3498-503.
Wiegand S, Terasawa E, Bridson W, RW G (1980) Effects of discrete lesions of preoptic and suprachiasmatic structures in the female rat. Alterations in the feedback regulation of gonadotropin secretion. Neuroendocrinology 31:147–157.
Wijnen H, Young MW (2006) Interplay of circadian clocks and metabolic rhythms. Annu Rev Genet 40:409–448.
Williams W 3rd, Jarjisian S, Mikkelsen J, LJ K (2011) Circadian control of kisspeptin and a gated GnRH response mediate the preovulatory luteinizing hormone surge. Endocrinology 152:595–606.
Williams WP, Kriegsfeld LJ (2012) Circadian control of neuroendocrine circuits regulating female reproductive function. Front Endocrinol (Lausanne) 3:1–14.
Willison LD, Kudo T, Loh DH, Kuljis D, Colwell CS (2013) Circadian dysfunction may be a key component of the non-motor symptoms of Parkinson's disease: Insights from a transgenic mouse model. Exp Neurol 243:57–66.
Wirz-justice A (1987) Circadian rhythms in mammalian neurotransmitter receptors. Prog Neurobiol 29:219–259.
Wirz-Justice A (2006) Biological rhythm disturbances in mood disorders. Int Clin Psychopharmacol 21 Suppl 1:S11–S15.
Wittert G (2014) The relationship between sleep disorders and testosterone. Curr Opin Endocrinol Diabetes Obes 21:239–243.

Wollnik F, Turek FW (1988) Estrous correlated modulations of circadian and ultradian wheel-running activity rhythms in LEW/Ztm rats. Physiol Behav 43:389–396.
Wood NI, Goodman AOG, van der Burg JMM, Gazeau V, Brundin P, Björkqvist M, Petersén A, Tabrizi SJ, Barker R a, Morton a J (2008) Increased thirst and drinking in Huntington's disease and the R6/2 mouse. Brain Res Bull 76:70–79.
Yamazaki S, Kerbeshian MC, Hocker CG, Block GD, Menaker M (1998) Rhythmic properties of the hamster suprachiasmatic nucleus in vivo. J Neurosci 18:10709–10723.
Yan L, Karatsoreos I, Lesauter J, Welsh DK, Kay S, Foley D, Silver R (2007) Exploring spatiotemporal organization of SCN circuits. Cold Spring Harb Symp Quant Biol 72:527–541.
Yan L, Okamura H (2002) Gradients in the circadian expression of Per1 and Per2 genes in the rat suprachiasmatic nucleus. Eur J Neurosci 15:1153–1162.
Yan L, Silver R (2004) Resetting the brain clock: Time course and localization of mPER1 and mPER2 protein expression in suprachiasmatic nuclei during phase shifts. Eur J Neurosci 19:1105–1109.
Yoo S-H, Yamazaki S, Lowrey PL, Shimomura K, Ko CH, Buhr ED, Siepka SM, Hong H-K, Oh WJ, Yoo OJ, Menaker M, Takahashi JS (2004) PERIOD2::LUCIFERASE real-time reporting of circadian dynamics reveals persistent circadian oscillations in mouse peripheral tissues. Proc Natl Acad Sci U S A 101:5339–5346.
Yoshikawa T, Sellix M, Pezuk P, Menaker M (2009) Timing of the ovarian circadian clock is regulated by gonadotropins. Endocrinology 150:4338–4347.
Zhou J-NN, Hofman MA, Swaab DF (1995) VIP neurons in the human SCN in relation to sex, age, and Alzheimer's disease. Neurobiol Aging 16:571–576.
Zielonka D, Marinus J, Roos R a C, De Michele G, Di Donato S, Putter H, Marcinkowski J, Squitieri F, Bentivoglio AR, Landwehrmeyer GB (2013) The influence of gender on phenotype and disease progression in patients with Huntington's disease. Parkinsonism Relat Disord 19:192–197.
Zucker I, Fitzgerald KM, Morin LP (1980) Sex differentiation of the circadian system in the golden hamster. Am J Physiol Regul Integr Comp Physiol 238:R97–R101.
Zucker I, Stephan FK (1973) Light-dark rhythms in hamster eating, drinking and locomotor behaviors. Physiol Behav 11:239–250.